University of Alberta

Designed zinc finger proteins as novel therapeutics inhibiting the transcription of hepatitis B and duck hepatitis B viruses

by

Kimberley Anne Zimmerman

A thesis submitted to the Faculty of Graduate Studies and Research
in partial fulfillment of the requirements for the degree of

Doctor of Philosophy

in

Virology

Department of Medical Microbiology and Immunology

Fall 2010
Edmonton, Alberta

Examining Committee

Lorne Tyrrell, Department of Medical Microbiology and Immunology

David Evans, Department of Medical Microbiology and Immunology

Edan Foley, Department of Medical Microbiology and Immunology

Luis Schang, Department of Biochemistry

Chris Richardson, Department of Microbiology and Immunology, Dalhousie University

Abstract

The Hepatitis B virus (HBV) chronically infects 350 million individuals worldwide, leading to mortality by end-stage liver disease, liver cirrhosis, and hepatocellular carcinoma. The vaccine to prevent HBV infection is highly effective but is not extensively available in endemic areas, resulting in high infection rates. Nucleoside analogue treatment of HBV has allowed for higher rates of viral clearance in infected individuals, but most patients must remain on therapy long term and viral resistance to the drugs is growing.

The HBV viral genome is an episome in the nucleus of infected hepatocytes. It is called covalently closed circular (ccc) DNA and is highly stable, has a long half-life, and is the template for all viral transcription and progeny production. Nucleoside analogues do not directly target cccDNA, therefore many patients experience rebound when antiviral therapy is stopped. I have designed novel DNA binding proteins called zinc finger proteins (ZFPs) to specifically bind to the cccDNA in infected cells and inhibit viral transcription. Seven ZFPs targeting the model duck HBV (DHBV) and ten ZFPs targeting HBV were developed. Kinetic analyses of the purified ZFPs were performed, characterizing their specificity and binding properties. Using the DHBV tissue culture model system, I have demonstrated that the DHBV-specific ZFPs can specifically inhibit transcription from the viral template, resulting in reduced viral RNA, protein products and progeny virions. The DHBV-specific ZFPs were tested in primary duck hepatocytes (PDH) and *in vivo* in the Pekin duck model. ZFPs failed to

express in PDH transduced by baculovirus vectors when DHBV was present in the cells. *In vivo* gene delivery of the ZFPs was carried out by portal vein injection of chitosan-based nanospheres. Unfortunately, non-specific reductions in viral levels masked any direct effect by the ZFPs. Testing of the HBV-specific ZFPs in tissue culture was hindered by a lack of transfectable cell culture model. A number of different transfection methods were tested to express the HBV-specific ZFPs, all without success. Further work is being carried out using baculovirus vectors to deliver the HBV-specific ZFPs to HBV-harbouring cell lines and HBV-infected *scid*-Alb/uPA chimeric mice with human liver cells.

Acknowledgements

I would like to acknowledge my husband, Garrett, for all of his support over the years of graduate school. He has been patient, encouraging and caring throughout it all.

I must also thank my family for their encouragement on this venture called "PhD". Without the many phone calls to my mom, Nivea, and my sister, Amanda, the journey would have been more difficult. I would also like to thank my father, Allan, for instilling in me a love of learning, and my brother, Kyle, for being there when I needed him.

I am indebted to all of my friends, both inside and outside of the department. Without the many coffee breaks with Jöelle and Melany, the days would have seemed much longer and the research much harder. As well, I have many other friends who have been encouraging and inspirational, including Bonnie, Bindi, Catherine and Leslie. Further, my lab mates, especially Lindsay, Kristen, Nicola, Darci, Rineke and Mike, were indispensible during my navigation through research, whether they offered scientific advice or brightened my day with a well-timed joke. My thanks to all of them for their support.

I would especially like to thank Karl, who has been a great resource and friend during my time in the lab. Without him, so much of my research would not have gone so smoothly. Additionally, I would like to thank Suellen Lamb for her help with histology, and Lin Fu Zhu for completing the microsurgical experiments.

Lastly, I would like to acknowledge my supervisor, Dr. Lorne Tyrrell, who has been an excellent mentor and has taught me that an optimistic outlook and a strong sense of respect for your co-workers are key principles in building healthy relationships and achieving goals that require the cooperation of a large group of individuals. His continued enthusiasm for research is inspirational, and I hope to one day be the kind of researcher and mentor to others that Dr. Tyrrell has been for me.

Table of Contents

List of Tables

List of Figures

Abbreviations and Units

Units

Å	Angstrom
Ω	Ohms
µF	Microfarads
µg	Micrograms
µL	Microlitres
µM	Micromolar
ng	Nanogram
nL	Nanolitres
nm	Nanometers
nM	Nanomolar
pM	Picomolar
Da	Daltons
G	Grams
kb	Kilobases
kDa	Kilodaltons
Kg	Kilogram
L	Litres
M	Molar
mA	Milliampere
mg	Milligrams
mL	Millilitres

mm	Millimeters
mM	Millimolar
mV	Millivolts
rpm	Rotations per minute
V	Volts

Abbreviations

3TC	3'-thiacytidine
9-mers	ZFPs recognizing 9-bps of target sequence
18-mers	ZFPs recognizing 18-bps of target sequence
AAV	Adeno-associated virus
ADV	Adefovir dipivoxil
Amp	Ampicillin
APS	Ammonium persulfate
ARE	Androgen response element
ATP	Adenosine triphosphate
β-Gal	β-galactosidase
bp	Base pairs
BSA	Bovine serum albumin
BSCTV	Beet severe curly top virus
cccDNA	Covalently closed circular DNA
cDNA	Complementary deoxyribonucleic acid
C/EBP	CCAAT/enhancer binding protein

CHO	Chinese Hamster Ovary
CLV	Clevudine
CMV	Cytomegalovirus
CO_2	Carbon dioxide
COUP-TF	Chicken ovalbumin upstream promoter transcription factor
CPD	Carboxypeptidase D
CTL	Cytotoxic T lymphocytes
Dε	DHBV epsilon sequence
dCTP	Deoxycytidine triphosphate
dEnI	DHBV Enhancer I
DEPC	Diethyl pyrocarbonate
dGMP	Deoxyguanosine nucleotide
dGTP	Deoxyguanosine triphosphate
dH_2O	Distilled water
dHBV	Defective HBV particles
DHBV	Duck hepatitis B virus
DMEM	Dulbecco's modified eagle medium
DMSO	Dimethyl sulfoxide
DNA	Deoxyribonucleic acid
dNTP	Deoxyribonucleotide triphosphate
DP	Deproteinized
DR	Direct repeat

ds	Double stranded
DSL	Double stranded linear
DTT	Dithiothreitol
dTTP	Deoxythymidine triphosphate
E.coli	*Escherichia coli*
ECV	Extracellular virus
EDTA	Ethylenediaminetatraacetic acid
EGFP	Enhanced green fluorescent protein
EGP-2	Epithelial glycoprotein-2
EMC	Emtricitabine
EMSA	Electrophoretic mobility shift assay
EnI	HBV Enhancer I
EnII	HBV Enhancer II
ER	Endoplasmic reticulum
EtBr	Ethidium bromide
ETV	Entecavir
FCS	Fetal calf serum
FP	Footprint region
FXR-α	Farnesoid X receptor alpha
GAPDH	Glyceraldehyde-3-phosphate dehydrogenase
GBP	Guanylate binding protein
GFP	Green fluorescent protein
GRE	Glucocorticoid-responsive element

Hε	HBV epsilon sequence
HbA	Adult hemoglobin
HBcAg	Hepatitis B core antigen
HBeAg	Hepatitis B E antigen
HbF	Fetal hemoglobin
HBsAg	Hepatitis B surface antigen
HBSP	HBV splice-generated protein
HBV	Hepatitis B virus
HBx	Hepatitis B X protein
HCC	Hepatocellular carcinoma
HCV	Hepatitis C virus
HIV-1	Human immunodeficiency virus 1
HNF	Hepatocyte nuclear factor
HPV	Human papillomavirus
HPVNA	High Pure Viral Nucleic Acid kit
HRP	Horseradish peroxidase
HSLα	HBV stem loop alpha
HSLβ1	HBV stem loop beta 1
HSP-60	Heat shock protein 60
HSV	Herpes simplex virus
ICAM-1	Intercellular cell adhesion molecule 1
ICV	Intracellular virus
IFN-α	Interferon alpha

IFN-β	Interferon beta
IFN-γ	Interferon gamma
IL1β	Interleukin 1 beta
IL-2	Interleukin 2
IL-6	Interleukin 6
IPTG	Isopropyl β-D-1-thiogalactopyranoside
IRF4	Interferon regulatory factor 4
ISG-15	Interferon stimulated gene 15
ISG-20	Interferon stimulated gene 20
Kan	Kanamycin
KRAB	Krüppel-associated box repressor domain
L	Large surface protein
LAM	Lamivudine
LB	Luria Broth
LF2000™	Lipfectamine™ 2000
LMH	Longhorn male hepatoma
LTR	Long terminal repeat
LV	Lentivirus
M	Medium surface protein
MBP	Maltose binding protein
MEM	Minimal Essential Medium
MOPS	3-(N-morpholino)propanesulfonic acid
mRNA	Messenger RNA

mtDNA	Mitochondrial DNA
MTT	3-(4,5-Dimethylthiazol-2-yl)-2,5-diphenyltetrazolium bromide
MW_A	Molecular weight of analyte
MW_L	Molecular weight of ligand
NA	Nucleoside analogue
NEB	New England Biolabs
net	Negative effector of transcription
NF	Nuclear factor
NF-κB	Nuclear factor kappa B
NLS	Nuclear localization signal
NPC	Nuclear pore complex
OAS1	Oligoadenylate synthetase 1
ONPG	Ortho-nitrophenyl-beta-galactoside
PAMP	Pathogen associated molecular patter
PBS	Phosphate buffered saline
PCR	Polymerase chain reaction
pcRNA	Precore RNA
PDH	Primary duck hepatocytes
PEG	Polyethylene glycol
pet	Positive effector of transcription
PGC-1α	Peroxisome proliferator-activated receptor-γ coactivator 1 alpha
pgRNA	Pregenomic RNA

PKC	Protein kinase C
PKR	Protein kinase R
pNPP	Para-nitrophenyl phosphate
Pol	Polymerase
polyA	polyadenylated
PPAR	Peroxisome proliferator-activated receptor
PRE	Posttranscriptional regulatory element
preS	DHBV large surface protein
preS1	Large surface protein
preS2	Medium surface protein
PS1	Processing signal 1
PS2	Processing signal 2
PTB	Polypyrmidine tract binding protein
rcDNA	Relaxed circular DNA
RIPA	Radioimmunoprecipitation assay
R_L	Immobilization level
RNA	Ribonucleic acid
RT	Reverse transcriptase
RU	Resonance units
RXR-α	Retinoic X receptor alpha
S	Small surface protein
SA	Streptavidin
SAP	Shrimp alkaline phosphatase

SDS	Sodium dodecyl sulfate
SDS-PAGE	SDS-polyacrylamide gel electrophoresis
SID	mSIN3 interaction domain
Sm	Stoichiometry of binding
SOB	Super Optimal Broth
SOC	Super Optimal Broth with Catabolite repression
SPI	preS1 promoter
SPII	preS2 promoter
SPR	Surface Plasmon resonance
SV40	Simian virus 40
T	Triangulation number
TBE	Tris borate EDTA
TBP	TATA-binding protein
TBS	Tris buffered saline
TBS-T	Tris buffered saline with Tween-20
TBV	Telbivudine
TEMED	N,N,N,N'-Tetramethyl-ethylenediamine
TNF	Tenofovir disoproxil fumarate
TNF-α	Tumor necrosis factor alpha
TP	Terminal protein
tRNA	Transfer ribonucleic acid
TYLCV	Tomato yellow leaf curl virus
UV	Ultraviolet

VDAC	Voltage dependent anion channel
VEGF-A	Vascular endothelial growth factor A
VV	Vaccinia virus
WHBV	Woodchuck hepatitis B virus
WHO	World Health Organization
X-Gal	bromo-chloro-indolyl-galactopyranoside
ZFN	Zinc finger nuclease
ZFP	Zinc finger protein
ZFP-TF	Zinc finger protein transcription factor

1 Chapter 1: Literature Review

1.1 Global health burden of the Hepatitis B Virus

The Hepatitis B virus (HBV) represents a significant global health burden because it causes severe liver diseases such as fibrosis, cirrhosis and hepatocellular carcinoma (HCC) (1, 2). The preventative vaccine and therapeutic drugs for HBV are also costly and difficult to access in developing countries, where HBV infection rates are high. Additionally, the emergence of strains resistant to therapeutic drugs makes this chronic disease a serious global health problem.

There are 350 million individuals chronically infected with HBV. Surprisingly, only 5% of adults acutely infected with HBV become chronically infected, however over 90% of infants exposed to the virus at birth, and 30% of children exposed between the ages of 1 to 6 years, become chronically infected (3, 4). These chronic infection rates are concerning due to the high transmission rate of HBV within households, and from mother to child (3, 4). It is estimated that at least 50% of the chronically infected individuals worldwide acquired HBV perinatally or during early childhood (4). Chronic infection in children is worrisome because these patients will manifest severe liver disease as young adults, and will contribute to the continued presence of the virus in the population.

HBV was definitively associated with HCC in 1981, when it was shown that carriers of the hepatitis B surface antigen (HBsAg) had a much higher incidence of HCC than non-carriers (2, 5). Furthermore, HCC and liver cirrhosis accounted for 54.3% of deaths in the HBsAg carriers, but only 1.5% of deaths in non-carriers, demonstrating a close linkage between HBV infection and the highly lethal HCC (2). It has been clearly demonstrated since then that the risk of development of HCC due to long-term HBV infection is high.

HCC is the second most lethal cancer in the United States, with a 5-year survival rate of only 8.9% (6). The worldwide estimated incidence rate for HCC is 3.1

cases per 100,000, which averages the high-rate regions, such as Asia and Africa, with the low-rate regions, such as Europe and North America (7). In Asia and Africa, HBV infection is endemic and 8-10% of adults are chronically infected (2, 3). In Europe and North America, approximately 1% of adults are infected, although HBV prevalence has risen in recent years due to increased infection rates during the 1970's (8). During that period, greater numbers of individuals were exposed to HBV and the hepatitis C virus (HCV), a second HCC-related pathogen. Infection occurred most often through unscreened blood products, contaminated needles from recreational drug use and unsafe sex (8). Since the progression to HCC due to HBV or HCV infection occurs over 20 – 30 years, these patients are only now developing serious liver disease as a result of their infection. There are few effective therapies for HCC, as evidenced by a mortality rate that closely reflects the incidence rate (8). It is estimated that approximately 600,000 individuals die each year due to HBV-related sequelae (9). Globally, the health burden due to HBV-associated liver disease and HCC is high, because prevention and treatment are often too costly for a large group of afflicted individuals.

Prevention of infection with HBV is an important step to reduce the incidence of HCC worldwide. A licensed vaccine for HBV has been available for the past 25 years, and is effective at producing neutralizing antibodies for protective immunity with almost no side effects (1, 10). It contains purified HBsAg and can be administered to infants, children and adults, providing protective immunity for 90 – 100% of individuals (1). Since the advent of its use, the rates of HBV infection have decreased in First World countries, although rates of HCC prevalence have yet to drop, due to the delayed nature of disease progression (1). Rates have been slower to drop in Asia and Africa, where the cost of the HBV vaccine has prevented it from being widely used. The original HBV vaccine costs $150 USD, which was prohibitive for widespread purchase in Third World countries. In 1992, the World Health Organization (WHO) made a resolution to have an international immunization program for HBV in place by 1997 (3).

However, this goal was not met and has been updated to have all countries with a national immunization rate of 90% by the end of 2010 (3). Great progress has been made in the vaccination program by improved low cost production of the vaccine and financial support from the WHO, and it is estimated that half a million premature deaths have been prevented since 2003 as a result of the program (3).

Therapeutic treatment of chronic HBV infection with nucleoside analogues (NA) can also reduce the rates of HBV-related liver disease. A number of NAs have been developed to treat HBV infection. The first NA licensed for treatment of chronic HBV was lamivudine (LAM). LAM, a cytosine analogue, is the (-)-enantiomer of 3'-thiacytidine (3TC) and has been shown to potently inhibit the replication of HBV. In patients receiving 100-mg/day doses, HBV DNA was undetectable in the serum in 100% of the cases, although rebound occurred in 81% of patients after therapy was completed (11, 12). This rebound effect first highlighted the potential problems with NA treatment of HBV: nucleoside analogues completely clear chronic HBV infection in only 20-30% of cases, but in the remaining 70-80%, patients experience viral rebound after cessation of therapy.

Other second and third generation NAs have been further developed. These include adefovir dipivoxil (ADV), entecavir (ETV), emtricitabine (EMC), telbivudine (TBV), clevudine (CLV), and tenofovir disoproxil fumarate (TNF). Of these, only EMC, which has a similar structure to 3TC, is not licensed for use to treat chronic HBV in adults. It is also the least promising new candidate because it has a high rate of resistance (13, 14). ADV is an adenosine analogue with a demonstrated ability to reduce HBV DNA serum levels during treatment (14, 15). For example, patients treated with ADV for one year had over a 4-log reduction in serum HBV DNA (15). ETV is a guanosine analogue with greater efficacy than LAM (14, 16, 17). 90% of HBeAg-negative patients and 67% of HBeAg-positive patients treated with ETV for 48 weeks had undetectable HBV

DNA in the serum (16, 17). TBV is an L-nucleoside analogue and TNF is an acyclic nucleotide analogue (14). TBV and TNF both appear to have potent anti-HBV activity (14). In fact, TBV appears to have superior suppression of HBV DNA than LAM, and has lower rates of resistance (18). CLV is a pyrimidine analogue that has shown efficacy in chronic HBV patients, and is currently licensed for use in South Korea (19). Of note, though, only LAM and ADV are licensed for use in children, whereas adults can make use of nearly the full range of drugs (13). Moreover, although LAM is relatively inexpensive, the newer generations of NAs are more expensive, limiting the ability of poor countries to access the new therapeutics.

NAs function by irreversible inhibition and chain termination during the reverse transcription step of viral maturation (20, 21). They are very successful at suppressing viral replication and are generally well tolerated by patients, having a good safety profile (14). However, viral levels can quickly return to that seen prior to treatment once therapy stops (16, 17, 22, 23). Additionally, the rates of resistance to NAs is a growing problem, since standard treatment guidelines use mono-therapy of NAs for chronic HBV infection (14). Mono-therapy allows for the emergence of escape mutants that can have cross-resistance to other NAs. However, utilization of multi-drug therapy for HBV would not be optimal with NAs alone, since they all function in a similar manner. Ideally, diversified therapies would be employed in combination therapy to effect greater clearance of chronic HBV.

Resistance to LAM was predicted and first demonstrated in the duck models of HBV, duck hepatitis B virus (DHBV) (24). Mutations in the reverse transcriptase resulted in 20-fold increased resistance to LAM in tissue culture (24). These mutations were later demonstrated in patients resistant to LAM and were associated with an exacerbation of liver damage and higher HBV DNA levels in the serum (25-27). After 4 years of therapy, LAM resistance can reach rates of 70%, much higher than that observed for any of the other NAs used to treat HBV

(28, 29). Resistance to ADV occurs in approximately 18% of patients after 4 years of mono-therapy, and can be cross-resistant to TNF (29). CLV resistance has not been identified in human subjects after 2 years on therapy, but the woodchuck hepatitis B virus model (WHBV) has demonstrated that resistant virus strains can occur in response to CLV after 32 weeks of therapy (19). These mutants were also cross-resistant to LAM (19). ETV resistance is rare in patients without any prior NA therapy (~1% after 5 years of therapy), but more frequent in patients with a LAM-resistant strain, since a second additional mutation is all that is required to impute full ETV resistance (30). NAs are rarely used in combination, but one study investigated LAM and ADV combination therapy in LAM-resistant patients (31). This treatment was effective for many LAM-resistant patients, however it resulted in multi-drug resistant phenotypes in some cases, including cross-resistance to ADV and ETV (31). TBV has a low rate of selecting for resistant strains of HBV, and can be used against ADV-resistant strains (18). TNF also selects for resistant strains at low rates, with no resistant strains detected after 4 years of mono-therapy (18). Additionally, TNF is superior than ADV or ETV when used to treat LAM-resistant patients (18). In summary, resistance and cross-resistance to NAs is a serious and complicated problem when treating patients long-term for HBV infection. Diversification of the therapeutic options could provide for a multi-drug treatment protocol that would make it more difficult for drug resistance to arise.

Despite the success of NAs in treating chronic HBV infection, 70-80% of patients still experience viral rebound upon cessation of therapy. This phenomenon is a result of the presence of a stable viral reservoir in the nucleus of hepatocytes called covalently closed circular (ccc) DNA (32, 33). The viral reverse transcription event is the target of NAs, which prevents the maturation of progeny virions and also prevents the replenishment of the cccDNA pool in the nucleus of hepatocytes, which can range from 3 – 50 copies per nucleus (34, 35). NAs do not directly target the pool of cccDNA, which has a long half-life, and can remain in the nucleus of hepatocytes during therapy (36). The minimal loss of cccDNA

during treatment with NAs appears to reflect the loss of hepatocytes rather than a direct effect on cccDNA (36). After therapy, the cccDNA is responsible for the rebound in virus production.

In summary, although there is a good vaccine and a number of therapeutic options available for HBV infection, HBV remains a major global health burden. Increased access to the vaccine can help shape a better future with lower HBV infection rates, but those individuals currently infected with the virus face difficult treatment options, especially if they develop drug-resistant strains. Furthermore, there are currently no therapies addressing the viral reservoir, found in the form of cccDNA. In this thesis, I will outline a novel therapeutic option that directly targets the cccDNA of HBV and the model virus, DHBV, based upon DNA binding proteins called zinc finger proteins (ZFP). ZFPs can directly target specific DNA sequences within the cccDNA genome. This is the first approach that can directly address the problem of cccDNA persistence in patients.

1.2 Molecular biology of the Hepatitis B Virus

1.2.1 Hepadnaviridae characteristics

HBV and DHBV belong to the *Hepadnaviridae* family. Members of this family have small, double-stranded (ds) DNA genomes with similar genome organization and life cycle. Two genera are contained within this family, including the avihepadnaviridae, which infect birds and includes the prototypic model DHBV, and the orthohepadnaviridae, which infect mammals and includes the human virus, HBV (37, 38).

1.2.2 Overview of HBV life cycle

The viral life cycle initiates by binding of the HBV virion to the surface of the host liver cell, via the surface glycoproteins found on the viral envelope. The entry mechanism has not been elucidated in detail, but it is thought that receptor-mediated endocytosis brings the viral particle into the endosomal pathway. Subsequently, the viral nucleocapsid is released into the cytoplasm, where it

tracks to the nuclear pore complex at the nuclear membrane. The viral genome is then released into the nucleoplasm, where it undergoes a number of completion steps, presumably by host enzymes, to form the cccDNA episome. The cccDNA is transcribed by RNA Polymerase II to produce five main HBV transcripts (two at 3.5-kilobases (kb) and one each at 2.4-kb, 2.1-kb, 0.7-kb), from which seven gene products are produced: (1) the core protein, which forms the nucleocapsid structure; (2-4) three surface glycoproteins, which are found in the viral envelope and are responsible for receptor identification and entry into host cells; (5) the DNA polymerase (Pol), which has RNA-dependent and DNA-dependent DNA polymerase activity. Pol is also known as the reverse transcriptase (RT), and is packaged into virion particles and participates in reverse transcription of the progeny RNA genomes; (6) the X protein, which has an unclear role but appears to be involved in pathogenesis and carcinogenesis; and (7) the precore protein, which does not appear to have a biological function is found in patients and is a useful diagnostic marker. Following translation of the viral protein products, core proteins spontaneously form nucleocapsid structures packaged with a progeny genome, consisting of the 3.5-kb transcript called pregenomic RNA (pgRNA) and the Pol protein. Once enclosed, Pol uses pgRNA as the template to reverse transcribe the minus- and plus-strands of the viral DNA genome, producing the relaxed circular dsDNA form found in mature virions. The nucleocapsid buds into the endoplasmic reticulum (ER) based upon interactions with the surface proteins, which are co-translationally inserted into this organelle during their synthesis. The enveloped virions then exit the cell via the constitutive pathway of vesicular transport.

1.2.3 Virion Structure

The infectious virus particle is called the Dane particle, which has a diameter of 42 to 47 nanometers (nm) (39-41). It has a lipid layer (envelope) surrounding an icosahedral nucleocapsid with a diameter of 28 nm (37, 42, 43). The nucleocapsid is composed of 120 dimers of core protein, with a triangulation number T=4 (37, 44). Dane particles have small (S), medium (M, preS2) and large (L, preS1)

surface proteins in their lipid layer at a ratio of 4:1:1 (37, 45, 46). The Dane particle contains the viral nucleic acid and the viral Pol (Figure 1.1) (47), as well as several host proteins, including protein kinase C (PKC) (48, 49). A fraction of Dane particles do not contain any nucleic acid or Pol (50).

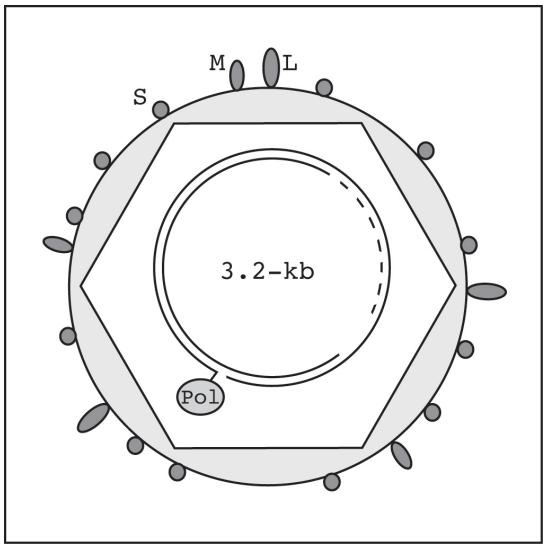

Figure 1.1 – The HBV Dane particle.
The general structure of the HBV Dane particle shows the three surface glycoproteins (S, M, L) as dark grey ovals in the viral envelope (outer circle). The viral nucleocapsid (white hexagon) contains the viral DNA genome in relaxed-circular form. The single stranded portion of the genome is shown by a dotted line and the viral polymerase (Pol) protein is covalently attached to the minus strand.

Infected cells also produce noninfectious subviral particles, called filaments and spheres (41, 51). Spheres, which are 20 nm in diameter, are the most abundant structure released into the blood of infected patients (41, 51), and contain M and S proteins at a ratio of 1:2, with only small amounts of L present (41, 46, 52, 53). Fewer filaments are produced than spheres, and contain M and L proteins at a ratio of 1:1 (37, 53). Neither of these particles contains nucleocapsids or viral nucleic acid (45, 53).

The majority of the DNA found within the Dane particles is double-stranded relaxed circular (rcDNA), with single stranded regions (39, 40, 54, 55). The single stranded regions are heterogeneous in a population of Dane particles, and can

vary in length from 15 to 50% of the full genome (39, 55-57). The DNA genome is covalently linked to Pol at the 5' end of the minus-strand (37, 58). Viral genomes within the Dane particles are most commonly found in rcDNA forms, although double-stranded linear forms can be detected (57).

1.2.4 Viral attachment and entry

Carboxypeptidase D (CPD; also known as gp180) is the viral entry receptor for DHBV (59). It is essential for viral entry, and binds with high affinity to the ectodomain of the preS region of the preS protein (59). Similarly, the preS1 region of the large surface protein in HBV is responsible for infectivity, although the receptor for HBV has not been identified (38).

After attachment to the surface receptor, which occurs quite quickly, the rate-limiting step is internalization of the viral particle (37). Internalization likely occurs via endocytosis, after which the nucleocapsids are released to the cytoplasm (37, 60). Contradictory evidence can be found as to whether escape from the endosome into the cytoplasm is pH-dependent or not, suggesting that part, but not all, of the trafficking and fusion events are pH-dependent (38).

1.2.5 Nucleocapsid disassembly and nuclear import of viral DNA

After release of the nucleocapsids into the cytoplasm, the nucleocapsid undergoes a maturation step. This maturation step is caused by completion of the plus-strand of the rcDNA, which was previously only partially completed (61). The completion of the plus-strand results in release of the covalently attached Pol from the minus-strand, a structural change in the nucleocapsid and the subsequent exposure of the carboxy-terminus of the core protein (61). This region of the core protein contains a classical nuclear localization signal (NLS) signal that interacts with the nuclear transport proteins Impβ and Impα (61-63). Once at the nucleus, the intact capsids are imported through the nuclear pore complex (NPC) into the nuclear basket, where the DNA genome is released to the nucleoplasm (62).

1.2.6 cccDNA formation

cccDNA is a supercoiled DNA molecule found in the nucleus of infected hepatocytes. As the template for viral transcription, the pool of cccDNA is generated, maintained and regulated during persistent infection.

The rcDNA genome of the infecting viral particle is converted to cccDNA in the nucleus of hepatocytes. The conversion of rcDNA to cccDNA involves several steps, including (1) removal of the covalently bound Pol from the 5' end of the minus strand, (2) removal of the RNA primer on the 5' end of the plus strand, (3) removal of one copy of the short terminal redundancy (r) from the minus strand, (4) completion of the partially dsDNA plus-strand and (5) ligation of both DNA strands. The covalently bound Pol is removed from the minus-strand within the nucleocapsid in the cytoplasm, after completion of the plus-strand DNA synthesis (61). This produces the deproteinized (DP) form of rcDNA, which is subsequently released into the nucleoplasm (61, 64). Production of DP-rcDNA is the rate-limiting step during cccDNA formation (64). Pol appears to be removed by cleavage of the phosphodiester bond between the tyrosine of Pol and the 5' phosphoryl group of the minus-strand DNA (64). Little is known about the remaining steps; removal of the RNA primer, removal of the short terminal redundancy and ligation of DNA strands. However, it is presumed that host factors play a role in these processes, since cccDNA can only be formed in certain cell lines or host organs.

Viral transcripts and progeny genomes are produce after the conversion of the incoming rcDNA genome to cccDNA. The new genomes are packaged into capsids and reverse transcribed into rcDNA. Early in the infectious cycle, these genomes are trafficked back to the nucleus of the same infected cell, where the rcDNA genomes are released and converted into cccDNA, effectively increasing the pool of cccDNA (65). DHBV preS protein and the HBV surface proteins control the level of cccDNA in the nucleus (60, 64, 66). As the cccDNA pool increases in the early stages of infection, greater amounts of viral gene products

accumulate. When preS levels become high, the rcDNA genomes within capsids are enveloped and trafficked out of the cells as mature virions, therefore these genomes are not templates to increase cccDNA levels (67). The number of cccDNA particles in each hepatocyte can vary from 3 – 50 copies. It has a half-life of approximately 33 – 50 days, making it a very stable reservoir of the viral genome (33-35).

Double stranded linear (DSL) genomes can also be converted into cccDNA by intra- and intermolecular non-homologous recombination (68, 69). This is called "illegitimate replication", as compared to the conversion of rcDNA to cccDNA in "legitimate replication" (68). Illegitimate replication results in cccDNA molecules with deletions and insertions at the site of joining, as well as oligomeric linear DNA forms (68). This method of cccDNA production is inefficient and slow compared to legitimate replication, and the resulting cccDNA pool is heterogeneous, rather than the homogenous pool seen with legitimate replication (68).

cccDNA is organized into "mini-chromosomes" in the nucleus of hepatocytes. It is associated with histone proteins and forms the typical "beads-on-a-string" conformation by electron microscopy (70). There is an average of 18 ± 3 beads per cccDNA molecule (70). The histones form a classical nucleosome structure on the cccDNA, although the nucleosomal spacing is reduced by 10% compared to cellular chromatin (71, 72). This altered spacing is due to the preferential binding of the HBV core protein to the mini-chromosome (70, 72).

1.2.7 Characteristics of the viral genome

The HBV genome is approximately 3,200-base pairs (bp) long, with minor variations in length depending on the genotype. It is composed of four open reading frames (ORF), producing five major transcripts and seven protein products (Figure 1.2). The major transcripts include two at 3.5-kilobases (kb) in length and one each at 2.4-kb, 2.1-kb and 0.7-kb in length. These transcripts

encode for the three surface proteins, the core protein (HBcAg), the precore protein (HBeAg), the viral polymerase and the X protein (HBx). The genome contains four promoters and two enhancers, which coordinate to specify the relative levels of each protein and the liver specificity of viral replication. The four promoters are called the precore promoter, the preS1 promoter (SPI), the preS2 promoter (SPII) and the X promoter. The two enhancers are called Enhancer I (EnI) and Enhancer II (EnII). Within virions, the DNA genome is partially double-stranded. The minus-strand is complete across the genome and is the sense strand for transcription. The plus-strand is incomplete, and spans two thirds of the genome, with the remaining one third complete to varying degrees (37).

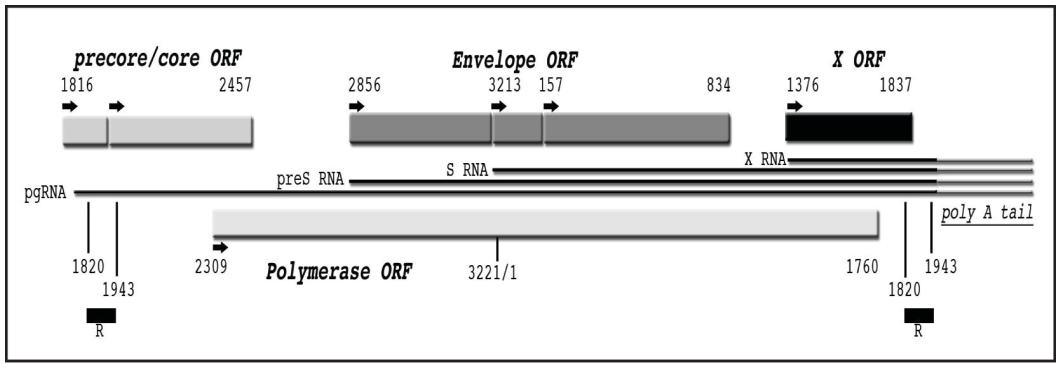

Figure 1.2 - The open reading frames and transcripts of HBV.
The HBV ORFs are shown as rectangular boxes, the translation initiation sites are shown as black arrows, and the nucleotide numbers are listed adjacent to the ORF. Numbers are relative to the defined start of the genome at a unique *EcoRI* restriction site. The five different transcripts (pgRNA & pcRNA/3.5-kb, preS/2.4-kb, S/2.1-kb and X/0.7-kb RNA) produced from the HBV genome are depicted. pgRNA contains the terminal redundancy (R) and all transcripts share a common 3' end and polyA tail. Modified from (37).

1.2.7.1 Enhancer I and X promoter

Enhancer I (EnI) is located from nt 966-1308 (73-76) and is composed of three main regions: (i) an upstream modulatory region from nt 971 – 1045 (FPVI-FPVIII), (ii) the core enhancer region from nt 1120 – 1164 (FPIII-FPV), and (iii) the basal X promoter region from nt 1168 – 1238 (FPI-FPII) (76) (Figure 1.3). The enhancer is liver-specific, causing greater amplification effects in liver cells

compared to non-liver cells (77-80). It is also one of the main drives of virus production, since EnI is required to up-regulate the production of HBcAg and virus particles (73, 78, 81). EnI can up-regulate the transcription from both the preS1 and preS2 promoters, however this was shown using re-structured vectors and not with the natural order of the HBV genome (82, 83). In studies where the endogenous structure of the HBV genome was preserved, there was little effect of EnI on the preS1 promoter (84). In addition to functioning as a typical enhancer, EnI also increased the levels of HBV products by increasing the stability of the transcripts (75).

The X promoter is closely linked to EnI, since they overlap from FPI-FPII. It is also liver-specific, and does not contain an apparent canonical TATA-box (76, 85). The entire X promoter, which spans nt 1168-1323 is required for production of X transcripts, since the basal X promoter is insufficient to support promoter activity on its own (76).

Eight protected regions within the EnI region have been identified using DNase I footprinting assays (80, 86-88). These regions are named FPI-FPVIII: other groups have used different nomenclature, which has been reconciled in Figure 1.3 (80, 86, 88-94). An additional region between FPIII and FPV has been identified and named “GB” (95, 96). The FPVI-FPVIII region constitutes the upstream modulatory region, which is not essential for enhancer activity, but increases its activity when present. In addition, the liver-specificity of the enhancer is partially conferred by this region (80). The FPIII-FPV region, which includes GB, constitutes the core enhancer region, which is capable of reproducing most of the enhancer activity (76). FPIII, in particular, is crucial for the activity of EnI, although it has no intrinsic enhancer activity itself (89). The FPI-FPII region makes up the basal X promoter, where the full X promoter overlaps with EnI. FPII is an important region of the enhancer, and has intrinsic enhancer activity when multimers of itself are strung in tandem, suggesting that recruitment of multiple binding partners is required and normally facilitated by the other FP

regions in the cognate enhancer (89). A number of different transcription factors bind to this region of the viral genome, as shown in Figure 1.3.

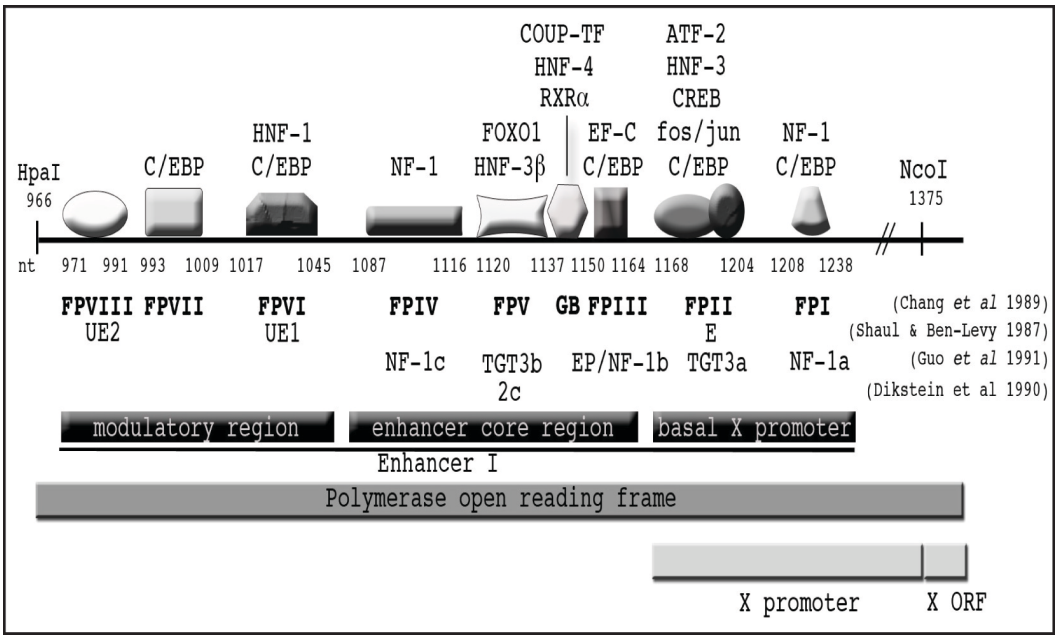

Figure 1.3 – Schematic of Enhancer I and the X promoter of HBV.
The different footprint (FP) regions in EnI and the X promoter are shown with the protein binding partners (PBP) listed above each FP region. The three sub-regions of EnI are shown as black boxes, the overlapping Pol ORF is shown as a dark grey box and the X promoter and X ORF are shown as a light grey box. The nucleotides representing the edge of each FP region are shown below the respective FP region. The different nomenclature for the FP regions is shown below each region (81, 86, 88, 89).

1.2.7.2 Androgen response elements and glucocorticoid response element

Slightly upstream of FPVIII in EnI, two androgen response elements (ARE) were identified from nt 913 to 927 (ARE-1) and nt 949 to 963 (ARE-2) (97). Ligand-stimulated androgen receptor increased the transcription of HBV in cell culture by binding the AREs (97). This effect is interesting, since androgen is found at a higher level in males and is suggested to relate to the higher rates of HCC in males (97).

An additional distinct region of regulation was found upstream of EnI, identified due to the responsiveness of HBV gene expression to corticosteroid treatments in

cell lines and patients (98). This region, termed the glucocorticoid-responsive element (GRE), is located between nt 30 – 735, with a putative binding site between nt 351 – 366. When the GRE was present upstream of EnI, transcription was increased in the presence of glucocorticoids (98). However, it is unclear whether this element can act as an enhancer on its own, although other similar "conditioned" enhancers have been identified in other viruses (98). Conditioned enhancers depend on exogenous factors for their enhancer activities.

1.2.7.3 Precore promoter and Enhancer II

The precore promoter is the strongest of the four promoters (77), from which the two 3.5-kb RNA transcripts are produced: precore RNA (pcRNA) and pgRNA. The precore promoter is located between nt 1591 to 1850 (79, 99) and can be subdivided into two main regions: (i) the basal precore promoter from nt 1744 to 1851 (includes FPV to FPVII) (100) and (ii) an upstream regulatory sequence from nt 1627 to 1732 (includes FPII-FPIV) (Figure 1.4) (101-103). Within this region, a number of proteins bind and influence the transcriptional activity of the precore promoter. Seven protein-binding sites have been mapped in this region using DNase I footprinting assays, which are named FPI – FPVII (99). Several groups have identified these same regions but used different nomenclature – the nomenclature is reconciled in Figure 1.4 (99, 100, 102, 104). The PBPs have been identified for all but one region in the precore promoter. A predominant binding partner is C/EBP, which binds twice within FPIII and once within FPV, FPVI and FPVII (99). Over-expression of C/EBP in hepatoma cell lines, but not non-liver cell lines, leads to transcription from the precore promoter (99). This indicates that C/EBP plays a role in the transcriptional regulation of this promoter, however other liver-specific factors are also important (99).

The TATA-binding protein (TBP) binds to the basal core promoter region from nt 1790 to 1804, a region called TA4 for its TA-rich nature (105). Although the precore promoter does not contain a canonical TATA-box, TA4 was found to be sufficient and essential for directing precise transcription initiation of both

pcRNA and pgRNA (105). TA4 (CATAAATT**GGTCTGC**) can be separated into two regions: (i) essential region for the transcriptional initiation of pgRNA (underlined), and (ii) region essential for correct initiation of precore message (bolded) (105).

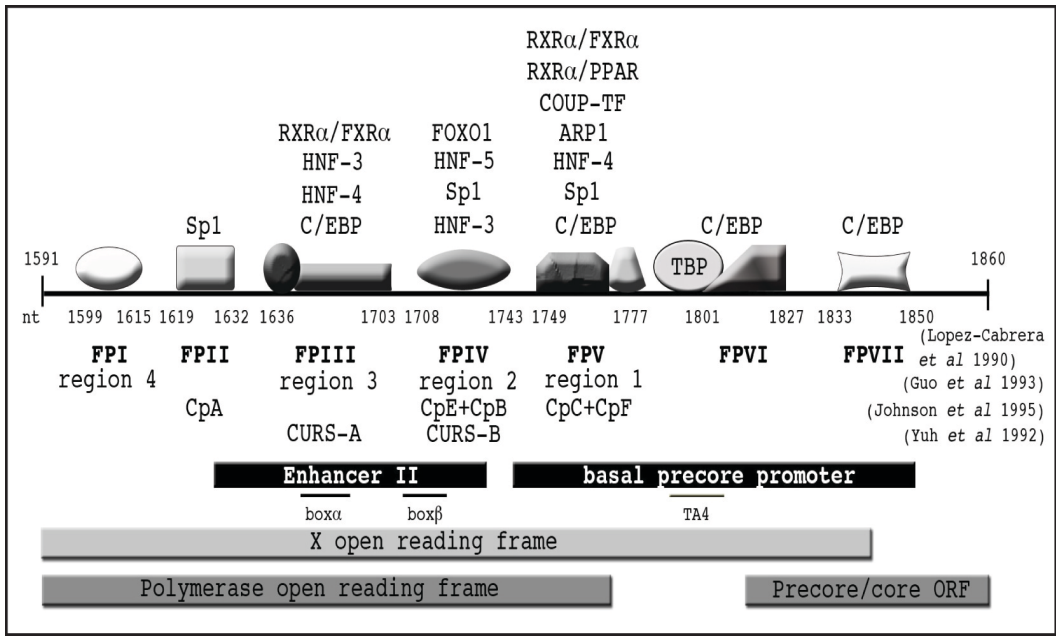

Figure 1.4 - Schematic of Enhancer II and the precore promoter of HBV.
The different FP regions in EnII and the precore promoter are shown with the PBPs listed above each FP region. EnII and the basal precore promoter are shown as labeled black boxes. The overlapping Pol ORF and the precore/core ORF are shown as labeled dark grey boxes, and the overlapping X ORF is shown as a light grey box. The nucleotides representing the edge of each FP region are shown below the respective FP region. The different nomenclature for the FP regions is shown below each region (99, 100, 102, 104).

The precore promoter, in conjunction with EnI, is responsible for the virus' tropism for liver cells (78, 79, 106). It has no activity in non-liver cell lines (78, 79, 106). There even appears to be a negative regulatory element in non-liver cells, upstream of the basal core promoter from nt 1404 – 1646 (102). This region resulted in a down-regulation of precore transcription in non-liver cells, whereas in liver cells, this effect was nonexistent (102). This suggests the liver specificity of the precore promoter is due to both the *presence* of hepatocyte-specific factors and the *absence* of non-liver repressor factors (102).

The second enhancer of the HBV genome, called Enhancer II (EnII), coincides with the precore promoter region from nt 1627-1732 (Figure 1.4) (101, 103, 107, 108). EnII completely overlaps with the upstream regulatory sequence characterized by other groups, indicating that the transactivation activity of this region on the precore promoter may be due to its properties as an enhancer (102, 103, 109). However, some data suggest this region might have a dual function, both as EnII (101, 103, 108) and as the upstream regulatory sequence of the precore promoter (100). That being said, it is difficult to separate the two functions, as they both require the same regions for their activity: box-α and box-β (100, 103, 108). The activity of EnII is limited to liver cells, and it also appears to be more sensitive to the differentiation state of cell lines compared to EnI (95, 101, 103, 110). EnII is able to up-regulate the precore, SPI and SPII promoters (95, 102, 103, 107).

EnII is composed of two main regulatory regions, called box-α and box-β (100, 102, 103, 108). Box-α is a positive regulatory element, and its cooperation with box-β makes them both indispensable and sufficient for EnII function (108). The spacing between the two elements does not appear to be crucial. Changes in the number of nucleotides between them had no effect on enhancer activity. However, their orientation relative to each other is important – reversing the direction of box-β resulted in 10-fold decreases in the EnII activity (108). Despite this, the orientation of the region containing *both* box-α and box-β is not important, indeed confirming that this region is an enhancer (101, 103).

1.2.7.4 preS1 and preS2 promoters

The preS1 promoter (SPI) is the only HBV promoter that contains the canonical TATA sequence (82, 111, 112). It controls transcription of the 2.4-kb transcript, from which the largest surface protein, preS1, is produced (81, 113). SPI spans nt 2668 – 2856 and can be subdivided into two regions: (i) the modulatory region, spanning nt 2668 – 2753 (FPI-FPIII); and (ii) the basal preS1 promoter region,

spanning nt 2754 – 2856 (FPIV-FPV) (114). Five protein-binding domains have been mapped and named FPI-FPV (Figure 1.5).

The preS2 promoter (SPII) has a divergent TATA-box (115), and shares homology with the simian virus 40 (SV40) major late promoter (82, 116, 117). The divergent TATA-box has the sequence (5'-TAAGAGA-3') and is similar to the adenovirus EIIaE1 TATA box-like region (115). SPII controls the transcription of the 2.1-kb transcript, from which both preS2 and S proteins are translated (82, 111, 113). SPII can be divided into several regions: (i) the upstream modulatory region from nt 2971 – 3055 (region A-C) (84, 117); (ii) the basal promoter from nt 3092 – 3136 (region D-E) (117); and (iii) the negative regulatory element from nt 3127 – 3150 (115, 117) (region F) (Figure 1.5). Different authors have described the same regions with different names – the nomenclature is reconciled in Figure 1.4. Region D is an essential region for SPII activity (117), and is bound by the Sp1 transcription factor (118, 119). Region E is essential for preventing the negative influence of region F, possibly by sterically hindering the binding of a negative factor to region F (117). Region G has the capacity to transcriptionally compensate for the loss of region E, suggesting redundancy in the promoter structure (117).

The binding of many different protein factors to the same region of DNA in the different HBV genome elements may indicate a transition of binding partners during the HBV replication cycle. It may also reflect differences in HBV gene expression according to different stimuli (96). As well, the presence or absence of certain factors in liver cells may explain the liver-tropism of the virus. Overall, it is the combinatorial effect of the liver-specific regions that gives HBV its liver tropism.

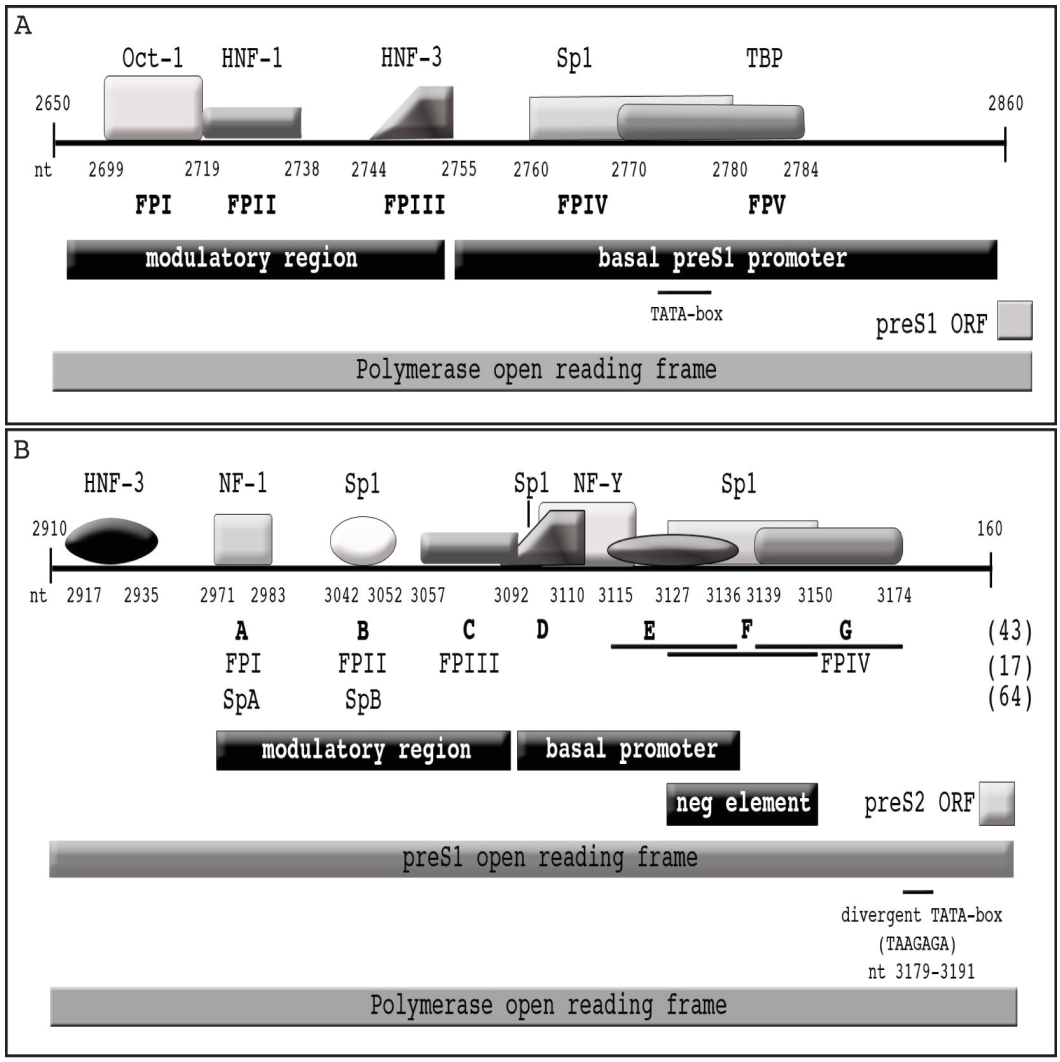

Figure 1.5 - Schematic of the preS1 and preS2 promoters of HBV.
The different FP regions in the preS1 promoter (A) and the preS2 promoter (B) are shown with the PBPs listed above each FP region. (A) The sub-regions of SPI are shown as labeled black boxes, the overlapping Pol ORF is shown as a dark grey box, and the preS1 ORF is shown as a light grey box. (B) The sub-regions of SPII are shown as labeled black boxes, the overlapping Pol ORF is shown as a dark grey box, the preS1 ORF is shown as a shaded grey box and the preS2 ORF is shown as a light grey box. The nucleotides representing the edge of each FP region are shown below the respective FP region. The different nomenclature for the FP regions is shown below each region.

1.2.7.5 DHBV Viral Genome

The DHBV genome is approximately 3021 nt in length, has three ORFs and encodes for five protein products (Figure 1.6) (120). Four major transcripts are produced: 1.95-kb, 2.1-kb and two that are 3.2-kb in length (121). These

transcripts produce the two surface proteins (S and preS), the core protein, the precore protein and the viral polymerase. A cryptic X ORF has been predicted to exist, but transcription of this gene has not been conclusively demonstrated.

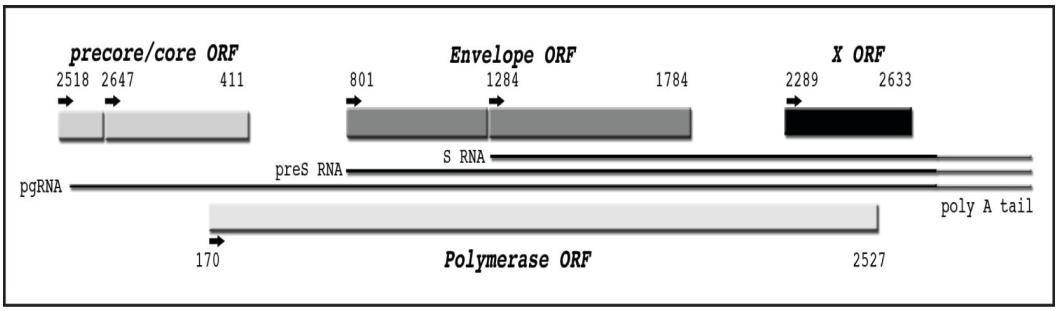

Figure 1.6 - The open reading frames and transcripts of DHBV.
The DHBV ORFs are shown as rectangular boxes, the translation initiation sites are shown as black arrows, and the nucleotide numbers are listed adjacent to the ORF. Numbers are relative to the defined start of the genome at a unique *EcoRI* restriction site. The three different transcripts (pgRNA/3.2-kb, preS/2.1-kb, and S/1.95-kb RNAs) produced from the DHBV genome are depicted. All transcripts share a common 3' end and polyA tail. A cryptic X ORF has been identified. Modified from (37).

DHBV has a single enhancer (dEnI) that can transactivate the precore/core and S promoters (122). Similarly to EnII of HBV, dEnI is located within the ORF of the polymerase gene (122, 123). dEnI spans nt 2159 to 2351 and has seven protein binding regions (122-125). These are named F1 (nt 2339 to 2350), F2 (nt 2302 to 2350), F3 (nt 2279 to 2298), F4 (nt 2255 to 2271), F5 (nt 2230 to 2250), F6 (nt 2213 to 2228) and F7 (nt 2179 to 2192) (Figure 1.7) (125). Regions F2, F3 and F7 are indispensable for proper enhancer function (126). HNF-1 is the sole factor binding at F3. This interaction is critical, since mutation of this site results in abolishment of enhancer activity (125-127). C/EBP binds at F7 and acts as a repressor, therefore it is likely that another important protein binds at this site to confer the indispensability of F7 (126, 127). HNF3 binds at F2, F4 and F6 (125, 127). Each of these sites is insufficient to independently stimulate enhancer activity (125, 127). HNF-1 appears to interfere with the binding of HNF-3 at F4, since the sites are adjacent, however this interference is not due to steric hindrance (127).

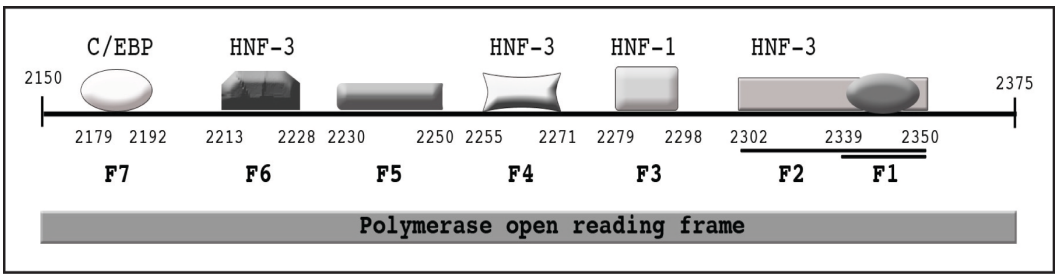

Figure 1.7 – Schematic of the Enhancer I region of DHBV.
The different FP regions in dEnI are shown with the PBPs listed above each FP region. The overlapping Pol ORF is shown as a dark grey box. The nucleotides representing the edge of each FP region are shown below the respective FP region.

The precore/core promoter consists of two main regions: the positive regulatory region from nt 2495 to 2533 and the negative regulator region from nt 2495 to 2447 (124). The preS promoter is not as cell-type specific as the S or precore/core promoters (122). The preS promoter is not up-regulated by dEnI: constructs with the preS promoter were active in the absence of dEnI, and were not further activated in the presence of dEnI (122). The minimal S promoter spans nt 720 to 1178 (128). It has an HNF-3 binding site at nt 948 to 959, just upstream of the S mRNA initiation site and within a region that is essential for promoter activity (nt 934 to 957) (128). In fact, HNF-3 over-expression releases the inhibition of S promoter activity in a non-permissive cell line (128). In contrast to the preS promoter, the S promoter is up-regulated by dEnI and appears to be dependent on dEnI for all expression (122).

1.2.8 Viral transcription

1.2.8.1 Characteristics of HBV transcripts

HBV produces five unspliced major transcripts with 5' caps and 3' polyA tails. The two largest transcripts are the nearly identically sized 3.5-kb pgRNA and pcRNA (112, 129). They both comprise the entire length of the genome plus extra sequences containing the terminal redundancy (130). pgRNA is a bicistronic mRNA for the production of the core protein and Pol, which are out of frame from each other (131). It is also packaged into progeny virions and is the template for reverse transcription into the rcDNA of infectious virus particles (130). The

pcRNA, as the template for the precore protein only, includes the 29 codons of the upstream precore sequence and is selectively excluded from virions (130). pcRNA is produced at a lower rate than pgRNA, accounting for less than one third of the 3.5-kb transcripts found in cells (132).

The 2.4-kb and the 2.1-kb transcripts code for the surface antigens (112, 129). The 2.4-kb transcript is produced from SPI and codes for the large surface antigen called 'L' or 'preS1'. The 2.1-kb transcript is produced from SPII and codes for both the major small surface antigen called 'S' and the medium surface antigen called 'M' or 'preS2' (37, 129). The 0.7-kb transcript corresponds to the X ORF and is produced from the X promoter (112, 129). All three of these smaller transcripts terminate at the same downstream location, approximately 15 nucleotides past the polyadenylation signal of HBV (112, 133, 134). Both the 2.1-kb and the 0.7-kb transcripts have heterogeneous 5' ends, as is common for promoters without TATA-boxes (112).

Spliced transcripts have been detected in tissue culture and infected human liver, however they do not appear to be required for replication *in vitro* (135-137). A 2.2-kb transcript with a polyA tail was isolated from cells expressing HBV (136, 137). This transcript contained a single splice event deleting 1,223 base pairs from nt 2448 to 488, resulting in truncation of Pol and surface proteins, and a one amino acid truncation of core (136, 137). In addition, the spliced transcript encodes for an HBV splice-generated protein (HBSP), which is expressed in infected-liver samples (138, 139). Although HBSP appears to play no direct role in HBV replication, it does appear to increase the severity of fibrosis and TNF-α secretion in chronically infected patients (138, 139). This same transcript can also undergo an alternate splicing event, where an upstream deletion of 300 nt occurs within the core ORF (140). These two splicing events do not occur simultaneously in tissue culture or liver (140). In patients, the 2.2-kb spliced transcripts can be packaged into capsids and reverse transcribed, leading to the circulation of defective virus particles, called dHBV, which may play a role in

viral persistence by acting as defective interfering particles (141, 142). A total of eleven types of spliced genomes were found in dHBV in patient serum, as a result of excision of 10 different introns and alternative usage of four splice acceptor sites and five splice donor sites (143). These sites are not all present in all genotypes (143).

Other truncated forms of HBV transcripts can be found when the HBV genome integrates into the host chromosomes, since chromosomally integrated DNA usually does not allow for full-length transcripts (144, 145). As well, hybrid viral-cellular transcripts can occur with integration (145). There is also a cryptic polyA motif (CAUAAA) within the X ORF that can be used when HBV integrates and the variant polyA signal is not accessible (146). This results in the production of truncated RNAs found in HCC and surrounding liver tissue (144-146). The appearance of truncated RNAs using the cryptic polyA motif is related to aging, with more frequent detection of truncated RNAs occurring at older ages (144, 146).

1.2.8.2 Characteristics of DHBV transcripts

The major transcripts of DHBV are the pgRNA and pcRNA (3.2-kb) transcripts and two subgenomic transcripts: the 2.1-kb transcript, encoding the preS/S RNA, and the 1.8-kb transcript, encoding the S RNA (147). DHBV also appears to have one spliced transcript of 2.1-kb in size, called spliced L RNA (148). This spliced RNA is produced by a deletion of 1.1-kb from pgRNA, between nt 2614 and 746 (148), and is hypothesized to produce the large surface antigen, L (148). Although not required for replication in transfected cells, this spliced RNA is required for productive infection *in vivo* (148).

1.2.8.3 *Cis*-transcriptional signals

There are several *cis*-elements within the HBV genome that optimize expression, stability and nuclear export of viral transcripts. All of the major HBV transcripts are unspliced and intronless, which makes them vulnerable to sequestration in the

nucleus and subsequent degradation (149). The posttranscriptional regulatory element (PRE) is a *cis*-acting element that supports the export of unspliced HBV transcripts and prevents their degradation (149-152). The PRE is a large region (nt 1239 to 1684) overlapping the untranslated region of the 2.1- and 2.4-kb transcripts and the ORFs of the X and Pol genes in the 0.7- and 3.5-kb transcripts, respectively (152-154). It can be subdivided into two main regions: HPRE-α and HPRE-β, which act interdependently for full activity (153, 154). There is one stem-loop within each of these two regions. The stem-loops are required for PRE function and are called HBV stem loop-α (HSLα; nt 1292 - 1391) and HBV stem loop-β1 (HSLβ1; nt 1410 - 1434) (154). HSLβ1 is highly conserved between HBV strains, and even with other mammalian hepadnaviruses (154). HSLα, on the other hand, has greater variation between strains, however all changes maintain the integrity of the HSLα stem loop (154). Both of these loops are further contained in a larger region of secondary structure (nt 1226 – 1444) (154). The PRE is orientation dependent and must be located within the transcript to have an effect (150, 151).

The PRE is not cell-specific and thus does not depend on viral or cell-specific *trans*-acting factors, although it does appear to have cellular protein binding partners (149, 153, 155). One of these proteins is glyceraldehyde-3-phosphate dehydrogenase (GAPDH), however the role this protein plays in the activity of the PRE is not clear (156). The PRE also binds the polypyrimidine tract binding protein (PTB), which is an RNA binding protein that plays a role in mRNA export (157). PTB binds to a pyrimidine-rich tract found between nt 1487 and 1582, and acts a positive regulatory factor (157). Mutations of the PTB-binding site resulted in decreases in activity of the PRE (157). PTB represses splicing by interfering with splice site definition (158).

The PRE appears to act similarly to a *cis*-acting element in a histone gene, which allows the intronless histone 2a mRNA to accumulate in the cytoplasm (159). The PRE enhances the level of polyadenylated subgenomic HBV transcripts, and it

increases the cytoplasmic to nuclear ratio of these transcripts (159). The PRE also inhibits the production of splicing products in a reporter model system (159). An HBV deletion mutant lacking the PRE resulted in increased amounts of pgRNA splicing, however the large region deleted in this mutant likely affected all of the HBV ORFs, therefore this effect may not be directly related to the PRE (160). In addition, the PRE appears to increase the half-life of pgRNA and is not critical for nuclear export of pgRNA (160). This contrasts to its activity in relation to the subgenomic transcripts (159, 160).

There is controversial evidence that the PRE uses the exportin 1 pathway (157, 161-164). Zang *et al* (2001) and Otero *et al* (1998) found the PRE does not utilize the exportin 1 pathway, as tested by a direct inhibitor of this pathway (157, 163). Roth and Dobbelstein (1997) used indirect techniques to conclude that the PRE uses the exportin 1 pathway, and Popa *et al* (2002) studied the model virus WHBV to conclude the same (161, 164). In addition, the WHBV PRE appears to function partially with CRM1-independent pathways, which may explain the discrepancies in the studies on human HBV (161).

1.2.8.4 Post-transcriptional modifications of HBV

Eukaryotic mRNAs are processed in several ways to ensure stability and recognition by ribosomes. This includes the addition of a 5' cap and a 3' tail. Transcription proceeds past the polyA signal, after which a precise cleavage event shortens the transcript and the addition of approximately two hundred adenosine residues by the polyA polymerase occurs (134). This event is signaled by the presence of a polyadenylation (polyA) signal of AAUAAA and a GU- or U-rich region located 10-30 nt downstream of the RNA cleavage site (134, 165). A polyadenylation factor binds to the polyA signal, followed by the binding of a cleavage factor to the GU-rich region (134).

Mammalian hepadnaviruses have a variant polyA signal sequence of UAUAAA, rather than the canonical sequence (134, 166). This variant polyA signal is

inefficient and allows approximately two-thirds of transcripts to read past the signal, facilitating the production of pgRNA species necessary for viral replication (112, 133, 167). Since the polyA signal is weak and the basal element (downstream GU- or U-rich region) is insufficient for proper site use (167), it has additional enhancer elements upstream to facilitate efficient processing of RNA transcripts (134, 165, 167). The enhancers also ensure that the proper polyA signal is processed, since pgRNA transcripts will have a copy of the polyA signal at both the 3' and 5' ends (165). The first of these enhancers is called processing signal 1 (PS1), and is located approximately at -215 to -107 upstream of the pgRNA transcriptional start site (165). Its distal nature ensures it is only transcribed at the 3' end of the transcript (165). PS1 functions to enhance the use of the polyA signal at the 3' end in an orientation- and distance-dependent manner (165). Another polyA-enhancer element is processing signal 2 (PS2), which is transcribed at both ends of pgRNA because it is located closer to the transcriptional start site (165). However, PS2 is not properly recognized at the 5' end because of its proximity to the cap site, thus it too can enhance the use of the polyA signal at the 3' end (134, 165). The presence of PS2 increases the processing efficiency of the variant polyA signal to nearly that of the canonical polyA signal (134).

1.2.8.5 Post-transcriptional modifications of DHBV

DHBV has a *cis*-acting element called *pet* (positive effector of transcription) found 3' to the transcription initiation site of pgRNA. *pet* is required to suppress premature termination of pgRNA (168). This element is position- and orientation-dependent, and is required in *cis* to promote read-through transcription of pgRNA past the transcription termination site on the first pass (168). *pet* may function through the formation of secondary structures within the transcript which may interact with a cellular protein, however this mechanism has not been proven (168).

DHBV has a second *cis*-acting element called *net* (negative effector of transcription) that is key to enhance termination of viral transcripts (169). *net* is located upstream of the preS promoter of DHBV, within the pgRNA transcript (169). It appears to work in balance with *pet*: in the absence of *pet* and the presence of *net*, pgRNA transcripts are reduced while surface transcripts increase (168, 169). However, high-molecular weight transcripts accumulate in the absence of *pet* and *net*, indicating that *net* is important for terminating transcription (169). Both *pet* and *net* appear to be functional substitutes in DHBV for HBV PS1 & PS2, although the locations within the genome and the mechanisms are different. Neither *pet* nor *net* have been found in HBV (169).

DHBV also has a single polyA signal from which all viral RNAs gain their polyA tail (147). DHBV appears to have two regions (regions A and B) found within pgRNA sequence that negatively regulate splicing and prevent excess accumulation of spliced L RNA (147). Located adjacent to the splice acceptor and donor sites, these two regions contain base pair homology and form a secondary structure that prevents splicing from occurring (147). Presumably, this mechanism prevents access of the splicing machinery to the splice acceptor and donor sites, thereby limiting splicing of DHBV transcripts (147).

1.2.9 Viral translation

The pgRNA is a bicistronic mRNA that encodes core protein and Pol. The two proteins are translated independently from each other (170). The Pol gene, found downstream of the core coding region, is not translated from pgRNA by internal ribosomal entry, but rather in a cap-dependent manner (171). Pol is translated by a scanning re-initiation mechanism, wherein ribosomes scan from the 5' end of the mRNA until the start codons are recognized (171). There are four start codons (C, C1, J, C2) in the core region upstream of the Pol start codon. Translation of the core protein is initiated at the C start codon. The other start codons play varying roles in the scanning and translation of the Pol protein. The process is predicted to occur as follows: ribosomes scan from the 5' end of pgRNA and initiate

translation from the C start codon (171). Some ribosomes will ignore this initiator codon and continue scanning toward C1, which most will ignore because it has an unfavorable Kozak context (171). The ribosomes will continue on to the J start codon, where they will translate a truncated core protein that allows the ribosomes to pass over the C2 start codon (171). C2 has a strong Kozak context, which would allow translation to be initiated and the downstream Pol start codon to be bypassed, therefore it is important for C2 to be skipped via translation from the J start codon (171). The J ORF is only seven codons in length and ends before the P start codon. After translating the J ORF, the polypeptide is released and the ribosomes continue scanning along the transcript to find the P start codon, wherein they being translating the Pol ORF (171, 172). This coordinated translation of core and Pol may indicate the requirement for coordinated production of core and Pol (171).

Unlike HBV, DHBV has thirteen start codons, called C2-C14, located between the core start codon and the Pol start codon, called C1 and P1, respectively (131). Four out of thirteen intermediate start codons are in a favorable Kozak sequence (131). This large number of favorable start codons argues against the use of leaky scanning to translate Pol, since the ribosomes would have to skip four favorable start codons and 9 unfavorable ones to reach P1 (131). In fact, mutation of each of the four favorable codons did not increase translation of Pol, suggesting they do not detract from Pol translation as ribosomes scan across them (131, 170). Instead, it appears that ribosomal shunting occurs: the ribosomes bind pgRNA at the cap and are then shunted to P1 without scanning the intervening sequences (131, 170). Once ribosomes reach the vicinity of P1, they scan normally, since mutations of P1 allow ribosomes to begin translation at downstream start codons P2 or P3 (131). Even though P1 is not an optimal start codon, the majority of ribosomes begin translation there, rather than at P2 or P3 (131). This suggests that other factors affect the translation efficiency from P1 (131). All of C2 to C14, except C10, are in frame with the P1 start codon (173). Ten stop codons also exist between C1 and P1 (S1 to S10), which terminate all upstream translation products

(173). In some DHBV strains lacking the S10 stop codon, a larger isoform of Pol, called pre-P, was produced as a result of initiation at C13 or C14 (173). This initiation also occurs through ribosomal shunting (173). The pre-P protein produced is not encapsidated and is N-glycosylated before being secreted out of cells (173).

1.2.10 Viral proteins

1.2.10.1 Core protein

The 21-kDa core protein of HBV is the unit structure for the viral nucleocapsid (174). The amino-terminal 149-residues are responsible for the spontaneous assembly of individual core proteins in the nucleocapsid structure, while the carboxy-terminal 36-residues are required for binding nucleic acids (174, 175). The carboxy-terminus contains four arginine-rich repeats (I to IV). Repeat I is responsible for RNA binding, and likely recruits pgRNA into the nucleocapsid during assembly (175). The other repeats (II to IV) are responsible for DNA binding, and likely play a role in the reverse transcription event within the nucleocapsid structure (175). The DNA binding activity of core is dependent upon the phosphorylation state of the repeats: greater levels of phosphorylation lead to the reduction of DNA binding activity (175). In HBV, three serines within SPRRR motifs are phosphorylated and crucial for the normal localization and binding activity of core protein (176). Similarly, three serines (S245, S257, S259) and a threonine (T239) were found to be the main sites of phosphorylation in the DHBV core protein (177). All four of these phosphorylation sites are adjacent to a proline residue, which was crucial for phosphorylation to occur (178). In DHBV, each of these phosphorylation sites seemed to distinctly contribute to the function of the core protein (177). Phosphorylation is generally required for the functions of immature capsids, such as minus- and plus-strand DNA synthesis, which requires phosphoserine 259 and phosphoserine 245, respectively (177). There is no requirement for phosphorylation of core protein at any sites for RNA encapsidation (177). For mature capsids, the lack of phosphorylation is generally required for virus assembly (S257 and S259) and dissociation of the nucleocapsid

from the envelope upon infection (S259) (177). It is presumed that the phosphorylation of the carboxy-terminus of the core protein results in conformational changes, which affects core protein function (177). The core protein is phosphorylated by host cell kinases, rather than a viral-encoded kinase (179). In fact, viral core particles isolated from mature virions contain protein kinase activity that is capable of phosphorylating the core protein in the particles (49, 179).

The structure of the core protein is dominated by a large alpha-helical hairpin (44). It also contains a large hydrophobic core and several other helices (44). The capsid structure starts to assemble when core monomers form dimers through interactions between these large alpha-helical hairpins (44). The dimers assemble into the full capsid, which has an inner radius of 130-Å and a thickness of 20-Å (44). The capsid has fenestrae on the two-fold and three-fold axes, which have been suggested to be essential for the entry of nucleotides during reverse transcription (44).

The carboxy-terminal region of core protein also contains two independently functioning NLS, resulting in the distribution of core protein in both the cytoplasm and the nucleus (180, 181). Phosphorylation of the core protein in the carboxy-terminus regulates its cellular distribution: more phosphorylation leads to a cellular distribution, and less leads to nuclear localization (176).

1.2.10.2 Precore protein

The precore protein, historically called HBeAg in its secreted form, is produced from a start codon 90-nt upstream of the core protein start codon on the precore RNA (182). The precore protein contains the entire core protein region, plus an additional amino-terminal sequence called the preC region (182). This region contains a 19-residue signal sequence that mediates the translocation of the precore protein into the endoplasmic reticulum (ER). The signal peptide is simultaneously cleaved off, creating the P22 precore derivative, which further

becomes glycosylated in the ER (183-185). An additional modification appears to be phosphorylation of P22 in the corresponding locations of the core protein. Proteolytic processing of P22 at the carboxy-terminus within the Golgi apparatus is the final processing step, producing P16. This step removes up to 37 residues of a strongly basic region, a step required for secretion of the 16-kDa HBeAg (182, 184, 186). The DHBV precore protein is secreted quite efficiently, whereas HBeAg appears to be poorly secreted (182). It is unclear what role HBeAg plays in the viral life cycle or pathogenesis, as it does not appear to have a biological function. The production and secretion of HBeAg is not required for persistent infection *in vivo*, but it can be detected in the liver of infected patients in both the cytoplasm and the nucleus of hepatocytes (181).

1.2.10.3 Surface proteins

HBV expresses three surface proteins: the major, small surface protein, called 'S' or 'HBsAg'; the medium surface protein, called 'M' or 'preS2'; and the large surface protein, called 'L' or 'preS1' (187). S and preS2 are both translated from the 2.1-kb subgenomic RNA transcript, while preS1 is translated from the 2.4-kb subgenomic RNA transcript. All three surface proteins share a common carboxy-terminal sequence and are glycosylated (187). preS1 and preS2 contain 163 and 55 additional amino-terminal residues, respectively, compared to the S protein (188). The preS1 protein is 39-kDa, the preS2 protein is 30-kDa and the S protein is 24-kDa in mass (189). Each surface protein is co-translationally inserted into the ER (190), where they are glycosylated or, for preS1, myristoylated. The surface proteins span the ER membrane several times, depending on the conformation of the protein. preS1 and S surface proteins are crucial for envelopment of nucleocapsids, whereas preS2 is dispensable (191). The expression levels of the three surface proteins are balanced to execute the proper viral life cycle. Over-expression of the preS1 protein results in suppression of secretion of subviral particles and mature virions (188, 189, 191).

DHBV expresses two surface proteins: the small surface protein, called 'S' and the large surface protein, called 'preS'. They are both translated from the 2.1-kb subgenomic RNA transcript. The preS protein is 36-kDa and the S protein is 17-kDa in mass (192). They have distinct amino-termini, but share a common carboxy-terminal sequence (192). The preS domain is responsible for determining the host range of DHBV - this region interacts with the viral receptor on the surface of host cells (193).

1.2.10.4 X protein

The HBV X protein, called HBx, appears to be involved in a wide-range of cellular processes. However, many conclusions about the function of HBx result from over-expression studies, which some believe masks the true functions of HBx. In general, HBx is thought to play a role in carcinogenesis during HBV infection. It has also been implicated in processes including signal transduction, cell cycle progression, protein degradation and apoptosis (194). DHBV and other avian hepadnaviruses have a cryptic HBx open reading frame, but a protein product has not been detected in the cytoplasm of hepatocytes (195).

HBx is 16.5-kDa in mass and is predominantly found within the cytoplasm adjacent to membranes. A small proportion is found within the nucleus (194, 196). HBx appears to shuttle between the nucleus and the cytoplasm through a CRM1-dependent pathway (196). It has no homology to any host proteins, but is conserved amongst mammalian hepadnaviruses (194). Structural information on HBx is lacking, because all characterization attempts using high-resolution crystallization and nuclear magnetic resonance have failed at determining a structure (196).

Expression of HBx may play a stimulatory role in HBV expression. Replicons lacking X expression have deficits in HBV replication (194). HBx also appears to be critical during *in vivo* infection, as WHBV infection of woodchucks was

abolished in HBx-mutant strains (196). However, HBx does not appear to be critical for HBV replication in transgenic mouse models of HBV (196).

HBx acts as a strong transcriptional activator for a large number of genes, including NF-κB, AP-1, AP-2, C/EBP, ATF/CREB and NF-AT (196-198). It does not directly bind DNA itself, but appears to have direct interactions with components of transcription complexes and activates cytosolic signaling pathways (196). HBx interacts with TFIIB, TFIIH and TBP (196, 199), and up-regulates AP-1-dependent transcription through the mitogen-activated protein kinase cascade (197). Additionally, HBx forms heterodimers with CREB and ATF-2 to enhance their binding to HBV EnI (200).

HBx also appears to play a role in the proteasome function in infected cells. It interacts with a number of proteasome complex components and appears to alter proteolysis functions (201, 202). For example, HBx prevents the proteasomal degradation of c-Myc, which plays a role in cell proliferation and tumor development (203). It has been suggested that the down-regulation of proteolysis in HBV infected cells contributes to the enhanced HBV replication that occurs in the presence of HBx, as less HBV products are also degraded and other factors that enhance HBV replication are maintained (194).

HBx contains a mitochondrial targeting sequence and interacts with two mitochondrial proteins - heat shock protein 60 (HSP60) and the voltage-dependent anion channel (VDAC) isoform VDAC3 (204). Over-expression of HBx results in its association with abnormally aggregated mitochondrial structures located around the periphery of the nucleus (205). This leads to an extreme decrease in the mitochondrial membrane potential, followed by cytochrome c release and apoptosis of the cell (205). Cell death can be prevented by the use of antioxidants, over-expression of the anti-apoptotic proteins Bcl-2 and Bcl-X_L, and mitochondrial permeability transition inhibitors (204). Since VDAC3 over-expression, mitochondrial dysfunction and mitochondrial

morphology alterations have been associated with chronic liver disease, these observations suggest another pathogenic feature of HBx (204).

In summary, HBx is a multi-functional viral protein that appears to play a role in many cellular functions. Clearer elucidation of the role HBx plays in the infection cycle is needed to truly appreciate the importance of this protein in the viral life cycle.

1.2.11 RNA encapsidation

The process of encapsidating pgRNA into the nucleocapsid must be selective. The epsilon sequence (Hε) at the 5' end of pgRNA is necessary and sufficient to encapsidate pgRNA (206). It does not overlap with direct repeat 1 (DR1), lying from nt 3134 to nt 36 of the genome (206, 207). Large fragments of pgRNA can be removed without affecting encapsidation (206). Pol protein is essential for pgRNA encapsidation, although none of its known enzymatic activities, such as the RT and RNase H activities, are required (208-210). Likewise, binding to Hε is required to render Pol competent for DNA synthesis (211). The conformational change that occurs upon Pol binding Hε appears to be reversible and is dependent on binding to Hε to maintain it (211).

Hε consists of a stem-loop structure composed of a lower stem, a 6-nt bulge, an upper stem with a single unpaired U residue and an apical 3-nt loop (207, 212, 213). Sequences downstream of Hε are not essential for encapsidation; however, the bulge and the loop are essential because weak encapsidation results when these regions are modified (207, 212). The sequence of the bulge can be altered and still be functional, however both the presence and the specific sequence of the loop are crucial for encapsidation (212). In addition, major sequence alterations in the stem loop impairs encapsidation (207). In the lower stem, base pairing is required but the specific sequence is flexible (212). In the lower part of the upper stem, base pairing is not required, but it is required in the rest of the upper stem (212).

Due to the terminal redundancy of pgRNA, Hε is found both at the 5' and 3' ends of the transcript, however only the 5' copy of Hε is functional for encapsidation (214). The presence of the 5' cap and the distance of Hε from the 5'-end cap structure are crucial to determine the usage of Hε for encapsidation (214). This scenario is also relevant for discriminating between pgRNA and pcRNA during encapsidation. pcRNA does not get encapsidated because of the additional 30-nt leader sequence at the 5' end, which makes the Hε too far from the 5' end for proper usage (206).

Unlike HBV, DHBV contains two regions that are essential for proper encapsidation of pgRNA. These regions contain the *cis*-sequences required for encapsidation: region I, also called epsilon (Dε) (nt 2560 - 2617) and region II (nt 551 - 719) (215, 216). Dε contains similar secondary structure to Hε, with the stem-loop structure, bulge and apical loop (217, 218). The secondary structure of Dε is critical for proper interaction with Pol and subsequent encapsidation (217). The presence of both Dε and region II are required for encapsidation, although the distance between these two regions is flexible (216). However, complete deletion of the intervening sequences or substitution of the intervening sequences with heterologous sequences abrogates encapsidation (216).

1.2.12 Nucleocapsid assembly

The core protein self-assembles into dimers and then complete capsid structures, a process that is heavily dependent on the large alpha-helical hairpin and the amino-terminal region of the core protein (174). The pgRNA and linked Pol protein are packaged inside the capsid during assembly, and the reverse transcription event occurs within the nucleocapsid, leading to the formation of mature virions.

1.2.13 Reverse transcription

1.2.13.1 Overview of reverse transcription

Reverse transcription of pgRNA by Pol occurs in the assembling nucleocapsids within the cytoplasm. Pol is covalently attached to pgRNA (58) and is packaged

into capsids with pgRNA during assembly (219). Reverse transcription proceeds similar to retroviral DNA synthesis, where a minus DNA strand is produced from an RNA template, followed by the plus strand of DNA, synthesized from the minus strand (220). Figure 1.8 gives an overview of the process.

1.2.13.2 Characteristics of the DNA polymerase

The DNA polymerase is encoded by the *pol* open reading frame and is transcribed from pgRNA (221). It is 90-kDa in mass and consists of three functional domains and a spacer region (221, 222). The three functional domains are highly conserved between avian and mammalian hepadnaviruses, whereas the spacer has no such conservation (222). The terminal protein (TP) domain is at the amino-terminus, spanning residues 1 to 179, and is unique to hepadnaviruses (222, 223). It acts as the primer protein for the minus-strand synthesis of pgRNA by forming a covalent bond between an amino-terminal tyrosine residue and a deoxyguanosine (dGMP) (223-225). A poorly conserved spacer region of approximately 180 residues adjacent to TP is presumed to function as a flexible hinge between the TP and RT domains (37). Downstream is the RT domain, from residues 336 to 679, which is responsible for the RNA-dependent and DNA-dependent DNA polymerase activities (222). Finally, at the C-terminus, the RNase H domain is found from residues 693 to 845, and is responsible for the degradation of pgRNA after the minus-strand has been synthesized (222). All of the domains must be present in *cis*, and mutations cannot be complemented by *trans* expression of any domain, therefore it is unlikely the subunits are processed into separate protein units (222).

The DHBV DNA polymerase has a similar structure to the HBV DNA polymerase, with an amino-terminal TP region, an RT region from residues 477 to 515 and an RNase H region from residues 665 to 755 (209). However, avian DNA polymerases have a 54 residue deletion in the RT domain compared to mammalian hepadnaviruses (222).

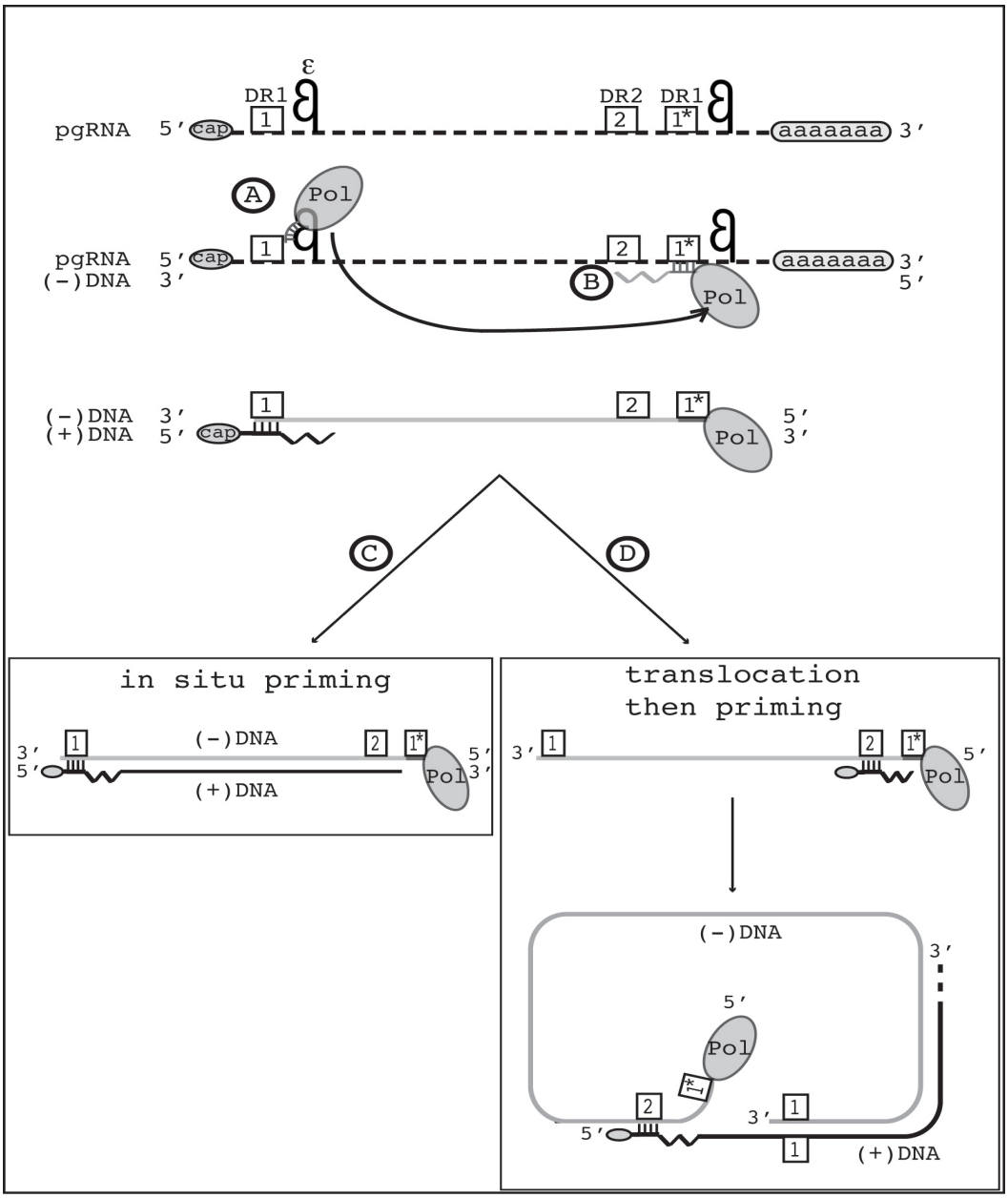

Figure 1.8 - Overview of the HBV genome replication process.

pgRNA is represented by a black dotted line, minus strand DNA by a solid grey line and plus strand DNA by a solid black line. The direct repeats (DR1, DR2 and DR1*) are shown as white boxes. (A) Pol becomes covalently linked to a dGMP complementary to the bulge region of epsilon (ε) and two to three nucleotides are synthesized using the ε bulge region as template. (B) The primer and attached Pol are translocated to DR1* at the 3' end of pgRNA and the minus strand of DNA is synthesized using pgRNA as template. During replication, the RNase H activity of Pol degrades the pgRNA template, except for an 18-19 nt RNA primer. The RNA primer maintains its 5' cap and is used to prime the plus strand of DNA. Two alternate events can occur next: (C) *In situ* priming can occur, wherein the RNA primer at DR1 is used as a template for production of the plus strand. This results in a linear genome; or (D) The RNA primer gets translocated to the DR2 site and completion of the plus strand can only occur through circularization of the genome, wherein the DR regions align to allow continuation of plus-strand synthesis.

1.2.13.3 Priming and Minus-strand synthesis

The first action for minus-strand DNA synthesis using pgRNA as template is a two-step priming event (226). In the first step, the TP domain of the DNA polymerase is covalently linked to the 5' end of the nascent minus-strand (223, 227). A phosphodiester linkage is formed between a tyrosine residue (Y65; Y96 for DHBV) near the amino-terminus of the TP domain and a dGMP that is complementary to a cytosine residue within the bulge region of ε (224, 225, 228). The second step in the priming event occurs when the dGMP is extended by two (80-90% of events) or three (10-20% of events) nucleotides to become the primer for minus-strand synthesis (226, 229). The 3' half of the bulge serves as the template for the DNA primer, while the 5' half of the bulge likely has a role in stopping primer elongation (229). Use of the bulge for initiation is ideal, since it is one of the few regions within ε that obviates the need for melting double-stranded structures (229).

The following steps in minus- and plus-strand synthesis involve the transfer of strands during synthesis. These transfer steps are dependent on the direct repeats DR1 and DR2 (10 to 12 nt), which are found within pgRNA and help to coordinate the minus- and plus-strand synthesis reactions from pgRNA (230). pgRNA contains terminal redundancy of DR1, while DR2 exists at the 3' end only (230). DR1 and DR2 are identical to each other in all sequenced clones of hepadnaviruses (120, 231).

After synthesis of the primer, it is translocated to the 3' DR1 site (DR1*), wherein the remainder of the minus-strand is synthesized (226, 232). The short length of the primer facilitates the release and transfer of the primer to DR1, however the short length is also a limitation in directing site-specific transfer, as there are a number of complementary sequences within pgRNA aside from that found within DR1 (229). Hence, there appear to be *cis*-acting elements outside of DR1 that account for the transfer to that site (233, 234). Further, it is likely that ε and DR1* are brought within close proximity by circularization of pgRNA (229, 235). Pol

remains covalently linked to the 5' end of the minus-strand for the duration of the replication process (227).

DNA synthesis ends by reaching the end of the template, resulting in an RNA-DNA hybrid (230). The protein primer remains attached to the 5' end of the minus-strand (230) until the relaxed circular DNA is converted to cccDNA within the nucleus of an infected cell. During synthesis of the minus-strand, the RNase H activity of the DNA Pol degrades the pgRNA template (236).

1.2.13.4 Plus-strand synthesis and circularization of the genome

Plus-strand synthesis is primed by an oligoribonucleotide of 18 – 19 nt in length, derived from the terminal bases of the pgRNA template (237). This RNA primer is produced by RNase H cleavage near the 5' DR1 of pgRNA (238). The cleavage event is not based upon any particular sequence at this region, but rather by the distance from the 5' end of pgRNA (238). After cleavage, the RNA primer can be translocated to the DR2 site (230, 237, 239). The translocation is dependent on sequences inside of and adjacent to DR1 (239). The cleavage and translocation events can be separated from each other, indicating that they are independent (239).

The RNA primer maintains the 5' cap of pgRNA, which is subsequently associated with the plus-strand (227). The primer also remains attached to the 5' end of the plus-strand (230) until conversion to cccDNA within the nucleus of an infected cell. Two types of mature genomes can be completed depending on whether the RNA primer remains at DR1 or is translocated to DR2. If the RNA primer translocates to DR2, the genome must circularize in order for the plus-strand to be completed (Figure 1.8) (230, 237, 239). Cohesive ends of approximately 310-nt in size allow for this circularization event, which results in mature viral rcDNA (56). If the RNA primer does not translocate to DR2, called *in situ* priming, the plus-strand will be synthesized linearly and a double-stranded linear genome will be formed (239). Small amounts of duplex linear genomes can

be found in virus particles (239). There is a key region, called Region 3E, is required for the circularization of the viral genome (240). This region is located near the 3' end of the minus strand, but is distinct from DR1 (240).

The plus-strand is only completed up to 15 – 50% of full length, resulting in heterologous 3' ends of the plus-strand (39, 55-57). Both space constraints and limitations in access to substrates are suggested to account for the lack of completion of the plus-strand. In the presences of excess nucleotides *in vitro*, Pol is capable of synthesizing complete plus-strands (37). However, limitation of substrates is not solely responsible, since space within the nucleocapsid has also been shown to limit the size of the genomes (37). Up to 10% larger genomes were tolerated for packaging into DHBV capsids (209). Once the plus-strand is as complete as possible given the space and reagents available within the nucleocapsid, the virion is mature and ready for exit from the host cell.

1.2.14 Nucleocapsid envelopment and virion release

Virion envelopment is linked to the state of genome maturation, since only 4% of extracellular virions have immature minus-strand DNA (241). Also, virions lacking mature genomes appear at a higher frequency in the cytoplasm of cells (241). DNA synthesis is required for envelopment and secretion, as it appears nucleocapsids gain the ability to interact with the amino-terminal domain of preS1 after DNA synthesis due to a conformational change in the core protein (37). The complete nucleocapsids gain their envelope by budding into the ER membrane containing the three surface proteins (191). The virions exit the cell via the constitutive pathway of vesicular transport (191).

1.3 Zinc finger proteins

The zinc finger protein (ZFP) family includes a large range of proteins that use zinc coordination to stabilize secondary structure. These proteins have multiple cysteine and/or histidine residues that anchor zinc ions within the structure of the protein. The founding members of this group are the Cys_2His_2 ZFPs, which are

commonly found in eukaryotic organisms and often function as transcription factors.

Cys_2His_2 ZFPs are DNA binding proteins that can also interact with RNA and other proteins (242). They are best known for their ability to bind specific DNA sequences with high affinity and have been used in protein therapeutic strategies in a variety of ways, as discussed below. The modular nature of the ZFPs allows them to be coupled to other functional domains, such as activation or repression domains to regulate transcription at the gene level. It is also apparent that ZFPs can control gene expression at the RNA level, as a few ZFPs bind RNAs (242). Additionally, ZFPs can form interactions with other proteins while coordinating with other transcription factors during gene regulation (242).

1.3.1 Structure of zinc finger proteins

ZFPs consist of tandem copies of zinc finger motifs. Zinc finger motifs are approximately 30 amino acids in length and contain two anti-parallel β–sheets and one α–helix. These structures are coordinated by a single zinc ion and form a ββα fold (242). In Cys_2His_2 zinc fingers, two cysteines and two histidines coordinate the zinc ion. The two cysteines are within one of the β–sheets and the two histidines are at the C-terminus of the α–helix (242). The consensus sequence for the zinc finger motif is (F/Y)-X-C-X_{2-5}-C-X_3-(F/Y)-X_5-ψ-X_2-H-X_{3-5}-H, where X represents any amino acid and ψ is a hydrophobic residue (242). This consensus demonstrates that there are very few conserved residues in the zinc finger motif. In general, the β–sheets play a role in the structure of the protein and stabilization of the DNA-protein interaction, whereas the α–helix is responsible for the site-specific recognition of the DNA target site.

ZFPs bind to DNA in an “anti-parallel” formation, such that the amino-terminus of the α-helix interacts with the 3’ end of the DNA subsite. The α–helix, which determines the DNA specificity, lies within the major groove of the DNA and forms hydrogen bonds with the DNA base pairs through its amino-terminal

residues. Each of the tandem zinc finger motifs of one ZFP lies within the major groove of the DNA, forming the protein into a "C" shape as it wraps around the DNA (Figure 1.9). This causes the conformation of the DNA to change to $B_{enlarged\ groove}$ DNA, which has a wider and deeper major groove due to a slight unwinding of the DNA and a shift of the base pairs from the helical axis (243). The DNA unwinds so that the average base pairs per turn is 11.4 rather than the standard 11.1, and the average displacement of the base pairs from the helical axis is 1.6 – 1.8 Å (243). As a result of this, the minor groove is subsequently compressed compared to B DNA (244).

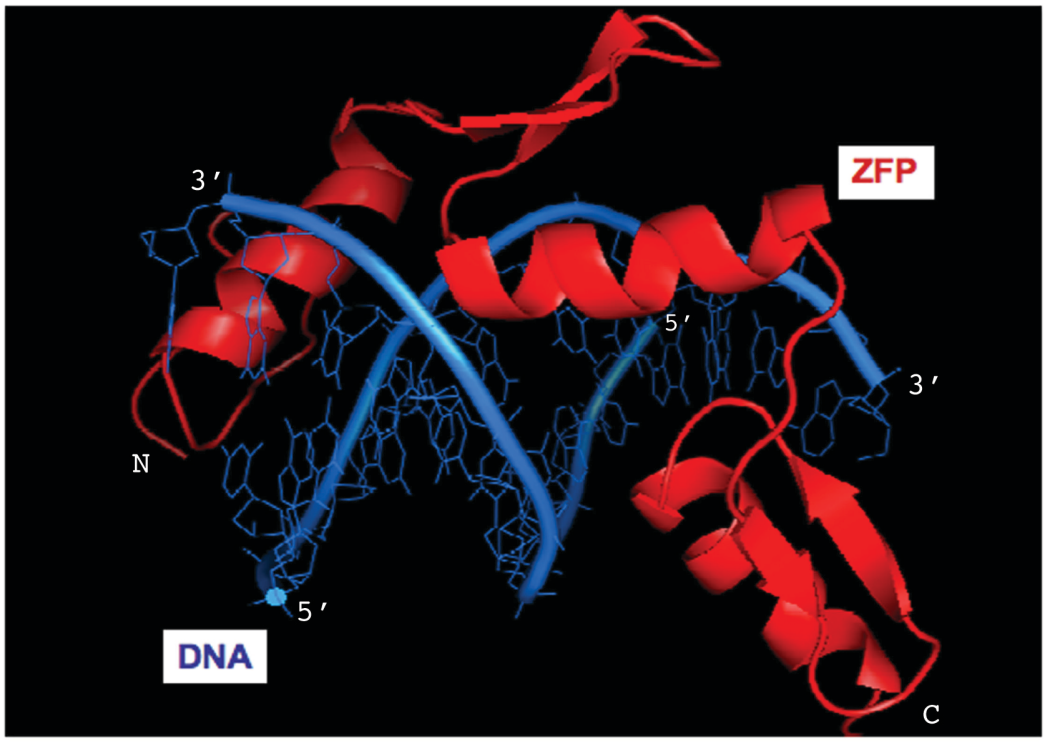

Figure 1.9 – Structure of the prototypic ZFP Zif268 bound to DNA.
Zif268 (red) lays in the major groove of the DNA (blue). The α-helix and β-sheets can be seen in the structure of Zif268, which consists of three zinc finger motifs. The 5' and 3' ends of each DNA strand are indicated, as well as the amino (N) and carboxyl (C) termini of Zif268.

The key amino acids of the α-helix are at positions -1, 2, 3, and 6. These residues lie within the major groove and form the majority of the interactions with the primary strand of the DNA subsite (244). Hydrogen bonds are formed between

the amino acid side chains of the α-helix and the DNA nucleotides, sometimes with a water molecule as an intermediate (243). Some interactions can also occur with the "secondary" strand of the DNA subsite, usually between the α-helix and the nucleotide found one base pair down from the DNA subsite (243). This results in interactions between the α-helix of one zinc finger motif and a base pair in the adjacent subsite. A schematic summary of the hydrogen bonding interactions between a prototypic ZFP called Zif268 and its DNA target site is shown in Figure 1.10.

A number of other interactions stabilize the DNA-protein complex. Hydrogen bonds form between the α-helix and the phosphodiester backbone of the DNA (245). Even though the two β-sheets play no role in DNA recognition, they can also interact with the phosphodiester backbone to increase the stability of ZFP binding (245). Furthermore, inter- and intra-finger interactions can occur when the ZFP is bound to DNA. Inter-finger interactions can stabilize the orientation of side chains within the major groove, helping to organize the protein-DNA interface at the zinc finger junctions within the ZFP (244). Intra-finger interactions appear to stabilize the protein-DNA interface during DNA recognition (244).

The linker region connecting zinc finger motifs is important for the proper spacing of the zinc finger motifs within the major groove. It allows each zinc finger motif to be properly lined up relative to its target DNA site. The consensus sequence for the linker is TGEKP, which is flexible in the free protein, but becomes rigid when bound to DNA (242, 246). A schematic of the ZFP substructure is shown in Figure 1.11, and indicates the location of the linker between the zinc finger motifs.

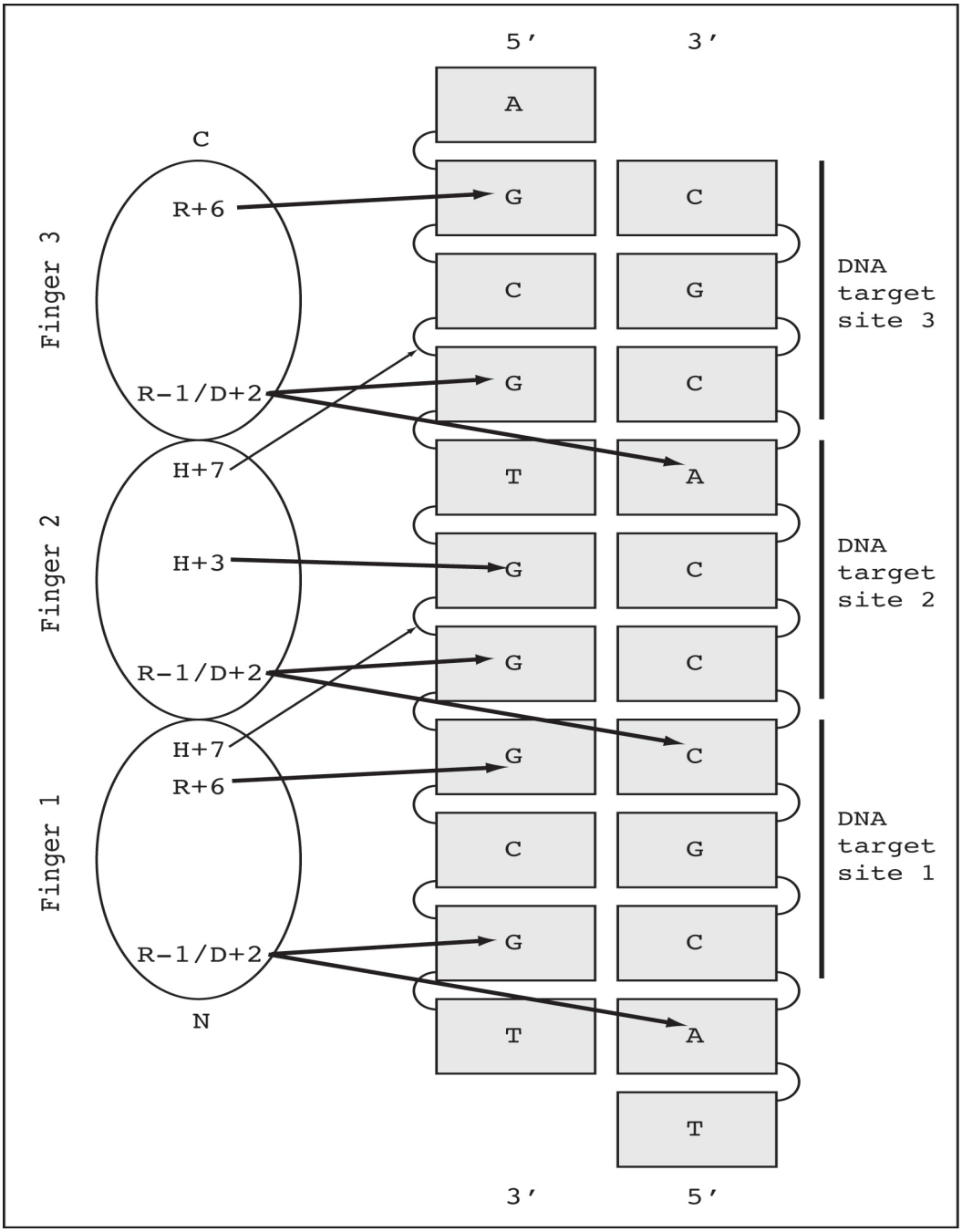

Figure 1.10 - Schematic of the key contacts between Zif268 and its target DNA sequence.

The three fingers of Zif268 are shown as ovals (Finger 1, 2, 3). The nucleotides of the DNA are shown as rectangles and the phosphodiester linkages are shown as curved lines connecting the nucleotides. DNA site specific hydrogen bonds between Zif268 and the DNA are represented by thick arrows and stabilizing hydrogen bonds between Zif268 and the phosphodiester backbone are shown as thin arrows. The interacting amino acids and their position in the α-helix are shown within each finger. Modified from (246).

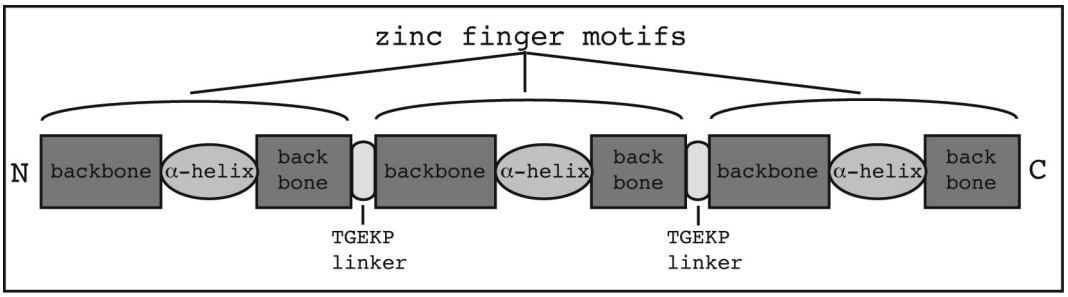

Figure 1.11 - Schematic representation of the substructure of a ZFP.
The substructure of a ZFP containing three zinc finger motifs is shown. The backbone regions are dark grey squares. The α-helices, which makes site-specific contact with the DNA target sequence, are grey ovals. Each zinc finger motif contains one α-helix flanked by two backbone regions. The motifs are joined by a linker composed of five amino acids (TGEKP), shown as light grey ovals. The amino (N) and carboxyl (C) termini are indicated.

1.3.2 Design of zinc finger proteins

There are a number of methods available to design zinc finger proteins to bind specific target sequences. Much research has been performed in recent years to develop a "recognition code", which describes the amino acid sequence of the α-helix in relation to the DNA target site. Although there does appear to be a one-to-one binding scenario for an amino acid within the α-helix and the base pair within its DNA target site, there is greater complexity to the interactions between the ZFP and the DNA.

The simplest method to design ZFPs is using the Zinc Finger Tools program, which is an online database that compiles a "recognition code" developed by Dr. Carlos Barbas III (247-250). This method employs modular assembly of zinc finger motifs. It uses the framework of the Sp1C ZFP as the backbone of the protein, while the N-terminal portion of the α-helix is variable for DNA recognition (251). This consists of an N-terminal backbone (YKCPECGKSFS) that contains the two β–sheets (underlined) and a C-terminal backbone that contains the C-terminal portion of the α-helix (HQRTH) (251). It also contains two terminal backbones at the N-terminus (LEPGEKP) and the C-terminus (TGKKTS) (251). After inputting the target DNA sequence, the readout is a sequence file for synthesizing a functional ZFP.

Other methods are more complicated and involve screening large libraries of possible zinc finger motifs against target DNA sequences. Phage display utilizes a library of ZFPs where the key recognition amino acids are varied. This library is displayed on the surface of phages and then mixed with the target DNA sequence. Those that bind the target DNA sequence are selected over several rounds and purified (252). ZFPs designed with this process are better able to take into account interactions between zinc finger motifs and adjacent DNA subsites. They generally have good specificity for their target sequence, but high-throughput application of this method is impractical.

A bi-partite method is available that is based upon phage-display libraries (253). This method allows selection of a 9-mer ZFP (recognizing a total of 9-bps) in two steps. Half of the 9-mer is varied in each of the two constructed libraries. Each half is selected to recognize 5-bps of DNA, and when the two halves are selected and identified, they are combined into one whole ZFP that recognizes the entire 9-bps of DNA (253). This method is rapid and convenient, and has been demonstrated to produce ZFPs with dissociation constants in the nanomolar range (253).

Yeast one- or two-hybrid, or bacterial two-hybrid selection systems are other methods for screening for ZFPs. Based upon the principles of standard two-hybrid techniques, the DNA binding activity of ZFPs is coupled to the recruitment of an RNA polymerase, leading to transcription of gene products that can be used as selection markers. The bacterial two-hybrid system may be superior compared to the yeast option, because it offers the ability to analyze larger libraries, has a faster growth rate, does not require an NLS on the proteins of interest and can be used with proteins that are toxic in yeast cells (254).

A domain shuffling approach is based upon the bacterial two-hybrid system, where each zinc finger of a ZFP 9-mer is altered independently within a synthetic ZFP framework. After screening three libraries, each with one of the three zinc

finger motifs as the variable region, the selected pools of ZFPs are randomly recombined and screened a final time against the entire DNA target site (255). The benefits of this approach are that it allows the use of very large libraries for selection and does not sacrifice combinatorial diversity; that is, it takes into account inter-finger interactions. However, the protocol is not as quick to implement as several other strategies.

In general, strategies to design ZFP by screening large libraries offer the best chance for identifying high affinity ZFPs. However, they have limitations due to the time required to perform the screens and the size of the libraries that can be functionally screened. Strategies that reduce the selection time generally reduce the design to a more modular viewpoint, which can ignore the inter-finger interactions and the connections between zinc finger motifs and adjacent DNA subsites. Nonetheless, high affinity ZFPs have been designed using "quick" methods, suggesting future improvements to the modular design strategy could make it even more functional.

1.3.3 Zinc finger proteins as antiviral therapeutics

ZFPs have been used as novel protein therapeutics in a number of viral systems. In some cases, ZFPs have been used to specifically bind to viral genomes and prevent the access of transcriptional machinery, effectively shutting down viral replication (256-259). In other cases, ZFPs have been fused to repressor domains to down-regulate viral transcription (260-262).

ZFPs have been used to inhibit the transcription of several plant and human viral pathogens. The beet severe curly top virus (BSCTV) is a dsDNA virus that causes severe disease in a wide range of host plants. BSCTV encodes a viral replication protein called Rep that is required for viral DNA replication. Rep binds to direct repeats within the viral origin and initiates DNA replication. ZFPs designed to occupy the Rep binding sites were expressed in *Arabidopsis thaliana* prior to infection with BSCTV (258). Plants expressing the ZFPs showed clear resistance

to BSCTV infection: 84% of transgenic *A. thaliana* showed no symptoms after exposure to BSCTV (258). The tomato yellow leaf curl virus (TYLCV) is another agriculturally relevant dsDNA virus. It causes severe disease in tomato plants, which affects a large agricultural field and currently has no treatment options for prevention of disease. ZFPs were designed to bind to the Rep binding site in the viral origin, to prevent the binding of the Rep protein and initiation of DNA replication (257). The designed ZFPs are currently being tested in *A. thaliana* as was done for BSCTV, with the anticipation of similar results (256).

Human papillomaviruses (HPV) are dsDNA viruses that cause benign lesions and cervical cancer (259). Similar to the plant viruses targeted above, HPV viruses encode two viral proteins, E1 and E2, which are required for DNA replication. E2 binds to the viral origin and recruits E1 to bind, resulting in the initiation of DNA replication (259). HPV type 18 (HPV-18) was targeted by two designed ZFPs to inhibit viral replication. The ZFPs were designed to have a higher affinity for the viral origin than E2, effectively preventing E2 from binding and blocking DNA replication initiation (259). HPV replication was reduced by almost 90% in the presence of the designed ZFPs, which was directly attributed to the ability of the ZFPs to inhibit the binding of E2 to the viral origin (259). Building on this work, a cell-penetrating peptide was fused to the designed ZFPs. The cell-penetrating peptide consisted of residues 47 – 57 of the human immunodeficiency virus 1 (HIV-1) Tat protein. The resulting cell-permeable protein was purified in *E.coli* and added to the media of tissue culture cells. In this context, the designed ZFPs were shown to enter cells and inhibit HPV replication without any toxic side effects (263).

ZFPs have also been fused to repressor domains to form ZFP transcription factors (ZFP-TF). Reynolds *et al* (2003), Segal *et al* (2004), and Eberhardy *et al* (2006) have designed ZFPs to target HIV-1, and fused the ZFPs to the Krüppel-associated box (KRAB) repressor domain from the KOX1 protein (260-262). The ZFPs were targeted to bind the HIV-1 5' long terminal repeat (LTR) promoter of

the integrated proviral form. The provirus becomes reactivated in infected T cells after their exposure to antigen or mitogen, which results in the nuclear translocation of NF-κB. Reynolds *et al* (2003) designed ZFP-TFs to bind upstream of the NF-κB binding sites (260). Repression by the ZFP-TF was sufficient to inhibit transcription from the LTR in unstimulated and stimulated T cells, and inhibited viral replication by up to 75% compared to controls (260). Segal *et al* (2004) designed ZFP-TFs to overlap the Sp1 binding sites located downstream of the NF-κB binding sites in the 5' LTR. These designed ZFP-TFs potently inhibited HIV-1 transcription 10- to 100-fold, without significant toxicity effects (261). Finally, Eberhardy *et al* (2006) redesigned ZFP-TFs to bind the primer-binding site (PBS) in the 5' LTR, which is identical in all identified HIV-1 subtypes. HIV-1 replication was inhibited greater than 90% using the designed ZFP-TFs. This approach has therapeutic applicability across many subtypes due to the conservation of the PBS sequence (262).

These examples demonstrate the feasibility of using ZFPs as antiviral therapeutics, whether they occlude the binding of proteins from the viral genome that are essential for viral replication, or if they act as transcriptional repressors to inhibit transcription and replication.

1.3.4 Zinc finger nucleases

The function of ZFPs as therapeutics has been optimized by the attachment of functional domains to their DNA binding specificity. The most common approach is to attach a nuclease domain, producing chimeric zinc finger nucleases (ZFN) that target dsDNA breaks to a particular site. ZFNs have been used to initiate site-directed homologous recombination events (264-267), and to edit or disrupt host gene function (268-270). Recently, ZFNs have also been used to target and cleave the cccDNA of HBV (271), which was an original goal of the work described in this thesis.

The endonuclease domain from the restriction enzyme *FokI*, produced by the bacterium *Flavobacterium okeanokoites* (also known as *Planobacterium okeanokoites*), is the most commonly used domain ZFN design. The *FokI* restriction endonuclease is a type IIS restriction enzyme that functions as a homodimer to mediate dsDNA breaks outside of the DNA binding site (272-274). The endonuclease domain of *FokI* has non-specific DNA cleavage activity and is easily uncoupled from its DNA binding domain, as the two regions function independently of each other. These properties allow the endonuclease domain of *FokI* to be re-coupled to another DNA binding domain, such as ZFPs, to form ZFN. In contrast to the *FokI* restriction enzyme, which only requires one monomer to be bound to the DNA for cleavage, *FokI*-based ZFNs require two inverted DNA binding sites separated by 6 – 18 bps of DNA (265, 273). Between the two binding sites, sticky-ended dsDNA breaks will occur when two *FokI* domains homodimerize (273). Generally, two ZFPs that each bind 9-bps of DNA are utilized as the DNA binding domains in ZFNs. This results in a heterodimer that recognizes a total of 18-bps of DNA, which is a statistically unique sequence within a mammalian genome.

A few other nuclease domains have been used in conjunction with ZFPs to form ZFNs. These include the *Saccharomyces cerevisiae* endonuclease Ho and the staphylococcal nuclease SNase. Ho is a member of the LAGLIDADG homing endonucleases and initiates a mating-type switch by making site-specific dsDNA breaks in the *MAT* gene (275). The last 120 residues of Ho encode an endogenous ZFP, which is easily replaced with a designed ZFP (276). Nahon and Raveh (1998) replaced the ZFP domain of Ho with the Swi5 ZFP domain, which is a yeast transcription factor, and were able to confer new site specificity for the DNA cleavage activity of Ho (276). The Swi5-Ho endonuclease was capable of cleaving a substrate plasmid when expressed in bacterial cells (276). The SNase approach was developed by Mineta *et al* (2008) to distinguish between the target DNA substrates and the cleavage products by sandwiching the SNase between two ZFPs (277). This approach utilizes two ZFPs that bind 9-bps of DNA on the

same strand, separated by the SNase domain between them. The entire complex only binds substrate DNA because the cleavage products do not contain the DNA target sites in close proximity (277). Mineta *et al* were able to demonstrate site-specific cleavage with greater efficiency than *FokI*-based ZFNs (278). The SNase-based ZFNs were able to cleave up to 2000-fold excess of target, demonstrating discrimination between substrates and products, and multiple turnover cleavage of target DNA (278).

Many groups have successfully used ZFNs as therapeutics in different model systems. In order to increase cell survival during biopharmaceutical and vaccine production processes, Cost *et al* (2010) demonstrated ZFN-mediated gene disruption of *BAX* and *BAK* could allow Chinese hamster ovary (CHO) cells to be resistant to apoptosis (268). These CHO cells were tested in scaled-down systems approximating large-scale bioreactors. The *BAX*- and *BAK*-deleted CHO cells were significantly more resistant to the apoptotic stimuli these conditions create, suggesting this approach could be useful for large-scale industrial protein production (268). Urnov *et al* (2005) and Lombardo *et al* (2007) used designed ZFNs to replace the deficient IL-2 receptor gene that causes X-linked severe combined immune deficiency (264, 269). After site-specific cleavage at the defective IL-2 receptor gene by the designed ZFNs, a wild-type version of the IL-2 receptor gene was inserted by homologous recombination (264, 269). Urnov *et al* (2005) achieved more than 18% gene-modified cells without selection, and Lombardo *et al* (2007) attained 13-39% of cells with an edited IL-2 receptor gene using integrase-defective lentiviral vectors to deliver the ZFNs (264, 269).

A similar approach was used by Shukla *et al* (2009) and Townsend *et al* (2009) for the crop species *Zea mays* (corn) and the tobacco plant, except that herbicide-resistant mutations were introduced into target genes associated with metabolism (266, 267). Shukla *et al* (2009) inserted the genes for resistance to two herbicides, bialaphos or quizalofop, into the inositol-1,3,4,5,6-pentakisphosphate 2-kinase (*IPK1*) gene. *IPK1* is an attractive target because it catalyzes the final step in

phytate biosynthesis. Phytate accounts for 75% of total seed phosphorus, which is a non-nutritional component of the seeds. Herbicide resistance occurred in 50 – 100% of treated plants, depending on the ZFN pairs used (266). Townsend *et al* (2009) likewise conferred herbicide-resistance in tobacco plants by inserting mutant strains of the acetolactate synthase gene, called *SuR*. Site-directed cleavage by designed ZFNs, followed by homologous recombination with the mutant *SuR* genes, resulted in up to 4% of plants with resistance to the herbicides chlorsulphuron and imazaquin (267).

Minczuk *et al* (2008) utilized ZFNs to target and selectively degrade mutated copies of mitochondrial DNA (mtDNA) (279). Over 100 point mutations and large rearrangements in human mtDNA have been associated with disease, ranging from progressive muscle weakness to fatal infant diseases (279). Minczuk *et al* designed ZFNs to target the m.8993T>G mutation, which causes two different mitochondrial diseases. The designed ZFNs could discriminated between wild-type and mutant mtDNA that differed by that one base-pair over a 12-bp long sequence. In cells containing 90% mutant mtDNA, expression of the ZFNs resulted in enrichment of wt mtDNA due to depletion of the mutant mtDNA. ZFN-treated cells had 40% wt mtDNA compared to 5-20% in control cells (279).

Two groups have utilized ZFNs as antiviral therapeutics. Perez *et al* (2008) altered the ability of HIV-1 to infect its target cells by designing ZFNs to disrupt CCR5 alleles in $CD4^+$ T cells (270). This resulted in robust, stable and heritable protection from HIV-1 infection, both in tissue culture and in a mouse model (270). Additionally, Cradick *et al* (2010) recently published using ZFNs to cleave the DNA genome of HBV. Cradick *et al* targeted a region within the core ORF and demonstrated 26% of a target plasmid was cleaved by ZFN in cell culture. The ZFNs also effected a 29% decrease in pgRNA in Huh7 cells transfected with an HBV-expression plasmid (271).

1.3.5 Zinc finger proteins and disease models

ZFPs have been used in a number of other disease model systems, mainly as transcription factors to repress or up-regulate endogenous expression levels of different transcripts.

ZFP-TFs were used to regulate the expression level of human vascular endothelial growth factor A (VEGF-A) (280-284). VEGF-A induces the growth of new blood vessels during embryogenesis and adult wound healing. It plays a key role in vasculogenesis and angiogenesis, and its dysregulation is related to tumor growth, diabetic retinopathy and ischemic heart and limb disease (280). Since the proper function of VEGF-A seems to depend upon the relative levels of its major splice variants, ZFP-TFs are a good approach because they can up-regulate transcription of the gene without affecting the post-transcriptional splicing processes (280).

ZFP-TFs were designed to target the accessible regions of the VEGF-A locus, and were linked to either the VP16 transcriptional activation domain or the activation domain from p65 (280). ZFP-TFs with either activation domain demonstrated a marked ability to up-regulate the transcription of VEGF-A in tissue culture cells, and were able to up-regulate each major splice variant of VEGF-A proportionally (280). The VP16-based ZFP-TFs were tested in a mouse model of angiogenesis using adenovirus vectors, which demonstrated increased angiogenesis and wound healing in the ears of mice (281). Additionally, the vasculature of the ZFP-TF-treated mice was not hyperpermeable, as was found when mice were treated with murine VEGF-A cDNA. This further suggested that the up-regulation of VEGF-A by ZFP-TFs is better at approximating the natural levels of VEGF-A splice variants (281). The ZFP-TFs were also assessed in a second mouse model looking at hind-limb ischemia in age-advanced mice (283). After adenovirus-mediated delivery of the ZFP-TFs, mice experienced greater blood flow, limb salvage and vascularization after surgically induced damage (283). Hind-limb ischemia in rabbits was also treated with VEGF-A-specific ZFP-TFs (284). ZFP-TF-treated rabbits again demonstrated greater capillary density, higher levels of all key

VEGF-A splice variants and greater blood flow into damaged limbs, compared to untreated animals (284). All of these studies suggest that ZFP-TFs are an effective therapeutic option to up-regulate the proper splice variants of VEGF-A to ablate disease symptoms and stimulate vascularization in wound healing.

VEGF-A was also targeted for repression during tumour proliferation. Constitutive high-level expression of VEGF-A can be detected in some human cancers. ZFPs targeting the VEGF-A locus were fused to the repression domain from the thyroid receptor α ErbA, or its viral relative, vErbA (282). Using a glioblastoma cell line, the ZFP-TFs were able to reduce the VEGF-A levels by 20-fold, a level that approximates the level in a nonangiogenic cancer line (282).

ZFP-TFs have also been used in several other approaches to cancer therapeutics. Beerli *et al* (1998) and Lund *et al* (2005) have used ZFP-TFs to target the promoter of the proto-oncogenes *erbB-2/HER-2* and *erbB-3/HER-3* (285, 286). The overexpression of ErbB receptors is associated with cancers in the breast, head and neck, kidney, prostrate, colon, pancreas, bladder, lung and ovaries (286). Beerli *et al* (1998) fused ZFPs to the KRAB repressor domain, the ERF repressor domain or the mSIN3 interaction domain (SID), then assessed their ability to repress the transcription from an *erbB-2* promoter using a luciferase assay (285). The KRAB-fused ZFP was capable of completely repressing the *erbB-2* promoter and the other repressor domains exhibited varying degrees of repression (285). Lund *et al* (2005) designed KRAB-based ZFP-TFs capable of regulating *erbB-3* and *ICAM-1* or *erbB-2* and *erbB-3*. Stable expression of the ZFP-TFs after retroviral transduction and integration resulted in 68-79% of cells having a 10-fold reduction in ErbB2 and ErbB3 levels. As well, cells exhibited decreased migration on collagen and decreased ERK1/2 phosphorylation when ErbB2 was repressed (286).

ZFP-TFs fused to the KRAB repressor domain have been designed to down-regulate the epithelial glycoprotein-2 (EGP-2) promoter, which has limited

expression in normal tissues and is up-regulated in ovarian, prostate, colon and breast cancers (287). The ZFP-TFs repressed expression of EGP-2 in human ovarian cancer and human colon cancer cell lines by 50-60% (287). Intercellular cell adhesion molecule 1 (ICAM-1) can be up-regulated in endothelial and cancer cells during tumor angiogenesis and metastasis (288). ICAM-1 expression was also down-regulated in novel anti-cancer therapies based upon ZFP-TFs (288). Magnenat *et al* (2004) fused the KRAB repression domain to ZFPs targeting the ICAM-1 promoter. ICAM-1 expression was down-regulated by 77% and 98% in primary endothelium cells and a melanoma cancer cell line, respectively (288). Lund *et al* (2005) also targeted ICAM-1 expression with a ZFP-KRAB fusion repressor and showed decreases of nearly 100% in ICAM-1 surface expression using an epidermoid carcinoma cell line (286).

Choo *et al* (1994) used ZFPs to preferentially bind the reciprocal chromosomal translocation associated with chronic myelogenous leukemia and acute lymphoblastic leukemia (289). This translocation is located at t(9;22)(q34;q11) and results in a truncation of the Philadelphia chromosome (chromosome 22) (289). The most common breakpoint occurs between the *c-ABL* proto-oncogene and the *BCR* gene (289). The *BCR-ABL* fusion acts as a dominant transforming oncogene in cell culture and mouse models (289). Choo *et al* designed ZFPs to bind specifically to the *BCR-ABL* fusion oncogene over the parental sequences (289). When the ZFPs bound to the *BCR-ABL* oncogene in transformed tissue culture cells, transcription was blocked and cells resumed a non-transformed phenotype that was dependent on exogenous growth factors (289). This approach represents a therapeutic that will specifically target cancer cells and will have little effect on cells lacking the chromosomal translocation.

β–thalassemia and sickle cell disease were targeted by ZFP-TFs to regulate the expression of γ-globin (290). β-globin is a normal component of hemoglobin (HbA). In β–thalassemia and sickle cell disease, β-globin expression is defective. These disease states can be rescued by the expression of the fetal globin chain γ to

replace the missing β-globin, forming fetal hemoglobin (HbF) (290). Graslund *et al* (2005) linked the VP16 activation domain to ZFPs targeting the γ-globin promoter. Retroviral transduction of the ZFP-TFs into an erythroleukemia cell line resulted in 16-fold higher levels of γ-globin expression (290). A similar approach was undertaken by Lu *et al* (2008) to target the utrophin A promoter. Up-regulation of endogenous utrophin A in Duchene muscular dystrophy can compensate for the defective dystrophin gene associated with the disease (291). Lu *et al* designed ZFP-TFs based on the VP16 activation domain and demonstrated expression of twice the amount of utrophin A mRNA and protein in mouse myoblasts (291). Additionally, in dystrophin-deficient mice, adenovirus transduction of the ZFP-TFs resulted in 3-fold more utrophin A protein, and 4- and 5-fold more utrophin A mRNA after 20 and 80 days, respectively (291). The treated mice had enhanced muscle function and decreased necrosis, all signs of an improved disease state (291).

1.3.6 Summary of ZFPs as therapeutics

The versatility and therapeutic effectiveness of ZFPs has been demonstrated in numerous papers. ZFPs have been used to treat and prevent viral infections, to up- or down-regulate expression of host genes in different disease systems, and to target cancer cells for growth inhibition. The relative ease of designing ZFPs to any desired DNA sequence makes them a desirable tool for targeting therapeutics to certain DNA regions. Further, their low toxicity level encourages their use as a protein therapeutic, and their versatility through fusion to a wide-range of functional domains, such as repressor, activation and nuclease domains, increases the range of their functionality.

1.4 References

1. Shepard CW, Simard EP, Finelli L, Fiore AE, & Bell BP (2006) Hepatitis B virus infection: epidemiology and vaccination. *Epidemiol Rev* 28:112-125.
2. Beasley RP, Hwang LY, Lin CC, & Chien CS (1981) Hepatocellular carcinoma and hepatitis B virus. A prospective study of 22 707 men in Taiwan. *Lancet* 2(8256):1129-1133.
3. Anonymous (2008) Hepatitis B: Fact sheet No.204. (World Health Organization).
4. Jonas MM (2009) Hepatitis B and pregnancy: an underestimated issue. *Liver Int* 29 Suppl 1:133-139.
5. Szmuness W (1978) Hepatocellular carcinoma and the hepatitis B virus: evidence for a causal association. *Prog Med Virol* 24:40-69.
6. Farazi PA & DePinho RA (2006) Hepatocellular carcinoma pathogenesis: from genes to environment. *Nat Rev Cancer* 6(9):674-687.
7. Herath NI, Leggett BA, & MacDonald GA (2006) Review of genetic and epigenetic alterations in hepatocarcinogenesis. *J Gastroenterol Hepatol* 21(1 Pt 1):15-21.
8. Colombo M & Donato MF (2005) Prevention of hepatocellular carcinoma. *Semin Liver Dis* 25(2):155-161.
9. Organization WH (2008) Hepatitis B: Fact sheet No.204.
10. Andre FE (1990) Overview of a 5-year clinical experience with a yeast-derived hepatitis B vaccine. *Vaccine* 8 Suppl:S74-78; discussion S79-80.
11. Tyrrell DLJ, Mitchell MC, A. DR, W. SS, J. M, Thomas HC, J. F, F. N, P. B, & Vicary C (1993) Phase II Trial of Lamivudine for Chronic Hepatitis B. *American Association of Liver Disease*, (Hepatology), p 112A.
12. Dienstag JL, Perrillo RP, Schiff ER, Bartholomew M, Vicary C, & Rubin M (1995) A preliminary trial of lamivudine for chronic hepatitis B infection. *N Engl J Med* 333(25):1657-1661.
13. Yeung LT & Roberts EA (2010) Current issues in the management of paediatric viral hepatitis. *Liver Int* 30(1):5-18.
14. Buster EH & Janssen HL (2006) Antiviral treatment for chronic hepatitis B virus infection--immune modulation or viral suppression? *Neth J Med* 64(6):175-185.
15. Werle-Lapostolle B, Bowden S, Locarnini S, Wursthorn K, Petersen J, Lau G, Trepo C, Marcellin P, Goodman Z, Delaney WEt, Xiong S, Brosgart CL, Chen SS, Gibbs CS, & Zoulim F (2004) Persistence of cccDNA during the natural history of chronic hepatitis B and decline during adefovir dipivoxil therapy. *Gastroenterology* 126(7):1750-1758.
16. Chang TT, Gish RG, de Man R, Gadano A, Sollano J, Chao YC, Lok AS, Han KH, Goodman Z, Zhu J, Cross A, DeHertogh D, Wilber R, Colonno R, & Apelian D (2006) A comparison of entecavir and lamivudine for HBeAg-positive chronic hepatitis B. *N Engl J Med* 354(10):1001-1010.
17. Lai CL, Shouval D, Lok AS, Chang TT, Cheinquer H, Goodman Z, DeHertogh D, Wilber R, Zink RC, Cross A, Colonno R, & Fernandes L

(2006) Entecavir versus lamivudine for patients with HBeAg-negative chronic hepatitis B. *N Engl J Med* 354(10):1011-1020.

18. Jiang L, Jiang LS, Cheng NS, & Yan LN (2009) Current prophylactic strategies against hepatitis B virus recurrence after liver transplantation. *World J Gastroenterol* 15(20):2489-2499.
19. Kwon SY, Park YK, Ahn SH, Cho ES, Choe WH, Lee CH, Kim BK, Ko SY, Choi HS, Park ES, Shin GC, & Kim KH (2010) Identification and characterization of clevudine-resistant mutants of hepatitis B virus isolated from chronic hepatitis B patients. *J Virol* 84(9):4494-4503.
20. Severini A, Liu XY, Wilson JS, & Tyrrell DL (1995) Mechanism of inhibition of duck hepatitis B virus polymerase by (-)-beta-L-2',3'-dideoxy-3'-thiacytidine. *Antimicrob Agents Chemother* 39(7):1430-1435.
21. Howe AY, Robins MJ, Wilson JS, & Tyrrell DL (1996) Selective inhibition of the reverse transcription of duck hepatitis B virus by binding of 2',3'-dideoxyguanosine 5'-triphosphate to the viral polymerase. *Hepatology* 23(1):87-96.
22. Fischer KP, Gutfreund KS, & Tyrrell DL (2001) Lamivudine resistance in hepatitis B: mechanisms and clinical implications. *Drug Resist Updat* 4(2):118-128.
23. Allen MI, Deslauriers M, Andrews CW, Tipples GA, Walters KA, Tyrrell DL, Brown N, & Condreay LD (1998) Identification and characterization of mutations in hepatitis B virus resistant to lamivudine. Lamivudine Clinical Investigation Group. *Hepatology* 27(6):1670-1677.
24. Fischer KP & Tyrrell DL (1996) Generation of duck hepatitis B virus polymerase mutants through site-directed mutagenesis which demonstrate resistance to lamivudine [(--)-beta-L-2', 3'-dideoxy-3'-thiacytidine] in vitro. *Antimicrob Agents Chemother* 40(8):1957-1960.
25. Liaw YF, Chien RN, Yeh CT, Tsai SL, & Chu CM (1999) Acute exacerbation and hepatitis B virus clearance after emergence of YMDD motif mutation during lamivudine therapy. *Hepatology* 30(2):567-572.
26. Ling R, Mutimer D, Ahmed M, Boxall EH, Elias E, Dusheiko GM, & Harrison TJ (1996) Selection of mutations in the hepatitis B virus polymerase during therapy of transplant recipients with lamivudine. *Hepatology* 24(3):711-713.
27. Tipples GA, Ma MM, Fischer KP, Bain VG, Kneteman NM, & Tyrrell DL (1996) Mutation in HBV RNA-dependent DNA polymerase confers resistance to lamivudine in vivo. *Hepatology* 24(3):714-717.
28. Chen CH, Lee CM, Tung WC, Wang JH, Hung CH, Hu TH, Wang JC, Lu SN, & Changchien CS (2010) Evolution of full-length HBV sequences in chronic hepatitis B patients with sequential lamivudine and adefovir dipivoxil resistance. *J Hepatol* 52(4):478-485.
29. Locarnini S & Omata M (2006) Molecular virology of hepatitis B virus and the development of antiviral drug resistance. *Liver Int* 26(S2):11-22.
30. Walsh AW, Langley DR, Colonno RJ, & Tenney DJ (2010) Mechanistic characterization and molecular modeling of hepatitis B virus polymerase resistance to entecavir. *PLoS One* 5(2):e9195.

31. Inoue J, Ueno Y, Wakui Y, Niitsuma H, Fukushima K, Yamagiwa Y, Shiina M, Kondo Y, Kakazu E, Tamai K, Obara N, Iwasaki T, & Shimosegawa T (2010) Four-year study of lamivudine and adefovir combination therapy in lamivudine-resistant hepatitis B patients: influence of hepatitis B virus genotype and resistance mutation pattern. *J Viral Hepat*.
32. Dean J, Bowden S, & Locarnini S (1995) Reversion of duck hepatitis B virus DNA replication in vivo following cessation of treatment with the nucleoside analogue ganciclovir. *Antiviral Res* 27(1-2):171-178.
33. Addison WR, Walters KA, Wong WW, Wilson JS, Madej D, Jewell LD, & Tyrrell DL (2002) Half-life of the duck hepatitis B virus covalently closed circular DNA pool in vivo following inhibition of viral replication. *J Virol* 76(12):6356-6363.
34. Zhu Y, Yamamoto T, Cullen J, Saputelli J, Aldrich CE, Miller DS, Litwin S, Furman PA, Jilbert AR, & Mason WS (2001) Kinetics of hepadnavirus loss from the liver during inhibition of viral DNA synthesis. *J Virol* 75(1):311-322.
35. Addison WR, Wong WW, Fischer KP, & Tyrrell DL (2000) A quantitative competitive PCR assay for the covalently closed circular form of the duck hepatitis B virus. *Antiviral Res* 48(1):27-37.
36. Moraleda G, Saputelli J, Aldrich CE, Averett D, Condreay L, & Mason WS (1997) Lack of effect of antiviral therapy in nondividing hepatocyte cultures on the closed circular DNA of woodchuck hepatitis virus. *J Virol* 71(12):9392-9399.
37. Ganem D & Schneider R (2005) Hepadnaviridae. *Fields Virology*, eds Knipe DM & Howley PM (Lippincott Williams & Wilkins, Philadelphia), 5 Ed Vol 2, pp 2977-3030.
38. Glebe D & Urban S (2007) Viral and cellular determinants involved in hepadnaviral entry. *World J Gastroenterol* 13(1):22-38.
39. Summers J, O'Connell A, & Millman I (1975) Genome of hepatitis B virus: restriction enzyme cleavage and structure of DNA extracted from Dane particles. *Proc Natl Acad Sci U S A* 72(11):4597-4601.
40. Robinson WS, Clayton DA, & Greenman RL (1974) DNA of a human hepatitis B virus candidate. *J Virol* 14(2):384-391.
41. Dane DS, Cameron CH, & Briggs M (1970) Virus-like particles in serum of patients with Australia-antigen-associated hepatitis. *Lancet* 1(7649):695-698.
42. Almeida JD, Rubenstein D, & Stott EJ (1971) New antigen-antibody system in Australia-antigen-positive hepatitis. *Lancet* 2(7736):1225-1227.
43. Hirschman SZ, Gerber M, & Garfinkel E (1974) Purification of naked intranuclear particles from human liver infected by hepatitis B virus. *Proc Natl Acad Sci U S A* 71(9):3345-3349.
44. Wynne SA, Crowther RA, & Leslie AG (1999) The crystal structure of the human hepatitis B virus capsid. *Mol Cell* 3(6):771-780.
45. Hruska JF & Robinson WS (1977) The proteins of hepatitis B Dane particle cores. *J Med Virol* 1(2):119-131.

46. Shih JW & Gerin JL (1975) Immunochemistry of hepatitis B surface antigen (HBsAg): preparation and characterization of antibodies to the constituent polypeptides. *J Immunol* 115(3):634-639.
47. Robinson WS & Greenman RL (1974) DNA polymerase in the core of the human hepatitis B virus candidate. *J Virol* 13(6):1231-1236.
48. Albin C & Robinson WS (1980) Protein kinase activity in hepatitis B virus. *J Virol* 34(1):297-302.
49. Kann M & Gerlich WH (1994) Effect of core protein phosphorylation by protein kinase C on encapsidation of RNA within core particles of hepatitis B virus. *J Virol* 68(12):7993-8000.
50. Kaplan PM, Ford EC, Purcell RH, & Gerin JL (1976) Demonstration of subpopulations of Dane particles. *J Virol* 17(3):885-893.
51. Dreesman GR, Hollinger FB, Suriano JR, Fujioka RS, Brunschwig JP, & Melnick JL (1972) Biophysical and biochemical heterogeneity of purified hepatitis B antigen. *J Virol* 10(3):469-476.
52. Heermann KH, Goldmann U, Schwartz W, Seyffarth T, Baumgarten H, & Gerlich WH (1984) Large surface proteins of hepatitis B virus containing the pre-s sequence. *J Virol* 52(2):396-402.
53. Heermann KH, Kruse F, Seifer M, & Gerlich WH (1987) Immunogenicity of the gene S and Pre-S domains in hepatitis B virions and HBsAg filaments. *Intervirology* 28(1):14-25.
54. Hruska JF, Clayton DA, Rubenstein JL, & Robinson WS (1977) Structure of hepatitis B Dane particle DNA before and after the Dane particle DNA polymerase reaction. *J Virol* 21(2):666-672.
55. Landers TA, Greenberg HB, & Robinson WS (1977) Structure of hepatitis B Dane particle DNA and nature of the endogenous DNA polymerase reaction. *J Virol* 23(2):368-376.
56. Sattler F & Robinson WS (1979) Hepatitis B viral DNA molecules have cohesive ends. *J Virol* 32(1):226-233.
57. Scotto J, Hadchouel M, Wain-Hobson S, Sonigo P, Courouce AM, Tiollais P, & Brechot C (1985) Hepatitis B virus DNA in Dane particles: evidence for the presence of replicative intermediates. *J Infect Dis* 151(4):610-617.
58. Gerlich WH & Robinson WS (1980) Hepatitis B virus contains protein attached to the 5' terminus of its complete DNA strand. *Cell* 21(3):801-809.
59. Breiner KM, Urban S, & Schaller H (1998) Carboxypeptidase D (gp180), a Golgi-resident protein, functions in the attachment and entry of avian hepatitis B viruses. *J Virol* 72(10):8098-8104.
60. Walters KA, Joyce MA, Addison WR, Fischer KP, & Tyrrell DL (2004) Superinfection exclusion in duck hepatitis B virus infection is mediated by the large surface antigen. *J Virol* 78(15):7925-7937.
61. Guo H, Mao R, Block TM, & Guo JT (2010) Production and function of the cytoplasmic deproteinized relaxed circular DNA of hepadnaviruses. *J Virol* 84(1):387-396.

62. Rabe B, Vlachou A, Pante N, Helenius A, & Kann M (2003) Nuclear import of hepatitis B virus capsids and release of the viral genome. *Proc Natl Acad Sci U S A* 100(17):9849-9854.
63. Kann M, Sodeik B, Vlachou A, Gerlich WH, & Helenius A (1999) Phosphorylation-dependent binding of hepatitis B virus core particles to the nuclear pore complex. *J Cell Biol* 145(1):45-55.
64. Guo H, Jiang D, Zhou T, Cuconati A, Block TM, & Guo JT (2007) Characterization of the intracellular deproteinized relaxed circular DNA of hepatitis B virus: an intermediate of covalently closed circular DNA formation. *J Virol* 81(22):12472-12484.
65. Tuttleman JS, Pourcel C, & Summers J (1986) Formation of the pool of covalently closed circular viral DNA in hepadnavirus-infected cells. *Cell* 47(3):451-460.
66. Lenhoff RJ & Summers J (1994) Coordinate regulation of replication and virus assembly by the large envelope protein of an avian hepadnavirus. *J Virol* 68(7):4565-4571.
67. Summers J, Smith PM, & Horwich AL (1990) Hepadnavirus envelope proteins regulate covalently closed circular DNA amplification. *J Virol* 64(6):2819-2824.
68. Yang W & Summers J (1995) Illegitimate replication of linear hepadnavirus DNA through nonhomologous recombination. *J Virol* 69(7):4029-4036.
69. Yang W, Mason WS, & Summers J (1996) Covalently closed circular viral DNA formed from two types of linear DNA in woodchuck hepatitis virus-infected liver. *J Virol* 70(7):4567-4575.
70. Bock CT, Schranz P, Schroder CH, & Zentgraf H (1994) Hepatitis B virus genome is organized into nucleosomes in the nucleus of the infected cell. (Translated from eng) *Virus Genes* 8(3):215-229 (in eng).
71. Newbold JE, Xin H, Tencza M, Sherman G, Dean J, Bowden S, & Locarnini S (1995) The covalently closed duplex form of the hepadnavirus genome exists in situ as a heterogeneous population of viral minichromosomes. *J Virol* 69(6):3350-3357.
72. Bock CT, Schwinn S, Locarnini S, Fyfe J, Manns MP, Trautwein C, & Zentgraf H (2001) Structural organization of the hepatitis B virus minichromosome. *J Mol Biol* 307(1):183-196.
73. Shaul Y, Rutter WJ, & Laub O (1985) A human hepatitis B viral enhancer element. *EMBO J* 4(2):427-430.
74. Tognoni A, Cattaneo R, Serfling E, & Schaffner W (1985) A novel expression selection approach allows precise mapping of the hepatitis B virus enhancer. *Nucleic Acids Res* 13(20):7457-7472.
75. Vannice JL & Levinson AD (1988) Properties of the human hepatitis B virus enhancer: position effects and cell-type nonspecificity. *J Virol* 62(4):1305-1313.
76. Trujillo MA, Letovsky J, Maguire HF, Lopez-Cabrera M, & Siddiqui A (1991) Functional analysis of a liver-specific enhancer of the hepatitis B virus. *Proc Natl Acad Sci U S A* 88(9):3797-3801.

77. Antonucci TK & Rutter WJ (1989) Hepatitis B virus (HBV) promoters are regulated by the HBV enhancer in a tissue-specific manner. *J Virol* 63(2):579-583.
78. Jameel S & Siddiqui A (1986) The human hepatitis B virus enhancer requires trans-acting cellular factor(s) for activity. *Mol Cell Biol* 6(2):710-715.
79. Honigwachs J, Faktor O, Dikstein R, Shaul Y, & Laub O (1989) Liver-specific expression of hepatitis B virus is determined by the combined action of the core gene promoter and the enhancer. *J Virol* 63(2):919-924.
80. Patel NU, Jameel S, Isom H, & Siddiqui A (1989) Interactions between nuclear factors and the hepatitis B virus enhancer. *J Virol* 63(12):5293-5301.
81. Chang HK, Wang BY, Yuh CH, Wei CL, & Ting LP (1989) A liver-specific nuclear factor interacts with the promoter region of the large surface protein gene of human hepatitis B virus. *Mol Cell Biol* 9(11):5189-5197.
82. Bulla GA & Siddiqui A (1988) The hepatitis B virus enhancer modulates transcription of the hepatitis B virus surface antigen gene from an internal location. *J Virol* 62(4):1437-1441.
83. Chang HK, Chou CK, Chang C, Su TS, Hu C, Yoshida M, & Ting LP (1987) The enhancer sequence of human hepatitis B virus can enhance the activity of its surface gene promoter. *Nucleic Acids Res* 15(5):2261-2268.
84. Raney AK, Milich DR, & McLachlan A (1989) Characterization of hepatitis B virus major surface antigen gene transcriptional regulatory elements in differentiated hepatoma cell lines. *J Virol* 63(9):3919-3925.
85. Treinin M & Laub O (1987) Identification of a promoter element located upstream from the hepatitis B virus X gene. *Mol Cell Biol* 7(1):545-548.
86. Shaul Y & Ben-Levy R (1987) Multiple nuclear proteins in liver cells are bound to hepatitis B virus enhancer element and its upstream sequences. *EMBO J* 6(7):1913-1920.
87. Dikstein R, Faktor O, & Shaul Y (1990) Hierarchic and cooperative binding of the rat liver nuclear protein C/EBP at the hepatitis B virus enhancer. *Mol Cell Biol* 10(8):4427-4430.
88. Guo WT, Bell KD, & Ou JH (1991) Characterization of the hepatitis B virus EnhI enhancer and X promoter complex. *J Virol* 65(12):6686-6692.
89. Dikstein R, Faktor O, Ben-Levy R, & Shaul Y (1990) Functional organization of the hepatitis B virus enhancer. *Mol Cell Biol* 10(7):3683-3689.
90. Ben-Levy R, Faktor O, Berger I, & Shaul Y (1989) Cellular factors that interact with the hepatitis B virus enhancer. *Mol Cell Biol* 9(4):1804-1809.
91. Ostapchuk P, Scheirle G, & Hearing P (1989) Binding of nuclear factor EF-C to a functional domain of the hepatitis B virus enhancer region. *Mol Cell Biol* 9(7):2787-2797.
92. Faktor O, Budlovsky S, Ben-Levy R, & Shaul Y (1990) A single element within the hepatitis B virus enhancer binds multiple proteins and responds to multiple stimuli. *J Virol* 64(4):1861-1863.

93. Chen M, Hieng S, Qian X, Costa R, & Ou JH (1994) Regulation of hepatitis B virus ENI enhancer activity by hepatocyte-enriched transcription factor HNF3. *Virology* 205(1):127-132.
94. Ori A & Shaul Y (1995) Hepatitis B virus enhancer binds and is activated by the Hepatocyte nuclear factor 3. *Virology* 207(1):98-106.
95. Huan B & Siddiqui A (1992) Retinoid X receptor RXR alpha binds to and trans-activates the hepatitis B virus enhancer. *Proc Natl Acad Sci U S A* 89(19):9059-9063.
96. Garcia AD, Ostapchuk P, & Hearing P (1993) Functional interaction of nuclear factors EF-C, HNF-4, and RXR alpha with hepatitis B virus enhancer I. *J Virol* 67(7):3940-3950.
97. Wang SH, Yeh SH, Lin WH, Wang HY, Chen DS, & Chen PJ (2009) Identification of androgen response elements in the enhancer I of hepatitis B virus: a mechanism for sex disparity in chronic hepatitis B. *Hepatology* 50(5):1392-1402.
98. Tur-Kaspa R, Burk RD, Shaul Y, & Shafritz DA (1986) Hepatitis B virus DNA contains a glucocorticoid-responsive element. *Proc Natl Acad Sci U S A* 83(6):1627-1631.
99. Lopez-Cabrera M, Letovsky J, Hu KQ, & Siddiqui A (1990) Multiple liver-specific factors bind to the hepatitis B virus core/pregenomic promoter: trans-activation and repression by CCAAT/enhancer binding protein. *Proc Natl Acad Sci U S A* 87(13):5069-5073.
100. Yuh CH, Chang YL, & Ting LP (1992) Transcriptional regulation of precore and pregenomic RNAs of hepatitis B virus. *J Virol* 66(7):4073-4084.
101. Wang Y, Chen P, Wu X, Sun AL, Wang H, Zhu YA, & Li ZP (1990) A new enhancer element, ENII, identified in the X gene of hepatitis B virus. *J Virol* 64(8):3977-3981.
102. Guo W, Chen M, Yen TS, & Ou JH (1993) Hepatocyte-specific expression of the hepatitis B virus core promoter depends on both positive and negative regulation. *Mol Cell Biol* 13(1):443-448.
103. Yuh CH & Ting LP (1990) The genome of hepatitis B virus contains a second enhancer: cooperation of two elements within this enhancer is required for its function. *J Virol* 64(9):4281-4287.
104. Johnson JL, Raney AK, & McLachlan A (1995) Characterization of a functional hepatocyte nuclear factor 3 binding site in the hepatitis B virus nucleocapsid promoter. *Virology* 208(1):147-158.
105. Chen IH, Huang CJ, & Ting LP (1995) Overlapping initiator and TATA box functions in the basal core promoter of hepatitis B virus. *J Virol* 69(6):3647-3657.
106. Junker M, Galle P, & Schaller H (1987) Expression and replication of the hepatitis B virus genome under foreign promoter control. *Nucleic Acids Res* 15(24):10117-10132.
107. Zhou DX & Yen TS (1990) Differential regulation of the hepatitis B virus surface gene promoters by a second viral enhancer. *J Biol Chem* 265(34):20731-20734.

108. Yuh CH & Ting LP (1991) C/EBP-like proteins binding to the functional box-alpha and box-beta of the second enhancer of hepatitis B virus. *Mol Cell Biol* 11(10):5044-5052.
109. Su H & Yee JK (1992) Regulation of hepatitis B virus gene expression by its two enhancers. *Proc Natl Acad Sci U S A* 89(7):2708-2712.
110. Yuh CH & Ting LP (1993) Differentiated liver cell specificity of the second enhancer of hepatitis B virus. *J Virol* 67(1):142-149.
111. Malpiece Y, Michel ML, Carloni G, Revel M, Tiollais P, & Weissenbach J (1983) The gene S promoter of hepatitis B virus confers constitutive gene expression. *Nucleic Acids Res* 11(13):4645-4654.
112. Saito I, Oya Y, & Shimojo H (1986) Novel RNA family structure of hepatitis B virus expressed in human cells, using a helper-free adenovirus vector. *J Virol* 58(2):554-560.
113. Siddiqui A, Jameel S, & Mapoles J (1986) Transcriptional control elements of hepatitis B surface antigen gene. *Proc Natl Acad Sci U S A* 83(3):566-570.
114. Raney AK, Easton AJ, & McLachlan A (1994) Characterization of the minimal elements of the hepatitis B virus large surface antigen promoter. *J Gen Virol* 75 (Pt 10):2671-2679.
115. De-Medina T, Faktor O, & Shaul Y (1988) The S promoter of hepatitis B virus is regulated by positive and negative elements. *Mol Cell Biol* 8(6):2449-2455.
116. Shaul Y, Ben-Levy R, & De-Medina T (1986) High affinity binding site for nuclear factor I next to the hepatitis B virus S gene promoter. *EMBO J* 5(8):1967-1971.
117. Raney AK, Milich DR, & McLachlan A (1991) Complex regulation of transcription from the hepatitis B virus major surface antigen promoter in human hepatoma cell lines. *J Virol* 65(9):4805-4811.
118. Raney AK, Le HB, & McLachlan A (1992) Regulation of transcription from the hepatitis B virus major surface antigen promoter by the Sp1 transcription factor. *J Virol* 66(12):6912-6921.
119. Lu CC & Yen TS (1996) Activation of the hepatitis B virus S promoter by transcription factor NF-Y via a CCAAT element. *Virology* 225(2):387-394.
120. Mandart E, Kay A, & Galibert F (1984) Nucleotide sequence of a cloned duck hepatitis B virus genome: comparison with woodchuck and human hepatitis B virus sequences. *J Virol* 49(3):782-792.
121. Mason WS, Seal G, & Summers J (1980) Virus of Pekin ducks with structural and biological relatedness to human hepatitis B virus. *J Virol* 36(3):829-836.
122. Liu C, Condreay LD, Burch JB, & Mason W (1991) Characterization of the core promoter and enhancer of duck hepatitis B virus. *Virology* 184(1):242-252.
123. Crescenzo-Chaigne B, Pillot J, Lilienbaum A, Levrero M, & Elfassi E (1991) Identification of a strong enhancer element upstream from the

pregenomic RNA start site of the duck hepatitis B virus genome. *J Virol* 65(7):3882-3886.
124. Schneider R & Will H (1991) Regulatory sequences of duck hepatitis B virus C gene transcription. *J Virol* 65(11):5693-5701.
125. Liu C, Mason WS, & Burch JB (1994) Identification of factor-binding sites in the duck hepatitis B virus enhancer and in vivo effects of enhancer mutations. *J Virol* 68(4):2286-2296.
126. Lilienbaum A, Crescenzo-Chaigne B, Sall AA, Pillot J, & Elfassi E (1993) Binding of nuclear factors to functional domains of the duck hepatitis B virus enhancer. *J Virol* 67(10):6192-6200.
127. Crescenzo-Chaigne B, Pillot J, & Lilienbaum A (1995) Interplay between a new HNF3 and the HNF1 transcriptional factors in the duck hepatitis B virus enhancer. *Virology* 213(1):231-240.
128. Welsheimer T & Newbold JE (1996) A functional hepatocyte nuclear factor 3 binding site is a critical component of the duck hepatitis B virus major surface antigen promoter. *J Virol* 70(12):8813-8820.
129. Doitsh G & Shaul Y (2003) A long HBV transcript encoding pX is inefficiently exported from the nucleus. *Virology* 309(2):339-349.
130. Fouillot N & Rossignol JM (1996) Translational stop codons in the precore sequence of hepatitis B virus pre-C RNA allow translation reinitiation at downstream AUGs. *J Gen Virol* 77 (Pt 6):1123-1127.
131. Sen N, Cao F, & Tavis JE (2004) Translation of duck hepatitis B virus reverse transcriptase by ribosomal shunting. *J Virol* 78(21):11751-11757.
132. Baumert TF, Marrone A, Vergalla J, & Liang TJ (1998) Naturally occurring mutations define a novel function of the hepatitis B virus core promoter in core protein expression. (Translated from eng) *J Virol* 72(8):6785-6795 (in eng).
133. Cattaneo R, Will H, & Schaller H (1984) Hepatitis B virus transcription in the infected liver. (Translated from eng) *EMBO J* 3(9):2191-2196 (in eng).
134. Cherrington J, Russnak R, & Ganem D (1992) Upstream sequences and cap proximity in the regulation of polyadenylation in ground squirrel hepatitis virus. *J Virol* 66(12):7589-7596.
135. Su TS, Lui WY, Lin LH, Han SH, & P'Eng F K (1989) Analysis of hepatitis B virus transcripts in infected human livers. *Hepatology* 9(2):180-185.
136. Su TS, Lai CJ, Huang JL, Lin LH, Yauk YK, Chang CM, Lo SJ, & Han SH (1989) Hepatitis B virus transcript produced by RNA splicing. *J Virol* 63(9):4011-4018.
137. Suzuki T, Masui N, Kajino K, Saito I, & Miyamura T (1989) Detection and mapping of spliced RNA from a human hepatoma cell line transfected with the hepatitis B virus genome. *Proc Natl Acad Sci U S A* 86(21):8422-8426.
138. Soussan P, Garreau F, Zylberberg H, Ferray C, Brechot C, & Kremsdorf D (2000) In vivo expression of a new hepatitis B virus protein encoded by a spliced RNA. *J Clin Invest* 105(1):55-60.

139. Soussan P, Tuveri R, Nalpas B, Garreau F, Zavala F, Masson A, Pol S, Brechot C, & Kremsdorf D (2003) The expression of hepatitis B spliced protein (HBSP) encoded by a spliced hepatitis B virus RNA is associated with viral replication and liver fibrosis. *J Hepatol* 38(3):343-348.
140. Wu HL, Chen PJ, Tu SJ, Lin MH, Lai MY, & Chen DS (1991) Characterization and genetic analysis of alternatively spliced transcripts of hepatitis B virus in infected human liver tissues and transfected HepG2 cells. *J Virol* 65(4):1680-1686.
141. Rosmorduc O, Petit MA, Pol S, Capel F, Bortolotti F, Berthelot P, Brechot C, & Kremsdorf D (1995) In vivo and in vitro expression of defective hepatitis B virus particles generated by spliced hepatitis B virus RNA. *Hepatology* 22(1):10-19.
142. Terre S, Petit MA, & Brechot C (1991) Defective hepatitis B virus particles are generated by packaging and reverse transcription of spliced viral RNAs in vivo. *J Virol* 65(10):5539-5543.
143. Gunther S, Sommer G, Iwanska A, & Will H (1997) Heterogeneity and common features of defective hepatitis B virus genomes derived from spliced pregenomic RNA. *Virology* 238(2):363-371.
144. Su Q, Wang SF, Chang TE, Breitkreutz R, Hennig H, Takegoshi K, Edler L, & Schroder CH (2001) Circulating hepatitis B virus nucleic acids in chronic infection : representation of differently polyadenylated viral transcripts during progression to nonreplicative stages. *Clin Cancer Res* 7(7):2005-2015.
145. Hilger C, Velhagen I, Zentgraf H, & Schroder CH (1991) Diversity of hepatitis B virus X gene-related transcripts in hepatocellular carcinoma: a novel polyadenylation site on viral DNA. *J Virol* 65(8):4284-4291.
146. Kairat A, Beerheide W, Zhou G, Tang ZY, Edler L, & Schroder CH (1999) Truncated hepatitis B virus RNA in human hepatocellular carcinoma: its representation in patients with advancing age. *Intervirology* 42(4):228-237.
147. Loeb DD, Mack AA, & Tian R (2002) A secondary structure that contains the 5' and 3' splice sites suppresses splicing of duck hepatitis B virus pregenomic RNA. *J Virol* 76(20):10195-10202.
148. Obert S, Zachmann-Brand B, Deindl E, Tucker W, Bartenschlager R, & Schaller H (1996) A splice hepadnavirus RNA that is essential for virus replication. *EMBO J* 15(10):2565-2574.
149. Huang ZM & Yen TS (1995) Role of the hepatitis B virus posttranscriptional regulatory element in export of intronless transcripts. *Mol Cell Biol* 15(7):3864-3869.
150. Huang ZM & Yen TS (1994) Hepatitis B virus RNA element that facilitates accumulation of surface gene transcripts in the cytoplasm. (Translated from eng) *J Virol* 68(5):3193-3199 (in eng).
151. Huang J & Liang TJ (1993) A novel hepatitis B virus (HBV) genetic element with Rev response element-like properties that is essential for expression of HBV gene products. *Mol Cell Biol* 13(12):7476-7486.

152. Donello JE, Beeche AA, Smith GJ, 3rd, Lucero GR, & Hope TJ (1996) The hepatitis B virus posttranscriptional regulatory element is composed of two subelements. *J Virol* 70(7):4345-4351.
153. Huang DS, Emancipator SN, Fletcher DR, Lamm ME, & Mazanec MB (1996) Hepatic pathology resulting from mouse hepatitis virus S infection in severe combined immunodeficiency mice. (Translated from eng) *Lab Anim Sci* 46(2):167-173 (in eng).
154. Smith GJ, 3rd, Donello JE, Luck R, Steger G, & Hope TJ (1998) The hepatitis B virus post-transcriptional regulatory element contains two conserved RNA stem-loops which are required for function. *Nucleic Acids Res* 26(21):4818-4827.
155. Huang ZM, Zang WQ, & Yen TS (1996) Cellular proteins that bind to the hepatitis B virus posttranscriptional regulatory element. *Virology* 217(2):573-581.
156. Zang WQ, Fieno AM, Grant RA, & Yen TS (1998) Identification of glyceraldehyde-3-phosphate dehydrogenase as a cellular protein that binds to the hepatitis B virus posttranscriptional regulatory element. *Virology* 248(1):46-52.
157. Zang WQ, Li B, Huang PY, Lai MM, & Yen TS (2001) Role of polypyrimidine tract binding protein in the function of the hepatitis B virus posttranscriptional regulatory element. *J Virol* 75(22):10779-10786.
158. Wagner EJ & Garcia-Blanco MA (2001) Polypyrimidine tract binding protein antagonizes exon definition. *Mol Cell Biol* 21(10):3281-3288.
159. Huang Y, Wimler KM, & Carmichael GG (1999) Intronless mRNA transport elements may affect multiple steps of pre-mRNA processing. *EMBO J* 18(6):1642-1652.
160. Heise T, Sommer G, Reumann K, Meyer I, Will H, & Schaal H (2006) The hepatitis B virus PRE contains a splicing regulatory element. *Nucleic Acids Res* 34(1):353-363.
161. Popa I, Harris ME, Donello JE, & Hope TJ (2002) CRM1-dependent function of a cis-acting RNA export element. *Mol Cell Biol* 22(7):2057-2067.
162. Zang WQ & Yen TS (1999) Distinct export pathway utilized by the hepatitis B virus posttranscriptional regulatory element. *Virology* 259(2):299-304.
163. Otero GC, Harris ME, Donello JE, & Hope TJ (1998) Leptomycin B inhibits equine infectious anemia virus Rev and feline immunodeficiency virus rev function but not the function of the hepatitis B virus posttranscriptional regulatory element. *J Virol* 72(9):7593-7597.
164. Roth J & Dobbelstein M (1997) Export of hepatitis B virus RNA on a Rev-like pathway: inhibition by the regenerating liver inhibitory factor IkappaB alpha. *J Virol* 71(11):8933-8939.
165. Russnak RH (1991) Regulation of polyadenylation in hepatitis B viruses: stimulation by the upstream activating signal PS1 is orientation-dependent, distance-independent, and additive. (Translated from eng) *Nucleic Acids Res* 19(23):6449-6456 (in eng).

166. Simonsen CC & Levinson AD (1983) Analysis of processing and polyadenylation signals of the hepatitis B virus surface antigen gene by using simian virus 40-hepatitis B virus chimeric plasmids. *Mol Cell Biol* 3(12):2250-2258.
167. Russnak R & Ganem D (1990) Sequences 5' to the polyadenylation signal mediate differential poly(A) site use in hepatitis B viruses. *Genes Dev* 4(5):764-776.
168. Huang M & Summers J (1994) pet, a small sequence distal to the pregenome cap site, is required for expression of the duck hepatitis B virus pregenome. *J Virol* 68(3):1564-1572.
169. Beckel-Mitchener A & Summers J (1997) A novel transcriptional element in circular DNA monomers of the duck hepatitis B virus. *J Virol* 71(10):7917-7922.
170. Chang LJ, Ganem D, & Varmus HE (1990) Mechanism of translation of the hepadnaviral polymerase (P) gene. (Translated from eng) *Proc Natl Acad Sci U S A* 87(13):5158-5162 (in eng).
171. Fouillot N, Tlouzeau S, Rossignol JM, & Jean-Jean O (1993) Translation of the hepatitis B virus P gene by ribosomal scanning as an alternative to internal initiation. (Translated from eng) *J Virol* 67(8):4886-4895 (in eng).
172. Roychoudhury S & Shih C (1990) cis rescue of a mutated reverse transcriptase gene of human hepatitis B virus by creation of an internal ATG. *J Virol* 64(3):1063-1069.
173. Cao F, Scougall CA, Jilbert AR, & Tavis JE (2009) Pre-P is a secreted glycoprotein encoded as an N-terminal extension of the duck hepatitis B virus polymerase gene. *J Virol* 83(3):1368-1378.
174. Machida A, Ohnuma H, Tsuda F, Yoshikawa A, Hoshi Y, Tanaka T, Kishimoto S, Akahane Y, Miyakawa Y, & Mayumi M (1991) Phosphorylation in the carboxyl-terminal domain of the capsid protein of hepatitis B virus: evaluation with a monoclonal antibody. *J Virol* 65(11):6024-6030.
175. Hatton T, Zhou S, & Standring DN (1992) RNA- and DNA-binding activities in hepatitis B virus capsid protein: a model for their roles in viral replication. *J Virol* 66(9):5232-5241.
176. Liao W & Ou JH (1995) Phosphorylation and nuclear localization of the hepatitis B virus core protein: significance of serine in the three repeated SPRRR motifs. *J Virol* 69(2):1025-1029.
177. Yu M & Summers J (1994) Multiple functions of capsid protein phosphorylation in duck hepatitis B virus replication. *J Virol* 68(7):4341-4348.
178. Yu M & Summers J (1994) Phosphorylation of the duck hepatitis B virus capsid protein associated with conformational changes in the C terminus. *J Virol* 68(5):2965-2969.
179. Yeh CT & Ou JH (1991) Phosphorylation of hepatitis B virus precore and core proteins. *J Virol* 65(5):2327-2331.

180. Eckhardt SG, Milich DR, & McLachlan A (1991) Hepatitis B virus core antigen has two nuclear localization sequences in the arginine-rich carboxyl terminus. *J Virol* 65(2):575-582.
181. Mondelli M, Tedder RS, Ferns B, Pontisso P, Realdi G, & Alberti A (1986) Differential distribution of hepatitis B core and E antigens in hepatocytes: analysis by monoclonal antibodies. *Hepatology* 6(2):199-204.
182. Schlicht HJ (1991) Biosynthesis of the secretory core protein of duck hepatitis B virus: intracellular transport, proteolytic processing, and membrane expression of the precore protein. *J Virol* 65(7):3489-3495.
183. Ou JH, Laub O, & Rutter WJ (1986) Hepatitis B virus gene function: the precore region targets the core antigen to cellular membranes and causes the secretion of the e antigen. *Proc Natl Acad Sci U S A* 83(6):1578-1582.
184. Standring DN, Ou JH, Masiarz FR, & Rutter WJ (1988) A signal peptide encoded within the precore region of hepatitis B virus directs the secretion of a heterogeneous population of e antigens in Xenopus oocytes. *Proc Natl Acad Sci U S A* 85(22):8405-8409.
185. Schlicht HJ, Salfeld J, & Schaller H (1987) The duck hepatitis B virus pre-C region encodes a signal sequence which is essential for synthesis and secretion of processed core proteins but not for virus formation. (Translated from eng) *J Virol* 61(12):3701-3709 (in eng).
186. Wang J, Lee AS, & Ou JH (1991) Proteolytic conversion of hepatitis B virus e antigen precursor to end product occurs in a postendoplasmic reticulum compartment. *J Virol* 65(9):5080-5083.
187. Stibbe W & Gerlich WH (1983) Structural relationships between minor and major proteins of hepatitis B surface antigen. *J Virol* 46(2):626-628.
188. Persing DH, Varmus HE, & Ganem D (1986) Inhibition of secretion of hepatitis B surface antigen by a related presurface polypeptide. *Science* 234(4782):1388-1391.
189. Ou JH & Rutter WJ (1987) Regulation of secretion of the hepatitis B virus major surface antigen by the preS-1 protein. *J Virol* 61(3):782-786.
190. Eble BE, Lingappa VR, & Ganem D (1990) The N-terminal (pre-S2) domain of a hepatitis B virus surface glycoprotein is translocated across membranes by downstream signal sequences. (Translated from eng) *J Virol* 64(3):1414-1419 (in eng).
191. Bruss V & Ganem D (1991) The role of envelope proteins in hepatitis B virus assembly. *Proc Natl Acad Sci U S A* 88(3):1059-1063.
192. Chassot S, Lambert V, Kay A, Godinot C, Trepo C, & Cova L (1994) Identification of major antigenic domains of duck hepatitis B virus pre-S protein by peptide scanning. *Virology* 200(1):72-78.
193. Ishikawa T & Ganem D (1995) The pre-S domain of the large viral envelope protein determines host range in avian hepatitis B viruses. *Proc Natl Acad Sci U S A* 92(14):6259-6263.
194. Tang H, Oishi N, Kaneko S, & Murakami S (2006) Molecular functions and biological roles of hepatitis B virus x protein. *Cancer Sci* 97(10):977-983.

195. Feitelson MA & Miller RH (1988) X gene-related sequences in the core gene of duck and heron hepatitis B viruses. *Proc Natl Acad Sci U S A* 85(16):6162-6166.
196. Bouchard MJ & Schneider RJ (2004) The enigmatic X gene of hepatitis B virus. *J Virol* 78(23):12725-12734.
197. Benn J, Su F, Doria M, & Schneider RJ (1996) Hepatitis B virus HBx protein induces transcription factor AP-1 by activation of extracellular signal-regulated and c-Jun N-terminal mitogen-activated protein kinases. *J Virol* 70(8):4978-4985.
198. Kanda T, Yokosuka O, Nagao K, & Saisho H (2006) State of hepatitis C viral replication enhances activation of NF-kB- and AP-1-signaling induced by hepatitis B virus X. *Cancer Lett* 234(2):143-148.
199. Qadri I, Conaway JW, Conaway RC, Schaack J, & Siddiqui A (1996) Hepatitis B virus transactivator protein, HBx, associates with the components of TFIIH and stimulates the DNA helicase activity of TFIIH. *Proc Natl Acad Sci U S A* 93(20):10578-10583.
200. Maguire HF, Hoeffler JP, & Siddiqui A (1991) HBV X protein alters the DNA binding specificity of CREB and ATF-2 by protein-protein interactions. *Science* 252(5007):842-844.
201. Hu Z, Zhang Z, Kim JW, Huang Y, & Liang TJ (2006) Altered proteolysis and global gene expression in hepatitis B virus X transgenic mouse liver. *J Virol* 80(3):1405-1413.
202. Zhang Z, Torii N, Furusaka A, Malayaman N, Hu Z, & Liang TJ (2000) Structural and functional characterization of interaction between hepatitis B virus X protein and the proteasome complex. *J Biol Chem* 275(20):15157-15165.
203. Kalra N & Kumar V (2006) The X protein of hepatitis B virus binds to the F box protein Skp2 and inhibits the ubiquitination and proteasomal degradation of c-Myc. *FEBS Lett* 580(2):431-436.
204. Boya P, Pauleau AL, Poncet D, Gonzalez-Polo RA, Zamzami N, & Kroemer G (2004) Viral proteins targeting mitochondria: controlling cell death. *Biochim Biophys Acta* 1659(2-3):178-189.
205. Takada S, Shirakata Y, Kaneniwa N, & Koike K (1999) Association of hepatitis B virus X protein with mitochondria causes mitochondrial aggregation at the nuclear periphery, leading to cell death. *Oncogene* 18(50):6965-6973.
206. Junker-Niepmann M, Bartenschlager R, & Schaller H (1990) A short cis-acting sequence is required for hepatitis B virus pregenome encapsidation and sufficient for packaging of foreign RNA. *EMBO J* 9(10):3389-3396.
207. Knaus T & Nassal M (1993) The encapsidation signal on the hepatitis B virus RNA pregenome forms a stem-loop structure that is critical for its function. *Nucleic Acids Res* 21(17):3967-3975.
208. Bartenschlager R, Junker-Niepmann M, & Schaller H (1990) The P gene product of hepatitis B virus is required as a structural component for genomic RNA encapsidation. *J Virol* 64(11):5324-5332.

209. Chang LJ, Hirsch RC, Ganem D, & Varmus HE (1990) Effects of insertional and point mutations on the functions of the duck hepatitis B virus polymerase. *J Virol* 64(11):5553-5558.
210. Hirsch RC, Lavine JE, Chang LJ, Varmus HE, & Ganem D (1990) Polymerase gene products of hepatitis B viruses are required for genomic RNA packaging as wel as for reverse transcription. *Nature* 344(6266):552-555.
211. Tavis JE & Ganem D (1996) Evidence for activation of the hepatitis B virus polymerase by binding of its RNA template. *J Virol* 70(9):5741-5750.
212. Pollack JR & Ganem D (1993) An RNA stem-loop structure directs hepatitis B virus genomic RNA encapsidation. *J Virol* 67(6):3254-3263.
213. Flodell S, Schleucher J, Cromsigt J, Ippel H, Kidd-Ljunggren K, & Wijmenga S (2002) The apical stem-loop of the hepatitis B virus encapsidation signal folds into a stable tri-loop with two underlying pyrimidine bulges. *Nucleic Acids Res* 30(21):4803-4811.
214. Jeong JK, Yoon GS, & Ryu WS (2000) Evidence that the 5'-end cap structure is essential for encapsidation of hepatitis B virus pregenomic RNA. *J Virol* 74(12):5502-5508.
215. Calvert J & Summers J (1994) Two regions of an avian hepadnavirus RNA pregenome are required in cis for encapsidation. *J Virol* 68(4):2084-2090.
216. Ostrow KM & Loeb DD (2002) Characterization of the cis-acting contributions to avian hepadnavirus RNA encapsidation. (Translated from eng) *J Virol* 76(18):9087-9095 (in eng).
217. Beck J & Nassal M (1997) Sequence- and structure-specific determinants in the interaction between the RNA encapsidation signal and reverse transcriptase of avian hepatitis B viruses. *J Virol* 71(7):4971-4980.
218. Beck J, Bartos H, & Nassal M (1997) Experimental confirmation of a hepatitis B virus (HBV) epsilon-like bulge-and-loop structure in avian HBV RNA encapsidation signals. *Virology* 227(2):500-504.
219. Kaplan PM, Greenman RL, Gerin JL, Purcell RH, & Robinson WS (1973) DNA polymerase associated with human hepatitis B antigen. *J Virol* 12(5):995-1005.
220. Fowler MJ, Monjardino J, Tsiquaye KN, Zuckerman AJ, & Thomas HC (1984) The mechanism of replication of hepatitis B virus: evidence of asymmetric replication of the two DNA strands. *J Med Virol* 13(1):83-91.
221. Bavand M, Feitelson M, & Laub O (1989) The hepatitis B virus-associated reverse transcriptase is encoded by the viral pol gene. *J Virol* 63(2):1019-1021.
222. Radziwill G, Tucker W, & Schaller H (1990) Mutational analysis of the hepatitis B virus P gene product: domain structure and RNase H activity. *J Virol* 64(2):613-620.
223. Bartenschlager R & Schaller H (1988) The amino-terminal domain of the hepadnaviral P-gene encodes the terminal protein (genome-linked protein) believed to prime reverse transcription. *EMBO J* 7(13):4185-4192.

224. Weber M, Bronsema V, Bartos H, Bosserhoff A, Bartenschlager R, & Schaller H (1994) Hepadnavirus P protein utilizes a tyrosine residue in the TP domain to prime reverse transcription. *J Virol* 68(5):2994-2999.
225. Zoulim F & Seeger C (1994) Reverse transcription in hepatitis B viruses is primed by a tyrosine residue of the polymerase. *J Virol* 68(1):6-13.
226. Wang GH & Seeger C (1993) Novel mechanism for reverse transcription in hepatitis B viruses. *J Virol* 67(11):6507-6512.
227. Lien JM, Petcu DJ, Aldrich CE, & Mason WS (1987) Initiation and termination of duck hepatitis B virus DNA synthesis during virus maturation. *J Virol* 61(12):3832-3840.
228. Molnar-Kimber KL, Summers JW, & Mason WS (1984) Mapping of the cohesive overlap of duck hepatitis B virus DNA and of the site of initiation of reverse transcription. *J Virol* 51(1):181-191.
229. Nassal M & Rieger A (1996) A bulged region of the hepatitis B virus RNA encapsidation signal contains the replication origin for discontinuous first-strand DNA synthesis. *J Virol* 70(5):2764-2773.
230. Seeger C, Ganem D, & Varmus HE (1986) Biochemical and genetic evidence for the hepatitis B virus replication strategy. *Science* 232(4749):477-484.
231. Seeger C, Ganem D, & Varmus HE (1984) Nucleotide sequence of an infectious molecularly cloned genome of ground squirrel hepatitis virus. *J Virol* 51(2):367-375.
232. Tavis JE, Perri S, & Ganem D (1994) Hepadnavirus reverse transcription initiates within the stem-loop of the RNA packaging signal and employs a novel strand transfer. *J Virol* 68(6):3536-3543.
233. Loeb DD & Tian R (1995) Transfer of the minus strand of DNA during hepadnavirus replication is not invariable but prefers a specific location. *J Virol* 69(11):6886-6891.
234. Tavis JE & Ganem D (1995) RNA sequences controlling the initiation and transfer of duck hepatitis B virus minus-strand DNA. *J Virol* 69(7):4283-4291.
235. Rieger A & Nassal M (1996) Specific hepatitis B virus minus-strand DNA synthesis requires only the 5' encapsidation signal and the 3'-proximal direct repeat DR1. *J Virol* 70(1):585-589.
236. Chen Y & Marion PL (1996) Amino acids essential for RNase H activity of hepadnaviruses are also required for efficient elongation of minus-strand viral DNA. *J Virol* 70(9):6151-6156.
237. Lien JM, Aldrich CE, & Mason WS (1986) Evidence that a capped oligoribonucleotide is the primer for duck hepatitis B virus plus-strand DNA synthesis. (Translated from eng) *J Virol* 57(1):229-236 (in eng).
238. Loeb DD, Hirsch RC, & Ganem D (1991) Sequence-independent RNA cleavages generate the primers for plus strand DNA synthesis in hepatitis B viruses: implications for other reverse transcribing elements. *EMBO J* 10(11):3533-3540.
239. Staprans S, Loeb DD, & Ganem D (1991) Mutations affecting hepadnavirus plus-strand DNA synthesis dissociate primer cleavage from

translocation and reveal the origin of linear viral DNA. *J Virol* 65(3):1255-1262.
240. Havert MB & Loeb DD (1997) cis-Acting sequences in addition to donor and acceptor sites are required for template switching during synthesis of plus-strand DNA for duck hepatitis B virus. *J Virol* 71(7):5336-5344.
241. Wei Y, Tavis JE, & Ganem D (1996) Relationship between viral DNA synthesis and virion envelopment in hepatitis B viruses. *J Virol* 70(9):6455-6458.
242. Wolfe SA, Nekludova L, & Pabo CO (2000) DNA recognition by Cys2His2 zinc finger proteins. *Annu Rev Biophys Biomol Struct* 29:183-212.
243. Elrod-Erickson M, Benson TE, & Pabo CO (1998) High-resolution structures of variant Zif268-DNA complexes: implications for understanding zinc finger-DNA recognition. *Structure* 6(4):451-464.
244. Wolfe SA, Grant RA, Elrod-Erickson M, & Pabo CO (2001) Beyond the "recognition code": structures of two Cys2His2 zinc finger/TATA box complexes. *Structure* 9(8):717-723.
245. Pavletich NP & Pabo CO (1991) Zinc finger-DNA recognition: crystal structure of a Zif268-DNA complex at 2.1 A. *Science* 252(5007):809-817.
246. Elrod-Erickson M, Rould MA, Nekludova L, & Pabo CO (1996) Zif268 protein-DNA complex refined at 1.6 A: a model system for understanding zinc finger-DNA interactions. *Structure* 4(10):1171-1180.
247. Dreier B, Segal DJ, & Barbas CF, 3rd (2000) Insights into the molecular recognition of the 5'-GNN-3' family of DNA sequences by zinc finger domains. *J Mol Biol* 303(4):489-502.
248. Dreier B, Beerli RR, Segal DJ, Flippin JD, & Barbas CF, 3rd (2001) Development of zinc finger domains for recognition of the 5'-ANN-3' family of DNA sequences and their use in the construction of artificial transcription factors. *J Biol Chem* 276(31):29466-29478.
249. Dreier B, Fuller RP, Segal DJ, Lund CV, Blancafort P, Huber A, Koksch B, & Barbas CF, 3rd (2005) Development of zinc finger domains for recognition of the 5'-CNN-3' family DNA sequences and their use in the construction of artificial transcription factors. *J Biol Chem* 280(42):35588-35597.
250. Segal DJ, Dreier B, Beerli RR, & Barbas CF, 3rd (1999) Toward controlling gene expression at will: selection and design of zinc finger domains recognizing each of the 5'-GNN-3' DNA target sequences. *Proc Natl Acad Sci U S A* 96(6):2758-2763.
251. Mandell JG & Barbas CF, 3rd (2006) Zinc Finger Tools: custom DNA-binding domains for transcription factors and nucleases. *Nucleic Acids Res* 34(Web Server issue):W516-523.
252. Wu H, Yang WP, & Barbas CF, 3rd (1995) Building zinc fingers by selection: toward a therapeutic application. *Proc Natl Acad Sci U S A* 92(2):344-348.

253. Isalan M, Klug A, & Choo Y (2001) A rapid, generally applicable method to engineer zinc fingers illustrated by targeting the HIV-1 promoter. *Nat Biotechnol* 19(7):656-660.
254. Joung JK, Ramm EI, & Pabo CO (2000) A bacterial two-hybrid selection system for studying protein-DNA and protein-protein interactions. *Proc Natl Acad Sci U S A* 97(13):7382-7387.
255. Hurt JA, Thibodeau SA, Hirsh AS, Pabo CO, & Joung JK (2003) Highly specific zinc finger proteins obtained by directed domain shuffling and cell-based selection. *Proc Natl Acad Sci U S A* 100(21):12271-12276.
256. Koshino-Kimura Y, Takenaka K, Domoto F, Ohashi M, Miyazaki T, Aoyama Y, & Sera T (2009) Construction of plants resistant to TYLCV by using artificial zinc-finger proteins. *Nucleic Acids Symp Ser (Oxf)* (53):281-282.
257. Takenaka K, Koshino-Kimura Y, Aoyama Y, & Sera T (2007) Inhibition of tomato yellow leaf curl virus replication by artificial zinc-finger proteins. *Nucleic Acids Symp Ser (Oxf)* (51):429-430.
258. Sera T (2005) Inhibition of virus DNA replication by artificial zinc finger proteins. *J Virol* 79(4):2614-2619.
259. Mino T, Hatono T, Matsumoto N, Mori T, Mineta Y, Aoyama Y, & Sera T (2006) Inhibition of DNA replication of human papillomavirus by artificial zinc finger proteins. *J Virol* 80(11):5405-5412.
260. Reynolds L, Ullman C, Moore M, Isalan M, West MJ, Clapham P, Klug A, & Choo Y (2003) Repression of the HIV-1 5' LTR promoter and inhibition of HIV-1 replication by using engineered zinc-finger transcription factors. *Proc Natl Acad Sci U S A* 100(4):1615-1620.
261. Segal DJ, Goncalves J, Eberhardy S, Swan CH, Torbett BE, Li X, & Barbas CF, 3rd (2004) Attenuation of HIV-1 replication in primary human cells with a designed zinc finger transcription factor. *J Biol Chem* 279(15):14509-14519.
262. Eberhardy SR, Goncalves J, Coelho S, Segal DJ, Berkhout B, & Barbas CF, 3rd (2006) Inhibition of human immunodeficiency virus type 1 replication with artificial transcription factors targeting the highly conserved primer-binding site. *J Virol* 80(6):2873-2883.
263. Mino T, Mori T, Aoyama Y, & Sera T (2008) Cell-permeable artificial zinc-finger proteins as potent antiviral drugs for human papillomaviruses. *Arch Virol* 153(7):1291-1298.
264. Urnov FD, Miller JC, Lee YL, Beausejour CM, Rock JM, Augustus S, Jamieson AC, Porteus MH, Gregory PD, & Holmes MC (2005) Highly efficient endogenous human gene correction using designed zinc-finger nucleases. *Nature* 435(7042):646-651.
265. Bibikova M, Carroll D, Segal DJ, Trautman JK, Smith J, Kim YG, & Chandrasegaran S (2001) Stimulation of homologous recombination through targeted cleavage by chimeric nucleases. *Mol Cell Biol* 21(1):289-297.
266. Shukla VK, Doyon Y, Miller JC, DeKelver RC, Moehle EA, Worden SE, Mitchell JC, Arnold NL, Gopalan S, Meng X, Choi VM, Rock JM, Wu

YY, Katibah GE, Zhifang G, McCaskill D, Simpson MA, Blakeslee B, Greenwalt SA, Butler HJ, Hinkley SJ, Zhang L, Rebar EJ, Gregory PD, & Urnov FD (2009) Precise genome modification in the crop species Zea mays using zinc-finger nucleases. *Nature* 459(7245):437-441.

267. Townsend JA, Wright DA, Winfrey RJ, Fu F, Maeder ML, Joung JK, & Voytas DF (2009) High-frequency modification of plant genes using engineered zinc-finger nucleases. *Nature* 459(7245):442-445.
268. Cost GJ, Freyvert Y, Vafiadis A, Santiago Y, Miller JC, Rebar E, Collingwood TN, Snowden A, & Gregory PD (2010) BAK and BAX deletion using zinc-finger nucleases yields apoptosis-resistant CHO cells. *Biotechnol Bioeng* 105(2):330-340.
269. Lombardo A, Genovese P, Beausejour CM, Colleoni S, Lee YL, Kim KA, Ando D, Urnov FD, Galli C, Gregory PD, Holmes MC, & Naldini L (2007) Gene editing in human stem cells using zinc finger nucleases and integrase-defective lentiviral vector delivery. *Nat Biotechnol* 25(11):1298-1306.
270. Perez EE, Wang J, Miller JC, Jouvenot Y, Kim KA, Liu O, Wang N, Lee G, Bartsevich VV, Lee YL, Guschin DY, Rupniewski I, Waite AJ, Carpenito C, Carroll RG, Orange JS, Urnov FD, Rebar EJ, Ando D, Gregory PD, Riley JL, Holmes MC, & June CH (2008) Establishment of HIV-1 resistance in CD4+ T cells by genome editing using zinc-finger nucleases. *Nat Biotechnol* 26(7):808-816.
271. Cradick TJ, Keck K, Bradshaw S, Jamieson AC, & McCaffrey AP (2010) Zinc-finger Nucleases as a Novel Therapeutic Strategy for Targeting Hepatitis B Virus DNAs. *Mol Ther* 18(5):947-954.
272. Smith J, Berg JM, & Chandrasegaran S (1999) A detailed study of the substrate specificity of a chimeric restriction enzyme. *Nucleic Acids Res* 27(2):674-681.
273. Smith J, Bibikova M, Whitby FG, Reddy AR, Chandrasegaran S, & Carroll D (2000) Requirements for double-strand cleavage by chimeric restriction enzymes with zinc finger DNA-recognition domains. *Nucleic Acids Res* 28(17):3361-3369.
274. Bitinaite J, Wah DA, Aggarwal AK, & Schildkraut I (1998) FokI dimerization is required for DNA cleavage. *Proc Natl Acad Sci U S A* 95(18):10570-10575.
275. Bakhrat A, Jurica MS, Stoddard BL, & Raveh D (2004) Homology modeling and mutational analysis of Ho endonuclease of yeast. *Genetics* 166(2):721-728.
276. Nahon E & Raveh D (1998) Targeting a truncated Ho-endonuclease of yeast to novel DNA sites with foreign zinc fingers. *Nucleic Acids Res* 26(5):1233-1239.
277. Mineta Y, Okamoto T, Takenaka K, Doi N, Aoyama Y, & Sera T (2008) Enhanced cleavage of double-stranded DNA by artificial zinc-finger nuclease sandwiched between two zinc-finger proteins. *Biochemistry* 47(47):12257-12259.

278. Mineta Y, Okamoto T, Takenaka K, Doi N, Aoyama Y, & Sera T (2009) Multiple-turnover cleavage of double-stranded DNA by sandwiched zinc-finger nuclease. *Nucleic Acids Symp Ser (Oxf)* (53):279-280.
279. Minczuk M, Papworth MA, Miller JC, Murphy MP, & Klug A (2008) Development of a single-chain, quasi-dimeric zinc-finger nuclease for the selective degradation of mutated human mitochondrial DNA. *Nucleic Acids Res* 36(12):3926-3938.
280. Liu PQ, Rebar EJ, Zhang L, Liu Q, Jamieson AC, Liang Y, Qi H, Li PX, Chen B, Mendel MC, Zhong X, Lee YL, Eisenberg SP, Spratt SK, Case CC, & Wolffe AP (2001) Regulation of an endogenous locus using a panel of designed zinc finger proteins targeted to accessible chromatin regions. Activation of vascular endothelial growth factor A. *J Biol Chem* 276(14):11323-11334.
281. Rebar EJ, Huang Y, Hickey R, Nath AK, Meoli D, Nath S, Chen B, Xu L, Liang Y, Jamieson AC, Zhang L, Spratt SK, Case CC, Wolffe A, & Giordano FJ (2002) Induction of angiogenesis in a mouse model using engineered transcription factors. *Nat Med* 8(12):1427-1432.
282. Snowden AW, Zhang L, Urnov F, Dent C, Jouvenot Y, Zhong X, Rebar EJ, Jamieson AC, Zhang HS, Tan S, Case CC, Pabo CO, Wolffe AP, & Gregory PD (2003) Repression of vascular endothelial growth factor A in glioblastoma cells using engineered zinc finger transcription factors. *Cancer Res* 63(24):8968-8976.
283. Yu J, Lei L, Liang Y, Hinh L, Hickey RP, Huang Y, Liu D, Yeh JL, Rebar E, Case C, Spratt K, Sessa WC, & Giordano FJ (2006) An engineered VEGF-activating zinc finger protein transcription factor improves blood flow and limb salvage in advanced-age mice. *FASEB J* 20(3):479-481.
284. Dai Q, Huang J, Klitzman B, Dong C, Goldschmidt-Clermont PJ, March KL, Rokovich J, Johnstone B, Rebar EJ, Spratt SK, Case CC, Kontos CD, & Annex BH (2004) Engineered zinc finger-activating vascular endothelial growth factor transcription factor plasmid DNA induces therapeutic angiogenesis in rabbits with hindlimb ischemia. *Circulation* 110(16):2467-2475.
285. Beerli RR, Segal DJ, Dreier B, & Barbas CF, 3rd (1998) Toward controlling gene expression at will: specific regulation of the erbB-2/HER-2 promoter by using polydactyl zinc finger proteins constructed from modular building blocks. *Proc Natl Acad Sci U S A* 95(25):14628-14633.
286. Lund CV, Popkov M, Magnenat L, & Barbas CF, 3rd (2005) Zinc finger transcription factors designed for bispecific coregulation of ErbB2 and ErbB3 receptors: insights into ErbB receptor biology. *Mol Cell Biol* 25(20):9082-9091.
287. Gommans WM, McLaughlin PM, Lindhout BI, Segal DJ, Wiegman DJ, Haisma HJ, van der Zaal BJ, & Rots MG (2007) Engineering zinc finger protein transcription factors to downregulate the epithelial glycoprotein-2 promoter as a novel anti-cancer treatment. *Mol Carcinog* 46(5):391-401.
288. Magnenat L, Blancafort P, & Barbas CF, 3rd (2004) In vivo selection of combinatorial libraries and designed affinity maturation of polydactyl zinc

finger transcription factors for ICAM-1 provides new insights into gene regulation. *J Mol Biol* 341(3):635-649.

289. Choo Y, Sanchez-Garcia I, & Klug A (1994) In vivo repression by a site-specific DNA-binding protein designed against an oncogenic sequence. *Nature* 372(6507):642-645.
290. Graslund T, Li X, Magnenat L, Popkov M, & Barbas CF, 3rd (2005) Exploring strategies for the design of artificial transcription factors: targeting sites proximal to known regulatory regions for the induction of gamma-globin expression and the treatment of sickle cell disease. *J Biol Chem* 280(5):3707-3714.
291. Lu Y, Tian C, Danialou G, Gilbert R, Petrof BJ, Karpati G, & Nalbantoglu J (2008) Targeting artificial transcription factors to the utrophin A promoter: effects on dystrophic pathology and muscle function. *J Biol Chem* 283(50):34720-34727.

2 Chapter 2: DHBV-specific ZFP production and *in vitro* assessment

2.1 Introduction

ZFPs were designed with the purpose of specifically binding DHBV genomic sequences within the context of duck or chicken nuclei, with the ability to discriminate between viral and host genomic sequences. Binding of ZFPs to the viral genome was expected to inhibit the binding of transcription factors required for the viral life cycle, and would also potentially prevent the movement of the transcriptional machinery along the viral genome. Since DHBV is known to have a chromosome structure with the presence of histones on the viral episome (1), it was important to consider targeting the ZFPs to 'accessible' regions of the DHBV genome; that is, to regions where other proteins are known to have access to the DNA through the chromatin structure. Promoters and enhancers are regions that commonly bind a variety of transcription factors. In fact, DHBV has one enhancer (dEnI) and three promoters (precore promoter, preS promoter and the S promoter), all of which interact with protein-binding partners (PBP). The PBPs of the DHBV enhancer have been extensively studied, thus I chose to target the ZFPs to this region, which spans nucleotides 2170 to 2361. In addition, the dEnI plays an integral role in enhancing the transcription from both the core promoter and the S promoter (2) and is located in a region shared by all three DHBV transcripts, making it an ideal target region. Three different transcription factors are known to bind within this region, including hepatocyte nuclear factor 1 (HNF-1), HNF-3 and CCAAT/enhancer binding protein (C/EBP). Since HNF-1 is essential for enhancer activity (3-5), prevention of its binding by competition with a bound ZFP is an additional benefit of targeting this region.

Two main types of ZFPs were designed: those that bind an 18-bp sequence (18-mers) and those that bind a 9-bp sequence (9-mers). The 9-mers were to be fused to the endonuclease domain of *FokI* to form ZFNs. *FokI* functions independently from its DNA binding domain and requires dimerization of the endonuclease domain in order to have activity. By replacing the endogenous DNA binding

domain with the designed ZFP 9-mers, an endonuclease with specificity for the DHBV genome would be created, wherein the ZFP-FokI chimeras would act as heterodimers. In both the 18-mer design and the heterodimer 9-mer design, a total of 18-bps of sequence are recognized, which statistically represents a unique sequence within the human genome. By targeting a unique sequence, the ZFPs can therefore discriminate between viral and host genomes, in line with the goals of the project.

The designed ZFPs were examined by *in vitro* kinetic experiments to determine their binding characteristics. Subsequently, their ability to impact the DHBV viral life cycle was examined in tissue culture cells by over-expressing the DHBV-specific ZFPs. These topics will be discussed in the following sections.

2.2 Materials and Methods

2.2.1 Design of DHBV-specific ZFPs

ZFPs were designed to target DHBV Canada isolate (AF047045) using the program 'Zinc Finger Tools' (http://www.scripps.edu/mb/barbas/zfdesign /zfdesignhome.php) (6). To generate the amino acid sequence for the ZFPs, the Zinc Finger Tools program models each zinc finger repeat as two invariant chain sequences (the amino- and carboxy-terminal backbones) surrounding the variant helix whose sequence depends on the triplet of DNA (6). The linker sequence (TGEKP) (7) is placed between successive zinc finger repeats and the entire construct is flanked by the amino- (LEPGEKP) and carboxy-terminal (TGKKTS) fixed sequences (6). The invariant chain sequences and the fixed terminal sequences are based on the framework of the Sp1C ZFP (6). The invariant chains consist of the carboxy-terminal portion of the α-helix (HQRTH) and the amino-terminal backbone (YKCPECGKSFS) that contains the two β–sheets (underlined) (see Appendix B for entire sequence) (6). ZFPs were designed with flanking *XhoI* (5') and *SpeI* (3') restriction endonuclease sites.

All ZFPs were designed to bind to target sites within the enhancer region of DHBV (2170-2361) (Figure 2.2). Three ZFPs targeting 18-bp sequences (18-mers) were designed to function as monomers (ZFP18A, ZFP18B, ZFP18C). Two pairs of ZFPs targeting 9-bp sequences each (9-mers) were designed to function as heterodimers (ZFP9A1 and ZFP9A2, ZFP9B1 and ZFP9B2). The zinc finger domains of the experimental ZFP were scrambled to produce control ZFPs. Thus for ZFP18A, ZFP18B and ZFP18C, 18-mer controls were produced called ZFP18cA, ZFP18cB and ZFP18cC. Similarly for ZFP9A1, ZFP9A2, ZFP9B1 and ZFP9B2, respective controls were ZFP9cA1, ZFP9cA2, ZFP9cB1 and ZFP9cB2. ZFP target sites and the corresponding zinc finger amino acid sequences that mediate binding are shown in Tables 2.1 & 2.2. The entire nucleotide and amino acid sequences for each designed ZFP can be found in Appendix B.

2.2.2 Synthesis of DHBV-specific ZFPs

ZFPs were optimized for codon usage by the Pekin duck (*Anas platyrhynchos*) using a database from Blue Heron Biotechnology (Bothell ,WA), then synthesized and cloned into pUC19 vectors by Blue Heron Biotechnology. The ZFPs were produced in *cis*-formation, such that ZFP18A, ZFP18B and ZFP18C were within one vector (pUC19-ZFP18), ZFP18cA, ZFP18cB and ZFP18cC were within another vector (pUC19-ZFPc18), ZFP9A1, ZFP9A2, ZFP9B1 and ZFP9B2 were within another vector (pUC19-ZFP9) and ZFP9cA1, ZFP9cA2, ZFP9cB1 and ZFP9cB2 were within another vector (pUC19-ZFPc9).

ZFP Name	Putative DNA Targets		Finger Designs [b]
	Sequence 5'-3' [a]	Subsites 5'-3' [b]	-1 1 2 3 4 5 6
ZFP18A	GCCAAGATAATGATTAAAc	GCCa	DCRDLAR
		AAGa	RKDNLKN
		ATAa	QKSSLIA
		ATGa	RRDELNV
		ATTa	HKNALQN
		AAAc	QRANLRA
ZFP18B	ATGGCAAACAAAAGTTGAa	ATGg	RRDELNV
		GCAa	QSGDLRR
		AACa	DSGNLRV
		AAAa	QRANLRA
		AGTt	HRTTLTN
		TGAa	QAGHLAS
ZFP18C	ATAAGAGACAGCGCGGTTt	ATAa	QKSSLIA
		AGAg	QLAHLRA
		GACa	DPGNLVR
		AGCg	ERSHLRE
		GCGg	RSDDLVR
		GTTt	TSGSLVR
ZFP9A1	AGAGATATAc	AGAg	QLAHLRA
		GATa	TSGNLVR
		ATAc	QKSSLIA
ZFP9A2	AAAAGCAAAc	AAAa	QRANLRA
		AGCa	ERSHLRE
		AAAc	QRANLRA
ZFP9B1	ATAATGATTa	ATAa	QKSSLIA
		ATGa	RRDELNV
		ATTa	HKNALQN
ZFP9B2	AACAAGACAt	AACa	DSGNLRV
		AAGa	RKDNLKN
		ACAt	SPADLTR

Table 2.1 - DNA binding sites and corresponding amino acid sequences of DHBV-specific experimental ZFPs.

[a] The entire DNA binding site sequence is shown from 5' to 3'.

[b] Each subsite is shown with its corresponding zinc finger amino acid sequence displayed, with amino acid positions from -1 up to +6 representing the amino acids of the alpha helix that make site specific contacts with the DNA. The 3' base pair of the DNA subsite (small case) makes minor interactions with the alpha helix of the zinc finger (Adapted from (8)).

ZFP Name	Putative DNA Targets		Finger Designs [b]
	Sequence 5'-3' [a]	Subsites 5'-3' [b]	-1 1 2 3 4 5 6
ZFP18cA	ATAAAAATGAAGGCCATTa	ATAa	QKSSLIA
		AAAa	QRANLRA
		ATGa	RRDELNV
		AAGg	RKDNLKN
		GCCa	DCRDLAR
		ATTa	HKNALQN
ZFP18cB	AACTGAAAAGCAATGAGTt	AACt	DSGNLRV
		TGAa	QAGHLAS
		AAAg	QRANLRA
		GCAa	QSGDLRR
		ATGa	RRDELNV
		AGTt	HRTTLTN
ZFP18cC	GACGTTAGCAGAATAGCGg	GACg	DPGNLVR
		GTTa	TSGSLVR
		AGCa	ERSHLRE
		AGAa	QLAHLRA
		ATAg	QKSSLIA
		GCGg	RSDDLVR
ZFP9cA1	ATAAGAGATa	ATAa	QKSSLIA
		AGAg	QLAHLRA
		GATa	TSGNLVR
ZFP9cA2	AAAAAAAGCa	AAAa	QRANLRA
		AAAa	QRANLRA
		AGCa	ERSHLRE
ZFP9cB1	ATTATAATGa	ATTa	HKNALQN
		ATAa	QKSSLIA
		ATGa	RRDELNV
ZFP9cB2	ACAAACAAGa	ACAa	SPADLTR
		AACa	DSGNLRV
		AAGa	RKDNLKN

Table 2.2 - DNA binding sites and corresponding amino acid sequences of DHBV-specific control ZFPs.

[a] The entire DNA binding site sequence is shown from 5' to 3'.

[b] Each subsite is shown with its corresponding zinc finger amino acid sequence displayed, with amino acid positions from -1 up to +6 representing the amino acids of the alpha helix that make site specific contacts with the DNA. The 3' base pair of the DNA subsite (small case) makes minor interactions with the alpha helix of the zinc finger (Adapted from (8)).

2.2.3 Cloning of DHBV-specific ZFPs into a bacterial expression vector

The backbone vector pMALc-gg1 (map in Appendix A) was received from Dr. Carlos Barbas III at the Scripps Research Institute (La Jolla, CA). pMALc-gg1 and the pUC19-ZFP plasmids were doubly digested with 15 units each of *XhoI* (Invitrogen 15231-012) and *SpeI* (Invitrogen 15443-013) in New England Biolabs (NEB) Buffer 4 with 1X bovine serum albumin (BSA) for 3 hours at 37°C. The restriction digests were run in their entirety on a 0.8% (w/v) agarose gel containing 1.5-ng/μL of ethidium bromide (EtBr) and visualized using ultraviolet (UV) light and the G:box Gel Documentation System (Syngene). The resulting backbone and inserts (546-bp: 18-mers and 294-bp: 9-mers) were excised from the agarose gel using a scalpel blade and the DNA was isolated using the QIAquick Gel Extraction Kit (Qiagen 28706) according to the manufacturer's protocol. Briefly, samples were weighed then 3 volumes of Buffer QG were added to 1 volume of gel. Samples were incubated at 50°C for 10 minutes, with periodic inversion to facilitate melting. Once the agarose was melted, 1 volume of isopropanol was added, then samples were loaded onto the provided column and centrifuged for 30 seconds at 14,000-rpm in a micro-centrifuge (Beckman Coulter Microfuge® 18 Centrifuge). Columns were washed twice with Buffer PE by adding 750-μL to the column, centrifuging for 30 seconds at 14,000-rpm, and discarding the flow-through. The columns were spun an additional time for 30 seconds at 14,000-rpm without the addition of liquid to the column, to ensure complete removal of alcohol traces from the DNA. DNA was then eluted with the addition of 30-μL of dH_2O by adding the dH_2O to the filter, incubating for 2 minutes and centrifuging for 1 minute at 12,000-rpm.

The purified inserts were ligated to the pMALc backbone in a 10-μL reaction containing 6-μL of insert DNA, 2-μL of 5X T4 DNA Ligase Buffer, 1-μL of the pMALc backbone and 1-μL (1 unit) of T4 DNA Ligase (Invitrogen 15224-017). Control reactions substituted 6-μL of water for insert. The ligations were incubated overnight at 16°C. The following day, 1-μL of the ligation reaction was transformed into 100-μL of chemically competent TOP10 *Escherichia coli*

(*E.coli*) (Invitrogen C664-11) by incubating the DNA mix with the TOP10 cells on ice for 30 minutes, followed by heat-shock at 42°C for 45 seconds. Next, 900-μL of Luria Broth (LB) was added to the cells, which were allowed to recover by incubation at 37°C for 1 hour with slight agitation. During this wait, two plates of LB/ampicillin (Amp: 100-μg/mL) were spread with 40-μL of X-Gal (bromo-chloro-indolyl-galactopyranoside at 20-mg/mL in dimethylformamide) and 40-μL of IPTG (isopropyl β-D-1-thiogalactopyranoside at 0.1-M stock in dH_2O) and allowed to absorb for 30 minutes. After the 1-hour incubation time, the transformed cells were spread plated onto the plates using aseptic technique. One plate was spread with 100-μL of the undiluted transformation mixture then the remaining transformation mixture was concentrated by centrifugation for 30 seconds at 14,000-rpm. All but 100-μL of the supernatant was aspirated and the pellet was re-suspended by vortexing before spreading it all upon the second LB/Amp plate. Plates were incubated at 37°C overnight and isolated white colonies were used to inoculate 2-mL of liquid LB/Amp (100-μg/mL) cultures in 14-mL (17-mm x 100-mm) polypropylene culture tubes (Simport T406-2A), which were incubated at 37°C overnight with agitation.

Miniprep DNA was isolated using the QIAprep Spin Miniprep Kit (Qiagen 27106) according to the manufacturer's protocol. Specifically, 1-mL of liquid culture was transferred to a 1.7-mL microcentrifuge tube and bacteria were pelleted by centrifugation for 30 seconds at 14,000-rpm. The supernatant was aspirated and the pellet was resuspended in 250-μL of Buffer P1 (plus RNase A) by vortexing. Cells were lysed by the addition of 250-μL of Buffer P2 and gentle inversion to mix. Finally, the sample was neutralized with the addition of 350-μL of Buffer N3 and inverted to mix. The sample was centrifuged for 10 minutes at 14,000-rpm to pellet the cellular debris and precipitated sodium dodecyl sulfate (SDS), and the supernatant subsequently transferred to the provided column. The column was centrifuged for 30 seconds at 14,000-rpm, and the flow-through was discarded. The column was washed twice with 750-μL of Buffer PE, each wash

followed by centrifugation for 30 seconds at 14,000-rpm and discard of the flow-through, finished up with one last spin to remove traces of ethanol from the column. The plasmid DNA was eluted by the addition of 30-µL of dH_2O to the column and letting it sit for 2 minutes before centrifuging for 1 minute at 12,000-rpm. Positive clones were confirmed by restriction digest of 5-µL of miniprep DNA with *XhoI* and *SpeI* as described above, followed by visualization using EtBr-agarose gel electrophoresis and UV light. The identity of the insert was determined by sequencing positive clones at the DNA Core Service Lab (University of Alberta, Department of Biochemistry) using the M13/pUC primer (5'-CGCCAGGGTT TTCCCAGTCA CGAC-3').

2.2.4 Bacterial expression and purification of ZFPs

pMALc-ZFP constructs were transformed into chemically competent BL21(DE3) *E. coli* (NEB C2527H) as follows: 100-µL of BL21(DE3) *E.coli* were thawed on ice, then 1.7-µL of 1.42-M β-mercaptoethanol (1/10 dilution of the stock, in dH_2O) was added and incubated for 10 minutes, with gentle flicking every 2 minutes. 50-ng of pMALc-ZFP DNA was added to the *E.coli* and incubated for 30 minutes on ice. During this time, Super Optimal Broth with Catabolite repression (SOC) media was prepared by adding 2-mL of 20% (w/v) glucose (filter sterilized) to 98-mL of Super Optimal Broth (SOB), and pre-warmed to 42°C. SOB was prepared ahead of time by combining 20-g tryptone, 5-g yeast extract and 0.5-g NaCl in 1-L of dH_2O, autoclaving the solution and subsequently adding 10-mL of filter sterilized 1-M $MgCl_2$ and 10-mL of filter sterilized 1-M $MgSO_4$. After 30 minutes, the *E.coli* were heat-shocked at 42°C for 45 seconds, then returned to ice for 2 minutes. 0.9-mL of the pre-warmed SOC was added to each transformation, and the *E.coli* allowed to recover at 37°C for 1 hour with gentle agitation. The entire transformation reaction (1-mL) was transferred into a 14-mL (17-mm x 100-mm) polypropylene culture tubes (Simport T406-2A) containing 2-mL of LB/Amp (100-µg/mL) and incubated at 37°C overnight with shaking.

The next day, 50-mL of Rich Broth in a baffled Erlenmeyer flask was inoculated with all of the overnight culture. Rich Broth was prepared by combining 10-g/L tryptone, 5-g/L yeast extract, 5-g/L NaCl and 2-g/L glucose, then autoclaving. Prior to use, 1-mL of filter sterilized 0.1-M $ZnCl_2$ (100-μM final concentration) and Amp (100-μg/mL final concentration) were added. The cultures were shaken at 250-rpm at room temperature (22 - 25°C) for approximately 4-hours, or until A_{600}~0.5. A sample (1-mL) was removed after 4-hours to monitor protein production (*uninduced cells*). This sample was centrifuged for 2-minutes at 14,000-rpm, then the supernatant was removed and the pellet re-suspended in 50-μL of SDS-PAGE loading buffer. After 4-hours, protein expression was induced by the addition of IPTG to a final concentration of 0.3-mM using a 0.1-M stock. The cultures continued to shake at 250-rpm at room temperature for a further 2-hours. 100-μL of culture supernatant was collected, centrifuged as before and the pellet re-suspended in 100-μL of SDS-PAGE loading buffer (*induced cells*). The cells were harvested by centrifugation for 10-minutes at 4000x*g* in a Beckman Coulter Avanti J-20XP Centrifuge. The supernatant was discarded and the pellet re-suspended in 5-mL of Column Buffer (10-mM Tris-HCl pH 7.4, 200-mM NaCl, 1-mM EDTA, 1-mM sodium azide and 1-mM β-mercaptoethanol. Store at 4°C). The suspensions were transferred to 15-mL tubes and frozen overnight at -20°C. The next day, the tubes were thawed in cold water, then place in an ice-water bath and sonicated in pulses of 15-seconds for a total sonication time of 2-minutes using the Mandell Sonicator Ultrasonic Processor XL. The samples were transferred to 15-mL screw-cap centrifuge tubes and centrifuged in a Beckman Coulter Avanti J-20XP Centrifuge for 20 minutes at 9000x*g* at 4°C. The supernatant was decanted and retained, and a 5-μL sample was mixed with 5-μL of SDS-PAGE loading buffer for analysis (*crude extract*). A sample was also obtained from the pellet by re-suspending it in 5-mL of Column Buffer and mixing 5-μL with 5-μL of SDS-PAGE loading buffer (*insoluble material*). The ZFP-MBP fusion protein was then isolated from the crude extract by purification on an amylose column.

All of the following steps were performed at 4°C. 200-µL of amylose resin (NEB E8021L) in 70% (v/v) ethanol was added to 0.8 x 0.4-cm chromatography columns (BioRad PolyPrep Chromatography Columns 731-1550). The amylose resin was washed 3 – 4 times with Column Buffer by filling the column to the top and allowing it to flow through by gravity. The crude extract was added to the column and allowed to flow through by gravity. The column was washed 3-4 times with Column Buffer as before. The ZFP-MBP fusion protein was eluted by the addition of 3-mL of Elution Buffer (Column Buffer plus 10-mM maltose and 15% (v/v) glycerol, autoclaved). Aliquots of 500 – 600-µL were collected from the column, and in general, fractions 2-4 were combined and assayed by the MicroBCA Protein Assay (Pierce 23235). Confirmation of the presence of eluted protein was performed by running 10-µL of each fraction, plus 5-µL of SDS-PAGE loading buffer, on a 10% SDS-polyacrylamide gel (see Section 2.2.21 for details) and staining 30-minutes with warm Coomassie Blue stain (0.25% (w/v) Coomassie R250 in 50% (v/v) methanol and 10% (v/v) acetic acid), followed by overnight destaining with Coomassie Blue destain (50% (v/v) methanol and 10% (v/v) acetic acid). Pictures were obtained by UV light exposure on a NovaGlo Visible light converter in the G:box Gel Documentation System. In addition, 5-µL of the eluate was mixed with 5-µL of SDS-PAGE loading buffer to complete the collection of samples throughout the procedure, and were also run on a 10% SDS-polyacrylamide gel, followed by staining by Coomassie blue. The eluate was aliquoted at 100-µL and stored at -80°C.

2.2.5 Electrophoretic mobility shift assay: Determination of the apparent equilibrium dissociation constant

The oligonucleotide sequences for the electrophoretic mobility shift assays (EMSA) can be found in Table 2.3 & 2.4. Each DNA recognition region was flanked by a 6-nt sequence (AGTACT) to increase stability of the annealed oligonucleotide and provide a larger backbone for ZFP binding. The top and bottom strands were annealed together at a concentration of 10-µM each in 10-

mM Tris-HCl pH 7.5, 10-mM $MgCl_2$ and 50-mM NaCl by boiling for 5 minutes, followed by a slow cool to room temperature.

Name	Oligonucleotide sequence [a, b]
18A.top	*AGTACT* GCCAAGATAATGATTAAA *AGTACT*
18A.bottom	*AGTACT* TTTAATCATTATCTTGGC *AGTACT*
18B.top	*AGTACT* ATGGCAAACAAAAGTTGA *AGTACT*
18B.bottom	*AGTACT* TCAACTTTTGTTTGCCAT *AGTACT*
18C.top	*AGTACT* ATAAGAGACAGCGCGGTT *AGTACT*
18C.bottom	*AGTACT* AACCGCGCTGTCTCTTAT *AGTACT*
9A1.top	*AGTACT* AGAGATATA *AGTACT*
9A1.bottom	*AGTACT* TATATCTCT *AGTACT*
9A2.top	*AGTACT* AAAAGCAAA *AGTACT*
9A2.bottom	*AGTACT* TTTGCTTTT *AGTACT*
9B1.top	*AGTACT* ATAATGATT *AGTACT*
9B1.bottom	*AGTACT* AATCATTAT *AGTACT*
9B2.top	*AGTACT* AACAAGACA *AGTACT*
9B2.bottom	*AGTACT* TGTCTTGTT *AGTACT*

Table 2.3 - DHBV-specific ZFP oligonucleotide sequences for EMSA and SPR.
[a] The sequences are shown from 5' to 3'.
[b] The ZFP-specific binding region is shown in straight font and the stabilizing nucleotides are shown in italics.

Name	Oligonucleotide sequence [a, b]
18cA.top	*AGTACT* ATAAAAATGAAGGCCATT *AGTACT*
18cA.bottom	*AGTACT* AATGGCCTTCATTTTTAT *AGTACT*
18cB.top	*AGTACT* AACTGAAAAGCAATGAGT *AGTACT*
18cB.bottom	*AGTACT* ACTCATTGCTTTTCAGTT *AGTACT*
18cC.top	*AGTACT* GACGTTAGCAGAATAGCG *AGTACT*
18cC.bottom	*AGTACT* CGCTATTCTGCTAACGTC *AGTACT*

Table 2.4 - DHBV-specific control ZFP oligonucleotide sequences for EMSA.
[a] The sequences are shown from 5' to 3'.
[b] The ZFP-specific binding region is shown in straight font and the stabilizing nucleotides are shown in italics.

Double stranded DNA oligonucleotides were added to a final concentration of 2.5-µM (ZFP18A, ZFP18B, ZFP18C, ZFP18cA, ZFP18cB, ZFP9A2, ZFP9B2) or 1-µM (ZFP9A1, ZFP9B1) with varying amounts of purified ZFP-MBP fusion proteins starting at 150-nM and serially diluted 1 in 2 down to 9.5-nM (9, 10). Reactions were in a total volume of 30-µL in Gel Shift Buffer (25-mM Tris-HCl pH 8, 100-mM NaCl, 2-mM DTT, 100-µM $ZnCl_2$, 10% (v/v) glycerol, 50-µg/mL BSA, 4-µg/mL polyI:C and 0.01% (w/v) bromophenol blue). Importantly, ZFP-MBP fusion proteins were added to the mixture last. A control sample contained dsDNA oligonucleotides without ZFP-MBP added. Reactions were incubated for 1 hour at room temperature. During this time, a 7% non-denaturing polyacrylamide gel was prepared as follows: 3.5-mL of 40% acrylamide/bis-acrylamide (19:1), 4-mL of 5X TBE (0.45-M Tris base, 0.45-M boric acid, 10-mM EDTA), 140-µL 10% (w/v) ammonium persulfate and 12.46-mL dH_2O were combined in a 50-mL tube. Because these gels shrink a great deal, 2-mL of the mixture was removed and set aside in a separate tube. 8-µL of TEMED (N,N,N,N'-Tetramethyl-ethylenediamine) was added and the mixture was poured into two mini-gel cast with 1.5-mm spacers and well combs. The gels were allowed to set for 30-minutes, then 2-µL of TEMED was added to the extra 2-mL of gel mixture, which was subsequently used to fill up the top of the gels. After another 15-minutes to set, the gels were placed into the gel box and pre-run for 30-minutes at 100-V at 4°C. Reactions were run on the 7% non-denaturing polyacrylamide gels at 100-V for 1 hour at 4°C, then the gel was removed from the glass, the wells were cut off, and the entire gel was stained while protected from light for 20-minutes at room temperature, using 5-µL of SYBR-Green (Molecular Probes EMSA kit; Invitrogen E33075) diluted in 50-mL of 1X TBE. The gels were then rinsed twice with 150-mL of dH_2O before being scanned using the Fujifilm FLA-5100 phosphorimager on the "1 laser/1 image" setting with excitation at 488-nm and emission at 520-nm. Gels were subsequently stained with SYPRO-Ruby stain (Molecular Probes EMSA kit; Invitrogen E33075) for 3-hours at room temperature while protected from light. After one rinse with 150-mL of dH_2O, gels were destained in 10% (v/v) methanol, 7% (v/v) acetic acid for

1 hour at room temperature. Lastly, one more rinse with 150-mL of dH_2O preceded scanning by the Fujifilm FLA-1500 phosphorimager on the "1 laser/1 image" setting with excitation at 488-nm and emission at 610-nm. EMSAs were quantified using Fujifilm ImageGauge v4.22 (2003) software. Non-linear regression plots were produced from this data using the program Enzyme Kinetics v1.11 (Trinity Software).

2.2.6 EMSA: Determination of specificity for target sequence

DsDNA oligonucleotides were prepared as in Section 2.2.5. The sequences of the oligonucleotides can be found in Table 2.3. The dsDNA oligonucleotides were made into radioactive ^{32}P-probes using T4 polynucleotide kinase (Invitrogen 18004-010) by adding the following to a 1.7-mL microcentrifuge tube, in this order: 5-pmol dsDNA oligonucleotide, 5-µL 5X Forward Reaction Buffer, dH_2O to 21.5-µL, 1-µL (10 units) T4 polynucleotide kinase and 2.5-µL (25-µCi) [γ-^{32}P]dATP. These were mixed gently and centrifuged briefly, then incubated 10 minutes at 37°C. The reaction was heat inactivated for 10 minutes at 65°C. Unincorporated [γ-^{32}P]dATP was removed using the QIAquick Nucleotide Removal Kit (Qiagen 28304) (10). Specifically, 10 volumes of Buffer PN was added to the reaction mix then transferred to a QIAquick spin column. The column was centrifuged for 1 minute at 6000-rpm. The flow through was discarded in the liquid radioactive waste container then two washes of 500-µL each were applied to the column, followed by centrifugation for 1 minute at 6000-rpm. After discarding the flow through in the liquid radioactive waste container, the column was centrifuged one more time for 1 minute at 14,000-rpm, to remove all traces of alcohol. The DNA was eluted by adding 50-µL of dH_2O to the column, letting it stand for 1 minute, then centrifuging for 2 minutes at 12,000-rpm. The probe activity was determined by spotting a 1:10 dilution on a DE81 filter paper (Whatman Ion Exchange Paper 3658324), placing it in a scintillation vial, adding 5-mL of EcoLite Scintillation Fluid (882475) and measuring on the Beckman LS6000TA liquid scintillator.

In a total volume of 30-µL in Gel Shift Buffer, 1-µL of [γ-^{32}P]-labeled probe with a count of 10,000-cpm/µL was added. Next, 5X, 10X or 50X the amount of probe was added as unlabeled oligonucleotide of the same sequence as the probe. Controls included no addition of unlabeled oligonucleotide or addition of 50X unlabeled non-specific oligonucleotide. The non-specific oligonucleotides used were one of the oligonucleotides containing the target site for a different ZFP. Lastly, 150-nM of ZFP was added to the reaction mixture and the reaction was allowed to proceed for 1 hour at room temperature. During this incubation time, a 7% non-denaturing polyacrylamide gel was prepared and pre-run, as described in Section 2.2.5. Samples were loaded on the gels and run at 100-V for 1 hour at 4°C. Once the run was completed, the gel was removed from the glass plates and the wells cut off with a scalpel. The gel was sealed inside a plastic bag and exposed to an image plate overnight at room temperature. The image plate was scanned using the Fujifilm FLA-5100 phosphorimager.

2.2.7 Surface Plasmon resonance for DHBV-specific ZFPs

Surface Plasmon resonance (SPR) was performed using BIAcore technology, which measures real-time interactions between a ligand anchored to a detection surface and an analyte that flows over the detection surface. ZFPs were dialyzed with 1X HBS-EP (Hank's Balanced Salts plus 3-mM EDTA and 0.005% (v/v) Surfactant P20) (BIAcore BR-1001-88) overnight at 4°C using 10-mm standard cellulose dialysis tubing (Spectrapor 132697) with molecular weight cut-off of 12,000 – 14,000 Da. 1X HBS-EP was used as running and sample buffers. All solutions were filtered and degassed before use, and protein samples were centrifuged at 14,000-rpm for 5 minutes to remove any precipitates. Oligonucleotides were produced by Operon Biotechnologies (Huntsville, AL) and were biotinylated at the 5' end of the top strand only. The sequences for the oligonucleotides can be found in Table 2.3. Biotinylated oligonucleotides were annealed to the bottom oligonucleotide strands at 10-µM each in 10-mM $MgCl_2$ by boiling for 5 minutes, followed by a slow cool to room temperature. The biotinylated dsDNA ligands were then coupled to the Sensor Chip SA

(streptavidin-coated) (BIAcore BR-1003-98) on the BIAcore 3000 using manual inject mode. 50-nM solutions of biotinylated oligonucleotides were injected onto one flow cell at a rate of 5-μL/min until the calculated R_L (immobilization level) was reached. R_L is calculated as follows:

$$R_L = R_{MAX} (1/Sm) (MW_L/MW_A)$$

where R_{MAX} = set at 100 resonance units (RU) for kinetic analysis

Sm = stoichiometry of binding (1:1 for ZFP:DNA)

MW_L = molecular weight of ligand (20-kDa for biotinylated-DNA)

MW_A = molecular weight of analyte (19-kDa for DHBV-specific 18-mers, 21-kDa for HBV-specific 18-mers, 11-kDa for all 9-mers)

The calculated and actual immobilization levels for all the biotinylated oligonucleotides can be found in Table 2.5. Free streptavidin sites were blocked on the flow cell and an unloaded reference flow cell by injecting 30-μL of 1-μM biotin at a rate of 30-μL/min. After coupling, 3 – 5 rounds of surface regeneration tests were carried out using ZFP concentrations around the dissociation concentration calculated by EMSA (Table 2.9) or at 128-nM for those ZFPs whose dissociation constant was not calculated by EMSA (ZFP9A2, ZFP9B1, ZFP9B2). 30-μL of ZFP was injected at 30-μL/min, followed by 1 minute of 1X HBS-EP and 30-μL of 0.5% (w/v) SDS at 30-μL/min to remove the bound ZFP. Once baseline remained constant after regeneration tests, kinetic analysis with direct binding was carried out using ZFP concentrations ranging from 0.1X to 10X the dissociation constant (in doubling dilutions) for those ZFPs whose dissociation constant were calculated by EMSA (Table 2.9) or ranging from 1-nM to 256-nM (ZFP9A2), 1-nM to 512-nM (ZFP9B1) or 1-nM to 940-nM (ZFP9B2). The latter ranges were chosen to include as high a concentration as possible at the top end of the range, which was limited by the stock concentration. Samples were measured from low to high concentrations with a flow rate of 30-μL/min, an injection time of 3 minutes and a dissociation time of 15 minutes. Regeneration between concentrations was completed with a single 30-μL injection of 0.5%

(w/v) SDS at a flow rate of 30-µL/min, followed by 5 minute stabilization time between runs. Bulk shift was accounted for by subtracting the signal from the reference flow cell. Kinetic analysis was done on the BIAeval software program and curves were fit to a 1:1 binding with drifting baseline model, except for ZFP9B2, which fit a 1:1 Langmuir binding model because the baseline did not drift. The general equation for the BIAcore kinetic model is:

$$dR/dT = k_aC(R_{MAX}-R) - k_dR$$

where dR/dT = the change in binding over time (RU)

k_a = the association rate constant

k_d = the disassociation rate constant

C = the amount of ligand on the surface of the chip, which is constant

R_{MAX} = the total ligand loaded onto the chip

R = the amount of analyte binding to the chip surface at a given time

	Immobilization Level (R_L)	
Biotinylated-oligonucleotide	**Calculated**	**Actual**
ZFP18A	105 RU[a]	139 RU
ZFP18B	105 RU	158 RU
ZFP9A1	182 RU	181 RU
ZFP9A2	182 RU	80 RU[b]
ZFP9B1	182 RU	203 RU
ZFP9B2	182 RU	159 RU

Table 2.5 - Calculated versus actual immobilization levels of biotinylated-DNA oligonucleotides on Sensor Chips SA for SPR.
[a] Resonance units (RU).
[b] This chip could not be loaded more than this.

2.2.8 Cloning of ZFPs into eukaryotic expression vector

ZFPs were PCR amplified from pZFP18 (ZFP18A, ZFP18B), pZFPc18 (ZFP18cA, ZFP18cB, ZFP18cC) or pZFP9 (ZFP9A1, ZFP9A2, ZFP9B1, ZFP9B2) using the primers in Table 2.6. These primers added a *BamHI* restriction site, a simian virus 40 (SV40) nuclear localization signal, and a His_6 tag at the 5'

end of each ZFP, and an *EcoRI* restriction site and a *SpeI* restriction site (9-mers only) at the 3' end of each ZFP. The PCR reaction contained 1-μL of template plasmid, 1-μL of 10-mM dNTPs, 12.5 units recombinant *Taq* DNA Polymerase (Invitrogen 10342-053), 1.5-mM $MgCl_2$, 5-μL of 10X PCR Buffer (Invitrogen), 0.5-μM of each primer and dH_2O up to 50-μL. The reaction was annealed at 54°C, with an elongation time of 1 minute and 30 cycles. PCR products were separated on a 0.8% (w/v) agarose gel and cut out using a scalpel. DNA was recovered using the QIAquick Gel Extraction Kit as described in Section 2.2.3. PCR products were ligated to pCR4 using the TOPO TA cloning kit (Invitrogen K4530-20) by incubating 2-μL of PCR product with 0.5-μL of vector and 0.5-μL of salt solution for 1 hour at room temperature. The ligations were transformed into TOP10 *E.coli* as described in Section 2.2.3 and plated on LB/Amp plus X-Gal and IPTG. After overnight incubation at 37°C, positive (white) colonies were used to inoculate 2-mL LB/Amp mini-preps. DNA was isolated from the cultures the next day using the QIAprep Spin Miniprep Kit (Qiagen 27106), as described in Section 2.2.3. Clones were screened for positivity by *EcoRI* restriction digest, liberating the PCR insert. Positive clones were sequenced with the T7 primer (5'-TAATACGACT CACTATAGGG-3') to confirm the integrity of the ZFP sequence after PCR. Clones with no sequence changes were doubly digested with 10 units of *EcoRI* and 10 units of *BamHI* (Invitrogen 15201-023) in NEB Buffer 2 with 1X BSA for 1.5 hours at 37°C. The backbone, pcDNA3.1(+), was similarly digested. All digests were separated on 0.8% (w/v) agarose gels and the resulting backbone and inserts (546-bp: 18-mers and 294-bp: 9-mers) were excised using a scalpel. DNA was recovered using the QIAquick Gel Extraction Kit. The ZFPs were ligated to pcDNA3.1(+) in a 10-μL reaction containing 6-μL of insert DNA, 2-μL of 5X T4 DNA Ligase Buffer, 1-μL of the pcDNA3.1(+) backbone (diluted 1:10) and 1-μL (1 unit) of T4 DNA Ligase (Invitrogen 15224-017). Control reactions substituted 6-μL of water for insert. The ligations were incubated overnight at 16°C. The following day, 1-μL of the ligation reaction was transformed into chemically competent TOP10 *E.coli*, and plated on LB/Amp as described in Section 2.2.3. Isolated colonies were used to inoculate 2-mL

LB/Amp mini-preps, which were incubated overnight at 37°C with agitation. DNA was isolated using the QIAprep Spin Miniprep Kit, and positive clones were determined by restriction digest with *BamHI* and *EcoRI*, as described above. Positive clones were sequenced with the T7 primer.

Name	Primer sequence [a]
ZFP18A.fw	**GGATCC**ATGC ATCATCACCA TCACCAT*CCC AAGAAAAAGC GTAAGGTC*CT CGAACCCGGC GAAAAGCCTT AT[b]
ZFP18A.rv	**GAATTC**ACTT GTCTTCTTAC CTGTGTGG[c]
ZFP18B.fw	**GGATCC**ATGC ATCATCACCA TCACCAT*CCC AAGAAAAAGC GTAAGGTC*CT CGAACCAGGT GAAAAACCCT[b]
ZFP18B.rv	**GAATTC**TGAA GTCTTCTTTC CTGTGTGA[c]
ZFP9A1.fw	**GGATCC**ATGC ATCATCACCA TCACCAT*CCC AAGAAAAAGC GTAAGGTC*CT GGAGCCCGGT GAGAAGCCCT[b]
ZFP9A1.rv	**GAATTC***ACTA GT*GCTCGTCT TTTTACCTGT GTGT[c]
ZFP9A2.fw	**GGATCC**ATGC ATCATCACCA TCACCAT*CCC AAGAAAAAGC GTAAGGTC*TT GGAGCCCGGG GAGAAGCCCT AC[b]
ZFP9A2.rv	**GAATTC***ACTA GT*GCTGGTCT TTTTGCCTGT GTGT[c]
ZFP9B1.fw	**GGATCC**ATGC ATCATCACCA TCACCAT*CCC AAGAAAAAGC GTAAGGTC*CT CGAACCAGGA GAGAAGCCCT AT[b]
ZFP9B1.rv	**GAATTC***ACTA GT*AGAAGTCT TTTTACCTGT ATGAG[c]
ZFP9B2.fw	**GGATCC**ATGC ATCATCACCA TCACCAT*CCC AAGAAAAAGC GTAAGGTC*CT GGAGCCAGGT GAAAAGCCAT[b]
ZFP9B2.rv	**GAATTC***ACTA GT*AGTTGAGG TCTTCTTTCC AGTATG[c]
ZFP18cA.fw	**GGATCC**ATGC ATCATCACCA TCACCAT*CCC AAGAAAAAGC GTAAGGTC*CT GGAACCCGGC GAGAAAC[b]
ZFP18cA.rv	**GAATTC**GGAG GTCTTTTTTC CGGTGTG[c]

Table 2.6 - Primer sequences for cloning DHBV-specific ZFPs into a eukaryotic expression vector.

[a] Sequences are shown 5' to 3'.

[b] *BamHI* restriction site (**bold**), 6x histidine tag (underlined), SV40 nuclear localization signal (*italics*), unique ZFP sequence (plain text).

[c] *EcoRI* restriction site (**bold**), *SpeI* restriction site (*italics*), unique ZFP sequence (plain text).

2.2.9 Cloning of EGFP into pcDNA3.1(+)-ZFP plasmids

Enhanced green fluorescent protein (EGFP) was PCR amplified from pAdTrack-CMV using the primers EGFP.fw (5'-GAATTCGCCA CAATGGTGAG CAAGGGCGAG G-3') and EGFP.rv (5'-GTCTGACAGA ACATCAAAGA ACCC-3'). These primers add the restriction sites *EcoRI* at the 5' end and *NotI* at the 3' end of EGFP. The PCR reaction contained 1-μL of template plasmid, 1-μL of 10-mM dNTPs, 12.5 units recombinant *Taq* DNA Polymerase, 1.5-mM $MgCl_2$, 5-μL of 10X PCR Buffer, 0.5-μM of each primer and dH_2O up to 50-μL. The reaction was annealed at 54°C, with an elongation time of 1 minute and 30 cycles. The PCR product was ligated to pCR4 and transformed into TOP10 as described in Section 2.2.8. Positive clones were identified by *EcoRI* digest of mini-prep DNA isolated by the QIAprep Spin Miniprep Kit and sequencing with the T7 primer.

EGFP was then fused in frame to ZFPs in pcDNA3.1(+)-ZFP18A, ZFP18B, ZFP9A1, ZFP9A2, ZFP9B1, and ZFPB2 by double digestion with 10 units of *EcoRI* and 7.5 units of *NotI* (Invitrogen 15441-017) in NEB Buffer 3 with 1X BSA for 1.5 hours at 37°C. All digests were separated on 0.8% (w/v) agarose gels and the resulting pcDNA3.1(+)-ZFP backbones and EGFP insert were excised using a scalpel. DNA was recovered using the QIAquick Gel Extraction Kit. EGFP as ligated to each pcDNA3.1(+)-ZFP backbone in a 10-μL reaction containing 6-μL of insert DNA, 2-μL of 5X T4 DNA Ligase Buffer, 1-μL of the pcDNA3.1(+)-ZFP backbone (diluted 1 in 10) and 1-μL (1 unit) of T4 DNA Ligase. Control reactions substituted 6-μL of water for insert. EGFP was also ligated to pcDNA3.1(+) alone, without an accompanying ZFP. The ligations were incubated overnight at 16°C. The following day, 1-μL of the ligation reaction was transformed into chemically competent TOP10 *E.coli*, and plated on LB/Amp as described in Section 2.2.3. Isolated colonies were used to inoculate 2-mL LB/Amp mini-preps, which were incubated overnight at 37°C with agitation. DNA was isolated using the QIAprep Spin Miniprep Kit, and positive clones were

determined by restriction digest with *EcoRI* and *NotI*, as described above. Positive clones were not obtained for pcDNA3.1(+)-ZFP9A2.

2.2.10 Cloning of chicken GAPDH into pCR4

Chicken (*Gallus gallus*) glyceraldehyde-3-phosphate dehydrogenase (GAPDH) was PCR amplified using cDNA made from total RNA from LMH cells. The primers Chick.GAPDH.25.fw (5'-GTTGACGTGC AGCAGGAACA CT-3') and Chick.GAPDH.222.rv (5'-CTTGAAGTGT CCGTGTGTAG AATC-3') were used, which were designed based on the sequence NM_204305. The PCR reaction contained 1-μL of template cDNA, 1-μL of 10-mM dNTPs, 12.5 units recombinant *Taq* DNA Polymerase, 1.5-mM $MgCl_2$, 5-μL of 10X PCR Buffer, 0.5-μM of each primer and dH_2O up to 50-μL. The reaction was annealed at 52°C, with an elongation time of 30 seconds and 30 cycles. The PCR product was ligated to pCR4 using the TOPO TA cloning kit and transformed into TOP10 as described in Section 2.2.8. White colonies were used to inoculate 2-mL of LB/Amp mini-preps. Positive clones were identified by *EcoRI* digestion of mini-prep DNA isolated by the QIAprep Spin Miniprep Kit and sequencing with the T7 primer.

2.2.11 Cell lines and culture conditions

Longhorn male hepatoma (LMH) cells were maintained in 1:1 Minimal Essential Medium (MEM)/Ham's F-12 Nutrient Mixture (MEM: 11700-077 Gibco; F-12: 21700-026 Gibco) supplemented with 10% (v/v) fetal calf serum (FCS: 12483-020 Gibco), 50-IU/mL penicillin, 10-μg/mL streptomycin and 1-mM glutamine. The pH of this media is adjusted after preparation by the addition of approximately 2.5-mL (in 500-mL of media) filter sterilized 7.5% (w/v) sodium bicarbonate. LMH cells were incubated at 37°C with CO_2.

2.2.12 Transfection conditions

LMH cells were plated in 6-well tissue culture plates (Sarstedt 83.1839.300) at 1.0×10^5 cells/well in 2-mL of media without antibiotics. Plates were incubated

overnight at 37°C in a CO_2 incubator and transfected the following day. Lipofectamine™ 2000 (LF2000: Invitrogen 11668-027) was used to transfect cells as described by the manufacturer. Specifically, 4-µg of total DNA, composed of 1µg of pDHBV1.3 (see map in Appendix A) and 3µg of pcDNA3.1(+) or pcDNA3.1(+)-ZFP18A, ZFP18B, ZFP9A1, ZFP9A2, ZFP9B1, ZFP9B2, ZFP18cA, ZFP18cB or ZFP18cC were diluted in 250-µL of Opti-MEM® I reduced-serum medium (Invitrogen 51985-034). In a separate tube, 2-µL of LF2000 was diluted in 250-µL of Opti-MEM® I reduced-serum medium (DNA to LF2000 ratio of 2:1). Both tubes were incubated 5 minutes at room temperature then the LF2000 solution was slowly added to the DNA solution in a drop-wise manner. The combined solution was incubated 20 minutes at room temperature then added in a drop wise manner to LMH cells. One well of each experiment was also transfected as described with 4-µg of pd1-EGFPn1 (see map in Appendix A), which allowed the use of EGFP expression to determine transfection efficiency.

2.2.13 Total RNA isolation from transfected LMH cells

Total RNA was isolated 24 hours post-transfection using TRIzol® Reagent (Invitrogen 15596-018) according to the manufacturer's specifications. Specifically, media was removed from the cells and the cells were washed once with 1X phosphate buffered saline (PBS: 8.0-g/L NaCl, 0.2-g/L KCl, 0.92 g Na_2HPO_4, and 0.2 g KH_2PO_4. Adjust pH to 7.15 - 7.4 and filter sterilize). 1-mL of TRIzol® Reagent was added to each well of a 6-well plate, and allowed to sit at room temperature for several minutes. Lysates were transferred to 1.7-mL microcentrifuge tubes and incubated at room temperature for 5 minutes. 0.2-mL chloroform was added to each tube, which were capped and vigorously hand-shaken for 15 seconds. Samples were incubated at room temperature for 3 minutes then centrifuged at 11,000-rpm in a Beckman Coulter Microfuge® 18 Centrifuge for 10 minutes at 4°C. The aqueous layer was transferred to a new tube and 0.5-mL of isopropanol was added to precipitate the RNA. After incubation at room temperature for 10 minutes, the samples were centrifuged at 11,000-rpm in a Beckman Coulter Microfuge® 18 Centrifuge for 10 minutes at 4°C. The

supernatant was removed and the RNA pellet was washed by adding 1-mL of 75% (v/v) ethanol (prepared with RNase-free water) and vortexing briefly. The samples were centrifuged at 8000-rpm in a Beckman Coulter Microfuge® 18 Centrifuge for 5 minutes at 4°C. The supernatant was again removed and the pellet allowed to air-dry for 5 minutes. 20-µL of RNase-free water was used to resuspend the pellet by pipetting up and down several times and incubating at 55°C. RNA was measured by diluting 1 in 100 in RNase-free water and measuring on the spectrophotometer (Pharmacia Biotech UltraSpec® 3000) at A_{260}/A_{280}.

2.2.14 Synthesis of cDNA from total RNA

cDNA was produced from 1-µg of total RNA using oligo$(dT)_{20}$ (18418-020 Invitrogen) and SuperScript® II Reverse Transcriptase (RT) (18064-022 Invitrogen) according to manufacturer's specifications. Specifically, 1-µL of oligo$(dT)_{20}$, 1-µL of RNase-free dNTPS (10-mM stock) and 1-µg of total RNA were combined in a 1.7-mL microcentrifuge tube with RNase-free water up to a total volume of 12-µL. The sample was heated to 65°C for 5 minutes and quickly chilled on ice. The sample was centrifuged briefly to return the contents to the bottom, then 4-µL of 5X First Strand Buffer and 2-µL of 0.1-M dithiothreitol (DTT) were added. The contents were mixed gently then incubated at 42°C for 2 minutes. 1-µL (200 units) of SuperScript® II RT was added and the reaction allowed to proceed at 42°C for 50 minutes. The reaction was heat inactivated at 70°C for 15 minutes.

2.2.15 Quantitative PCR

Quantitative PCR was performed on the Roche LightCycler® 2.0 Carousel-Based System (03531414001) using the LightCycler® FastStart DNA Master^{PLUS} SYBR Green I kit (Roche 03515885001) and the primer pairs DHBV.2553.fw and DHBV.2752.rv, and Chick.GAPDH.25.fw and Chick.GAPDH.222.rv (see Table 2.7 for sequences).

Name	Primer sequence [a]
DHBV.2553.fw	AGCTGCTTGC CAAGGTATCT TT
DHBV.2752.rv	GCTCTAAAGC GTCTTTAGCA TCTC
Chick.GAPDH.25.fw	GTTGACGTGC AGCAGGAACA CT
Chick.GAPDH.222.rv	CTTGAAGTGT CCGTGTGTAG AATC

Table 2.7 - Primer sequences for quantitative PCR with Roche LightCycler.
[a] Sequences are shown 5' to 3'.

The plasmid pDHBV1.3 was used as the standard for pregenomic assessment and pCR4-Chick.GAPDH was used as the standard for GAPDH. The Master Mix was prepared by combining 14-µL of Enzyme with one vial of Reaction Mix from the LightCycler® FastStart DNA Master^{PLUS} SYBR Green I kit. 20-µL LightCycler® capillaries (Roche 04929292001) were placed into the LightCycler® Centrifuge Adaptors (Roche 11909312001), which were pre-cooled to 4°C within their aluminum cooling block. The PCR mix for one 20-µL reaction was prepared by combining, in this order: 9-µL of PCR-grade water, 2-µL of 10X PCR primers (0.5-µM stock of each primer), and 4-µL of Master Mix. The reaction was mixed by gentle pipetting, then 15-µL was transferred to the top of a capillary tube. A complete master mix of all three components can also be made and aliquoted into capillary tubes at a volume of 15-µL. 5-µL of sample was added to each tube, then the tubes were sealed with the provided stoppers. The capillary tubes in the centrifuge adaptors were centrifuged at 700x*g* for 10 seconds then the capillary tubes were placed in the LightCycler® Sample Carousel. The Instrument Protocol was run as described in the manual, using an annealing temperature of 54°C for all primers. The amplicons were 200 – 220-bp in length. Results were analyzed on the LightCycler® Software 3.5.

2.2.16 Production of DHBV-specific and chicken-GAPDH radioactive probes

The DHBV-specific and chicken-GAPDH radioactive probes were produced by digesting pDHBV1.3 and pCR4-Chicken.GAPDH each with 10 units of *EcoRI* in 10X NEB Buffer 4 at 37°C for 1.5 hours. The digests were separated on a 0.8% (w/v) agarose gel. The 1.3-mer DHBV genome equivalent (3.0-kb) and the

chicken GAPDH insert (197-bp) were gel purified using the QIAquick Gel Extraction kit as described in Section 2.2.3. The fragments were radiolabeled using the Random Primers DNA Labeling Kit (Invitrogen 18187-013) according to manufacturer's protocols. Specifically, 25-ng of the isolated DNA was diluted in 20-μL of water and boiled for 5 minutes to denature, then placed immediately onto ice. 15-μL of Random Primers Buffer Mixture and 2-μL each of dATP, dGTP and dTTP (0.5-mM each) were added to the tube. The total volume was brought up to 44-μL with water, after which 5-μL of [α-^{32}P]dCTP and 1-μL of Klenow fragment were added and incubated at room temperature for 4 hours. 12.5-μL of 1-M NaOH were added to denature for 5 minutes at room temperature, followed by 12.5-μL of 1-M HCl to neutralize.

2.2.17 Glyoxal-based RNA electrophoresis and Northern blot

10X MOPS solution, RNA loading buffer, 20X SSC, 50X Denhardt's Reagent, RNase-free water and deionized glyoxal were prepared ahead of time. 10X MOPS solution was made with 400-mM MOPS (3-(N-morpholino)propanesulfonic acid), 100-mM sodium acetate and 10-mM EDTA in water. 1-mL of diethyl pyrocarbonate (DEPC; Sigma D5758) was added to 1-L of 10X MOPS solution, incubated at 37°C overnight to remove RNases, then autoclaved to remove the DEPC. RNA loading buffer was made with 50% (v/v) glycerol, 1-mM EDTA, 0.25% (w/v) bromophenol blue and 0.25% (w/v) xylene cyanol in water. RNA loading buffer was treated with DEPC and autoclaved in a glass test tube. 20X SSC was made with 3-M NaCl and 280-mM sodium citrate in water and treated with DEPC. 50X Denhardt's Reagent was made with 10-g/L Ficoll (Type 400), 10-g/L polyvinylpyrrolidone and 10-g/L bovine serum albumin (fraction V) in water. The solution was filter-sterilized and treated with DEPC then stored at -20°C. RNase-free water was prepared by DEPC treatment, and was used for dilution of all of the buffers in this section. Deionized glyoxal was prepared by running 10-mL of 6-M glyoxal stock repeatedly over 0.8 x 4-cm disposable chromatography columns loaded with 5-mL of Mixed Bed Resin AG 501-X8 (Bio-Rad). The pH was measured at the start and after each cycle over the column

using pH paper, until the pH reached a steady state of pH 4.5 – 5.0. Once this pH was achieved, the deionized glyoxal was quickly dispensed in 50-mL aliquots and stored at -80°C.

A 1% (w/v) 1X MOPS agarose gel was prepared by preheating 10-mL of 10X MOPS solution to 55°C. 1.0-g of agarose was dissolved in 90-mL of RNase-free water by microwaving. The solution was then cooled to 55°C and 10-mL of 10X MOPS solution (preheated) was added. The gel was poured into an 8 x 10-cm casting tray and allowed to cool for an hour. During this time, 15 – 20-µg of total RNA was mixed with 15-µL DMSO, 5.4-µL of 6-M deionized glyoxal, 3-µL of 10X MOPS solution and RNase-free water up to 30-µL. The samples were heated in the thermocycler at 50°C for 60 minutes to denature, then 3-µL of RNA loading buffer was added. The denatured RNA was loaded onto the 1% (w/v) 1X MOPS agarose gel and separated at 5-V/cm using 1X MOPS solution as the electrophoresis buffer.

After separation, the gel was soaked in 50-mM NaOH for 20-minutes to partially hydrolyze the RNA and improve the efficiency of transfer. Then the RNA was transferred to a charged nylon membrane (Hybond-XL, Amersham Biosciences RPN303S) using 7.5-mM NaOH as the transfer buffer. The transfer was set up using a 13 x 9-inch Pyrex glass dish, with a glass plate across the top of the dish and ~1-L of 7.5-mM NaOH in the dish. Whatman 3MM filter paper was placed over the glass plate and allowed to hang in the NaOH. The gel was placed on the filter paper, and the remaining filter paper surface was covered with old pieces of film, to prevent buffer flow-through around the gel. Next, the charged nylon membrane was placed on top of the gel, a piece of filter paper was placed on top of the membrane, and a stack of paper towels was placed on top of the filter paper. A weight of 200 – 300-g was placed on top of the filter paper, and the transfer was allowed to proceed overnight at room temperature. The following day, the membrane was pre-hybridized in 6X SSC, 2X Denhardt's reagent and 0.1% (w/v) SDS for 4 hours at 65°C in the hybridization oven (Robbins

Scientific® Model 1000), then 10-µL of DHBV- or chicken-GAPDH-specific radioactive probe was added overnight. Membranes were washed twice with 10-mL of 1X SSC/0.1% (w/v) SDS and twice with 10-mL of 0.1X SSC/0.1% (w/v) SDS at 65°C for 15 minutes each wash. The membrane was exposed to an image plate overnight and the image plate was scanned on the Fujifilm FLA-5100 phosphorimager using the "IP S" setting.

2.2.18 Isolation of intracellular viral DNA from transfected LMH cells

Intracellular viral (ICV) DNA was isolated 48 hours post-transfection as previously described (11). Specifically, cells were washed once with 1X PBS and lysed in the well with 400-µL of ICV Solution 1 (10-mM Tris-HCl pH 7.5, 50-mM NaCl, 1-mM EDTA, 0.3% (v/v) Triton X-100 and 8% (w/v) sucrose). Lysates were collected in 1.7-mL microcentrifuge tubes. Nuclei and cellular debris were pelleted by centrifugation at 14,000-rpm for 10 minutes, then the supernatant transferred to a new tube. Samples were incubated at 37°C for 30 minutes with 6-mM $MgCl_2$, 100-µg/mL DNase I and 10-µg/mL RNase A to digest cellular nucleic acids. Samples were centrifuged again for 10 minutes at 14,000-rpm, then the supernatant transferred to a new tube. Virus was precipitated from the supernatants with 0.3 volumes of ICV Solution 2 (26% (w/v) polyethylene glycol (PEG) 8000, 1.4-M NaCl and 10-mM EDTA) overnight at 4°C. Samples were centrifuged for 10 minutes at 14,000-rpm to pellet the virus particles, which were resuspended in 100-µl of TSE (50-mM Tris-HCl pH 8, 150-mM NaCl and 10-mM EDTA). Samples were incubated overnight at 42°C with 800-µg/mL proteinase K (Invitrogen 25530-015) and 0.1% (w/v) SDS to digest capsid and polymerase. The next day, samples were phenol:chloroform extracted by adding 150-µL each of phenol and chloroform, shaking vigorously for 15 seconds and centrifuging 5-minutes at 14,000-rpm. The aqueous layer was transferred to a new tube and the viral DNA was precipitated overnight at -20°C with 10-µg yeast tRNA as carrier, 0.1 volume 3-M sodium acetate and 2X volume 95% (v/v) ethanol. Following centrifugation at 14,000-rpm for 10 minutes, the supernatant was removed and the viral DNA was resuspended in 15-µL DNA

loading buffer (30% (v/v) glycerol, 1% (w/v) SDS, 0.25% (v/v) bromophenol blue, 0.25% (v/v) xylene cyanol) and the entire sample was used for Southern analysis.

2.2.19 DNA gel electrophoresis and Southern blot analysis of ICV

ICV samples were loaded onto a 0.8% (w/v) agarose gel prepared and electrophoresed at 120-V. After separation, the gel was depurinated in 0.25-M HCl for 15-minutes at room temperature. The Southern transfer was assembled as described for the Northern transfer in Section 2.2.17, except the transfer buffer was 0.4-M NaOH. After overnight transfer, the membrane was neutralized in 1.5-M NaCl, 1-M Tris-HCl pH 8.0 for 15 minutes at room temperature. The membrane was dried face-up on paper towel for 30 minutes then exposed to UV-light for 3 minutes to cross-link the DNA to the membrane. The membrane was pre-hybridized in 10-mL 5X SSC, 2% (w/v) SDS, 1X Denhardt's solution and 50-µg/mL herring sperm DNA at 65°C for 4 hours in the hybridization over (Robbins Scientific® Model 1000). 10-µL of radioactive DHBV-specific probe was incubated overnight at 65°C, then the membrane was washed twice with 10-mL of 1X SSC/0.1% (w/v) SDS and twice with 10-mL of 0.1X SSC/0.1% (w/v) SDS at 65°C for 15 minutes each wash. The membrane was exposed to an image plate overnight and the image plate was scanned on the Fujifilm FLA-5100 phosphorimager using the "IP S" setting.

2.2.20 Isolation and quantification of extracellular viral DNA from transfected LMH cells

ECV was isolated from the supernatant of transfected LMH by collecting 1-mL of culture supernatant and centrifuging 5 minutes at 1500-rpm, to pellet any floating cells. The supernatant was transferred to a new tube and incubated at 37°C for 30 minutes with 6-mM $MgCl_2$, 100-µg/mL DNase I and 10-µg/mL RNase A to digest unprotected nucleic acids. Samples were centrifuged for 10 minutes at 14,000-rpm, then the supernatant transferred to a new tube. Virus was precipitated from the supernatants with 0.3 volumes of ICV Solution 2 (26% (w/v)

polyethylene glycol (PEG) 8000, 1.4-M NaCl and 10-mM EDTA) overnight at 4°C. The ECV isolation was then completed identically to ICV isolation described in Section 2.2.18. ECV was quantified using the Roche LightCycler® 2.0 using the DHBV primers in Table 2.7.

2.2.21 SDS-polyacrylamide gel electrophoresis

Whole cell lysates were collected 24 or 48 hours post-transfection. LMH cells were washed once with 1X PBS and lysed with 400-µL radioimmunoprecipitation assay (RIPA) buffer (10-mM Tris-HCl pH 8.0, 140-mM NaCl, 0.025% (w/v) sodium azide, 1% (v/v) Triton X-100, 0.1% (w/v) SDS and 1% (w/v) sodium deoxycholate in water). The lysates were transferred to a 1.7-mL microcentrifuge tube and protein concentrations were measured using the MicroBCA Protein Assay (Pierce Biotechnology 23235).

In general, 10% SDS-polyacrylamide gel electrophoresis was performed. The SDS-polyacrylamide gel electrophoresis (PAGE) loading buffer, and SDS-PAGE running buffer were made ahead of time. SDS-PAGE loading buffer was prepared with 125-mM Tris-HCl pH 6.8, 5% (w/v) SDS, 10% (v/v) 2-mercaptoethanol, 15% (v/v) glycerol and 0.1% (w/v) bromophenol blue. SDS-PAGE running buffer was prepared with 30-g/L Tris, 144-g/L glycine and 10-g/L SDS. The separating gel (for two gels) was prepared by combining 3.75-mL of 2.0-M Tris-HCl pH 8.8, 3.75-mL of 40% acrylamide/bisacrylamide (29:1), 200-µL of 10% (w/v) SDS, 200-µL of 10% (w/v) APS, 12.1-mL of water and 20-µL of TEMED. The mixture was poured into two mini-gel cast with 1.5-mm spacers and over-layed with butanol. The gel was allowed to polymerize for 30-minutes, then the butanol was cleaned off. The stacking gel was prepared by combining 2.5-mL of 0.5-M Tris-HCl pH 6.8, 974-µL 40% acrylamide/bisacrylamide (29:1), 100-µL of 10% (w/v) SDS, 100-µL of 10% (w/v) APS, 6.3-mL of water and 10-µL of TEMED. The well comb was placed in the gel cast and stacking gel was used to fill the cast to the top of the glass plates. The stacking gel was allowed to polymerize for 15 minutes and then the comb was removed. Samples were prepared by aliquoting 20

– 30-µg of whole cell lysate with 5-µL of SDS-PAGE loading buffer and boiling for 5 minutes. The mini-gels were assembled in the gel apparatus and the inner and outer chambers were filled with SDS-PAGE running buffer. The samples were loaded into the wells of the gel and run at 100-V for 15 minutes, then at 160-V until the bromophenol blue marker was 1-cm from the bottom of the gel. The Low Range Standards (unstained, Bio-Rad 161-0304) were used as a protein ladder.

2.2.22 Western transfer of SDS-polyacrylamide gels

Once the electrophoresis was completed from Section 2.2.21, the gel was removed from the glass plates and the stacking gel was cut away with a scalpel. The gel was transferred to a dish containing semi-dry transfer buffer (14.27-g/L glycine, 3.0-g/L Tris and 20% (v/v) methanol in water) and soaked for 5 minutes. In another dish, two Whatman 3MM filter pieces (just larger than the gel) and a nitrocellulose membrane (Hybond-ECL) were soaked in semi-dry transfer buffer for 5 minutes. The Western transfer was set up using a semi-dry transfer apparatus (Fischer Brand FB-SDB-2020) where the gel and the membrane are sandwiched between the two filter papers, and the membrane is on the top of the gel, closest to the positive panel of the apparatus. The lid of the apparatus was closed tightly and evenly, attached to a power pack (Bio-Rad Model 200/2.0 Power Supply) and run for 1 hour with a limit of 500-mA and a maximum voltage of 29-V. If four gels were transferred simultaneously, the run time was increased to 1.5 hours.

2.2.23 Western blot

Once the Western transfer was completed from Section 2.2.22, the membranes were removed from the transfer apparatus and stained with 1% (v/v) napthol blue black stain (stock was 0.2% (w/v) napthol blue black in 10% (v/v) acetone and 10% (v/v) methanol) in water for 3 minutes to verify transfer of proteins to the membrane. Membranes were subsequently blocked for 1 hour at room temperature with 50-mL of skim milk block (2.5% (w/v) skim milk powder, 0.1% (v/v) Tween-20 in 1X Tris buffered saline (TBS). 10X TBS is prepared with

15.76-g/L Tris base and 87.66-g/L NaCl). Membranes were washed three times for 5 minutes each with 25-mL TBS-T (1X TBS with 0.1% (v/v) Tween-20). Primary antibody was diluted in 2-mL of skim milk block and added to the membrane in a plastic bag for 1 hour at room temperature with gentle rotation. Primary antibodies to DHBV core (J112) and DHBV S (7C12) were provided by Jesse Summers (University of New Mexico) and were used at dilutions of 1:10,000 and 1:100, respectively. The primary antibody to DHBV preS (1H1) was provided by Pat Nakajima (Fox Chase Institute) and was used at the dilution of 1:500. The anti-actin antibody (Chemicon MAB1501) was used at a dilution of 1:10,000. The anti-GFP antibody (Zymed 33-2600) was used at a dilution of 1:500. Anti-serum against ZFPs was produced as described in Section 2.2.24. In general, anti-serum from rabbit GN-22,801 was used at a dilution of 1:5000. After incubation with primary antibody, the membranes were washed three times for 5 minutes each with 25-mL TBS-T. Secondary antibody was diluted in 2-mL of skim milk block and added to the membrane in a plastic bag for 1 hour at room temperature with gentle rotation. Goat anti-rabbit horseradish peroxidase (HRP) (1:5000, BioRad 1706515) was used as the secondary antibody for anti-DHBV core membranes. Goat anti-mouse HRP (1:5000, Jackson ImmunoResearch 115-035-174) was used as the secondary antibody for anti-DHBV preS, anti-DHBV S, anti-actin and anti-GFP membranes. After incubation with the secondary antibody, the membranes were washed three times for 5 minutes each with 25-mL TBS-T. The membranes were treated with Supersignal® West Dura Extended Duration Substrate (Pierce 34076) and exposed to film (Kodak XAR-5) to visualize the protein bands. The film was developed using the Kodak M35A X-OMAT Processor.

2.2.24 Custom anti-serum against ZFPs

Custom rabbit anti-serum against ZFPs was produced by Sigma Genosys (The Woodlands, TX) by injection of two New Zealand White Rabbits (animal ID GN-22,801 and GN-22,802) with purified ZFP18A-MBP fused to the KLH-peptide for immunization. The immunization protocol is as shown in Table 2.8. 0.1%

(w/v) sodium azide was added to the collected serum. The serum was aliquoted into 5-mL tubes and stored long-term at -80°C. Small aliquots were stored at -20°C and working aliquots were stored at 4°C.

Day	Task	Notes
0	Collect pre-immune serum	Approx. 5-mL.
0	Immunize	200-µg in Complete Freund's Adjuvant.
14	Immunize	100-µg in Incomplete Freund's Adjuvant.
28	Immunize	100-µg in Incomplete Freund's Adjuvant.
42	Immunize	100-µg in Incomplete Freund's Adjuvant.
49	Bleed	First production bleed & ELISA assessment.
		GN-22,801 (25-mL); GN-22,802 (30-mL)
56	Immunize	100-µg in Incomplete Freund's Adjuvant.
63	Bleed	Second production bleed.
		GN-22,801 (29-mL); GN-22,802 (30-mL)
70	Immunize	100-µg in Incomplete Freund's Adjuvant.
77	Bleed	Third production bleed.
		GN-22,801 (27-mL); GN-22,802 (30-mL)
84	Bleed	Terminal bleed.
		GN-22,801 (29-mL); GN-22,802 (30-mL)
87	Bleed	Terminal bleed.
		GN-22,801 (45-mL); GN-22,802 (45-mL)

Table 2.8 - Immunization protocol of New Zealand White Rabbits for production of custom anti-serum against ZFP18A-MBP.

2.2.25 MTT assay for assessment of metabolically active cells

LMH cells were plated at 2.0 x 10^4 cells/well in 96 well plates in 100-µL of media and transfected as described in Section 2.2.12, except 50-ng of pDHBV1.3, 150-ng of pcDNA3.1(+)-ZFP18A, ZFP18B, ZFP9A1, ZFP9A2, ZFP9B1, ZFP9B2, ZFP18cA, ZFP18cB or ZFP19cC, and 0.6-µL of LF2000 were used. 24 hours after transfection, 10-µL of 5-mg/mL MTT (3-(4,5-Dimethylthiazol-2-yl)-2,5-diphenyltetrazolium bromide) in 1X PBS was added to the cells for 2 hours and

incubated at 37°C in 5% CO_2. Cells were washed once with 1X PBS and then 100-µL of acid isopropanol (isopropanol with 0.1N HCl) was added to each well and allowed to dissolve the crystals for 5 minutes. The wells were measured at 570-nm on a Spectramax PLUS plate reader (Molecular Devices).

2.2.26 Confocal microscopy of ZFP-EGFP expression in transfected LMH cells

Dishes for live cell confocal microscopy were prepared using 35-mm dishes with 15-mm holes drilled in the middle. 18-mm round cover slips (Fischer 12-545-100) were glued over the holes with epoxy and the dishes were sterilized by UV-light exposure for 30 minutes. LMH cells were plated onto these dishes at 1.7 x 10^5 cells/well in 2-mL of media, and incubated overnight at 37°C in 5% CO_2. After 24 hours, the cells were transfected with 4-µg of pcDNA3.1(+)-ZFP18A-EGFP, -ZFP18B-EGFP, ZFP9A1-EGFP, -ZFP9B1-EGFP, or -ZFP9B2-EGFP. The positive control was pcDNA3.1(+)-EGFP and the negative control was pcDNA3.1(+). After 24 hours, 10-µL/mL of 0.1-mg/mL Hoechst 33342 (Biochemika 14533) was added to the media and cells were incubated at 37°C in 5% CO_2 for 15 minutes. The media was replaced and live cells were visualized using the Zeiss NLO510 multi-photon microscope. The emission and excitation wavelengths were 488-nm and 509-nm for EGFP and 355-nm and 465-nm for Hoechst 33342.

2.2.27 Flow cytometry of ZFP-EGFP expression in transfected LMH cells

LMH cells were plated in 6-well plates and transfected as described in Section 2.2.12, except that 4-µg of pcDNA3.1(+)-ZFP18A-EGFP, -ZFP18B-EGFP, ZFP9A1-EGFP, -ZFP9B1-EGFP, or -ZFP9B2-EGFP was used. The positive control was pcDNA3.1(+)-EGFP and the negative control was non-transfected cells. After 24 hours, the cells were removed from the plate by washing once with PBS then adding 0.5-mL/well ATV (8.0-g/L KCl, 0.4-g/L NaCl, 1.0-g/L NaHCO3, 0.58-g/L D-glucose, 0.5-g/L trypsin (1:250), 0.2-g/L disodium EDTA, pH 7.4 – 7.5) and incubating at 37°C for 10 minutes. 0.5-mL/well of media was

added and the cells were transferred into a tube. The cells were centrifuged for 5 minutes at 1500-rpm in a Beckman Coulter Allegra® X-15R centrifuge and resuspended in 0.5-mL of PBS plus 1% (v/v) FCS and 0.5-mM EDTA. The samples were added to the strainer caps of 5-mL polypropylene round-bottom tubes (Falcon 352235) and gently tapped to encourage flow-through. The samples were then sorted on EGFP (488-nm) using the BD FACScan™ Flow Cytometer (BD Biosciences).

2.2.28 Data and statistical analysis

Quantitative PCR results on cDNA made from total RNA using the Roche LightCycler® 2.0 were analyzed by normalizing the DHBV-specific results to the chicken GAPDH results using Microsoft Excel. The values were then converted into percentages, with the empty vector set as 100%. One-Way ANOVA, using StatPlus®:mac LE.2009 (AnalystSoft Inc. for MacOS), was performed on the data sets. One-Way ANOVA showed the means for treatment with DHBV-specific control ZFPs did not have a statistically significant difference; therefore no further analysis was applied. Single factor ANOVA showed the means for treatment with DHBV-specific experimental ZFPs were not equal. This analysis was followed up with pair-wise comparison of each mean using the Tukey Test in Microsoft Excel. Any pairs found not to be equal using the Tukey Test were then assessed directly using Two-Sample T-test assuming unequal variances. This test was used because the calculated variances of the samples were not equal.

Quantitative PCR results on ECV DNA using the Roche LightCycler® 2.0 were analyzed by converting the values into percentages, with the empty vector set at 100%. Single factor ANOVA was performed on the data sets. It showed the means for treatment with DHBV-specific ZFPs were not equal, however, follow-up with the Tukey Test did not detect any differences between empty vector and any of the ZFP-treatment samples.

Southern blot results on ICV DNA were quantified using the ImageGauge v4.22 software. The global background was subtracted from all samples and single factor ANOVA was performed on the data set. It showed the means for treatment with DHBV-specific ZFPs were all equal. The Tukey Test confirmed this finding.

Results using the MTT assay were analyzed by One-Way ANOVA. It showed the means were not equal. The pair-wise comparison using the Tukey Test demonstrated differences between some means, which were further analyzed using Two-Sample T-tests assuming unequal variances.

2.3 Results

2.3.1 Design of DHBV-specific ZFPs

ZFP 18-mers were designed to target either the plus- or the minus strand of DHBV. Each 18-mer consists of six zinc finger motifs linked in tandem by the canonical TGEKP linker (7). Three 18-mers were designed, called ZFP18A, ZFP18B and ZFP18C. Their binding sites can be found in Figure 2.1 A. ZFP18A binds the minus strand while ZFP18B and ZFP18C both bind the plus strand. ZFP18A overlaps a majority of footprint region 3 (F3), where HNF-1 is known to bind. ZFP18C overlaps part of F3 and part of F2, potentially interfering with both HNF-1 and HNF-3 binding regions. ZFP18B also binds within the centre of F2.

Four 9-mers were designed, called ZFP9A1, ZFP9A2, ZFP9B1 and ZFP9B2. Their binding sites are in Figure 2.1 B. Each zinc finger motif (three in each 9-mer) were linked in tandem with the canonical TGEKP linker (7). ZFP 9-mers were designed in pairs with the intention of adding the *FokI* endonuclease domain at the N-terminus of the ZFP. In order to allow dimerization through the *FokI* domains, one member of each 9-mer pair was designed inverted to the other. (Figure 2.2). Thus, ZFP9A1 and ZFP9A2 function as one pair, where ZFP9A1 binds to the minus strand and ZFP9A2 binds to the plus strand. Likewise, ZFP9B1 and ZFP9B2 function as the second pair, where ZFP9B1 binds to the minus strand and ZFP9B2 binds to the plus strand (Figure 2.2).

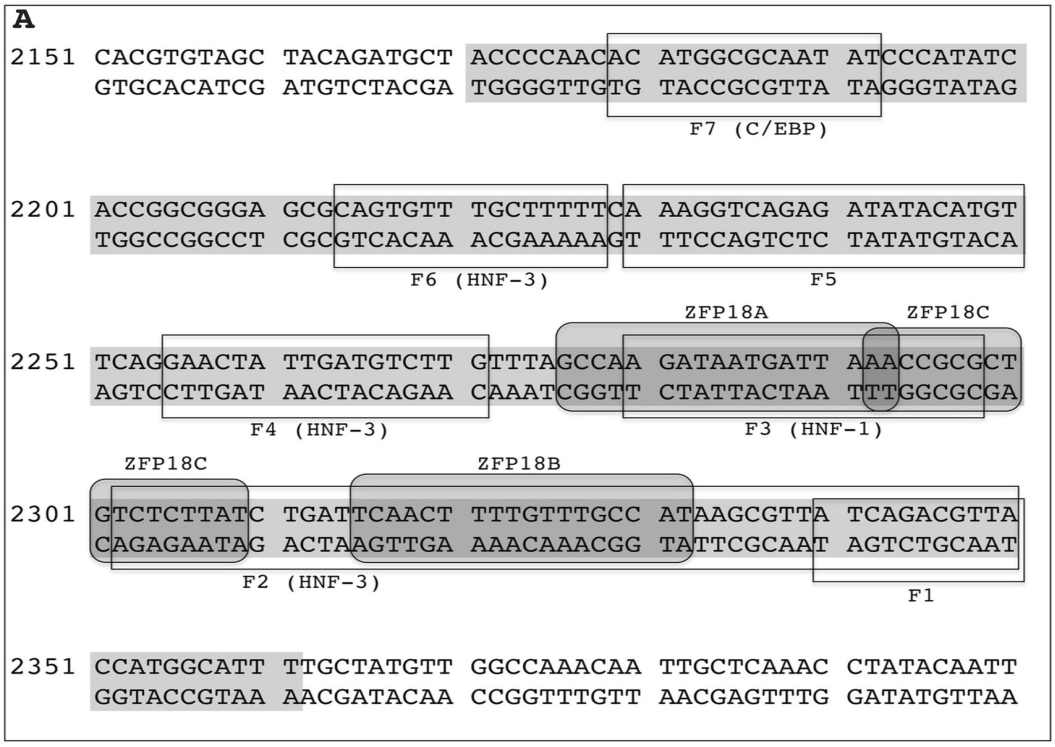

Figure 2.1 - Detailed map of the DHBV enhancer.
The nucleotide sequence of dEn1 is shown above in shaded grey, spanning nucleotides 2170 to 2361. The open boxes represent FP regions detected by other groups during DNase I footprinting assays. The PBPs are indicated in brackets. The binding sites of ZFP 18-mers (A) and ZFP 9-mers (B) are indicated by the rounded rectangles shaded grey.

In addition, the spacing between the pairs is important, because optimal cleavage by dimerized *FokI* domains occurs when there are 6 to 18-bps between the DNA binding domains, with an optimum of 8-bps (12). Thus, a space of 9-bps can be found between the binding sites of ZFP9A1 and ZFP9A2, and 8-bps between ZFP9B1 and ZFP9B2.

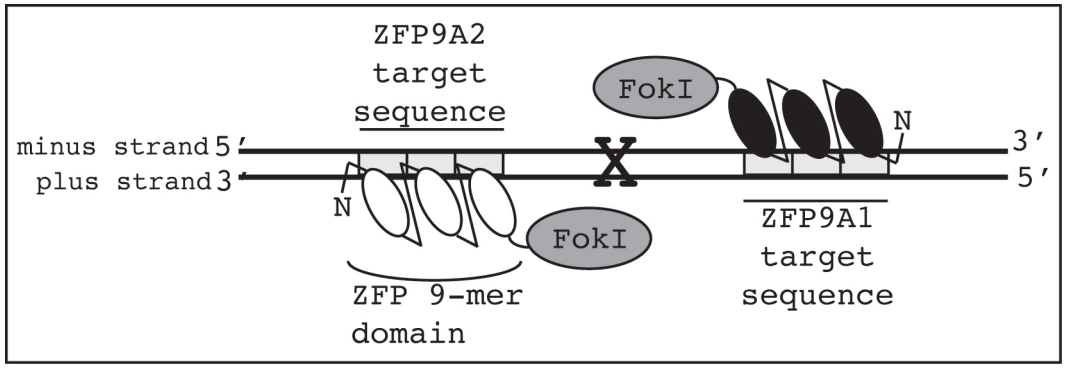

Figure 2.2 - Schematic representation of ZFNs formed by ZFP 9-mers acting as heterodimers around the FokI endonuclease domain.
Each zinc finger motif of the 9-mer is shown as an oval, with three modules linked in tandem. The FokI domain is located at the C-terminus of each 9-mer. The 9-mer pairs are designed to bind opposite strands of DNA, ensuring the FokI domains are both located at the intervening DNA sequence between the two target sites. The approximate cleavage site is shown by an 'X'.

In addition to the above-mentioned experimental ZFPs, control ZFPs were also created that did not bind to a specific sequence within the DHBV genome. One control ZFP was designed for each DHBV-specific ZFP. The controls contain the same zinc finger motifs as the related experimental ZFP, however the order of the motifs was shuffled. For example, if ZFP18A had zinc finger motifs ordered 1 through 6, ZFP18cA had a shuffled order of the same motifs, with an order of 3-6-4-2-1-5. All control 18-mers had this zinc finger motif order compared to their respective experimental ZFP. Likewise, control 9-mers had a zinc finger motif order of 3-1-2. Control 18-mers were named ZFP18cA, ZFP18cB and ZFP18cC. Control 9-mers were named ZFP9cA1, ZFP9cA2, ZFP9cB1 and ZFP9cB2.

The entire DHBV genome (AF047045) was entered into the 'Zinc Finger Tools' website using the "Search DNA Sequence for Contiguous or Separated Target

Sites" program. This program was chosen for designing ZFPs, rather than any of the other ZFP library methods, because of the speed and ease of design. The genome was scanned for either 9-bp or 18-bp sequences that ZFPs could be designed to target. Possible target sites were found throughout the genome, and those within the dEn1 region were investigated for use. First, the proposed target sequences were searched using the NCBI genomic BLAST database for their presence in the *Gallus gallus* genome. None of the proposed target sequences were found within the chicken genome. The proposed sequences could not be compared to the Pekin duck (*Anas platyrhynchos*) genome because it has not yet been sequenced. Thus, there is the potential that the target sequences may be found in duplicate within the duck genome, as this could not be tested.

After selecting the target sequences, they were then re-entered into the 'Zinc Finger Tools' website using the "Design a Zinc Finger Protein" program. The output consisted of the required amino acid sequence of the ZFP in order to target that DNA sequence. The output included both the standard backbone sequence and the unique α-helix sequences for specific DNA recognition (see Appendix B).

2.3.2 Synthesis, bacterial expression and purification of DHBV-specific ZFPs

The amino acid sequence of each ZFP provided by the 'Zinc Finger Tools' website was used to order custom sequence synthesis by Blue Heron Technologies. A codon usage table for *Anas platyrhynchos* was used to convert the amino acid sequence to the nucleotide sequence and the "codon-optimized sequence" was selected for synthesis. The ZFPs were produced in pUC19 vectors as described in the Materials and Methods section.

ZFPs were cloned into the pMal-gg1 vector (pMal-c backbone). ZFPs were expressed in BL21(DE3) *E.coli* and purified based on their fusion to the maltose binding protein (MBP). Samples were collected during the purification protocol and analyzed by SDS-PAGE and Coomassie Blue staining. The expression

pattern of the ZFPs can be seen in Figure 2.3, which shows typical patterns as seen for all ZFPs. Lysates from un-induced bacterial cultures (Figure 2.3 A & C, lane 1) versus cultures induced with IPTG for 2 hours (Figure 2.3 A & C, lane 2) or 3 hours (Figure 2.3 C, lane 2b) show the production of the ZFP-MBP fusion protein (asterisk) after induction. The soluble fraction (Figure 2.3 A & C, lane 3) maintains the majority of the ZFP-MBP fusion protein compared to the insoluble fraction (Figure 2.3 A & C, lane 4). The ZFP-MBP fusion protein was isolated from the soluble fraction using an amylose-resin column. The column eluate (Figure 2.3 A & C, lane 5) demonstrates the ZFP-MBP fusion protein in a concentrated and purified form. The column eluate was further evaluated by analyzing each fraction eluted from the amylose resin column by SDS-PAGE and Coomassie Blue staining. The elution pattern can be seen in Figure 2.3 (B & D), which shows typical patterns as seen for all ZFPs. The fractions with the greatest amount of ZFP-MBP fusion protein were pooled together for further experiments. All *in vitro* assessments of ZFPs were performed using the ZFP-MBP fusion protein.

2.3.3 EMSA: Determination of apparent equilibrium dissociation constant for DHBV-specific ZFPs

EMSAs were performed to both confirm that the designed ZFPs were capable of binding their target sequences and to calculate the apparent equilibrium dissociation constant (k_D). Bacterially purified ZFP-MBP fusion proteins were incubated with dsDNA oligonucleotides encoding the specific target sequence for each ZFP then separated on non-denaturing polyacrylamide gels. After staining with SYBR-green DNA stain and scanning with a phosphorimager, the shift of the dsDNA oligonucleotides up to a high molecular weight complex with the ZFP-MBP fusion proteins could be visualized (Figure 2.4 A, C & D, lanes 2 - 6). All ZFP 18-mers (ZFP18A, ZFP18B, ZFP18C) bound their target sequence with high affinity, as can be seen by the strong mobility shift bands produced in the presence of each ZFP. The gels were all subsequently stained with SYPRO-Ruby protein stain and scanned with a phosphorimager. A representative gel can be

seen in Figure 2.4 B, with ZFP18A as the example. This gel confirms the presence of protein in the lanes where a mobility shift occurred, and demonstrates the decreasing amount of protein in each sample.

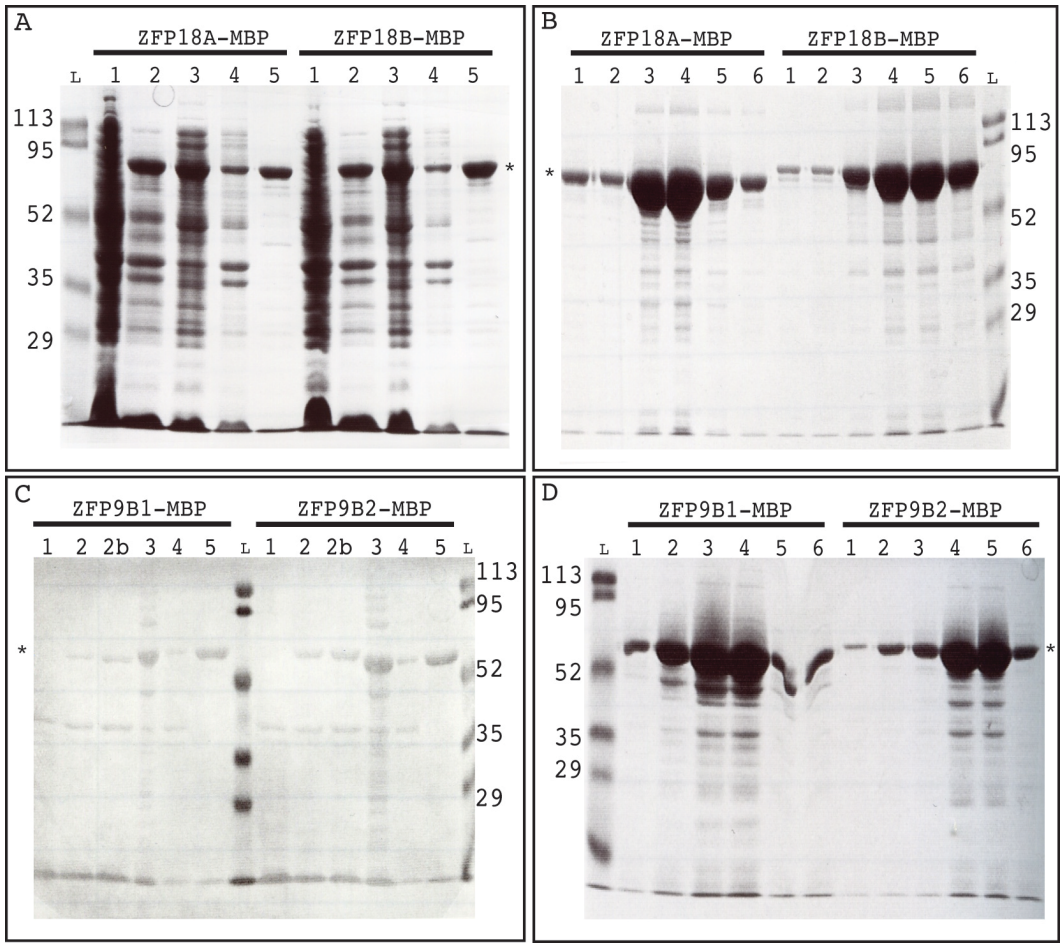

Figure 2.3 - Protein purification of DHBV-specific ZFPs.
Samples collected during the purification procedure were separated using 10% SDS-PAGE and stained with Coomassie Blue protein stain. Samples from the purification procedure for (A) ZFP18A-MBP and ZFP18B-MBP, and (C) ZFP9B1-MBP and ZFP9B2-MBP were collected from (1) un-induced bacterial cultures, (2) cultures induced for 2 hours with IPTG, (2b) cultures induced for 3 hours with IPTG, (3) soluble fraction after centrifugation, (4) insoluble fraction after centrifugation, and (5) column eluate. Fractions of 500-μL were collected from the column during elution for (B) ZFP18A-MBP and ZFP18B-MBP, and (D) ZFP9B1-MBP and ZFP9B2-MBP. Fractions 1–6 are shown, and the fractions with the greatest protein content were pooled for experimental use. The ladder (L) is shown on each figure and the MW sizes of the markers are shown on the side, in kDa. An asterisk (*) marks the band representing the ZFP-MBP fusion protein.

The ZFP 9-mers bound their targets less strongly than the 18-mers, as might be expected, considering they recognize a sequence half as long. Only ZFP9A1 demonstrated binding capacities similar to the 18-mers (Figure 2.5 A). ZFP9A2 consistently showed no to very little binding, as only a faint band can be seen in lane 2 of Figure 2.5 B. ZFP9B1 and ZFP9B2 showed weak binding patterns in Figure 2.5 C & D.

EMSAs were performed on purified MBP alone, to confirm that binding of ZFP-MBP fusion proteins to their target oligonucleotides was not due to the associated MBP component. As seen in Figure 2.6 A, MBP did not bind the dsDNA oligonucleotide carrying the ZFP18A target sequence. EMSAs were also performed on ZFP18cA and ZFP18cB (Figure 2.6). ZFP18cA has poor binding, with only a faint band detectable in lanes 2 and 3 (Figure 2.6 B). ZFP18cB exhibited strong binding (Figure 2.6 C). EMSAs were not performed upon control ZFP 9-mers because it became unnecessary to maintain all seven control ZFPs (three 18-mers and four 9-mers) throughout the cloning and tissue culture experiments.

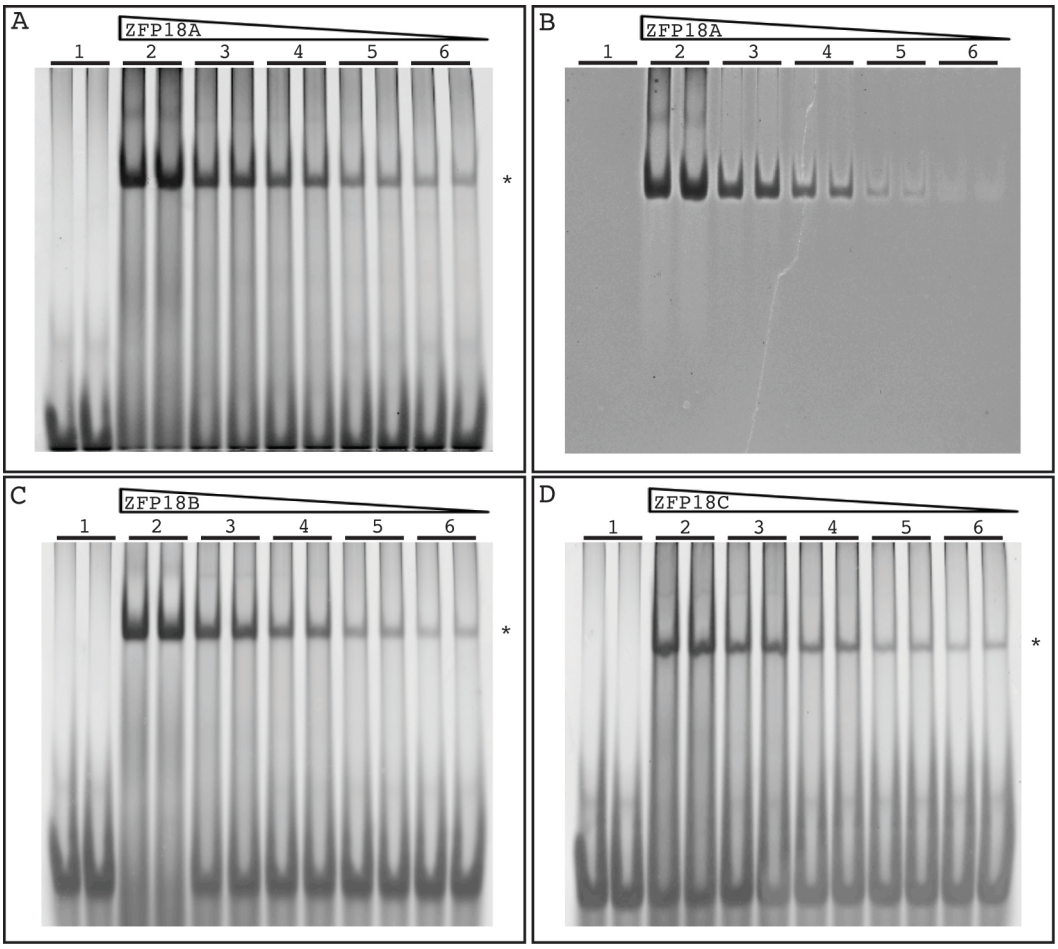

Figure 2.4 - EMSAs to determine the apparent equilibrium dissociation constant of DHBV-specific ZFP 18-mers.
DsDNA oligonucleotides with the specific target sequence for each ZFP were incubated alone (lane 1) or in the presence of ZFP18-MBP fusion proteins at 150-nM (lane 2), serially diluted 1 in 2 (lanes 3 to 5) down to 9.5-nM (lane 6). Each sample is in duplicate. The gels were stained with SYBR-green DNA stain (A, C, D) and subsequently stained with SYPRO-Ruby protein stain (B). The SYPRO-Ruby-stained gel for ZFP18A (B) is an example of a typical image for SYPRO-Ruby stained EMSAs. The asterisk (*) marks the DNA-protein complex. The bands next to the asterisks were quantified using Image Gauge software v4.22, and the dissociation constant was calculated using the Enzyme Kinetics software v1.11. Each EMSA was performed 2-3 times.

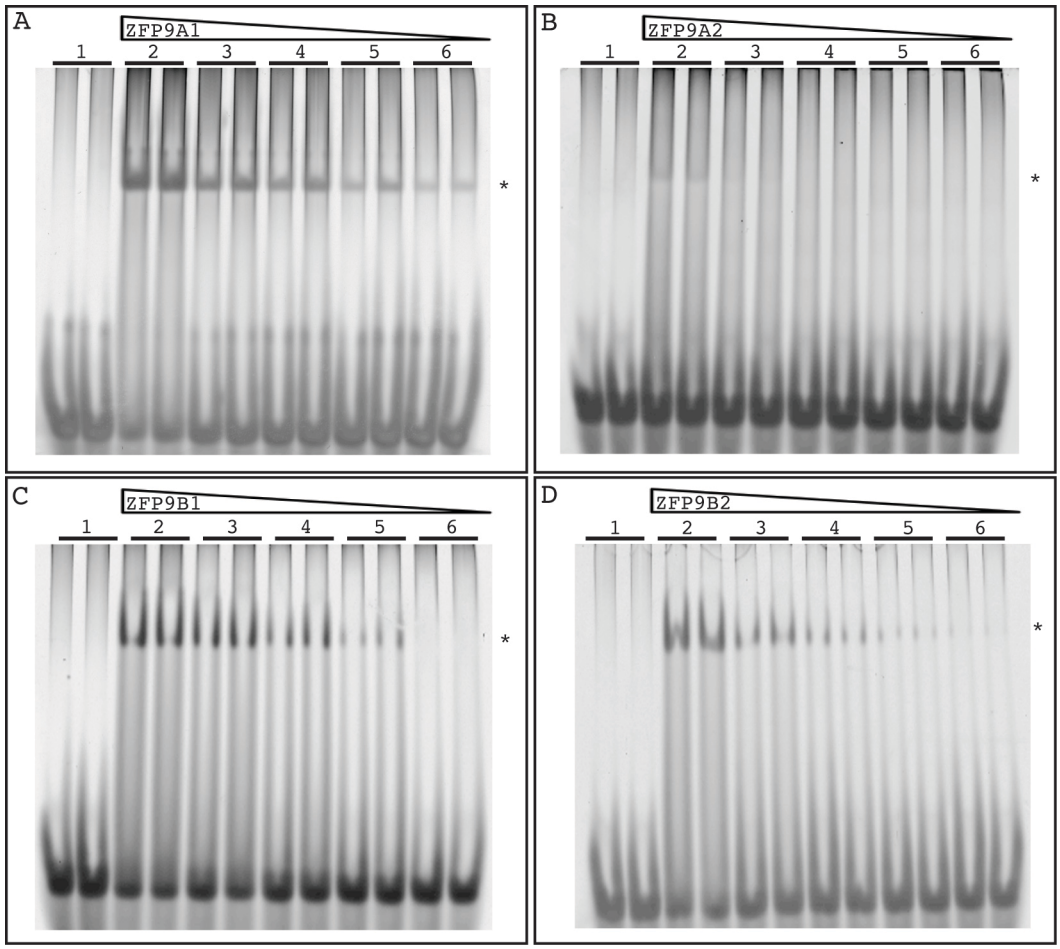

Figure 2.5 - EMSAs to determine the apparent equilibrium dissociation constant of DHBV-specific 9-mers.

DsDNA oligonucleotides with the specific target sequence for each ZFP were incubated alone (lane 1) or in the presence of ZFP9-MBP fusion proteins at 150-nM (lane 2), serially diluted 1 in 2 (lanes 3 to 5) down to 9.5-nM (lane 6). Each sample is in duplicate. The gels were stained with SYBR-green DNA stain. The asterisk (*) marks the DNA-protein complex. The bands next to the asterisks were quantified using Image Gauge software v4.22, and the dissociation constant was calculated using the Enzyme Kinetics software v1.11. Each EMSA was performed 2-3 times.

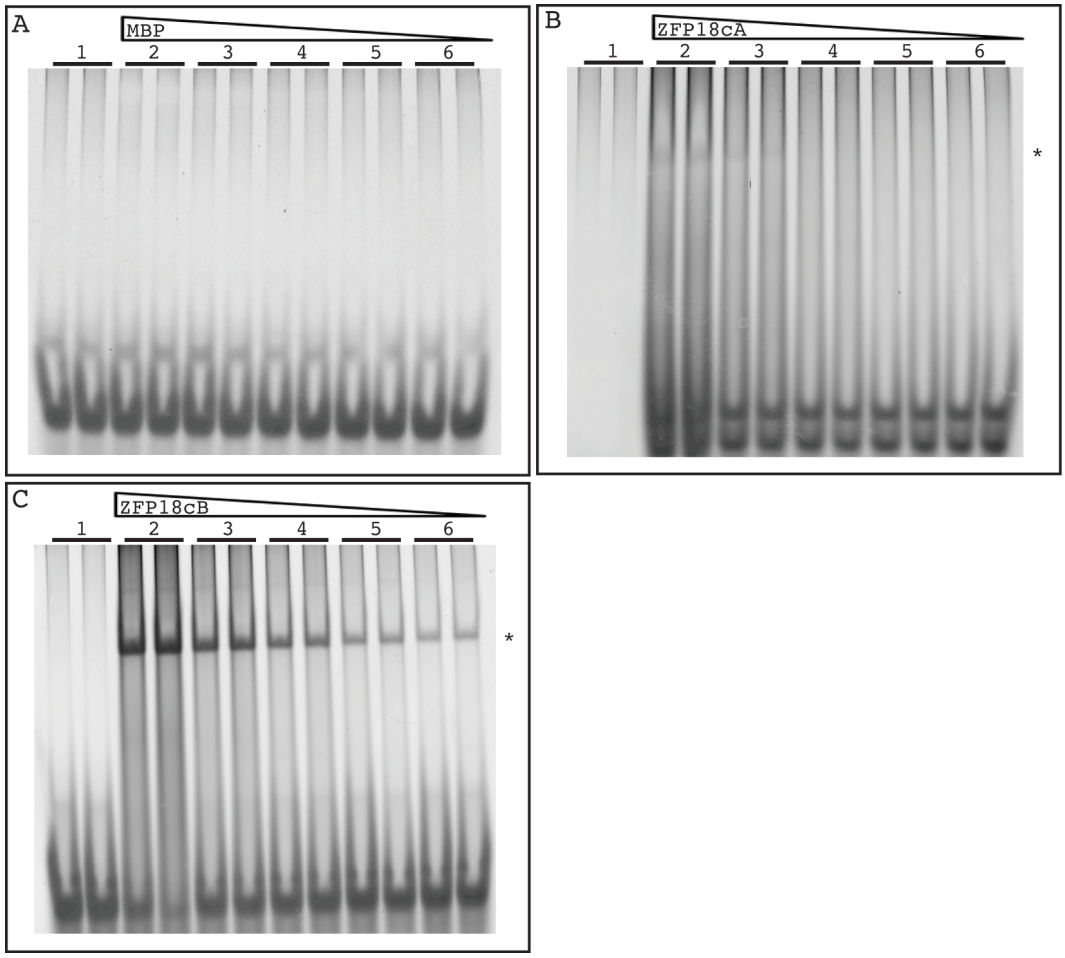

Figure 2.6 - EMSAs to determine the apparent equilibrium dissociation constant of DHBV-specific control ZFPs.
(A) MBP alone, (B) ZFP18cA-MBP or (C) ZFP18cB-MBP were incubated with dsDNA oligonucleotides with the specific target sequence for (A) ZFP18A, (B) ZFP18cA or (C) ZFP18cB, respectively. (Lane 1) dsDNA oligonucleotides without protein, (lane 2) protein added at 150-nM, serially diluted 1 in 2 (lanes 3 – 5) down to 9.5-nM (lane 6). Each sample is in duplicate. The gels were stained with SYBR-green DNA stain. The asterisk (*) marks the DNA-protein complex. The bands next to the asterisks were quantified using Image Gauge software v4.22, and the dissociation constant was calculated using the Enzyme Kinetics software v1.11. Each EMSA was performed 2-3 times.

The bands in the EMSAs representing the complexed ZFP-MBP and dsDNA oligonucleotide were quantified using ImageGauge v4.22 software. After subtracting both local and global background measurements, the values were plotted using the Enzyme Kinetics v1.11 software program. The non-linear regression plots for ZFP18A, ZFP18B, ZFP18C and ZFP9A1 can be found in

Figure 2.7 and show the concentration (nM) of ZFPs on the x-axis against the amount of binding (arbitrary units) on the y-axis.

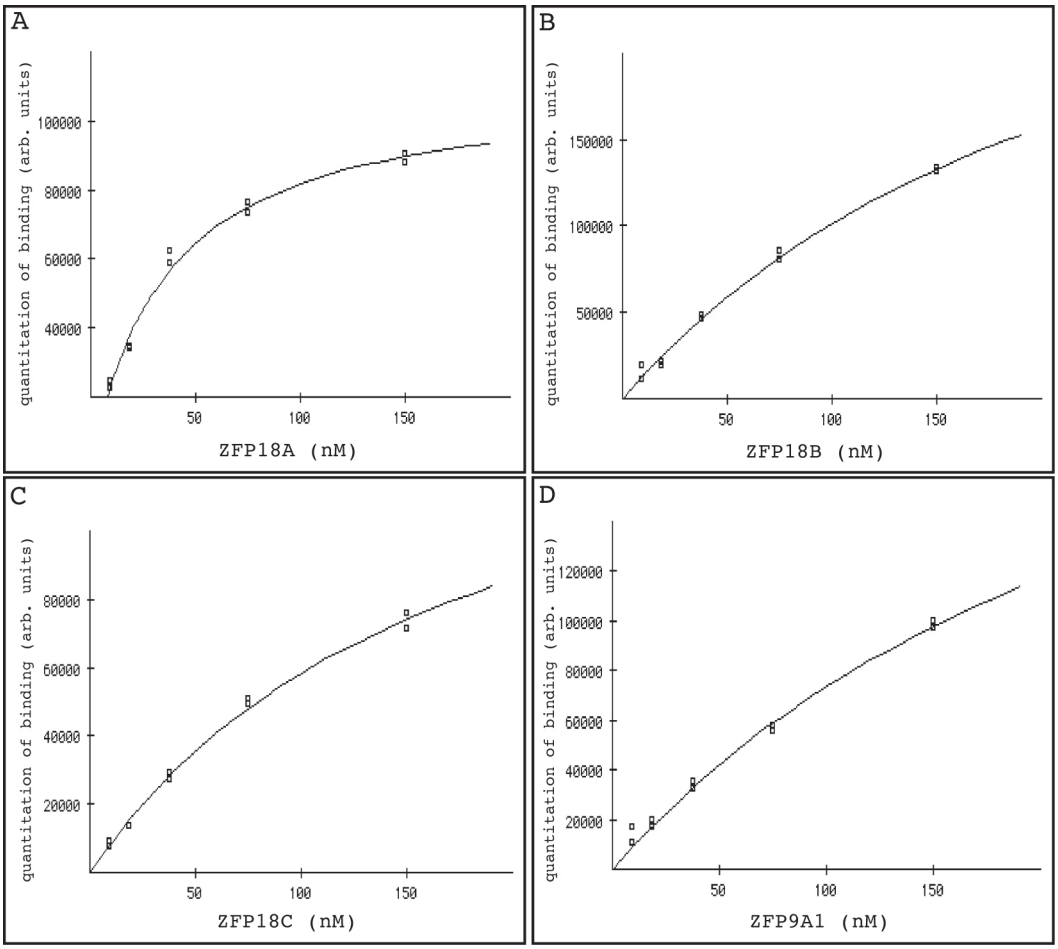

Figure 2.7 - Non-linear regression plots from the quantification of EMSAs of DHBV-specific ZFPs.
EMSAs were quantified and analyzed using the Enzyme Kinetics software v1.11. The non-linear regression plots were created by plotting the concentration (nM) of the ZFP (x-axis) against the amount of binding (y-axis). Graphs show the values for a single representative EMSA.

The dissociation constants, found in Table 2.9, were calculated from these graphs based upon the Michaelis-Menton equation. All four of these ZFPs had dissociation constants in the nanomolar range, which is frequently considered to be sufficient for therapeutic development. ZFP18A had the strongest binding with a dissociation constant of 37.0-nM, followed by ZFP9A1 with a dissociation

constant of 115.0-nM. ZFP18B was calculated to have a dissociation constant of 179.0-nM and ZFP18C of 203.0-nM. Dissociation constants for ZFP9B1 and ZFP9B2 could not be calculated because the bands in the EMSAs were not distinct. ZFP9A2 and ZFP18cA had no binding, and thus were not plotted nor calculated to have dissociation constants.

DHBV-specific ZFPs			
Name	EMSA	Name	EMSA
ZFP18A	37.0-nM	ZFP9A1	115.0-nM
ZFP18B	179.0-nM	ZFP9A2	n.b.[a]
ZFP18C	203.0-nM	ZFP9B1	n.c.[b]
		ZFP9B2	n.c.

Table 2.9 - Dissociation constants calculated by EMSA for DHBV-specific ZFPs.
[a] No binding. [b] Not calculated.

2.3.4 EMSA: Determination of specificity for target sequence by DHBV-specific ZFPs

The specificity of the ZFPs to their target sequences was assessed by competition-based EMSAs (Figure 2.8). The protocol is based upon the idea that a ZFP that exhibits specificity for its target sequence should preferentially bind to its target sequence, generally in the form of a radiolabeled probe (lane 2). The ZFP should not be competed off from this probe by the addition of unlabeled oligonucleotide with a non-specific sequence (lane 6). In addition, it should be competed off from the probe by the addition of increasing amounts of unlabeled specific oligonucleotide (lanes 3 – 5). Lastly, a specific ZFP should not bind a radiolabeled probe with a non-specific sequence (lane 7). Lane 1 contains radiolabeled probe without ZFP added.

Since only ZFP18A, ZFP18B, ZFP18C and ZFP9A1 exhibited strong binding as determined by their dissociation constants, competition-based EMSAs were

performed on these ZFPs (Figure 2.8). The competition EMSA of ZFP18A (Figure 2.8 A) demonstrates a ZFP that is specific for its target sequence. It binds to its target sequence (lane 2), and is incrementally competed off from the probe by the addition of unlabeled specific oligonucleotide (lanes 3 – 5). In these lanes, the ZFP becomes distributed between binding the probe and the unlabeled oligonucleotide, thus less ZFP is available to bind to the probe and the band is decreased in those lanes. Additionally, ZFP18A is bound to the probe in the presence of an unlabeled non-specific oligonucleotide (lane 6) to the same extent as in lane 2 indicates that it has a preference for its own target sequence and is not binding DNA unselectively. This is confirmed by lane 7, where a non-specific probe is incubated with ZFP18A, and binding is not detected.

ZFP18B (Figure 2.8 B) and ZFP9A1 (Figure 2.8 D) demonstrate similar patterns, wherein they are competed by unlabeled specific oligonucleotides (lanes 3 – 5), but not by non-specific competitors (lane 6). Further, they do not bind a non-specific probe (lane 7). ZFP18C (Figure 2.8 C), however, did not exhibit the same specificity profile. Instead, it appeared to bind the non-specific probe (lane 7) to an equal extent as its specific probe. This indication of non-specific binding prompted me to eliminate ZFP18C from further analysis.

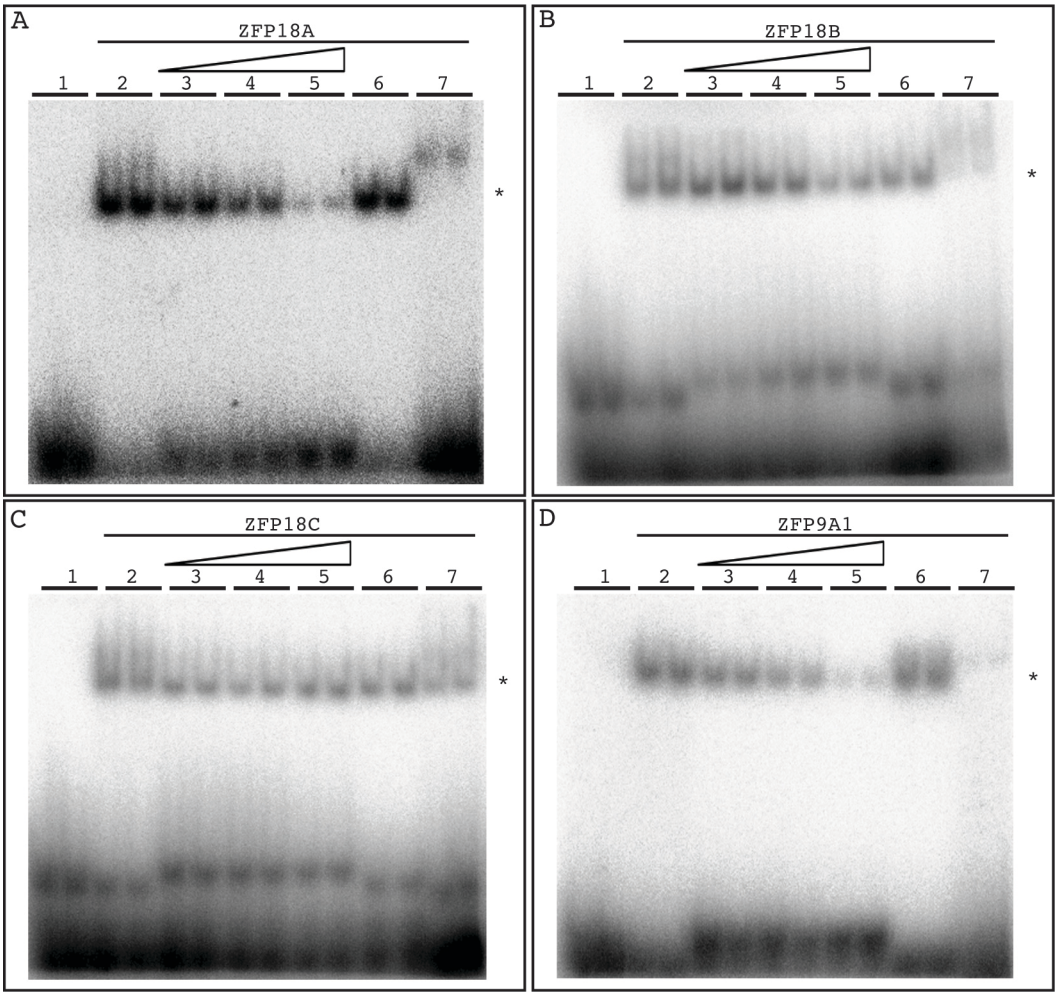

Figure 2.8 - EMSAs to determine the specificity of DHBV-specific ZFPs.
DsDNA oligonucleotides with the specific target sequence for each ZFP were radiolabeled with ^{32}P and incubated alone (lane 1) or in the presences of 150-nM ZFP-MBP fusion protein (lanes 2 – 7). In addition, unlabeled specific oligonucleotide competitor DNA was added at 5-μM, 10-μM or 50-μM concentrations (lanes 3 – 5, respectively), or unlabeled non-specific competitor DNA was added at 50-μM concentration (lane 6). Lastly, radiolabeled non-specific probe was incubated with 150-nM ZFP-MBP protein (lane 7). Each sample is in duplicate. The asterisk (*) marks the mobility shift formed when the dsDNA oligonucleotide is bound to the ZFP-MBP fusion protein.

2.3.5 Surface Plasmon resonance on DHBV-specific ZFPs

To further characterize the binding characteristics of the designed ZFPs, surface Plasmon resonance (SPR) was used, which measures association and disassociation rates in real time and calculates association and dissociation equilibrium constants. SPR measures the real-time interactions between a ligand

anchored to a detection surface and an analyte that flows over the detection surface. In the case of the ZFPs, biotinylated dsDNA oligonucleotides were anchored to a sensor chip flow cell (detection surface) coated with streptavidin. The analytes were the ZFPs, which flowed over the detection surface and produced a 1:1 binding scenario with the immobilized oligonucleotides. The analytes also flow over a second sensor chip flow cell without immobilized oligonucleotides, as a reference for non-specific binding. Any measurements from this flow cell were subtracted from the measurements of the detection surface.

SPR was performed using the automated BIAcore 3000 machine on ZFP18A, ZFP18B, ZFP9A1, ZFP9A2, ZFP9B1 and ZFP9B2. For each ZFP, a range of concentrations were passed over the sensor chip surface, from low to high concentrations, with a regeneration step in between each concentration to renew the surface of the sensor chip. Binding was measured as ZFPs passed over the surface, by measuring the change in refraction of light on the sensor surface, caused by analyte binding to ligand. This change is plotted as response difference in resonance units (RU), with more binding producing higher response differences than less binding. In Figure 2.9, the response difference (RU) on the *y*-axis is plotted against the time (seconds) on the *x*-axis for each ZFP18A (A), ZFP18B (B), ZFP9A1 (C) and ZFP9B1 (D). Each line on these graphs represents a different concentration of ZFP passed over the sensor chip surface. SPR was carried out for ZFP9A2 and ZFP9B2 as well, but these experiments produced data indicating no binding was occurring.

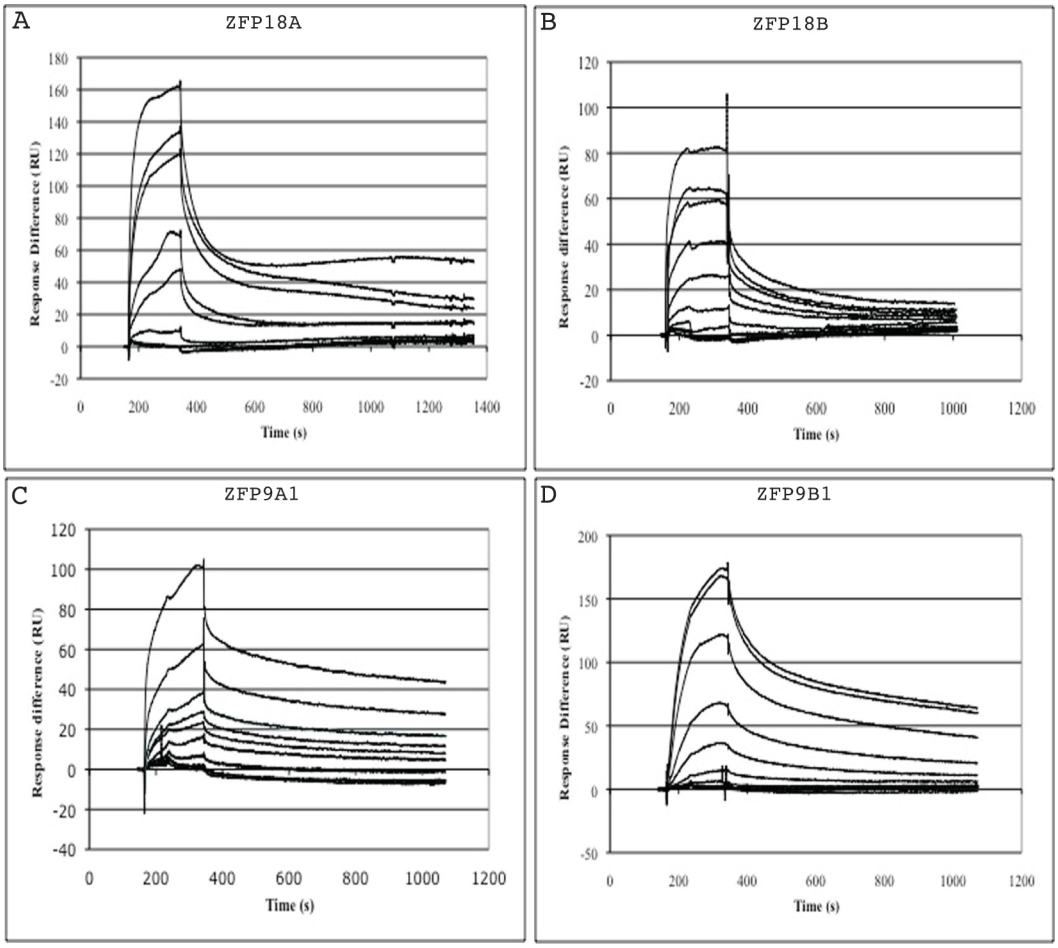

Figure 2.9 - SPR on DHBV-specific ZFPs.
SPR was performed on DHBV-specific ZFP-MBP fusion proteins using the BIAcore 3000 and biotinylated dsDNA oligonucleotides coupled to streptavidin on a Sensor Chip SA. ZFPs were flowed over the sensor chip surface and the amount of ZFP binding to the target DNA was measured by the change in the refractive index on the sensor chip surface. This change is calculated as the response difference in resonance units (RU), and is plotted on the *y*-axis, against time on the *x*-axis (seconds). ZFPs were flowed over the sensor chip surface for 3 minutes, followed by 15 minutes of dissociation time. ZFPs were injected at a range of concentrations in duplicate, running from low to high concentrations. Between each round of injections, the surface was regenerated with 0.5% SDS to remove any bound ZFP from the previous round. Each line represents the average of duplicate analysis of one concentration of ZFP. Three blanks were also performed in duplicate. For each sample, the measurements from a reference flow cell lacking the oligonucleotides were subtracted.

Fitting the data to a 1:1 binding with drifting baseline model produced the association and dissociation rates and constants. The baseline drift was likely due to incomplete renewal of the sensor chip surface after the regeneration step, due to incomplete removal of ligand bound ZFP during regeneration. The dissociation constants (Table 2.10) are in general agreement with those calculated by EMSA (Table 2.9). For example, the dissociation constant for ZFP18A was calculated as 36.9-nM by EMSA and 12.3-nM by SPR, which is a 3-fold difference. The dissociation constant for ZFP18B was 179.4-nM by EMSA and 40.2-nM by SPR; almost a 5-fold difference between the two protocols, with SPR suggesting a stronger binding affinity for its target than that suggested by the EMSA. ZFP9A1 exhibited a consistent dissociation constant for both protocols. The dissociation constant was calculated for ZFP9B1 by SPR was 67.1-nM. In agreement with that seen by EMSA, ZFP9A2 and ZFP9B2 demonstrated none or poor binding: the SPR data for these ZFPs could not be fit to the model.

DHBV-specific ZFPs					
Name	Association rate ($M^{-1}s^{-1}$)	Dissociation rate (s^{-1})	Association constant (M^{-1})	Dissociation constant (nM)	Chi^2 value
ZFP18A	2.74×10^5	3.37×10^{-3}	8.12×10^7	12.3	15.8
ZFP18B	1.11×10^5	4.45×10^{-3}	2.49×10^7	40.2	2.35
ZFP18C	n.d.[a]	n.d.	n.d.	n.d.	n.d.
ZFP9A1	1.84×10^4	1.82×10^{-3}	1.01×10^7	99.0	1.70
ZFP9A2	n.b.[b]	n.b.	n.b.	n.b.	n.b.
ZFP9B1	4.14×10^4	2.78×10^{-3}	1.49×10^7	67.1	3.9
ZFP9B2	n.b.	n.b.	n.b.	n.b.	n.b.

Table 2.10 - Kinetic data from SPR on DHBV-specific ZFPs.
[a] Not done. [b] No binding.

The association rate describes the number of ZFP-DNA complexes formed per second in a 1M solution of ZFP and DNA. The association rates ranged from $1.84 \times 10^4 - 2.74 \times 10^5$ $M^{-1}s^{-1}$ (Table 2.10), and shows that the 18-mers had more ZFP-

DNA complexes forming per second than the ZFP 9-mers. The dissociation rates ranged from 1.82 x 10^{-3} – 4.45 x 10^{-3} s^{-1} (Table 2.10). This rate describes the stability of the complex formed by ZFPs and DNA. For example, a dissociation rate of 4.45 x 10^{-3} s^{-1} (0.00445 s^{-1}) describes 0.445% of the complexes dissociating per second. There was little difference in the dissociation rates for the 18-mers compared to the 9-mers. The association constant describes the binding strength of the ZFP to the DNA, which was similar for all of the ZFPs (Table 2.10). Lastly, the Chi^2 value is a measurement of the goodness of fit to the model. Smaller values for Chi^2 indicate a better fit to the model.

2.3.6 Transfection of LMH cells expressing DHBV with ZFPs

ZFPs were cloned into the eukaryotic expression vector pcDNA3.1(+). ZFPs were then PCR amplified and cloned into pCR4-TOPO. The primers (Table 2.6) added a nuclear localization signal (NLS) to the N terminus of each ZFP, which will localize the expressed ZFPs with DHBV DNA in the nucleus. Subsequent restriction digest and directional ligation into pcDNA3.1(+) yielded positive clones that were used to transfect LMH cells.

LMH cells were plated in 6-well plates and co-transfected with pDHBV1.3 and pcDNA3.1(+)-ZFP18A, ZFP18B, ZFP9A1, ZFP9A2, ZFP9B1, ZFP9B2, ZFP18cA, ZFP18cB or ZFP18cC. The ratio of pDHBV1.3 to pcDNA3.1(+)-ZFP was 1:3, ensuring an excess of ZFP expression within cells compared to DHBV expression. When LMH cells are transfected with the pDHBV1.3 plasmid, they competently replicate the viral life cycle, including viral RNA and protein production, virus progeny production and secretion of infectious virus. However, LMH cells lack the receptors to allow infection of DHBV, thus there is no re-infection of the tissue culture cells by their production of infectious virus. Small amounts of cccDNA can also accumulate in LMH cells, however it generally takes four or more days for enough cccDNA to accumulate to be detectable, and even then it is a weak signal.

For each experiment, two wells were additionally transfected with pd1-EGFPn1 alone. These wells were assessed under the fluorescence microscope for GFP expression at 24 and 48 hours post-transfection to determine transfection efficiency. Transfection efficiencies were consistently between 40 – 60%.

2.3.7 Assessment of the effect of ZFPs on the DHBV RNA species in LMH cells

Total RNA from transfected LMH cells was harvested after 24 hours and converted into cDNA. The cDNA was assessed for DHBV pgRNA and GAPDH levels using quantitative PCR on the Roche LightCycler® 2.0. The DHBV results were normalized to GAPDH levels and then converted into percentages, with the empty vector sample set as 100%. In general, there was a decrease in the amount of DHBV pgRNA in cells expressing DHBV-specific ZFPs (Figure 2.10 A). Specifically, ZFP9B2 decreased DHBV pgRNA by 65.7%, and ZFP18A, ZFP9A2 and ZFP9B1 all decreased DHBV pgRNA by 68.4 ± 0.3%. All of these values were statistically significant compared to the empty vector control ($p < 0.05$). ZFP18B decreased the amount of DHBV pgRNA by 58.4% and ZFP9A1 decreased the amount by 45.3%, neither of which was statistically significant. In contrast, none of the control ZFPs demonstrated any ability to change the amount of DHBV pgRNA in LMH cells expressing them, compared to the empty vector control (Figure 2.10 B). The fact that the control ZFPs do not cause a similar decrease in pgRNA to the experimental ZFPs, suggests that the ZFPs do not simply usurp supplies and machinery from DHBV when the ZFPs are co-expressed with the virus. This demonstrates the ability of the DHBV-specific experimental ZFPs to cause a decrease in DHBV pgRNA in cells expressing them, which is not related to a supply limitation problem.

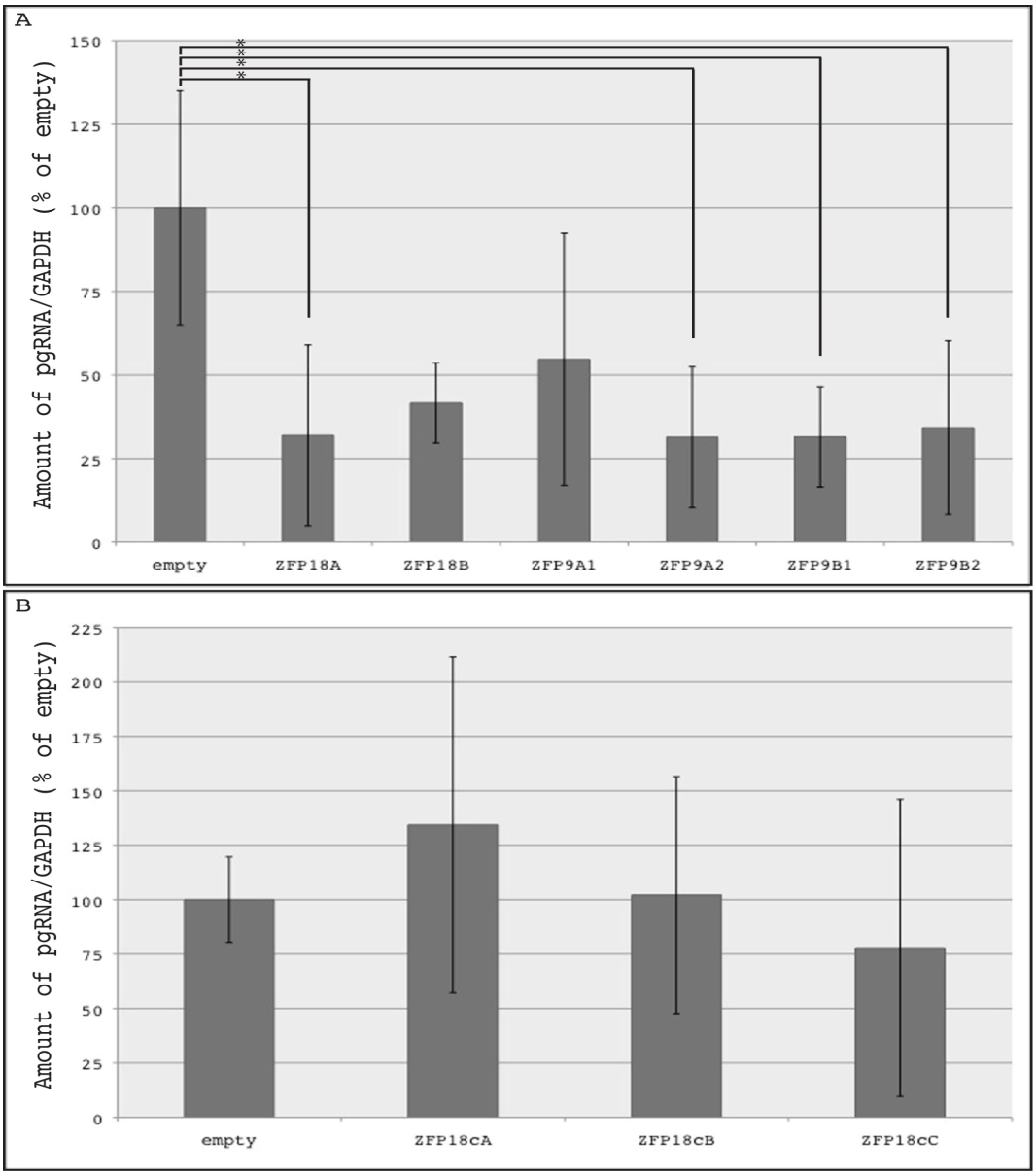

Figure 2.10 - Quantitative PCR for DHBV pgRNA in LMH cells expressing DHBV-specific ZFPs.

LMH cells were co-transfected with 1-μg of pDHBV1.3 and 3-μg of pcDNA3.1(+) (empty) or (A) pcDNA3.1(+)-ZFP18A, ZFP18B, ZFP9A1, ZFP9A2, ZFP9B1 and ZFP9B2, or (B) pcDNA3.1(+)-ZFP18cA, ZFP18cB or ZFP18cC. Total RNA was harvested after 24 hours and cDNA was made using oligo$(dT)_{20}$ as primer. Quantitative PCR was performed using the Roche LightCycler® and primers specific for DHBV pgRNA or chicken GAPDH. The DHBV values were normalized to chicken GAPDH and are presented as the combined mean from two (A) or three (B) experiments. The empty vector control was set to 100%. The error bars indicate the standard deviation. * indicates statistical significance between the empty vector control and the ZFP ($p < 0.05$).

Due to the overlapping nature of the viral RNA species, qPCR could only be used to determine the levels of pgRNA. Thus, in order to investigate the levels of all three DHBV transcripts, a Northern blot was performed on total RNA from transfected LMH cells harvested after 24 hours (Figure 2.11 A). The Northern blot was probed with a DHBV-specific probe, or in parallel with a GAPDH-specific probe. Since the bands for the DHBV transcripts were relatively indistinct except for the 3.0-kb band, the total RNA or the 3.0-kb band in each lane of Figure 2.11 A were quantified using the ImageGauge v4.22 software and normalized to the GAPDH signal in the associated blot. This was then plotted in (Figure 2.11 B), where you can better see the trend of decreased viral RNA in the presence of ZFP18A or ZFP18B, but not in the presence of the control, ZFP18cA. Overall, the designed ZFPs have a decreasing effect on the amount DHBV pgRNA in LMH cells.

2.3.8 Assessment of the effect of ZFPs on protein expression in LMH cells

Whole cell lysates were collected from LMH cells transfected with DHBV-specific ZFPs and analyzed by Western blot for protein expression. The expression of ZFPs in LMH cells co-expressing DHBV proteins resulted in a dramatic decrease in the amount of DHBV core and preS protein, and to a lesser extent, S protein (Figure 2.12 A & B). Specifically, ZFP 18-mers and ZFP 9-mers decreased the amount of viral protein products. In contrast, the control ZFPs (Figure 2.12 C) showed a small decrease in DHBV core, but no effect on either preS or S protein expression in LMH cells expressing them. Actin was used as a loading control for all blots.

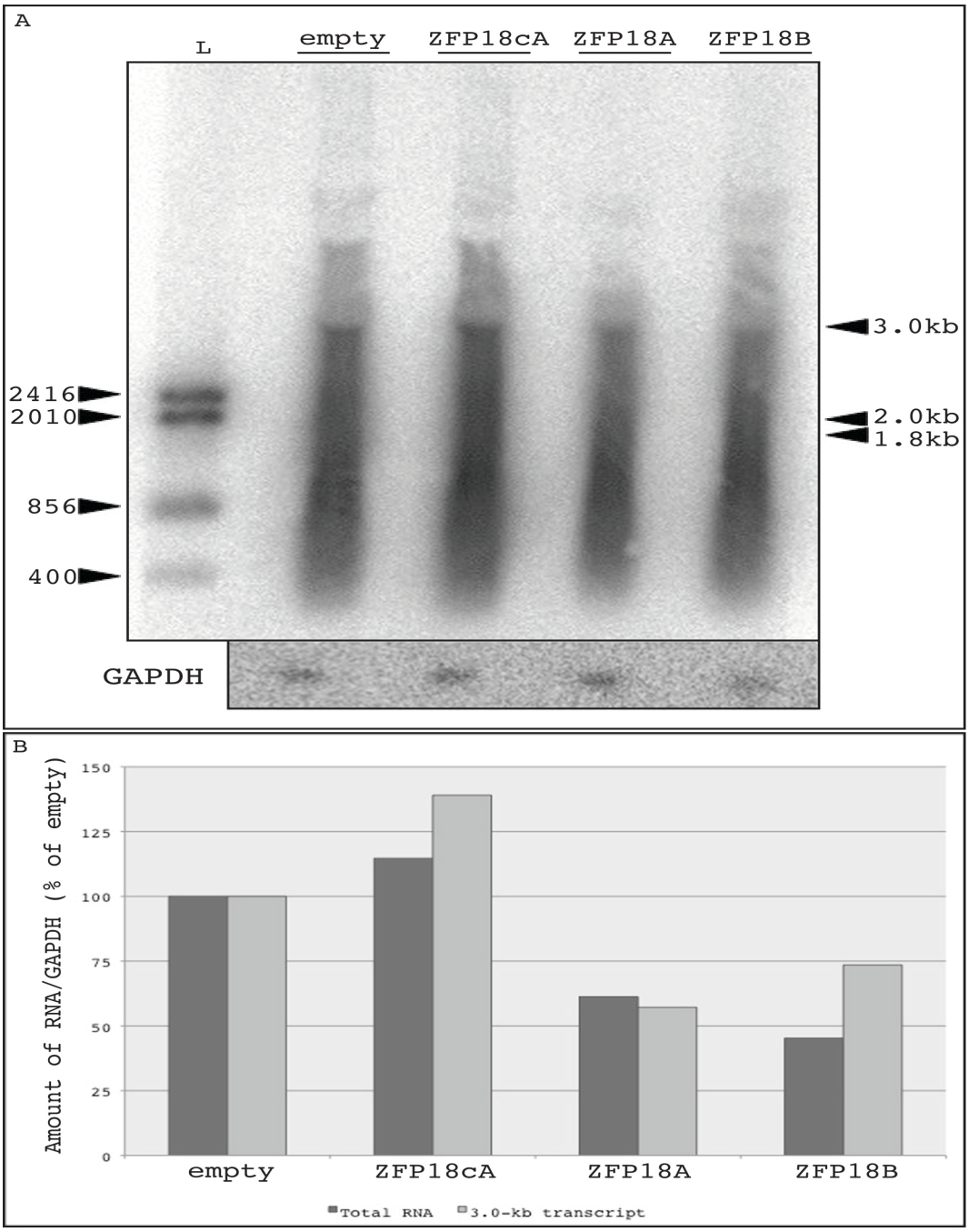

Figure 2.11 - Northern blot analysis of DHBV RNA and GAPDH in LMH cells expressing DHBV-specific ZFPs.

(A) LMH cells were co-transfected with 1-μg of pDHBV1.3 and 3-μg of pcDNA3.1(+) (empty) or pcDNA3.1(+)-ZFP18A, ZFP18B, and ZFP18cA. Total RNA was harvested after 24 hours and analyzed by Northern blot. The 3.0-kb, 2.0-kb and 1.8-kb DHBV transcripts are marked with a solid black arrow on the right. The ladder (L) sizes are marked with a solid black arrows on the left. The GAPDH Northern blot is aligned at the bottom of the DHBV Northern blot. (B) The total RNA or the 3.0-kb band in each lane of (A) was quantified and normalized to GAPDH, then plotted as a percentage of the empty vector control.

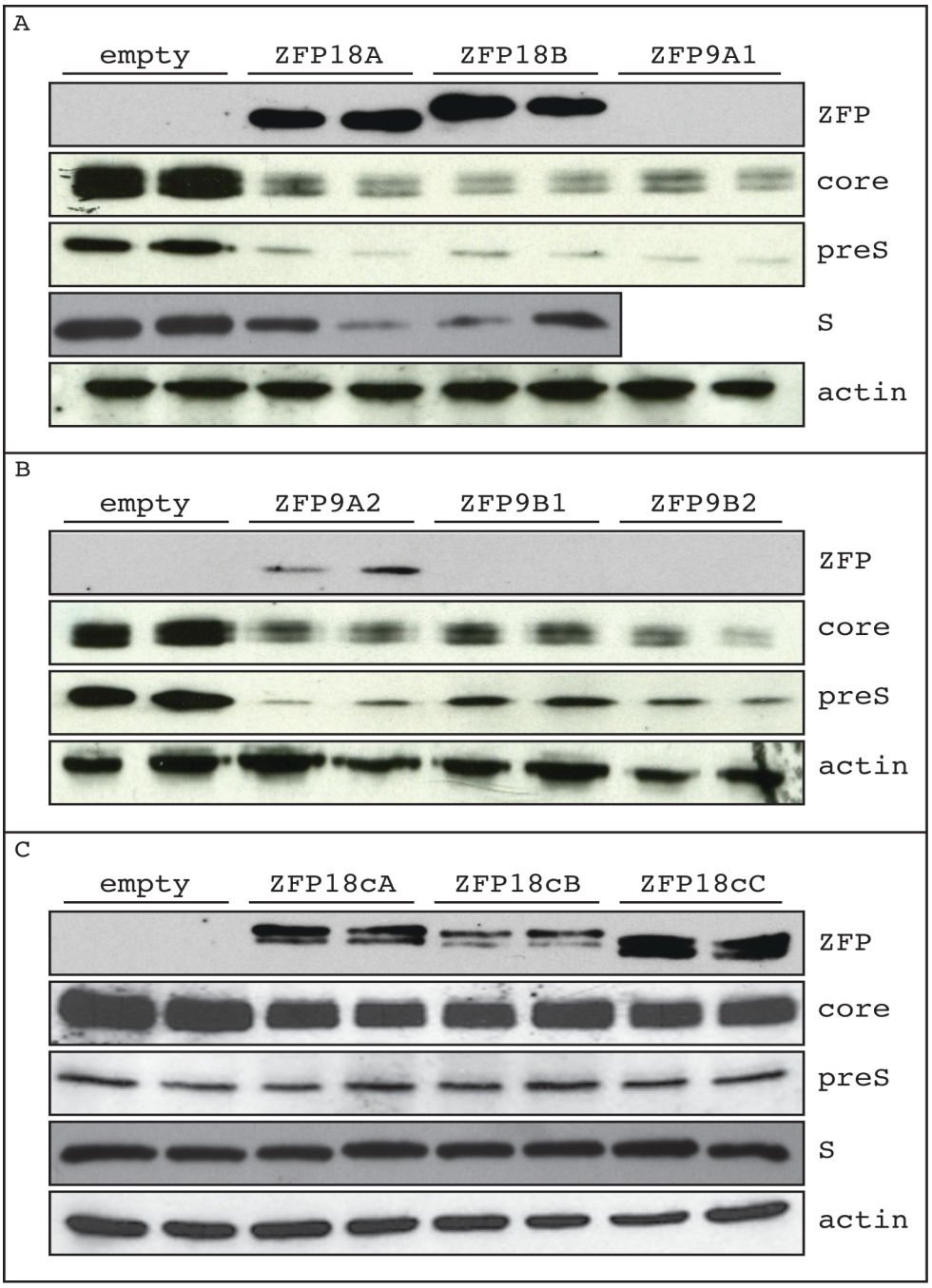

Figure 2.12 - Western blot analysis of protein expression in LMH cells expressing DHBV-specific ZFPs.

LMH cells were co-transfected with 1-μg of pDHBV1.3 and 3-μg of pcDNA3.1(+) (empty) or (A) pcDNA3.1(+)-ZFP18A, ZFP18B, and ZFP9A1, (B) pcDNA3.1(+)-ZFP9A2, ZFP9B1 and ZFP9B2, or (C) pcDNA3.1(+)-ZFP18cA, ZFP18cB or ZFP18cC. After 24 hours, whole cell lysates were collected using RIPA buffer and assessed for protein expression by Western blot using anti-ZFP antiserum (ZFP), anti-DHBV core (J112) (core), anti-DHBV preS (1H1) (preS), anti-DHBV S (7C12) (S) and anti-actin (actin) antibodies. These Western blots were repeated 2-3 times.

The presence of ZFPs in the transfected cells was detected using custom anti-serum produced against ZFP18A-MBP fusion protein, which produces a strong signal against ZFP18A, ZFP18B and all three control ZFPs (Figure 2.12 C). However, the anti-serum produces weak (ZFP9A2) or no signal against the 9-mers, which I have consistently noticed since receiving the custom anti-serum. As such, it is impossible to determine whether there was no expression of ZFP9A1, ZFP9B1 and ZFP9B2 in the LMH cells, or whether the custom anti-serum was not specific for detecting the 9-mers, which is the more likely case.

In summary, the Western blot results support the RNA data, wherein the presence of ZFPs results in a decrease in the amount of DHBV protein products in LMH cells.

2.3.9 Assessment of the effect of ZFPs on DHBV virus production in LMH cells

LMH cells were transfected with DHBV-specific ZFPs and virus production was analyzed after 24 hours by assessing both intracellular virus (ICV) and extracellular virus (ECV). ICV was assessed by Southern blot (Figure 2.13 A), which was subsequently quantified using ImageGauge v4.22 software. After subtracting background levels, the means of duplicate lanes were plotted using the arbitrary units calculated by ImageGauge (Figure 2.13 B). ZFP18A and ZFP18B decreased the amount of ICV the greatest compared to the empty vector control, although the difference was not statistically significant. ZFP18A decreased ICV production by 57.1% and ZFP18B by 71.1%. ZFP9A1, ZFP9A2 and ZFP9B1 also moderately decreased the amount of ICV, by 21.6%, 30.0% and 25.3%, respectively. Lastly, ZFP9B2 produced a widely variable result due to one lane out of two duplicates that was dramatically higher than the other one. Thus, while the mean of ZFP9B2 was 125% higher than the empty vector, the standard deviation (as shown by the error bars) was large, representing uncertainty in the validity of that result.

Compared to the ICV analysis, which showed a general trend of moderate decrease in the presence of ZFPs, ECV production did not seem greatly impacted by the expression of DHBV-specific ZFPs. ECV was assessed using quantitative PCR on isolated DNA using DHBV-specific primers. The results were converted to percentages, with the empty vector control set at 100% (Figure 2.13 C). ZFP18A demonstrated a very minimal decrease of 2.94%, whereas ZFP18B had a larger decrease of 28.4%. Both ZFP9A1 and ZFP9A2 produced no decrease. ZFP9B1 and ZFP9B2 decreased the ECV by 32.1% and 43.4%, respectively. None of these decreases were statistically significant. It was consistently difficult to see dramatic decreases in ECV production in transfected LMH cells, despite the demonstration of decreases in viral pgRNA and protein expression. This experiment was repeated three times, however results varied each time the experiment was performed.

2.3.10 Assessment of the metabolic activity of LMH cells expressing DHBV-specific ZFPs

In order to determine that decreases in viral products were not a result of cell death upon expression of ZFPs, LMH cells were transfected with pDHBV1.3 and pcDNA3.1(+)-ZFP18A, ZFP18B, ZFP9A1, ZFP9A2, ZFP9B1, ZFP9B2, ZFP18cA, ZFP18cB or ZFP19cC and assessed after 24 hours using the MTT assay. This assay is based upon the reduction of the MTT reagent into a purple formazan dye that can be measured at 570-nm. The MTT assay gives a measurement of metabolically active cells. Expression of the ZFPs was not associated with any changes in the metabolic activity of the transfected cells compared to non-transfected or empty vector control (Figure 2.14). There were, however, statistically significant differences between ZFP9B1 and ZFP9A1, ZFP9B1 and ZFP9B2, and ZFP9A1 and ZFP18cA, however these are not relevant with respect to the comparison of empty vector control to ZFPs in the previous sections.

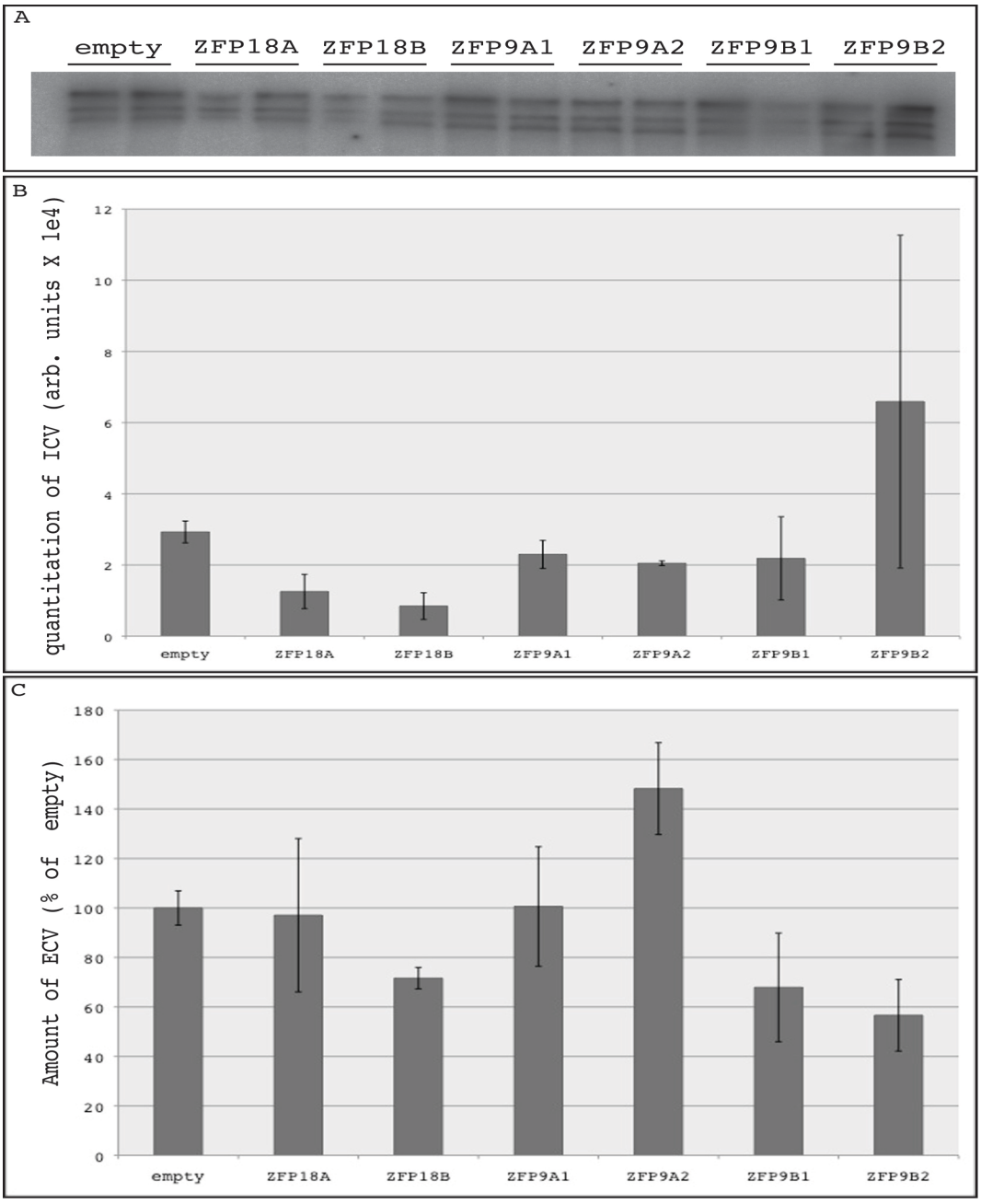

Figure 2.13 - Assessment of viral progeny production in LMH cells expressing DHBV-specific ZFPs.
LMH cells were co-transfected with 1-μg of pDHBV1.3 and 3-μg of pcDNA3.1(+) (empty) or pcDNA3.1(+)-ZFP18A, ZFP18B, and ZFP9A1, pcDNA3.1(+)-ZFP9A2, ZFP9B1 and ZFP9B2. ICV and ECV were harvested. ICV was assessed by Southern blot (A), which was quantified and plotted (B). ECV was quantified by quantitative PCR using the Roche LightCycler® and primers for DHBV (C). The results are presented as the mean from one experiment, with error bars to indicate the standard deviation. These experiments were performed twice.

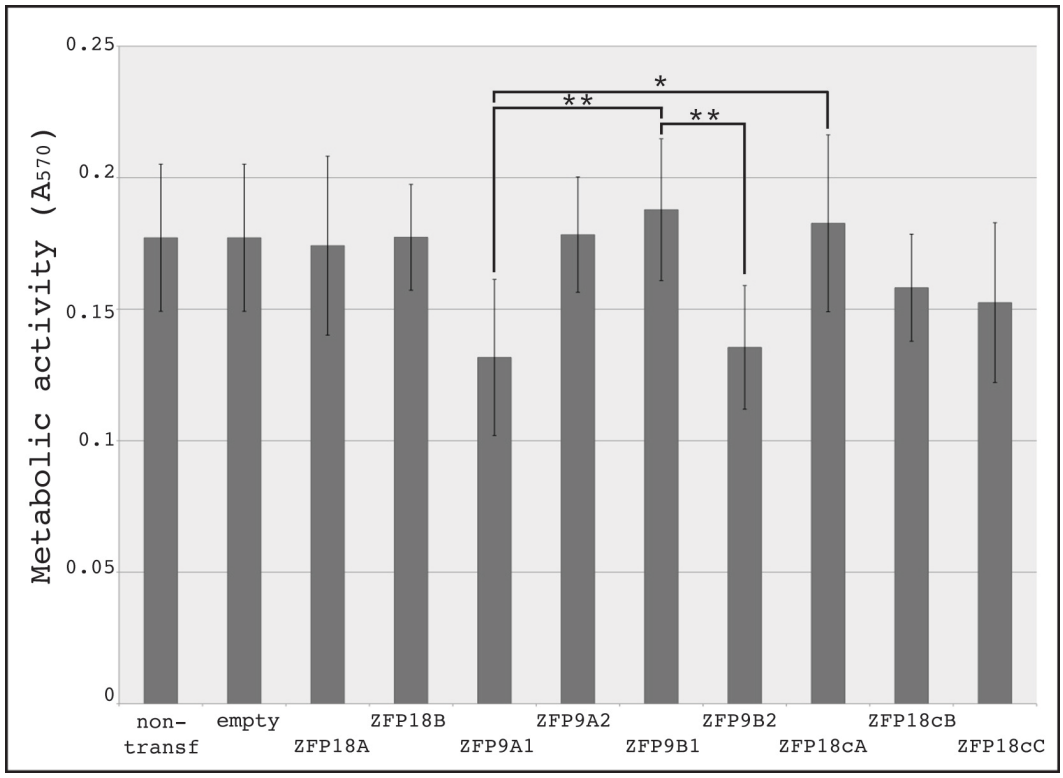

Figure 2.14 - MTT assay to test metabolic activity of LMH cells expressing DHBV-specific ZFPs.
The cell viability of LMH cells not transfected (non-transf), or transfected with pDHBV1.3 and pcDNA3.1(+) (empty) or pcDNA3.1(+)-ZFP18A, ZFP18B, ZFP9A1, ZFP9A2, ZFP9B1, ZFP9B2, ZFP18cA, zFP18cB or ZFP18cC was tested using the MTT assay. Absorbance (570-nm) is measured in each sample and is plotted on the y-axis. The results are presented as the mean of 6 wells, with error bars to indicate the standard deviation. * indicates statistical significance ($p < 0.05$) between the groups. ** indicates statistical significance ($p < 0.01$) between the groups. This experiment was repeated three times.

2.3.11 Visualization of DHBV-specific ZFPs expressed in LMH cells using confocal microscopy

Plasmids expressing ZFPs fused to EGFP were created in the pcDNA3.1(+) background by PCR amplifying EGFP from the pAdTrack-CMV1 plasmid. The PCR amplified product was ligated to pCR4-TOPO, and then transferred into pcDNA3.1(+)-ZFP18A, ZFP18B, ZFP9A1, ZFP9A2, ZFP9B1 or ZFP9B2 by restriction digest and directional ligation. No positive clones were successfully isolated for pcDNA3.1(+)-ZFP9A2, therefore confocal microscopy was not completed for this ZFP.

LMH cells were plated in plastic dishes with glass coverslips in the center. After 24 hours, they were transfected with one of the pcDNA3.1(+)-ZFP-EGFP plasmids. A further 24 hours after transfection, the nuclei were stained with Hoechst 33342, which allows live cell staining of nuclei. Using a multi-photon microscope, images of LMH cells expressing ZFP-EGFP (green) were collected, with the nuclei stained in blue. Z-stacks were arranged into orthogonal views for ZFP18A-EGFP and ZFP18B-EGFP (Figure 2.15 C&D). Both proteins are found predominantly within the nucleus, in contrast to EGFP alone in the positive control (Figure 2.15 A), which can be seen throughout the cell. This result is expected, since EGFP does not contain an NLS, but both ZFP18A and ZFP18B do contain an NLS. The negative control (Figure 2.15 B) demonstrates that pcDNA3.1(+) alone does not produce any EGFP signal, and that the ZFP18A-EGFP and ZFP18B-EGFP levels are above background levels.

The 9-mers were also visualized as ZFP-EGFP constructs (Figure 2.16). ZFP-EGFP expression can be seen for ZFP9A1 (Figure 2.16 C), ZFP9B1 (Figure 2.16 D) and ZFP9B2 (Figure 2.16 E). The 9-mers are not found as exclusively in the nucleus as seen for the 18-mers. ZFP9A1 appears to have the strongest expression of GFP, while ZFP9B1 and ZFP9B2 exhibit similar levels to each other. Again, the positive control can be seen throughout the cytoplasm and the nucleus (Figure 2.16 A) and the negative control demonstrates the fluorescence of the ZFP-EGFP constructs are above background levels (Figure 2.16 B).

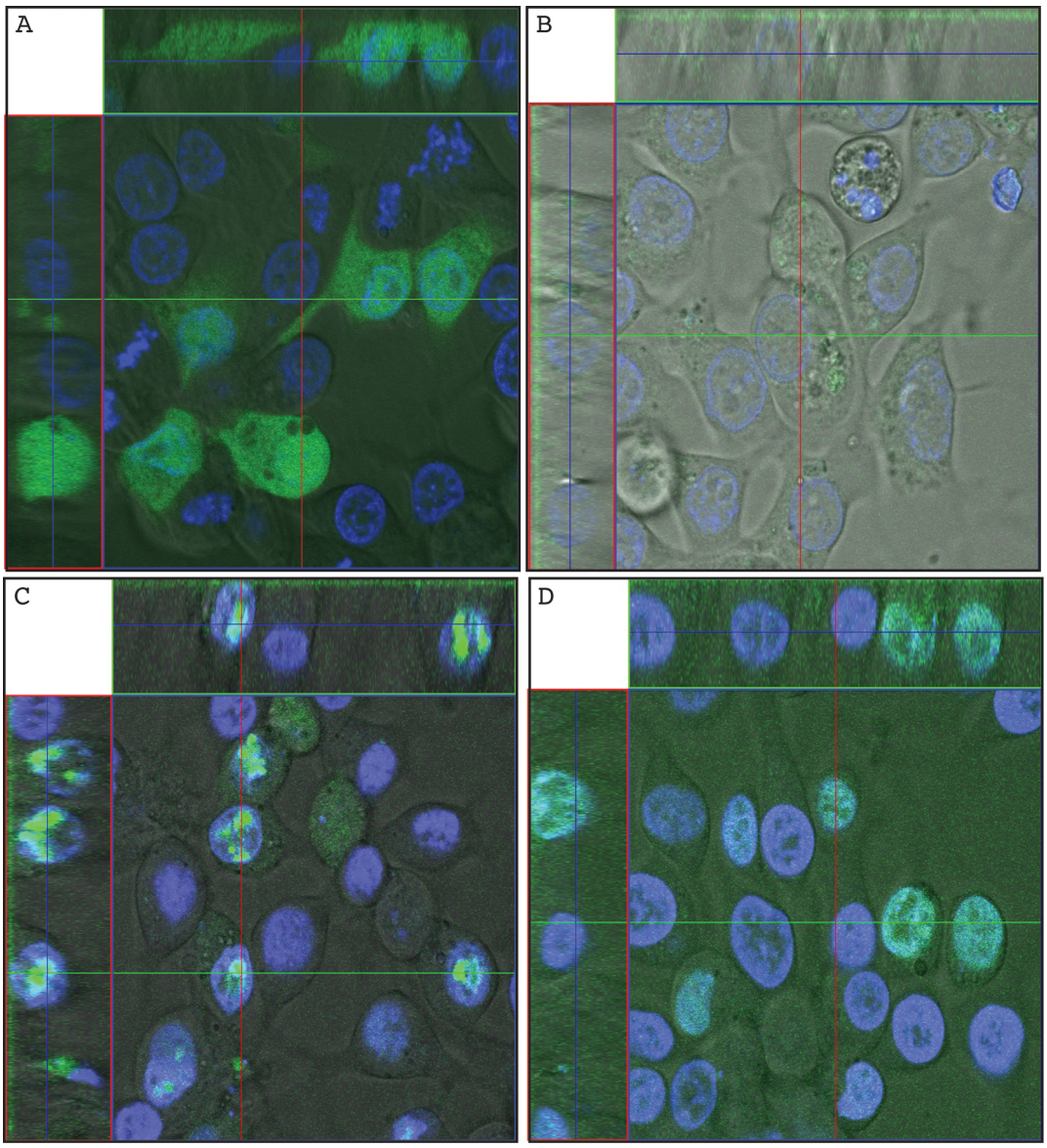

Figure 2.15 - Live cell imaging of DHBV-specific ZFP18-EGFP expression in transfected LMH cells.
LMH cells were plated in dishes with glass coverslips, then transfected with (A) pcDNA3.1(+)-EGFP (positive), (B) pcDNA3.1(+) (negative), (C) pcDNA3.1(+)-ZFP18A-EGFP or (D) pcDNA3.1(+)-ZFP18B-EGFP. After 24 hours, the nuclei were stained with Hoechst 33342 and visualized using a multi-photon microscope. EGFP is shown in green and nuclei are shown in blue. Z-stacks were collected and the orthogonal view is shown above. These experiments were performed twice.

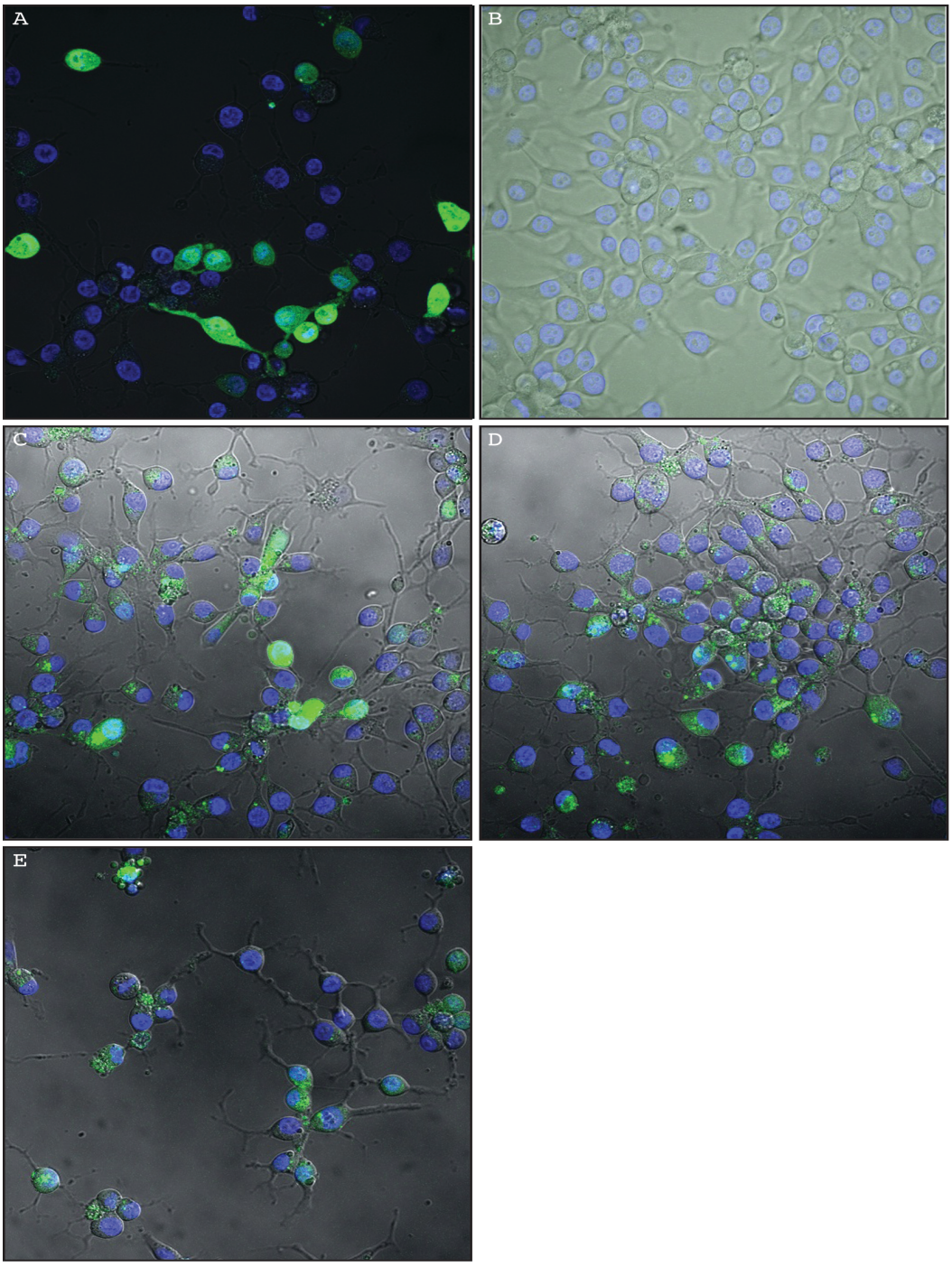

Figure 2.16 - Live cell imaging of DHBV-specific ZFP9-EGFP expression in transfected LMH cells.
LMH cells were plated in dishes with glass coverslips, then transfected with (A) pcDNA3.1(+)-EGFP (positive), (B) pcDNA3.1(+) (negative), (C) pcDNA3.1(+)-ZFP9A1-EGFP, (D) pcDNA3.1(+)-ZFP9B1-EGFP or (E) pcDNA3.1(+)-ZFP9B2-EGFP. After 24 hours, the nuclei were stained with Hoechst 33342 and visualized using a multi-photon microscope. EGFP is shown in green and nuclei are shown in blue. These experiments were performed twice.

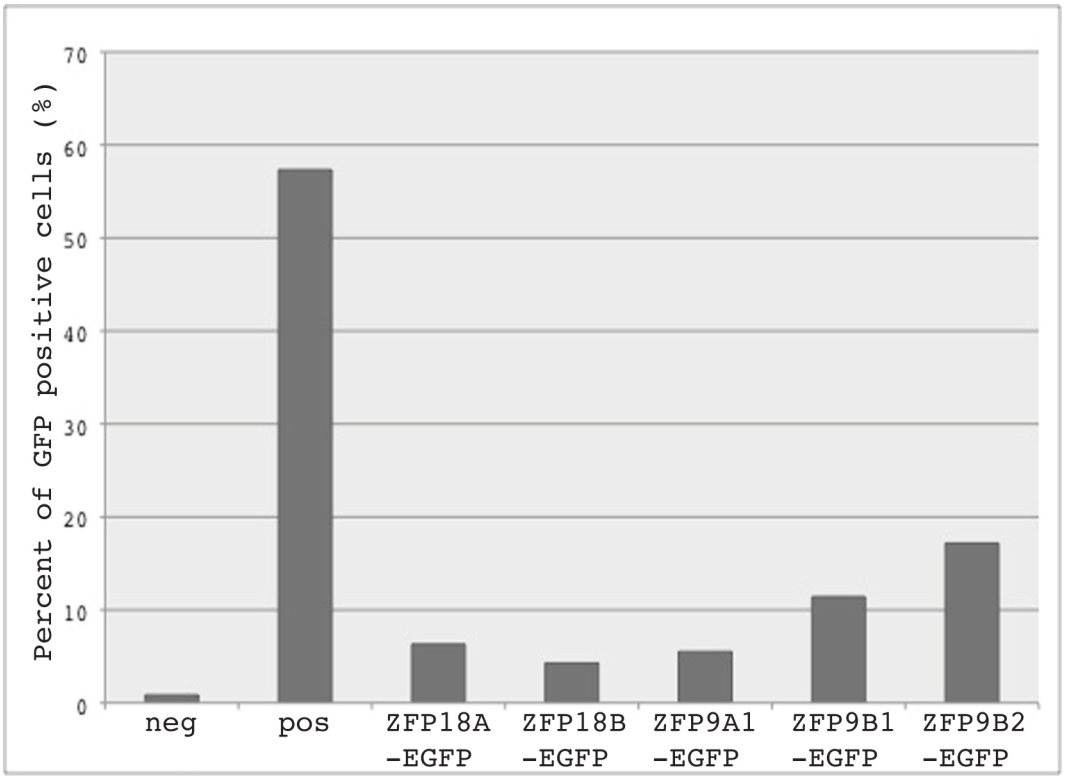

Figure 2.17 - Flow cytometry measurement of EGFP-expression in LMH cells transfected with ZFP-EGFP plasmids.
LMH cells were transfected with 4-µg of pcDNA3.1(+) (neg), pcDNA3.1(+)-EGFP (pos), pcDNA3.1(+)-ZFP18A-EGFP, -ZFP18B-EGFP, -ZFP9A1-EGFP, -ZFP9B1-EGFP or ZFP9B2-EGFP. After 24 hours, the cells were collected and sorted on EGFP using the BD FACScan™ Flow Cytometer. The percent of EGFP-positive cells were plotted (*y*-axis) for each treatment group. This experiment was performed twice.

2.3.12 Quantification of the ZFPs expressed in LMH cells using flow cytometry

LMH cells transfected with pcDNA3.1(+)-ZFP-EGFP plasmids were also assessed for GFP expression using flow cytometry. This allowed the quantification of ZFP expression, in the context of a ZFP-EGFP construct. Also, because WBs of ZFP 9-mers showed only faint or no bands using anti-ZFP18A antiserum (Figure 2.12) this confirms that ZFP9A1, ZFP9B1 and ZFP9B2 were expressed within transfected LMH cells. Again, since no positive clones for pcDNA3.1(+)-ZFP9A2-EGFP were obtained, this ZFP could not be analyzed by flow cytometry. Although the amount of cells expressing ZFP-EGFP was lower

than the positive control, there were detectable amounts of GFP expression in LMH cells expressing ZFP18A-EGFP, ZFP18B-EGFP, ZFP9A1-EGFP, ZFP9B1-EGFP and ZFP9B2-EGFP (Figure 2.17). 6.31% of LMH cells transfected with pcDNA3.1(+)-ZFP18A-EGFP were GFP positive. 4.29% of LMH cells expressed ZFP18B-EGFP, 5.52% expressed ZFP9A1-EGFP, 11.42% expressed ZFP9B1-EGFP and 17.18% expressed ZFP9B2-EGFP.

2.4 Discussion

As a novel approach to HBV therapy, ZFPs were designed to bind the cccDNA of the model virus DHBV. ZFPs were targeted to the DHBV enhancer region, which is known to be accessible to other transcription factors. Seven DHBV-specific ZFPs were designed: three recognizing 18-bps of target DNA (18-mers), and four recognizing 9-bps of DNA (9-mers). In general, the 18-mers bound their target sequences with greater affinity than the 9-mers. One of the 18-mers (ZFP18C) demonstrated off-target binding capabilities and was excluded from further analysis, but the remaining ZFPs were investigated in the context of DHBV replication in LMH cells.

LMH cells are chicken hepatoma cells that replicate the life cycle of DHBV when transfected with a plasmid encoding a greater-than-genome equivalent of DHBV. LMH cells cannot be infected with DHBV, but can produce infectious virus particles. They can also produce cccDNA, however in very small amounts after 4-7 days, making it difficult to detect. Thus, in this cell-system, expressed ZFPs actually bind to the transfected DHBV plasmid, rather than cccDNA.

All of the ZFPs were able to decrease the amount of viral RNA transcripts to varying degrees. This degree was further reflected in a decrease in the amount of viral protein products (core, preS, S) produced in the LMH cells in the presence of ZFPs. It was surprising that the ZFP 9-mers, especially ZFP9A2, ZFP9B1 and ZFP9B2, were able to decrease viral RNA transcripts and protein products to a similar degree compared to ZFP18A, ZFP18B and ZFP9A1, since the former ZFPs exhibited weak binding during *in vitro* binding assessments. However, the

bacterial expression and purification of ZFP9A2, ZFP9B1 and ZFP9B2 may have had a detrimental effect on the function of these ZFPs, due to possible misfolding. When ordering the synthesis of all the ZFPs from Blue Heron Technologies, the "codon-optimized" sequence was utilized, rather than the "expression-optimized" sequence. The codon-optimized sequence is preferable for eukaryotic expression of the sequences, whereas the expression-optimized sequence is better for prokaryotic expression for purification of proteins. This selection may have affected the production of some of the ZFPs in the bacterial expression systems, causing them to have poor binding characteristics that were not exhibited in tissue culture cells.

Despite dramatic reductions in the production of viral RNA and protein species, there were only moderate effects on the amount of ICV and ECV produced in the presence of ZFPs. One hypothesis for this may be that the assembly rate of virion particles is not dependent on the size of the pool of building blocks in the cytoplasm therefore the production of ICV and ECV would not be greatly affected by a decrease in the pool size. Thus, a reduction in the pool of viral RNA and protein species would not result in a change in the amount of ICV or ECV produced. Additionally, the poor consistency of the ICV Southern blots between repeat experiments may have been caused by the methodology. Total ICV is isolated from the cytoplasm of cells and it cannot be compared to any cell marker as standard. Thus, unlike Western blots that use actin as a loading control, isolation of ICV has no standard and any loss of material due to the isolation process can result in discrepancies during the final analysis.

Expression of the different ZFPs is presumed to be equivalent, however this cannot be confirmed, since the anti-ZFP antiserum does not strongly detect the ZFP 9-mers. ZFP18A and ZFP18B appear to be expressed to similar levels, suggesting that differences in the anti-DHBV effects are due to either binding affinity or the influence of the target site. For example, even though ZFP18B has a lower affinity than ZFP18A, it appears to have a greater effect on the amount of

ECV & ICV than ZFP18A. This could be due to the fact that ZFP18B binds in the middle of F2 in dEnI, whereas ZFP18A binds at the ends of F3 and may not be as effective at disrupting the binding of HNF-1. Both ZFP18A and ZFP18B were detected within the nucleus by live-cell imaging of cells transfected with ZFP-EGFP plasmids. This demonstrates that the NLS engineered onto the ZFPs is performing its function by delivering the ZFPs to the nucleus, the same compartment as the cccDNA target.

The expression levels of the ZFP 9-mers could not be determined by Western blot, however live-cell imaging and flow-cytometry of ZFP9A1, ZFP9B1 and ZFP9B2 as fusion proteins with EGFP showed that there is some expression of these proteins in LMH cells. By flow cytometry, ZFP9B1 and ZFP9B2 appear to have higher expression than the other ZFPs, however it is difficult to determine how the fusion to EGFP is influencing the expression level. Thus, while I am confident the ZFP 9-mers are being expressed in LMH cells, it is impossible to compare them to the ZFP 18-mers and determine how their expression levels may be affecting the levels of DHBV in the cell.

The designed ZFPs target the DHBV enhancer, which is known to control the core and small surface promoters, but not the large surface promoter (2, 3, 13, 14). However, the data show that the designed ZFPs inhibit not only core and small surface protein production but also large surface protein production, albeit to a lesser extent. All three DHBV transcripts include 3'-untranslated regions that span the enhancer region prior to the polyadenylation signal (13). It is likely that the bound ZFPs are sterically hindering the RNA polymerase and preventing read-through across the enhancer region. This would result in incomplete transcripts being produced that lack the stability of the poly(A) tail. In this way, the ZFPs may be having dual effects on DHBV: (i) inhibition of enhancer activity on core and small surface promoters and (ii) steric hindrance of RNA polymerase across the enhancer—resulting in a reduction of stable complete transcripts.

In summary, the data in this chapter offer a promising outlook on the potential of DHBV-specific ZFPs to act therapeutically and specifically against a hepadnavirus infection. Their high affinity, good specificity, low toxicity and antiviral effects make them candidates for a new type of antiviral therapy for HBV – one that directly targets the viral cccDNA reservoir in the nucleus of hepatocytes in chronic carriers of HBV.

2.5 References

1. Newbold JE, Xin H, Tencza M, Sherman G, Dean J, Bowden S, & Locarnini S (1995) The covalently closed duplex form of the hepadnavirus genome exists in situ as a heterogeneous population of viral minichromosomes. *J Virol* 69(6):3350-3357.
2. Schneider R & Will H (1991) Regulatory sequences of duck hepatitis B virus C gene transcription. *J Virol* 65(11):5693-5701.
3. Liu C, Condreay LD, Burch JB, & Mason W (1991) Characterization of the core promoter and enhancer of duck hepatitis B virus. *Virology* 184(1):242-252.
4. Lilienbaum A, Crescenzo-Chaigne B, Sall AA, Pillot J, & Elfassi E (1993) Binding of nuclear factors to functional domains of the duck hepatitis B virus enhancer. *J Virol* 67(10):6192-6200.
5. Crescenzo-Chaigne B, Pillot J, & Lilienbaum A (1995) Interplay between a new HNF3 and the HNF1 transcriptional factors in the duck hepatitis B virus enhancer. *Virology* 213(1):231-240.
6. Mandell JG & Barbas CF, 3rd (2006) Zinc Finger Tools: custom DNA-binding domains for transcription factors and nucleases. *Nucleic Acids Res* 34(Web Server issue):W516-523.
7. Elrod-Erickson M, Rould MA, Nekludova L, & Pabo CO (1996) Zif268 protein-DNA complex refined at 1.6 A: a model system for understanding zinc finger-DNA interactions. *Structure* 4(10):1171-1180.
8. Beerli RR, Segal DJ, Dreier B, & Barbas CF, 3rd (1998) Toward controlling gene expression at will: specific regulation of the erbB-2/HER-2 promoter by using polydactyl zinc finger proteins constructed from modular building blocks. *Proc Natl Acad Sci U S A* 95(25):14628-14633.
9. Moore M, Klug A, & Choo Y (2001) Improved DNA binding specificity from polyzinc finger peptides by using strings of two-finger units. *Proc Natl Acad Sci U S A* 98(4):1437-1441.
10. Smith J, Berg JM, & Chandrasegaran S (1999) A detailed study of the substrate specificity of a chimeric restriction enzyme. *Nucleic Acids Res* 27(2):674-681.
11. Walters KA, Joyce MA, Addison WR, Fischer KP, & Tyrrell DL (2004) Superinfection exclusion in duck hepatitis B virus infection is mediated by the large surface antigen. *J Virol* 78(15):7925-7937.

12. Bibikova M, Carroll D, Segal DJ, Trautman JK, Smith J, Kim YG, & Chandrasegaran S (2001) Stimulation of homologous recombination through targeted cleavage by chimeric nucleases. *Mol Cell Biol* 21(1):289-297.
13. Buscher M, Reiser W, Will H, & Schaller H (1985) Transcripts and the putative RNA pregenome of duck hepatitis B virus: implications for reverse transcription. *Cell* 40(3):717-724.
14. Crescenzo-Chaigne B, Pillot J, Lilienbaum A, Levrero M, & Elfassi E (1991) Identification of a strong enhancer element upstream from the pregenomic RNA start site of the duck hepatitis B virus genome. *J Virol* 65(7):3882-3886.

3 Chapter 3: HBV-specific ZFP production and *in vitro* assessment

3.1 Introduction

Similar to the design strategy for the DHBV-specific ZFPs, HBV-specific ZFPs were designed with the intention of discriminating between viral sequences and human genomic sequences. Binding of ZFPs to the viral genome of HBV was expected to inhibit the binding of transcription factors and read-through transcription of the transcriptional machinery along the viral genome. Also, similar to DHBV, the HBV episome is found associated with histone proteins and HBV core protein (1-3), protecting the DNA from unlimited access by any potential ZFPs. Thus, HBV-specific ZFPs were designed to target accessible regions of the HBV genome. HBV has four promoters (precore, X, SPI and SPII promoters) and two enhancers (EnI and EnII), all of which have been shown to interact with many PBPs (see Figures 1.3 – 1.5). SPII interacts with many PBPs, and should be accessible for binding by designed ZFPs. NF-1, Sp1 and NF-Y are the transcription factors that bind to SPII. In addition, both the Pol ORF and the preS1 ORF read through this region, allowing the potential to interrupt these two transcripts as well as the transcriptional initiation of the preS2 promoter. Ten HBV-specific ZFPs were designed to target SPII, which spans nucleotides 2971 to 3140.

The designed ZFPs were assessed using a variety of kinetic experiments to determine their binding characteristics. Examination of their ability to impact the HBV viral life cycle was not completed, however, because the cell lines harbouring HBV could not be readily transfected. A variety of transfection methods were utilized in an attempt to over-express the HBV-specific ZFPs, as is outlined in the following sections.

Additionally, the cloning strategy to develop ZFNs using the DHBV- and HBV-specific ZFPs is discussed herein. A summary of the barriers faced while cloning and future directions for that project are also discussed.

3.2 Materials and Methods

3.2.1 Design of HBV-specific ZFPs

ZFPs were designed to target HBV stain *ayw* (U95551) using the program 'Zinc Finger Tools' (http://www.scripps.edu.mb/barbas/zfdesign/zfdesignhome.php) (4). To generate the amino acid sequence for the ZFPs, the Zinc Finger Tools program models each zinc finger repeat as two invariant chain sequences (the amino- and carboxy-terminal backbones) surrounding the variant helix whose sequence depends on the triplet of DNA (4). The linker sequence (TGEKP) (5) is placed between successive zinc finger repeats and the entire construct is flanked by the amino- (LEPGEKP) and carboxy-terminal (TGKKTS) fixed sequences (4). The invariant chain sequences and the fixed terminal sequences are based on the framework of the Sp1C ZFP (4). The invariant chains consist of the carboxy-terminal portion of the α-helix (HQRTH) and the amino-terminal backbone (YKCPECGKSFS) that contains the two β–sheets (underlined) (see Appendix B for entire sequence) (4). ZFPs were designed with flanking *XhoI* and *EcoRV* (5') and *SpeI* and *EcoRV* (3') restriction endonuclease sites.

All ZFPs were designed to bind to target sites within the SPII promoter region of HBV (nt 3007-3150) (Figure 3.1). Four ZFPs targeting 18-bp sequences (18-mers) were designed to function as monomers (ZFP18K, ZFP18M, ZFP18N, ZFP18P). Three pairs of ZFPs targeting 9-bp sequences each (9-mers) were designed to function as heterodimers (ZFP9X1 and ZFP9X2, ZFP9Y1 and ZFP9Y2, ZFP9Z1 and ZFP9Z2). In addition, ZFP9X1 and ZFP18M were designed as alternate heterodimer pairs, as were ZFP18N and ZFP9Z2. These pairs will bind a total of 27-bps. Each ZFP was produced singly in its own pUC19 vector, as compared to the DHBV-specific ZFPs, which were prepared in *cis*-formation in one vector. ZFP target sites and the corresponding zinc finger amino acid sequences that mediate binding are shown in Table 3.1 & 3.2.

ZFP Name	Putative DNA Targets: Sequence 5'-3'[a]	Putative DNA Targets: Subsites 5'-3'[b]	Finger Designs [b] -1 1 2 3 4 5 6
ZFP9X1	AGGCCTCCGt	AGGc	RSDHLTN
		CCTc	TKNSLTE
		CCGt	RNDTLTE
ZFP9X2	AGCCCTCAGt	AGCc	ERSHLRE
		CCTc	TKNSLTE
		CAGt	RADNLTE
ZFP9Y1	AGTATGCCCt	AGTa	HRTTLTN
		ATGc	RRDELNV
		CCCt	SKKHLAE
ZFP9Y2	CCAGCAAATc	CCAg	TSHSLTE
		GCAa	QSGDLRR
		AATc	TTGNLTV
ZFP9Z1	GGCGATTGGt	GGCg	DPGHLVR
		GATt	TSGNLVR
		TTGt	RSDHLTT
ZFP9Z2	CAGCCTACCc	CAGc	RADNLTE
		CCTa	TKNSLTE
		ACCc	DKKDLTR

Table 3.1 - DNA binding sites and corresponding amino acid sequences of HBV-specific experimental 9-mer ZFPs.

[a] The entire DNA binding site sequence is shown from 5' to 3'.

[b] Each subsite is shown with its corresponding zinc finger amino acid sequence displayed, with amino acid positions from -1 up to +6 representing the amino acids of the alpha helix that make site specific contacts with the DNA. The 3' base pair of the DNA subsite (small case) makes minor interactions with the alpha helix of the zinc finger (Adapted from (6)).

ZFP Name	Putative DNA Targets: Sequence 5'-3'[a]	Putative DNA Targets: Subsites 5'-3'[b]	Finger Designs [b] -1 1 2 3 4 5 6
ZFP18K	ACCAATCGCCAGACAGGAa	ACCa	DKKDLTR
		AATc	TTGNLTV
		CGCc	HTGHLLE
		CAGa	RADNLTE
		ACAg	SPADLTR
		GGAa	QRAHLER
ZFP18M	GCTCAGGGCATACTACAAa	GCTc	TSGELVR
		CAGg	RADNLTE
		GGCa	DPGHLVR
		ATAc	QKSSLIA
		CTAc	QNSTLTE
		CAAa	QSGNLTE
ZFP18N	TGGTGGAGGCAGGAGGCGg	TGGt	RSDHLTT
		TGGa	RSDHLTT
		AGGc	RSDHLTN
		CAGg	RADNLTE
		GAGg	RSDNLVR
		GCCg	RSDDLVR
ZFP18P	CAGCGGGGTAGGCTGCCTt	CAGc	RADNLTE
		CGGg	RSDKLTE
		GGTa	TSGHLVR
		AGGc	RSDHLTN
		CTGc	RNDALTE
		CCTt	TKNSLTE

Table 3.2 - DNA binding sites and corresponding amino acid sequences of HBV-specific experimental 18-mer ZFPs.

[a] The entire DNA binding site sequence is shown from 5' to 3'.

[b] Each subsite is shown with its corresponding zinc finger amino acid sequence displayed, with amino acid positions from -1 up to +6 representing the amino acids of the alpha helix that make site specific contacts with the DNA. The 3' base pair of the DNA subsite (small case) makes minor interactions with the alpha helix of the zinc finger (Adapted from (6)).

3.2.2 Synthesis of HBV-specific ZFPs

ZFPs sequences were optimized for codon usage by *Homo sapiens* and synthesized by Blue Heron Biotechnology (Bothell, WA) into pUC19 vectors lacking the multiple cloning site (Amp resistant). They were also optimized to internally exclude commonly used restriction sites, including *BamHI*, *BglII*,

EcoRI, *EcoRV*, *HindIII*, *KpnI*, *NotI*, *SalI*, *SpeI*, *XbaI* and *XhoI*. Each ZFP was produced individually in its own pUC19 vector (pUC19-ZFP18K, pUC19-ZFP18M, pUC19-ZFP18N, pUC19-ZFP18P, pUC19-ZFP9X1, pUC19-ZFP9X2, pUC19-ZFP9Y1, pUC19-ZFP9Y2, pUC19-ZFP9Z1, pUC19-ZFP9Z2).

3.2.3 Cloning of HBV-specific ZFPs into a bacterial expression vector

HBV-specific ZFPs were cloned into pMALc as described in Section 2.2.3 for DHBV-specific ZFPs, except that the pUC19-ZFP plasmids were doubly digested with 10 units each of *Xho*I and *SpeI* in NEB Buffer 4 for 1.5 hours at 37°C. The HBV-specific ZFP 18-mers are 558-bp and 9-mers are 306-bp. The protocols for separation on agarose gel, gel purification, ligation, bacterial transformation and screening of clones were identical. ZFP9Z2 could not be cloned in the forward orientation in pMALc.

3.2.4 Bacterial expression and purification of ZFPs

The HBV-specific ZFPs were expressed and purified as described in Section 2.2.4.

3.2.5 EMSA: Determination of the apparent equilibrium dissociation constant

The oligonucleotide sequences for the EMSAs are in Table 3.3. The HBV-specific ZFPs were assessed as described in Section 2.2.5, except that dsDNA oligonucleotides were added to a final concentration of 1-μM (ZFP18K, ZFP18M, ZFP18N, ZFP18P, ZFP9X1, ZFP9X2, ZFP9Y1, ZFP9Y2, ZFP9Z1).

Name	Oligonucleotide sequence [a, b]
18K.top	*AGTACT* ACCAATCGCCAGACAGGA *AGTACT*
18K.bottom	*AGTACT* TCCTGTCTGGCGATTGGT *AGTACT*
18M.top	*AGTACT* GCTCAGGGCATACTACAA *AGTACT*
18M.bottom	*AGTACT* TTGTAGTATGCCCTGAGC *AGTACT*
18N.top	*AGTACT* TGGTGGAGGCAGGAGGCG *AGTACT*
18N.bottom	*AGTACT* CGCCTCCTGCCTCCACCA *AGTACT*
18P.top	*AGTACT* CAGCGGGGTAGGCTGCCT *AGTACT*
18P.bottom	*AGTACT* AGGCAGCCTACCCCGCTG *AGTACT*
9X1.top	*AGTACT* AGGCCTCCG *AGTACT*
9X1.bottom	*AGTACT* CGGAGGCCT *AGTACT*
9X2.top	*AGTACT* AGCCCTCAG *AGTACT*
9X2.bottom	*AGTACT* CTGAGGGCT *AGTACT*
9Y1.top	*AGTACT* AGTATGCCC *AGTACT*
9Y1.bottom	*AGTACT* GGGCATACT *AGTACT*
9Y2.top	*AGTACT* CCAGCAAAT *AGTACT*
9Y2.bottom	*AGTACT* ATTTGCTGG *AGTACT*
9Z1.top	*AGTACT* GGCGATTGG *AGTACT*
9Z1.bottom	*AGTACT* CCAATCGCC *AGTACT*
9Z2.top	*AGTACT* CAGCCTACC *AGTACT*
9Z2.bottom	*AGTACT* GGTAGGCTG *AGTACT*

Table 3.3 - HBV-specific ZFP oligonucleotide sequences for EMSA and SPR.
[a] The sequences are shown from 5' to 3'.
[b] The ZFP-specific binding region is shown in straight font and the stabilizing nucleotides are shown in italics.

Name	Oligonucleotide sequence [a, b, c]
18K.1C-T.fw	*AGTACT* AC**T**AATCGCCAGACAGGA *AGTACT*
18K.1C-T.rv	*AGTACT* TCCTGTCTGGCGATT**A**GT *AGTACT*
18K.1C-G.fw	*AGTACT* AC**G**AATCGCCAGACAGGA *AGTACT*
18K.1C-G.rv	*AGTACT* TCCTGTCTGGCGATT**C**GT *AGTACT*
18K.3G-A.fw	*AGTACT* ACCAATC**A**CCAGACAGGA *AGTACT*
18K.3G-A.rv	*AGTACT* TCCTGTCTGG**T**GATTGGT *AGTACT*
18K.3G-C.fw	*AGTACT* ACCAATC**C**CCAGACAGGA *AGTACT*
18K. 3G-C.rv	*AGTACT* TCCTGTCTGG**G**GATTGGT *AGTACT*
18K.5A-G.fw	*AGTACT* ACCAATCGCCAG**G**CAGGA *AGTACT*
18K. 5A-G.rv	*AGTACT* TCCTG**C**CTGGCGATTGGT *AGTACT*
18K. 5A-T.fw	*AGTACT* ACCAATCGCCAG**T**CAGGA *AGTACT*
18K. 5A-T.rv	*AGTACT* TCCTG**A**CTGGCGATTGGT *AGTACT*
18K.1.5.fw	*AGTACT* AC**T**AATCGCCAG**G**CAGGA *AGTACT*
18K.1.5.rv	*AGTACT* TCCTG**C**CTGGCGATT**A**GT *AGTACT*

Table 3.4 - ZFP18K-specific oligonucleotide sequences with one or two nucleotide changes for EMSA.
[a] The sequences are shown from 5' to 3'.
[b] The ZFP-specific binding region is shown in straight font and the stabilizing nucleotides are shown in italics.
[c] The nucleotide(s) altered from the original sequence is shown in bold font.

3.2.6 EMSA: Determination of tolerance for single or double nucleotide changes in target sequence

ZFP18K was assessed for its ability to bind oligonucleotides with one or two changes from the wild type target sequence. The oligonucleotide sequences can be found in Table 3.4. Each DNA recognition region was flanked by a 6-nt sequence (AGTACT) to increase stability of the annealed oligonucleotide and provide a larger backbone for ZFP binding. The top and bottom strands were annealed together at a concentration of 10-uM each in 10-mM Tris-HCl pH 7.5, 10-mM $MgCl_2$ and 50-mM NaCl by boiling for 5 minutes, followed by a slow cool to room temperature. DsDNA oligonucleotides were added to a final concentration

of 1-μM in Gel Shift Buffer with 75-nM purified ZFP18K-MBP fusion proteins, in a total volume of 25-μL. Importantly, ZFP-MBP fusion proteins were added to the mixture last. A control sample contained dsDNA oligonucleotides without ZFP18K-MBP added. Reactions were incubated for 1 hour at room temperature, then were run in their entirety on a 7% native acrylamide gel as described in Section 2.2.6. Gels were stained with SYBR-Green and SYPRO-Ruby as described in Section 2.2.6, and scanned using the Fujifilm FLA-5100 phosphorimager on the "1 laser/1 image" setting with excitation and emission wavelengths of 488-nm/520-nm and 488-nm/610-nm, respectively.

3.2.7 EMSA: Determination of specificity for target sequence

EMSAs for the HBV-specific ZFPs were performed as described in Section 2.2.6. The sequences of the oligonucleotides can be found in Table 3.4.

3.2.8 SPR for HBV-specific ZFPs

SPR was performed using BIAcore technology as described in Section 2.2.7. The sequences for the oligonucleotides can be found in Table 3.3 and the calculated and actual immobilization levels for all the biotinylated oligonucleotides can be found in Table 3.5. Surface regeneration tests were carried out using ZFP concentrations around the dissociation concentration calculated by EMSA (Table 3.7) or at 128-nM for those ZFPs whose dissociation constant was not calculated by EMSA (ZFP9X1, ZFP9X2, ZFP9Y1, ZFP9Y2). Kinetic analysis was carried out using ZFP concentrations ranging from 0.1X to 10X the dissociation constant (in doubling dilutions) for those ZFPs whose dissociation constant were calculated by EMSA (Table 3.7) or ranging from 1-nM to 256-nM (ZFP9X1, ZFP9X2, ZFP9Y1, ZFP9Y2, ZFP9Z1). Kinetic analysis was done on the BIAeval software program and curves were fit to a 1:1 binding with drifting baseline model.

Biotinylated-oligonucleotide	Immobilization Level (R_L)	
	Calculated	Actual
ZFP18K	95 RU[a]	110 RU
ZFP18M	95 RU	87 RU
ZFP18N	95 RU	95 RU
ZFP9X1	182 RU	194 RU
ZFP9X2	182 RU	180 RU
ZFP9Y1	182 RU	185 RU
ZFP9Y2	182 RU	167 RU
ZFP9Z1	182 RU	193 RU

Table 3.5 - Calculated versus actual immobilization levels of biotinylated-DNA oligonucleotides on Sensor Chips SA for SPR.
[a] Resonance units (RU).

3.2.9 Cloning of ZFPs into a eukaryotic expression vector

ZFPs were PCR amplified from pUC19-ZFP18K, pUC19-ZFP18M, pUC19-ZFP18N, pUC19-ZFP18P, pUC19-ZFP9X1, pUC19-ZFP9X2, pUC19-ZFP9Y1, pUC19-ZFP9Y2, pUC19-ZFP9Z1 and pUC19-ZFP9Z2 using the primers in Table 3.6. The PCR amplification and subsequent cloning steps were performed as described in Section 2.2.8. Positive clones were not successfully produced for pcDNA3.1(+)-ZFP18M and -ZFP9Z1.

3.2.10 Cloning of EGFP into pcDNA3.1(+)-ZFP plasmids

EGFP was PCR amplified and ligated into pCR4 as described in Section 2.2.9. EGFP was then fused in frame to ZFPs in pcDNA3.1(+)-ZFP18K, ZFP18N, ZFP9X1, ZFP9X2, ZFP9Y1, ZFPY2 and ZFP9Z2 as described in Section 2.2.9. Positive clones were not successfully produced for pcDNA3.1(+)-ZFP9X2, ZFP9Y1, ZFP9Y2 and ZFP9Z2.

Name	Primer sequence [a]
ZFP18K.fw	**GGATCC**ATGC ATCATCACCA TCACCAT*CCC AAGAAAAAGC*
	*GTAAGGTC*GG TGATATCCTG GAGCCCGGC[b]
ZFP18K.rv	**GAATTC**ACCG ATATCAGACG TCTTCTTAC[c]
ZFP18M.fw	**GGATCC**ATGC ATCATCACCA TCACCAT*CCC AAGAAAAAGC*
	*GTAAGGTC*GGTGATATCCTGGAGCCAGGAGAA[b]
ZFP18M.rv	**GAATTC***ACTA GT*ACCGATAT CTGATGTCTT TTTACC[c]
ZFP18N.fw	**GGATCC**ATGC ATCATCACCA TCACCAT*CCC AAGAAAAAGC*
	*GTAAGGTC*GG TGATATCCTC GAACCCGGTG A[b]
ZFP18N.rv	**GAATTC***ACTA GT*ACCGATAT CGGACGTCTT CTTT[c]
ZFP9X1.fw	**GGATCC**ATGC ATCATCACCA TCACCAT*CCC AAGAAAAAGC*
	*GTAAGGTC*GG TGATATCTTG GAACCCGGTG[b]
ZFP9X1.rv	**GAATTC***ACTA GT*ACCGATAT CGCTTGTCTT TTTGCC[c]
ZFP9X2.fw	**GGATCC**ATGC ATCATCACCA TCACCAT*CCC AAGAAAAAGC*
	*GTAAGGTC*GG TGATATCCTG GAGCCTGGCG AAA[b]
ZFP9X2.rv	**GAATTC***ACTA GT*ACCGATAT CAGAGGTTTT CTTCCCT[c]
ZFP9Y1.fw	**GGATCC**ATGC ATCATCACCA TCACCAT*CCC AAGAAAAAGC*
	*GTAAGGTC*GG TGATATCCTT GAGCCCGGAG A[b]
ZFP9Y1.rv	**GAATTC***ACTA GT*ACCGATAT CAGATGTCTT TTTGCC[c]
ZFP9Y2.fw	**GGATCC**ATGC ATCATCACCA TCACCAT*CCC AAGAAAAAGC*
	*GTAAGGTC*GG TGATATCCTG GAGCCCGGAG AGAA[b]
ZFP9Y2.rv	**GAATTC***ACTA GT*ACCGATAT CAGAGGTCTT CTTGCC[c]
ZFP9Z1.fw	**GGATCC**ATGC ATCATCACCA TCACCAT*CCC AAGAAAAAGC*
	*GTAAGGTC*GG TGATATCCTG GAGCCAGGCG AAA[b]
ZFP9Z1.rv	**GAATTC***ACTA GT*ACCGATAT CTGATGTCTT CTTGCC[c]
ZFP9Z2.fw	**GGATCC**ATGC ATCATCACCA TCACCAT*CCC AAGAAAAAGC*
	*GTAAGGTC*GG TGATATCCTC GAACCAGGCG AA[b]
ZFP9Z2.rv	**GAATTC***ACTA GT*ACCGATAT CGGACGTCTT TTTACC[c]

Table 3.6 - Primer sequences for cloning HBV-specific ZFPs into a eukaryotic expression vector.

[a] Sequences are shown 5' to 3'.

[b] BamHI restriction site (**bold**), 6x histidine tag (underlined), SV40 nuclear localization signal (*italics*), unique ZFP sequence (plain text).

[c] EcoRI restriction site (**bold**), SpeI restriction site (*italics*), unique ZFP sequence (plain text).

3.2.11 Cell lines and culture conditions

HepAD38 (7) cells were received from Dr. J.T. Guo (Drexel University College of Medicine, Doylestown PA) (8) and contain a tetracycline-inducible promoter controlling HBV strain *ayw* expression in the HepG2 background. They were maintained in 1:1 DMEM/F-12 medium (Gibco 12500-062) supplemented with 10% (v/v) FCS, 50-IU/mL penicillin and 10-µg/mL streptomycin, and incubated at 37°C with CO_2. LMH cells were maintained as described in Section 2.2.11.

3.2.12 HepAD38 transfection conditions

3.2.12.1 Lipofectamine™ 2000 transfection

HepAD38 cells were plated in 6-well tissue culture plates (Sarstedt 83.1839.300) at 2.0 x 10^5 cells/well in 2-mL of media without antibiotics. Plates were incubated overnight at 37°C in a CO_2 incubator and transfected the following day. LF2000 was used to transfect cells as described in Section 2.2.12, except 4-µg of the plasmid pd1-EGFPn1 was used to transfect the HepAD38 cells. Ratios of 1:1, 1:2, 2:1, 1:4 and 1:5 (DNA (µg) to LF2000 (µL)) were tested. After 24 and 48 hours, cells were inspected using the Zeiss Axiovert 200M fluorescence microscope and lasers for 488-nm excitation of GFP. Subsequently, different plating densities of HepAD38 cells were tested with a DNA to LF2000 ratio of 1:5. HepAD38 cells were plated at 2.0 x 10^5, 4.0 x 10^5, 8.0 x 10^5 and 1.6 x 10^6 cells/well, then transfected 24 hours later as described above.

3.2.12.2 Flow cytometry sorting of LF2000 transfected cells

HepAD38 cells were plated in 6-well tissue culture plates at 2.0 x 10^5 cells/well in 2-mL of media without antibiotics. Plates were incubated overnight at 37°C in a CO_2 incubator and transfected the following day. LF2000 was used to transfect cells with 0.8-µg of the plasmid pcDNA3.1(+)-EGFP and 3.2-µg of either pcDNA3.1(+) or pcDNA3.1(+)-ZFP18K, ZFP18M or ZFP18N, as described above. One whole plate was transfected with each treatment. After 24 hours, the cells were removed from the plate by washing once with PBS then adding 0.5-mL/well ATV and incubating at 37°C for 10 minutes. 0.5-mL/well of media was

added and the cells from the whole plate pooled in one tube. In addition, a plate of non-transfected cells was collected in a similar method, to act as negative control. The cells were centrifuged for 5 minutes at 1500-rpm in a Beckman Coulter Allegra® X-15R centrifuge and resuspended in 0.5-mL of PBS plus 1% (v/v) FCS and 0.5-mM EDTA. The samples were added to the strainer caps of 5-mL polypropylene round-bottom tubes (Falcon 352235) and gently tapped to encourage flow-through. This step removes cell clumps, an essential step with HepAD38s. The samples were then sorted on EGFP (488-nm) using the BD FACSAria™ II Flow Cytometer (BD Biosciences). The sorted cells were collected in a new tube and then centrifuged for 5 minutes at 1000-rpm. The pellet was washed once with 1X PBS, centrifuged again for 5 minutes at 1000-rpm then the cells were used for analysis.

3.2.12.3 TransIT®-LT1 transfection

HepAD38 cells were plated in 6-well tissue culture plates at 2.0 x 10^5 cells/well in 2-mL of media without antibiotics. Plates were incubated overnight at 37°C in a CO_2 incubator and transfected the following day. TransIT®-LT1 Transfection Reagent (Mirus Bio LLC 2300) was used to transfect cells as described by the manufacturer. Specifically, 7.5-µL of TransIT®-LT1 was added directly to 250-µL of Opti-MEM® I reduced-serum medium and incubated for 5-20 minutes at room temperature after mixing by pipetting. 2.5-µg of the plasmid pd1-EGFPn1 was added to the tube and mixed by gently pipetting. The sample incubated for 15-30 minutes at room temperature, then added drop-wise to the cells. After 24 and 48 hours, cells were inspected using the Zeiss Axiovert 200M fluorescence microscope and lasers for 488-nm excitation of GFP.

3.2.12.4 Fugene® 6 transfection

HepAD38 cells were plated in 6-well tissue culture plates at 4.0 x 10^5 cells/well in 2-mL of media without antibiotics. Plates were incubated overnight at 37°C in a CO_2 incubator and transfected the following day. Fugene® 6 Transfection Reagent (Roche 11814443001) was used to transfect cells as described by the

manufacturer. Specifically, 3-µL of Fugene® 6 was added to 97-µL of Opti-MEM® I reduced-serum medium and mixed gently. The sample was incubated for 5 minutes at room temperature then 1-µg or 2-µg of the plasmid pd1-EGFPn1 was added and mixed gently. The sample was incubated for 15-45 minutes then added drop-wise to the cells. Ratios of 1:3, 2:3 and 1:6 (DNA (µg) to Fugene® 6 (µL)) were tested. In addition, different cell densities (2.0 x 10^5 cells/well, 4.0 x 10^5 cells/well, 8.0 x 10^5 cells/well, 1.6 x 10^6 cells/well) were tested with a ratio of 1:5. After 24 and 48 hours, cells were inspected using the Zeiss Axiovert 200M fluorescence microscope and lasers for 488-nm excitation of GFP.

3.2.12.5 Electroporation

HepAD38 cells were resuspended in Opti-MEM® I reduced-serum medium at 7.5 x 10^6 cells/mL. 400-µL of cells were transferred to a 0.4-mm electroporation cuvette (Bio-Rad 165-2088). 10-µg of pd1-EGFPn1 plasmid DNA was added. The cells were electroporated in a Bio-Rad Gene Pulser electroporator at 260-V, 950-µF and 200-Ω. The cuvette was then placed on ice for 10 minutes, than cells were transferred into 16-mL of complete media and plated in 6-well plates. After 24 and 48 hours, cells were inspected using the Zeiss Axiovert 200M fluorescence microscope and lasers for 488-nm excitation of GFP.

3.2.12.6 Nucleofection

The Cell Line Optimization Nucleofector® Kit (Lonza Bio VCO-1001N) was used with HepAD38 cells on the Nucleofector® Device (Lonza Bio AAD-1001). Nucleofector® Solution L and V were prepared by combining 0.2-mL of Supplement with 0.9-mL of Solution L or V. 2.0 x 10^6 HepAD38 cells were suspended in 100-µL of Nucleofector® Solution L or Solution V, with 2-µg of the provided pmaxGFP (see map in Appendix A). The samples were transferred into the provided cuvettes, and the cuvettes placed in the cuvetter holder of the Nucleofector® Device one at a time. Each solution was tested with 7 different programs: A-020, T-020, T-030, X-001, X-005, L-029, D-023. Two controls were included, one in which cells are incubated with DNA and the Nucleofector®

Solution but without a program, and one in which the cells are treated with the T-020 program without DNA. After the program was run, cells were immediately transferred to pre-warmed complete media using the provided pipettes. Each reaction was placed in one well of a 6-well plate. After 24 and 48 hours, cells were inspected using the Zeiss Axiovert 200M fluorescence microscope and lasers for 488-nm excitation of GFP.

3.2.12.7 ZFP-polyplex transfection

3.2.12.7.1 Optimization of polyplex transfection protocol

The plasmid pEF1a-SEAP-wPRE-attB was assembled into chitosan-based polyplexes (batch EG-02) by Engene Inc. (Vancouver, BC). The polyplexes had a concentration of 150-µg/mL, a pH of 4.0, polydispersity index (distribution of molecular mass) of 0.156, particle diameter of 97-nm, N:P ratio of 20 and Zeta potential (electrostatic potential) of +38-mV. This polyplex allows the production and secretion of secreted alkaline phosphatase (SEAP), which is measurable in the supernatant of transfected cells. HepAD38 cells were plated at 1.5 x 10^5 cells/mL in 6-well plates. Plates were incubated overnight at 37°C in a CO_2 incubator and transfected the following day. Cells were washed once with 1-mL of Opti-MEM® I reduced-serum medium pH 6.0 (adjust the pH using filter sterilized 1-M HCl), then 1-mL of Opti-MEM® I reduced-serum medium pH 6.0 was added to each well. 2-µg of polyplex was added to the media and incubated at 37°C with 5% CO_2 for 2 or 6 hours, with or without 0.5% DMSO added. Cells were also incubated with 2-µg of polyplex for 24 hours. Mock transfected cells had their media changed to Opti-MEM® I reduced-serum medium pH 6.0 for 6 hours. After the polyplex treatment, regular media was returned to the cells. After 48 hours, the cells were assessed for SEAP in the media supernatant as follows: 1-mL of media was collected in a 1.7-mL microcentrifuge tube and heated to 65°C for 30 minutes to inactivate endogenous alkaline phosphatases. In a 96-well plate, 20-µL of the media was incubated with 10-µL of 0.05% Zwittergent in 1X PBS. Control wells contained 20-µL of water to normalize the volume. The standards were composed of calf intestine alkaline phosphatase (Sigma P-3877) ranging

from 100-ng/µL down to 100-fg/µL, using 1 in 10 dilutions. Then, 200-µL of 1-mg/mL para-nitrophenyl phosphate (pNPP; prepared in 1-mM $MaCl_2$, 1-M diethanolamine pH 9.8) was added to each well. The reaction was incubated at room temperature for 5 – 45 minutes and then measured at 405-nm using a SpectraMAX Plus 384 plate reader (Molecular Devices).

The cell density for polyplex transfection of HepAD38s was optimized by plating HepAD38 cells in 6-well plates at the following densities: 1.5 x 10^5, 2.0 x 10^5, 2.5 x 10^5, 3.0 x 10^5, 3.5 x 10^5 and 4.0 x 10^5 cells/well. After 24 hours, cells were washed once with 1-mL of Opti-MEM® I reduced-serum medium pH 6.0, then 1-mL of Opti-MEM® I reduced-serum medium pH 6.0 was added to each well. 2-µg of polyplex-ZFP18K was added to the media and incubated at 37°C with 5% CO_2 for 6 hours. After 24 hours, cells were stained for β–galactosidase expression as described in Section 3.2.12.7.3.

3.2.12.7.2 Transfection of HepAD38 cells with ZFP-polyplexes

The plasmid mlacZ was a gift from Dr. Jim Smiley and encodes the lacZ gene under control of the CMV promoter in the pcDNA3.1(+) backbone. The plasmid DNA for mlacZ and pcDNA3.1(+)-ZFP18A, -ZFP18K, -ZFP18N and –ZFP18cA were prepared using the EndoFree Plasmid Giga Kit (Qiagen 12391) and then assembled into chitosan-based polyplexes by Engene Inc with a ratio of 5:1 (pcDNA3.1(+)-ZFP to mlacZ). ZFP18A polyplexes (batch 124-89-A) had a concentration of 150-µg/mL, a polydispersity index of 0.18, an N:P ratio of 20 and a particle diameter of 113-nm. ZFP18K polyplexes (batch 124-89-K) had a concentration of 150-µg/mL, a polydispersity index of 0.23, an N:P ratio of 20 and a particle diameter of 127-nm. ZFP18N polyplexes (batch 124-89-N) had a concentration of 150-µg/mL, a polydispersity index of 0.16, an N:P ratio of 20 and a particle diameter of 114-nm. ZFP18cA polyplexes (batch 124-89-1) had a concentration of 150-µg/mL, a polydispersity index of 0.17, an N:P ratio of 20 and a particle diameter of 116-nm. The pH and Zeta potential were not calculated for these polyplexes. All polyplexes were aliquoted, stored at -80°C and thawed

on ice for use. HepAD38 cells were plated in 6-well tissue culture plates at 4.0 x 10^5 cells/well in 2-mL of media without antibiotics. Plates were incubated overnight at 37°C in a CO_2 incubator and transfected the following day. 2-µg of polyplex was added to culture media and incubated at 37°C with 5% CO_2 for 2 – 6 hours, after which the media was replaced. After 24 and 48 hours, the cells were assessed for protein expression and stained for β–galactosidase expression by the mlacZ plasmid, as an indicator of transfection efficiency.

3.2.12.7.3 X-Gal histochemistry of polyplex-transfected HepAD38 cells

The fixative and stain were prepared ahead of time. The fixative was prepared fresh for each use by dissolving 2% paraformaldehyde and 0.2% glutaraldehyde in 1X PBS. Stain was prepared fresh by combining 1-mg/mL X-gal, 2-mM $MgCl_2$, 41-mg potassium ferricyanide and 53-mg potassium ferrocyanide in 25-mL of 1X PBS (pH 7.3). The media was removed from the cells, which were then washed once with 1X PBS. The cells were fixed on ice for 5 minutes in 1-mL of fixative. The cells were washed three times with 1X PBS and then stained overnight at 37°C (without CO_2) with 1.5-mL of stain/well. The following day, the wells were rinsed once with 1X PBS and stored in 1-mL 1X PBS for viewing. Samples were viewed under white light using a Nikon light microscope.

3.2.12.8 Profect-P2 transfection

HepAD38 cells were plated in 6-well tissue culture plates at 2.0 x 10^5 cells/well in 2-mL of media. Plates were incubated overnight at 37°C in a CO_2 incubator and transfected the following day. Profect-P2 (Targeting Systems 0042) was vortexed vigorously. 1 – 10-µg of purified ZFP18K-MBP fusion protein was added to 100-µL of serum-free, high-glucose (4500-mg/mL) DMEM (Invitrogen 10313-039) in a tube. 1 – 10-µL of Profect-P2 was added to the tube and mixed gently. The solution was incubated for 20 minutes at room temperature. The cells were washed twice with serum-free, high-glucose DMEM then 1-mL of serum-free, high-glucose DMEM was added to each well. 100-µL of the transfection solution was added to each well, and the cells were incubated for 5 hours at 37°C in a CO_2

incubator. 1-mL of complete media was added to each well and the cells were incubated overnight at 37°C in a CO_2 incubator. The following day, the cells were washed once with 1X PBS and lysed with 400-µL of RIPA lysis buffer, then assessed for the presence of ZFP18K-MBP fusion protein within the cells by Western blot analysis using anti-ZFP antiserum, anti-HBV core and anti-actin antibodies, as described in Section 2.2.23.

3.2.12.9 Targefect-Hepatocyte transfection

HepAD38 cells were plated in 6-well tissue culture plates at 1.2 x 10^5 cells/well in 2-mL of media. Plates were incubated overnight at 37°C in a CO_2 incubator and transfected the following day. Targefect-Hepatocyte (Targeting Systems HEP01) was thawed and vortexed vigorously. 1 – 3-µg of the plasmid pd1-EGFPn1 was added to 500-µL of serum-free, high-glucose (4500-mg/mL) DMEM (Invitrogen 10313-039) in a tube and mixed gently. 2.5 – 7.5-µL of Targefect-Hepatocyte was added to the tube and mixed gently. The solution was incubated for 20 minutes at 37°C. The cells were washed twice with serum-free, high-glucose DMEM and the media removed completely. 500-µL of the transfection solution was added to each well, and the cells were incubated for 3 hours at 37°C in a CO_2 incubator. After 24 and 48 hours, cells were inspected the Zeiss Axiovert 200M fluorescence microscope and lasers for 488-nm excitation of GFP.

3.2.13 SDS-PAGE, Western transfer and Western blot

Western blotting was performed as described in Sections 2.2.21-2.2.23. Additionally, anti-HBV core antibody (Dako B0586) was used at a dilution of 1:5000.

3.2.14 MTT assay for assessment of metabolically active cells

The MTT assay was carried out as described in Section 2.2.25 using Huh7 cells transfected with 0.2-µg of pcDNA3.1(+) or pcDNA3.1(+)-ZFP18K, ZFP18N or ZFP18cA using a DNA:LF2000™ ratio of 2:1. The cells were assayed 24 hours after transfection.

3.2.15 Confocal microscopy of ZFP-EGFP expression in transfected LMH cells

Confocal microscopy was carried out as described in Section 2.2.26, except cells were transfected with 4-µg of pcDNA3.1(+)-ZFP18K-EGFP, -ZFP18N-EGFP, or ZFP9X1-EGFP.

3.2.16 Cloning of chimeric ZFP-FokI endonucleases

The plasmid pML109RM19-1 was purchased from ATCC® (40898). It contains a 6.0-kb insert of genomic DNA (including the methylase *FokI* and the restriction endonuclease *FokI*) from *Flavobacterium okeanokoites* in the pUC19 plasmid. The *FokI* endonuclease was isolated by PCR amplification using the following primers: link.Fok.Spe.fw (5'-CAGTATACTA GTGGAGGAGG AAGCGGAGGA GGAAGCGGAG GAGGAAGCCA ACTCGTCAAA AGTGAACTGG A-3') and Fok.Spe.st.rv (5'- GGATCTACTA GTAAAGTTTA TCTCGCCGTT ATTAAATTTC CG -3'). These primers add *SpeI* restriction digest sites at both ends of *FokI*. The PCR reaction contained 1-µL of pML109RM19-1, 1-µL of 10-mM dNTPs, 12.5 units recombinant *Taq* DNA Polymerase, 1.5-mM $MgCl_2$, 5-µL of 10X PCR Buffer, 0.5-µM of each primer and dH_2O up to 50-µL. The reaction was annealed at 54°C, with an elongation time of 50 seconds and 30 cycles. The PCR product was run on a 0.8% (w/v) agarose gel containing 1.5-ng/µL EtBr and visualized using UV light and the G:box Gel Documentation System. The PCR product was ligated to pCR4 using the TOPO TA cloning kit and transformed into TOP10 as described in Section 2.2.8. The ligation was transformed into TOP10 *E.coli* and plated on LB/Amp plus X-Gal and IPTG. After overnight incubation at 37°C, positive (white) colonies were used to inoculate 2-mL LB/Amp mini-preps. DNA was isolated from the cultures the next day using the QIAprep Spin Miniprep Kit. Clones were screened for positivity by *EcoRI* restriction digest, liberating the PCR insert. Positive clones were sequenced with the T7 primer. Clones with no sequence changes were digested with 10 units of *SpeI* in NEB Buffer 4 with 1X BSA for 1.5 hours at 37°C. The backbones, pMAL-ZFP9A1, ZFP9A2, ZFP9B1, ZFP9B2,

ZFP9X1, ZFP9X2, ZFP9Y1, ZFP9Y2, ZFP18M and ZFP18N were similarly digested, then de-phosphorylated with shrimp alkaline phosphatase (SAP) (Roche 1758 250) to dephosphorylate the ends. The entire, *SpeI*-digested backbone was treated with 2-µL (2 units) of SAP and 4-µL of 10X SAP Buffer in 40-µL total volume, brought up with dH_2O. After incubation at 37°C for 10 minutes, the enzyme was heat inactivated at 70°C for 10 minutes. Subsequently, the DNA was removed from protein and buffer using the PCR Purification protocol from the QIAquick Gel Extraction Kit. Specifically, 400-uL of Buffer PB was gently mixed with the sample then placed on a provided column. The sample was centrifuged for 30 seconds at 14,000-rpm and the flow-through discarded. The wash steps as described for gel extraction in Section 2.2.3 were performed, and the sample was eluted in 30-µL dH_2O. All digests were separated on 0.8% (w/v) agarose gels and the resulting backbone and inserts were excised using a scalpel. DNA was recovered using the QIAquick Gel Extraction Kit. *FokI* was ligated to pMAL- ZFP9A1, ZFP9A2, ZFP9B1, ZFP9B2 ZFP9X1, ZFP9X2, ZFP9Y1, ZFP9Y2, ZFP18M and ZFP18N in a 10-µL reaction containing 6-µL of insert DNA, 2-µL of 5X T4 DNA Ligase Buffer, 1-µL of the pMAL-ZFP18 backbone (diluted 1:10) and 1-µL (1 unit) of T4 DNA Ligase. Control reactions substituted 6-µL of water for insert. The ligations were incubated overnight at 16°C. The following day, 1-µL of the ligation reaction was transformed into chemically competent TOP10 *E.coli*, and plated on LB/Amp. Isolated colonies were used to inoculate 2-mL LB/Amp mini-preps, which were incubated overnight at 37°C with agitation. DNA was isolated using the QIAprep Spin Miniprep Kit, and positive clones were determined by restriction digest with *SpeI*. Positive clones were sequenced with the *FokI*-specific primer, Fok.263.fw (5'-ATAGCGGAGG TTATAATCTG CC-3').

3.2.17 Cloning of chimeric ZFP-Ho endonucleases

The plasmid YCpGAL::HO (Amp^R) (see map in Appendix A) was received as a gift from Dr. David Stuart in the Department of Biochemistry at the University of Alberta. The Ho endonuclease was isolated by PCR amplification using the

following primers: HO.Eco.fw (5'-GAATTCATGC TTTCTGAAAA CACGACTATT-3') and HO.Xho.1399.rv (5'-CTCGAGACAT GATTTCACTT CTATTTTGTT-3'). These primers add *EcoRI* and *XhoI* restriction digest sites at the 5' and 3' ends of Ho, respectively. The reverse primer excludes the last 360-bps of the full-length Ho, which contains the endogenous zinc finger protein region (9). The PCR reaction contained 1-µL of YCpGAL::HO, 1-µL of 10-mM dNTPs, 12.5 units recombinant *Taq* DNA Polymerase, 1.5-mM $MgCl_2$, 5-µL of 10X PCR Buffer, 0.5-µM of each primer and dH_2O up to 50-µL. The reaction was annealed at 54°C, with an elongation time of 1 minute 45 seconds and 30 cycles. The PCR product was run on a 0.8% (w/v) agarose gel containing 1.5-ng/µL of EtBr and visualized using UV light and the G:box Gel Documentation System. The PCR product (1399-bp) was ligated to pCR4 using the TOPO TA cloning kit and transformed into TOP10 as described in Section 2.2.8. The ligation was transformed into TOP10 *E.coli* and plated on LB/Amp plus X-Gal and IPTG. After overnight incubation at 37°C, positive (white) colonies were used to inoculate 2-mL LB/Amp mini-preps. DNA was isolated from the cultures the next day using the QIAprep Spin Miniprep Kit, as described in Section 2.2.3. Clones were screened for positivity by *EcoRI* and *XhoI* restriction digest, liberating the PCR insert. Positive clones were sequenced with the T7 primer. Clones with no sequence changes were doubly digested with 10 units of *EcoRI* and 10 units of *XhoI* in NEB Buffer 3 with 1X BSA for 1.5 hours at 37°C. The backbones, pMAL-ZFP18A, ZFP18B, ZFP18cA, ZFP18K and ZFP18N, were similarly digested. All digests were separated on 0.8% (w/v) agarose gels and the resulting backbone and inserts were excised using a scalpel. DNA was recovered using the QIAquick Gel Extraction Kit as described. Ho was ligated to pMAL-ZFP18A, ZFP19B, ZFP18cA, ZFP18K and ZFP18N in a 10-µL reaction containing 5-µL of insert DNA, 2-µL of 5X T4 DNA Ligase Buffer, 1-µL of the pMAL-ZFP18 backbone (diluted 1:10), 1-µL (1 unit) of T4 DNA Ligase and 1-µL of water. Control reactions substituted 5-µL of water for insert. The ligations were incubated overnight at 16°C. The following day, 1-µL of the ligation reaction was transformed into chemically competent TOP10 *E.coli*, and plated on LB/Amp.

Isolated colonies were used to inoculate 2-mL LB/Amp mini-preps, which were incubated overnight at 37°C with agitation. DNA was isolated using the QIAprep Spin Miniprep Kit, and positive clones were determined by restriction digest with *EcoRI* and *XhoI* as described above. Positive clones were sequenced with the M13/pUC primer, as well a Ho-specific primer called HO4 (5'-TATGGACGGA ATTGTCCATA TTT-3').

3.3 Results

3.3.1 Design of HBV-specific ZFPs

Four 18-mers and three pairs of 9-mers were designed to target SPII. ZFP 18-mers were designed to target either the plus or the minus strand of HBV, and each zinc finger motif was linked in tandem by the canonical TGEKP linker (5). The binding sites of the 18-mers, ZFP18K, ZFP18M, ZFP18N and ZFP18P, can be found in Figure 3.1 A. ZFP18K and ZFP18M bind the minus strand and ZFP18N and ZFP18P bind the plus strand. ZFP18K binds a section overlapping both regions D and E, potentially interfering with the binding of both Sp1 and NF-Y. ZFP18M binds near the end of region C, which interacts with unidentified binding partners. ZFP18N binds within region D, and is highly likely to interfere with Sp1 binding to this region. ZFP18P binding overlaps with region E and region F, with a small portion binding within region G. ZFP18P will interfere with a number of PBPs in this area of SPII.

Six 9-mers were designed, called ZFP9X1, ZFP9X2, ZFP9Y1, ZFP9Y2, ZFP9Z1 and ZFP9Z2. Their binding sites can be found in Figure 3.1 B. Each zinc finger motif was linked in tandem with the canonical TGEKP linker (5). As was the case for the DHBV-specific 9-mers, the ZFP pairs were designed inverted to each other with 6 – 18-bps of DNA in the spacer region (10) (Figure 3.2). The HBV-specific 9-mers were designed with the intention of fusing them in-frame to the *FokI* endonuclease domain. ZFP9X1 pairs with ZFP9X2, where ZFP9X1 binds to the plus strand and ZFP9X2 binds to the minus strand. Likewise, ZFP9Y1 pairs with ZFP9Y2, and ZFP9Z1 with ZFP9Z2, where ZFP9Y1 and ZFP9Z1 bind to

the plus strand and ZFP9Y2 and ZFP9Z2 bind to the minus strand. Note that the numbering of each pair is the opposite as seen for DHBV-specific ZFPs. 10-bp gaps are found between the binding sites of ZFP9X1 and ZFP9X2, and ZFP9Z1 and ZFP9Z2. An 11-bp gap is found between the binding sites of ZFP9Y1 and ZFP9Y2.

Additionally, two extra pairs were designed wherein ZFP18M can substitute for ZFP9X2 to pair with ZFP9X1. Similarly, ZFP18N can substitute for ZFP9Z1 by pairing with ZFP9Z2. The addition of these pairs provided additional options for the chimeric endonuclease design should some the 9-mers exhibit poor binding.

Control ZFPs were not created for the HBV-specific ZFPs, as was done for the DHBV-specific ZFPs. Instead, the DHBV-specific control ZFPs were used as the control ZFPs for the HBV-specific ZFPs.

The entire HBV genome (U95551) was entered into the 'Zinc Finger Tools' website using the "Search DNA Sequence for Contiguous or Separated Target Sites" program. The genome was scanned for either 9-bp or 18-bp sequences that ZFPs could be designed to target. Possible target sites were found throughout the genome, and those within the SPII region were further investigated. First, the proposed target sequences were searched using the NCBI genomic BLAST database for their presence in the *Homo sapiens* genome. None of the proposed target sequences were found within the human genome.

After selecting the target sequences, they were then re-entered into the 'Zinc Finger Tools' website using the "Design a Zinc Finger Protein" program. The output consisted of the required amino acid sequence of the ZFP in order to target that DNA sequence. The output included both the standard backbone sequence and the unique α-helix sequences for specific DNA recognition (see Appendix B for sequences and alignments).

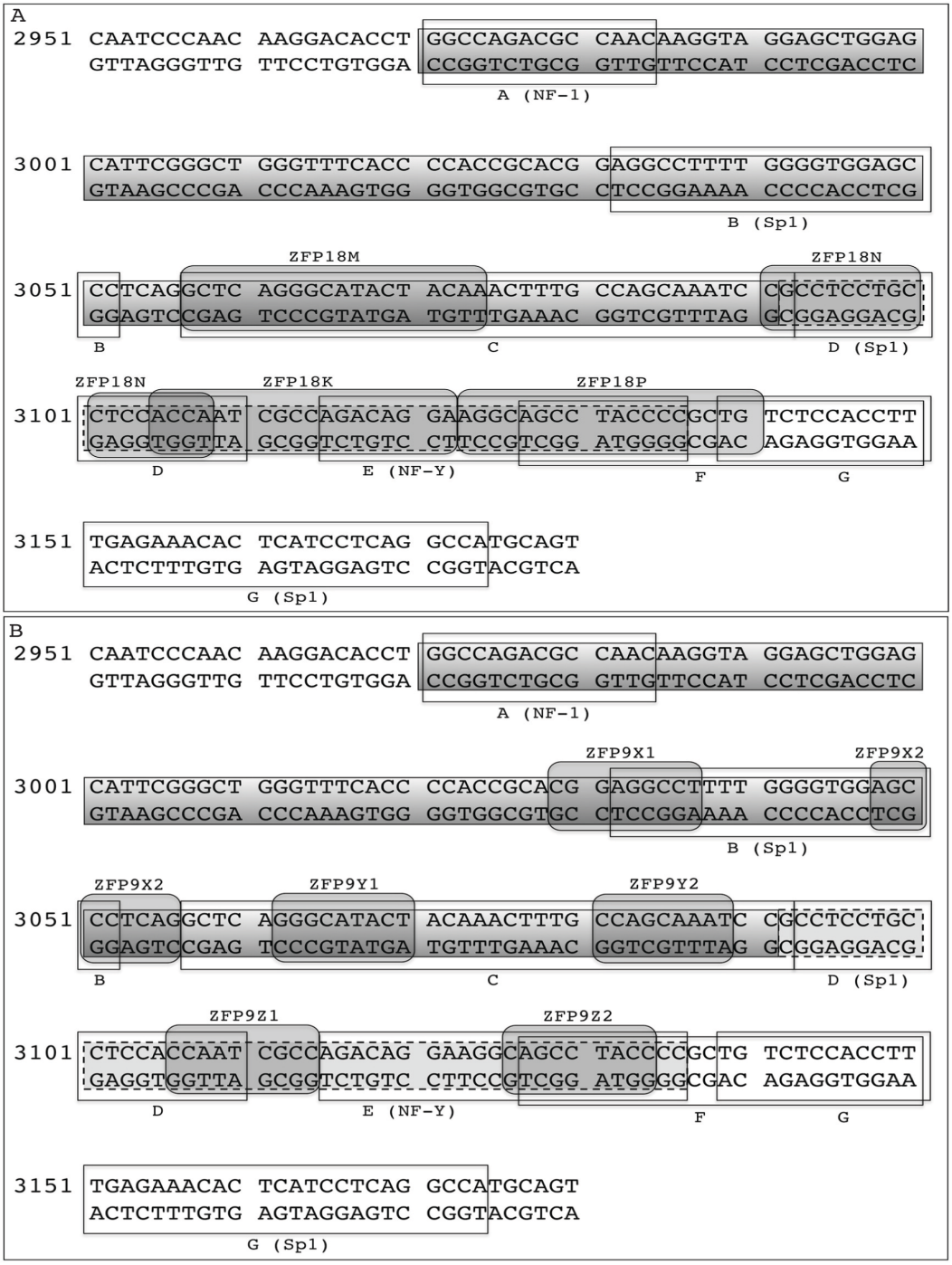

Figure 3.1 - Detailed map of the HBV SPII promoter region.
The two main regions of SPII are shown: the modulatory region spanning nucleotides 2971 – 3091 (shaded in grey gradient) and the basal promoter region spanning nucleotides 3092 – 3136 (grey box with dashed stroke line). The open boxes represent FP regions detected by other groups during DNase I footprinting assays. The PBPs are indicated in brackets. The binding sites of ZFP 18-mers (A) and ZFP 9-mers (B) are indicated by the rounded rectangles shaded grey.

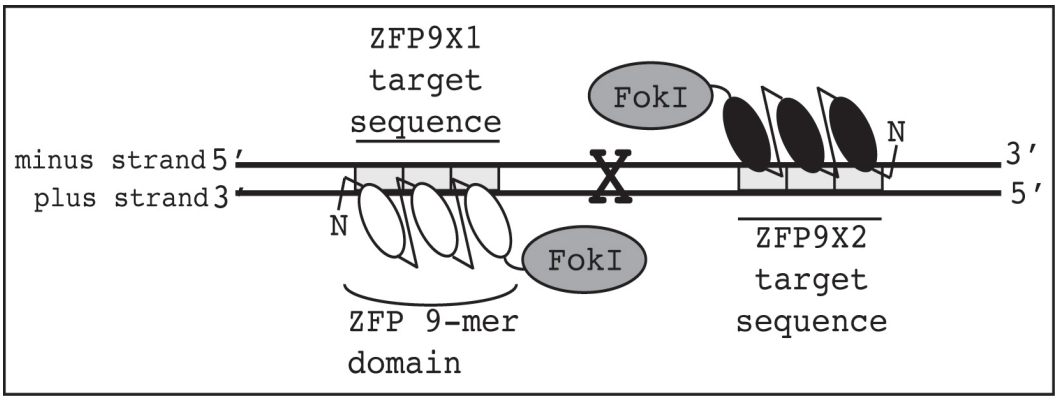

Figure 3.2 - Schematic representation of ZFNs formed by ZFP 9-mers acting as heterodimers around the FokI endonuclease domain.
Each zinc finger motif of the 9-mer is shown as an oval, with three modules linked in tandem. The grey boxes represent the target binding sites for each ZFP. The FokI domain is located at the C-terminus of each 9-mer. The 9-mer pairs are designed to bind opposite strands of DNA, ensuring the FokI domains are both located at the intervening DNA sequence between the two target sites. The "X" represents the DNA cleavage site.

3.3.2 Synthesis, bacterial expression and purification of HBV-specific ZFPs

The amino acid sequence of each ZFP provided by the 'Zinc Finger Tools' website was used to order custom sequence synthesis by Blue Heron Technologies. A codon usage table for *Homo sapiens* was used to convert the amino acid sequence to the nucleotide sequence and the "codon-optimized sequence" was selected for synthesis. The ZFPs were produced in pUC19 vectors as described in the Materials and Methods section.

ZFPs were cloned into the pMal-gg1 vector (pMal-c background). Positive clones were obtained for all ZFPs except ZFP9Z2. ZFPs were expressed in BL21(DE3) *E.coli* and purified based upon their fusion to the maltose binding protein (MBP). Samples were collected during the purification protocol and analyzed by SDS-PAGE and Coomassie Blue staining. Figure 3.3 shows a typical expression pattern for the ZFPs. Lysates from un-induced bacterial cultures (Figure 3.3 lane 1) versus cultures induced with IPTG for 2 hours (Figure 3.3 lane 2) show the production of the ZFP-MBP fusion protein (asterisk) after induction. The soluble fraction (Figure 3.3 lane 3) maintains the majority of the ZFP-MBP fusion protein

compared to the insoluble fraction (Figure 3.3 lane 4). The ZFP-MBP fusion protein was isolated from the soluble fraction using an amylose-resin column. The column eluate (Figure 3.3 lane 5) demonstrates the ZFP-MBP fusion protein in a concentrated and purified form. A small amount of purified MBP was run in the right hand lane for size comparison of the ZFP-MBP fusion proteins to MBP alone. The column eluate was further evaluated by analyzing each fraction eluted from the amylose resin column by SDS-PAGE and Coomassie Blue staining. The elution pattern is similar to a representative pattern seen in Figure 2.3 B. The fractions with the greatest amount of ZFP-MBP fusion protein were pooled together for further experiments. All *in vitro* assessments of ZFPs were performed using the ZFP-MBP fusion protein.

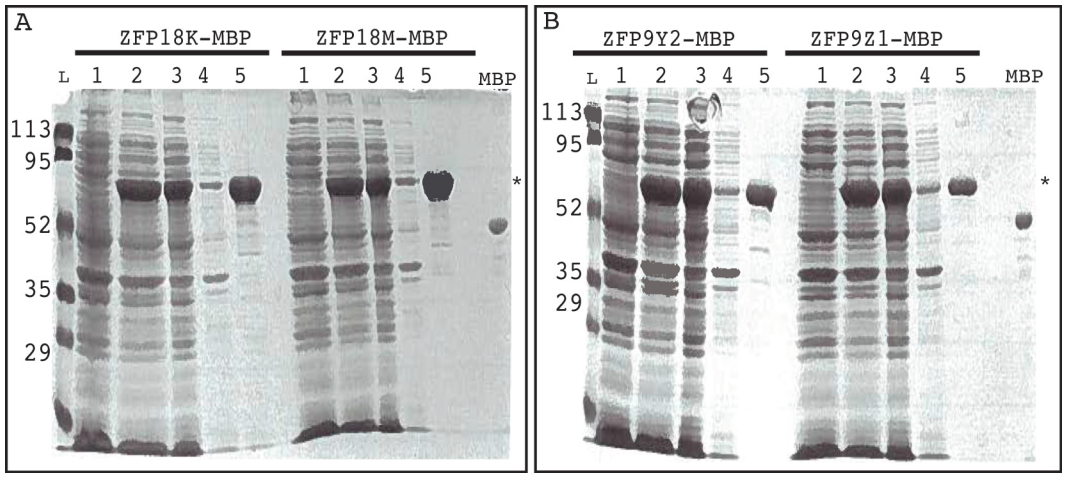

Figure 3.3 - Protein purification of HBV-specific ZFPs.
Samples collected during the purification procedure were separated using 10% SDS-PAGE and stained with Coomassie Blue protein stain. Samples from the purification procedure for (A) ZFP18K-MBP and ZFP18M-MBP, and (C) ZFP9Y2-MBP and ZFP9Z1-MBP were collected from (1) un-induced bacterial cultures, (2) cultures induced for 2 hours with IPTG, (3) soluble fraction after centrifugation, (4) insoluble fraction after centrifugation, and (5) column eluate. A small amount of purified MBP was run in the right hand land of each gel. The ladder (L) is shown on each figure and the MW sizes of the markers are shown on the side, in kDa. An asterisk (*) marks the band representing the ZFP-MBP fusion protein.

3.3.3 EMSA: Determination of apparent equilibrium dissociation constant for HBV-specific ZFPs

EMSAs were performed to determine the apparent equilibrium dissociation constants of the HBV-specific ZFPs. Bacterially purified ZFP-MBP fusion proteins were incubated with dsDNA oligonucleotides encoding the specific target sequence for each ZFP then separated on non-denaturing polyacrylamide gels. The gels were stained with SYBR-green DNA stain and scanned with a phosphorimager. This process shows the shift of the dsDNA oligonucleotides up to a high molecular weight complex composed of ZFP-MBP fusion protein bound to the oligonucleotide (Figure 3.4). All HBV-specific 18-mers (ZFP18K, ZFP18M, ZFP18N, ZFP18P) bound their target sequences with high affinity, as shown by the strong mobility shift bands produced in the presence of each ZFP.

The HBV-specific 9-mers exhibited poor target binding. Only ZFP9Z1 demonstrated any detectable binding (Figure 3.5 B). The EMSA for ZFP9X1 is shown in Figure 3.5 A, but is also representative for EMSAs obtained for ZFP9X2, ZFP9Y1 and ZFP9Y2. For these ZFP 9-mers, no binding was detectable by EMSA. ZFP9Z2 was not successfully cloned into the pMAL plasmid, therefore it was not purified and EMSA was not performed on it.

The bands in the EMSAs representing the complexed ZFP-MBP and dsDNA oligonucleotide were quantified using ImageGauge v4.22 software. After subtracting both local and global background, the values were plotted using the Enzyme Kinetics v1.11 software program. The non-linear regression plots for ZFP18K, ZFP18M, ZFP18N, ZFP18P and ZFP9Z1 (Figure 3.6) show the concentration (nM) of ZFPs on the x-axis against the amount of binding (arbitrary units) on the y-axis.

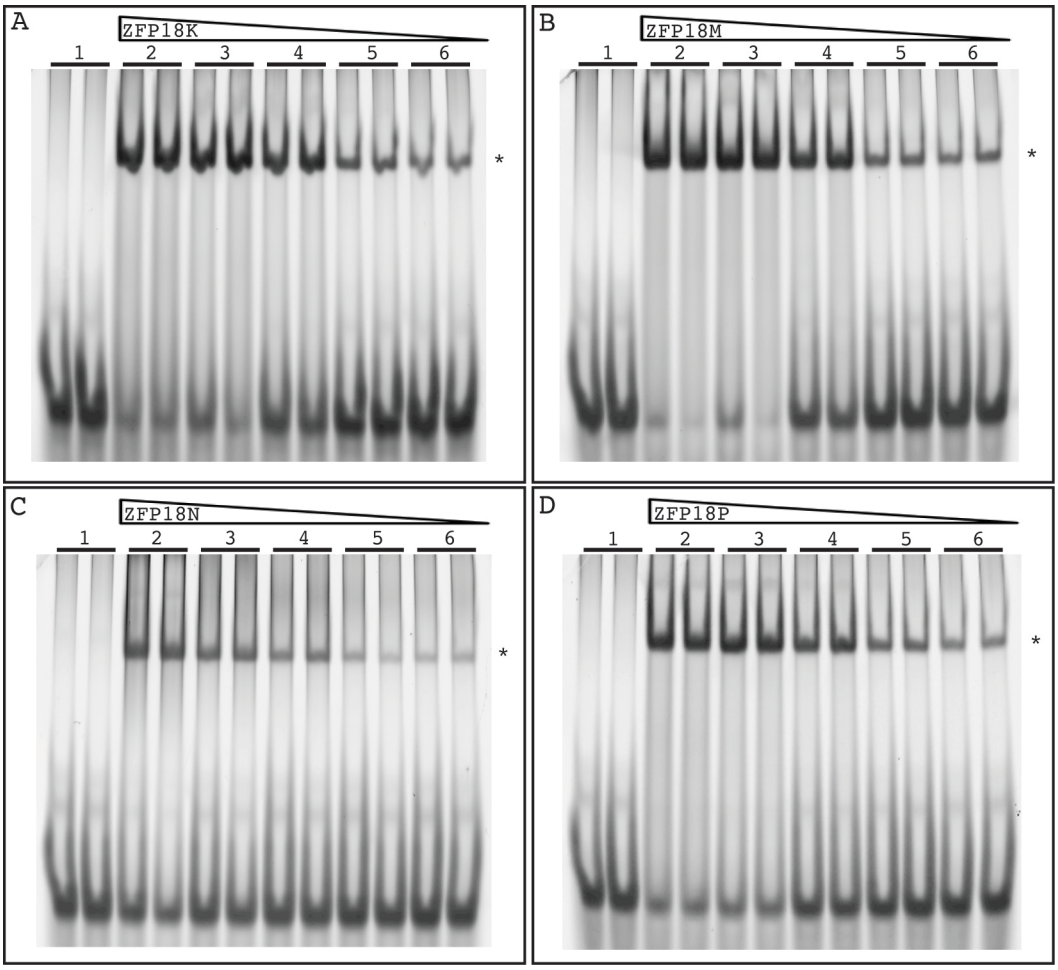

Figure 3.4 - EMSAs to determine the apparent equilibrium dissociation constant of HBV-specific ZFP 18-mers.
DsDNA oligonucleotides with the specific target sequence for each ZFP were incubated alone (lane 1) or in the presence of ZFP18-MBP fusion proteins at 150-nM (lane 2), serially diluted 1 in 2 (lanes 3 to 5) down to 9.5-nM (lane 6). Each sample is in duplicate. The gels were stained with SYBR-green DNA stain. The asterisk (*) marks the DNA-protein complex. The bands next to the asterisks were quantified using Image Gauge software v4.22, and the dissociation constant was calculated using the Enzyme Kinetics software v1.11. Each EMSA was performed 2-3 times.

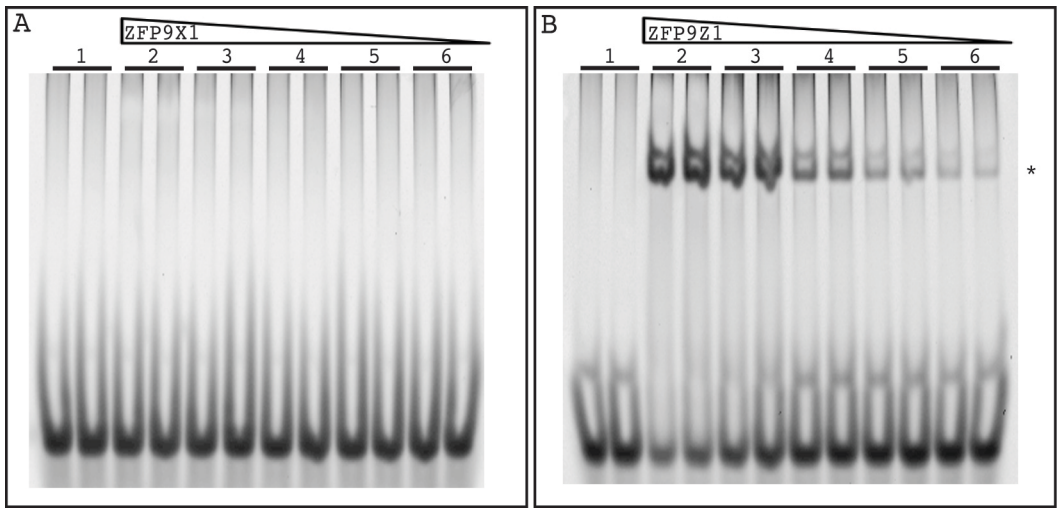

Figure 3.5 - EMSAs to determine the apparent equilibrium dissociation constant of HBV-specific ZFP 9-mers.
DsDNA oligonucleotides with the specific target sequence for each ZFP were incubated alone (lane 1) or in the presence of ZFP9-MBP fusion proteins at 150-nM (lane 2), serially diluted 1 in 2 (lanes 3 to 5) down to 9.5-nM (lane 6). Each sample is in duplicate. The gels were stained with SYBR-green DNA stain. The asterisk (*) marks the DNA-protein complex. The bands next to the asterisks were quantified using Image Gauge software v4.22, and the dissociation constant was calculated using the Enzyme Kinetics software v1.11. Each EMSA was performed 2-3 times.

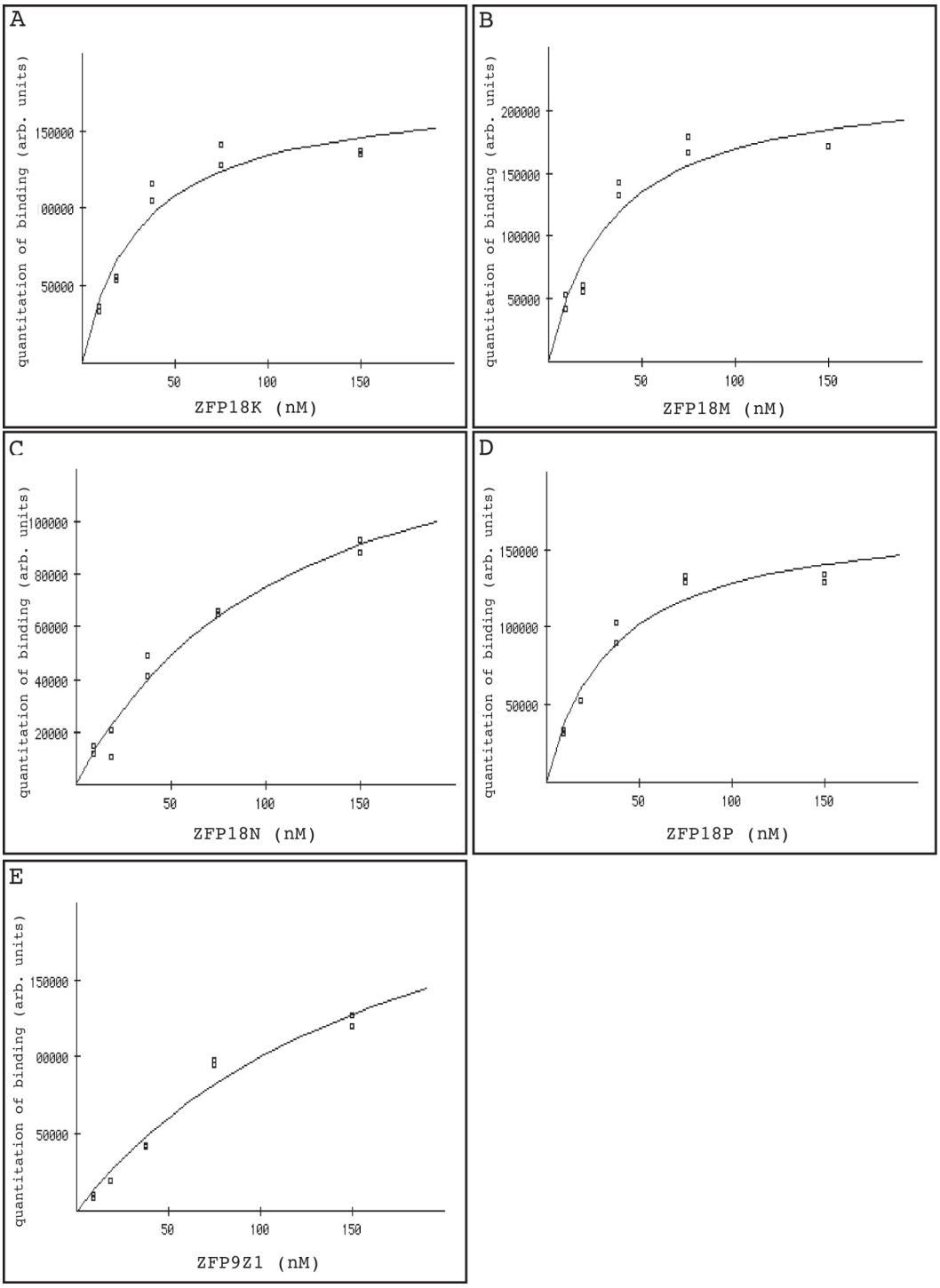

Figure 3.6 - Non-linear regression plots from the quantification of EMSAs on HBV-specific ZFPs.

EMSAs were quantified and analyzed using the Enzyme Kinetics software v1.11. The non-linear regression plots were created by plotting the concentration (nM) of the ZFP (x-axis) against the amount of binding (y-axis). Graphs show the values for a single representative EMSA.

The dissociation constants, found in Table 3.7, were calculated from these graphs based upon the Michaelis-Menton equation. All four of the 18-mers had dissociation constants in the nanomolar range, which is frequently considered to be sufficient for therapeutic development. ZFP18K, ZFP18M and ZFP18P had similarly strong dissociation constants of 44.0-nM, 41.0-nM and 46.0-nM, respectively. ZFP18N had a slightly weaker dissociation constant of 85.0-nM. ZFP9Z1, however, had a very weak dissociation constant of 1.2-μM, which is 26-fold weaker than the 18-mers. Since the other 9-mers (ZFP9Z1, ZFP9X2, ZFP9Y1, ZFP9Y2) did not demonstrate any binding by EMSA, their dissociation constant could not be calculated. Similarly, the EMSA could not be performed on ZFP9Z2 because it could not be cloned and purified.

HBV-specific ZFPs			
Name	EMSA	Name	EMSA
ZFP18K	44.0-nM	ZFP9X1	n.b [a]
ZFP18M	41.0-nM	ZFP9X2	n.b.
ZFP18N	85.0-nM	ZFP9Y1	n.b
ZFP18P	46.0-nM	ZFP9Y2	n.b
		ZFP9Z1	1.2-μM
		ZFP9Z2	n.b.

Table 3.7 - Summary of dissociation constants calculated by EMSA for HBV-specific ZFPs.
[a] No binding.

3.3.4 EMSA: Determination of tolerance for single or double nucleotide changes in target sequence

To investigate the ability of the designed ZFPs to bind sequences that have one or two nucleotide changes compared to the exact target sequence, EMSAs were performed on the ZFP18K-MBP fusion protein using oligonucleotides with altered target sequences (Figure 3.7). The sequences of the oligonucleotides are found in Table 3.4. The oligonucleotides 18K.1C-T and 18K.1C-G have a

cytosine changed to either a thymine or guanine, respectively, in the first triplet of the recognition sequence for ZFP18K. ZFP18K-MBP binds these target sequence variants with equal affinity to the wild type target sequence (Figure 3.7 A, lanes 3 and 4). In fact, ZFP18K-MBP even appears to bind 18K.1C-G (lane 4) with greater affinity than the wild type sequence (lane 2).

The oligonucleotides 18K.3G-A and 18K.3G-C have a guanine changed to either an adenine or cytosine, respectively, in the third triplet of the recognition sequence for ZFP18K. ZFP18K-MBP binds these target sequence variants (Figure 3.7 A, lanes 5 and 6) with equal affinity to the wild type target sequence (lane 2), although ZFP18K-MBP appears to bind 18K.3G-C with slightly lower affinity than wild type.

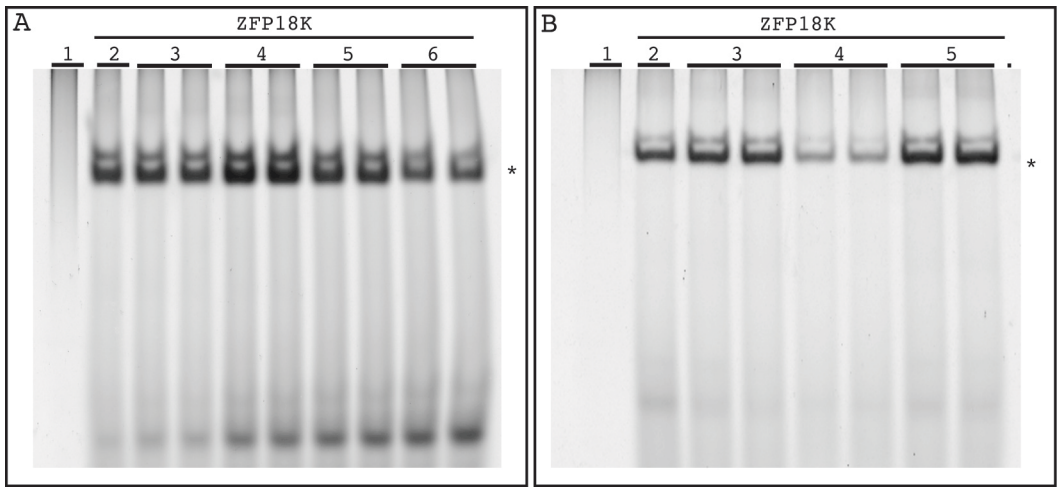

Figure 3.7 - EMSAs to explore the tolerance of ZFP18K-MBP to one or two nucleotide changes in the target nucleotide sequence.
(A) dsDNA oligonucleotides were incubated alone (lane 1) or with 150-nM of ZFP18K-MBP fusion protein (lanes 2–6). Exact target sequence for ZFP18K-MBP (lane 2), 18K.1C-T (lane 3), 18K.1C-G (lane 4), 18K.3G-A (lane 5), 18K.3G-C (lane 6). (B) dsDNA oligonucleotides were incubated alone (lane 1) or with 150-nM of ZFP18K-MBP fusion protein (lanes 2 – 5). Exact target sequence for ZFP18K-MBP (lane 2), 18K.5A-G (lane 3), 18K.5A-T (lane 4), 18K.1.5 (lane 5). The gels were stained with SYBR-green DNA stain. The asterisk (*) marks the DNA-protein complex.

The oligonucleotides 18K.5A-G and 18K.5A-T have an adenine changed to either a guanine or thymidine, respectively, in the fifth triplet of the recognition sequence for ZFP18K. While ZFP18K-MBP binds 18K.5A-G (Figure 3.7 B, lane 3) with equal affinity as the wild type sequence (lane 2), it has decreased binding of 18K.5A-T (lane 4). However, this is the only oligonucleotide with one nucleotide change that ZFP18K-MBP binds with noticeably decreased affinity, suggesting that the tolerance for single nucleotide changes in the target sequence is quite high. One oligonucleotide with two nucleotide changes, 18K.1.5, was also tested. This oligonucleotide combines the changes of 18K.1C-T and 18K.5A-G: in the first triplet, a cytosine is substituted by a thymidine, and in the fifth triplet, an adenine is substituted by a guanine. ZFP18K-MBP exhibits an equal, if not greater, ability to bind 18K.1.5 (Figure 3.7 B, lane 5) compared to the wild type sequence (Figure 3.7 B, lane 2). This further suggests the tolerance of ZFP18K-MBP is high. The off-target binding is of concern because if it occurs in the context of a cell, it can interfere with normal transcriptional process and decrease the effectiveness of the designed ZFPs to function as virus-specific therapeutics. The tolerance of ZFP18K-MBP is likely due to the method of production of the ZFPs – the ZFPs were not produced by screening a library of clones for the best binding, but rather by using an online library of known sequences. The combination of the zinc finger modules to bind multiple sequences is not optimized in the Zinc Finger Tools library. It is know that there are some interactions between one zinc finger module and the DNA of the adjacent zinc finger module's target sequence, which is not taken into consideration during the Zinc Finger Tools design process. As well, the amino acid sequences of the zinc finger modules can be quite similar, despite the difference in target binding sequence. For example, when comparing the amino acid sequences to bind the ACC triplet vs. the ACT triplet, 3 out of the 7 amino acids are identical in the α-helix recognition loop of the zinc finger module (see Appendix B Tables 7.1 & 7.2, for all α-helix amino acid sequences). This emphasizes the possibility of cross-interaction with non-cognate target sequences. However, the chromosome structure of the cellular DNA can protect near-target sequences from being bound

by a ZFP. This does not exclude the possibility that one or more of the HBV-specific ZFPs may bind off-target sites in tissue culture cells.

3.3.5 EMSA: Determination of specificity for target sequence by HBV-specific ZFPs

The specificity of the ZFPs to their target sequences was assessed by competition-based EMSAs (Figure 3.8). The protocol is based upon the idea that a ZFP that exhibits specificity for its target sequence should preferentially bind to its target sequence, generally in the form of a radiolabeled probe (lane 2), and should not be competed off from this probe by the addition of unlabeled oligonucleotide with a non-specific sequence (lane 6). In addition, it should be competed off from the probe by the addition of increasing amounts of unlabeled specific oligonucleotide (lanes 3 – 5). Lastly, a specific ZFP should not bind a radiolabeled probe with a non-specific sequence (lane 7). Lane 1 contains radiolabeled probe without ZFP added.

Competition-based EMSAs were only performed on ZFP18K, ZFP18M, ZFP18N and ZFP18P, which were the only ZFPs that exhibited strong binding as determined by their dissociation constants. The competition EMSA of ZFP18K demonstrates a ZFP that is specific for its target sequence (Figure 3.8 A). It binds to its target sequence (lane 2), and is incrementally competed off from the probe by the addition of unlabeled specific oligonucleotide (lanes 3 – 5). In these lanes, the ZFP becomes distributed between binding to the labeled probe and the unlabeled oligonucleotide competitor. Less ZFP is therefore available to bind to the probe and the band is decreased in those lanes. Additionally, ZFP18K binds to the probe in the presence of an unlabeled non-specific oligonucleotide (lane 6) to the same extent as in lane 2, indicating that it has a preference for its own target sequence. This is confirmed by lane 7, where a non-specific probe is incubated with ZFP18K and is not bound by it.

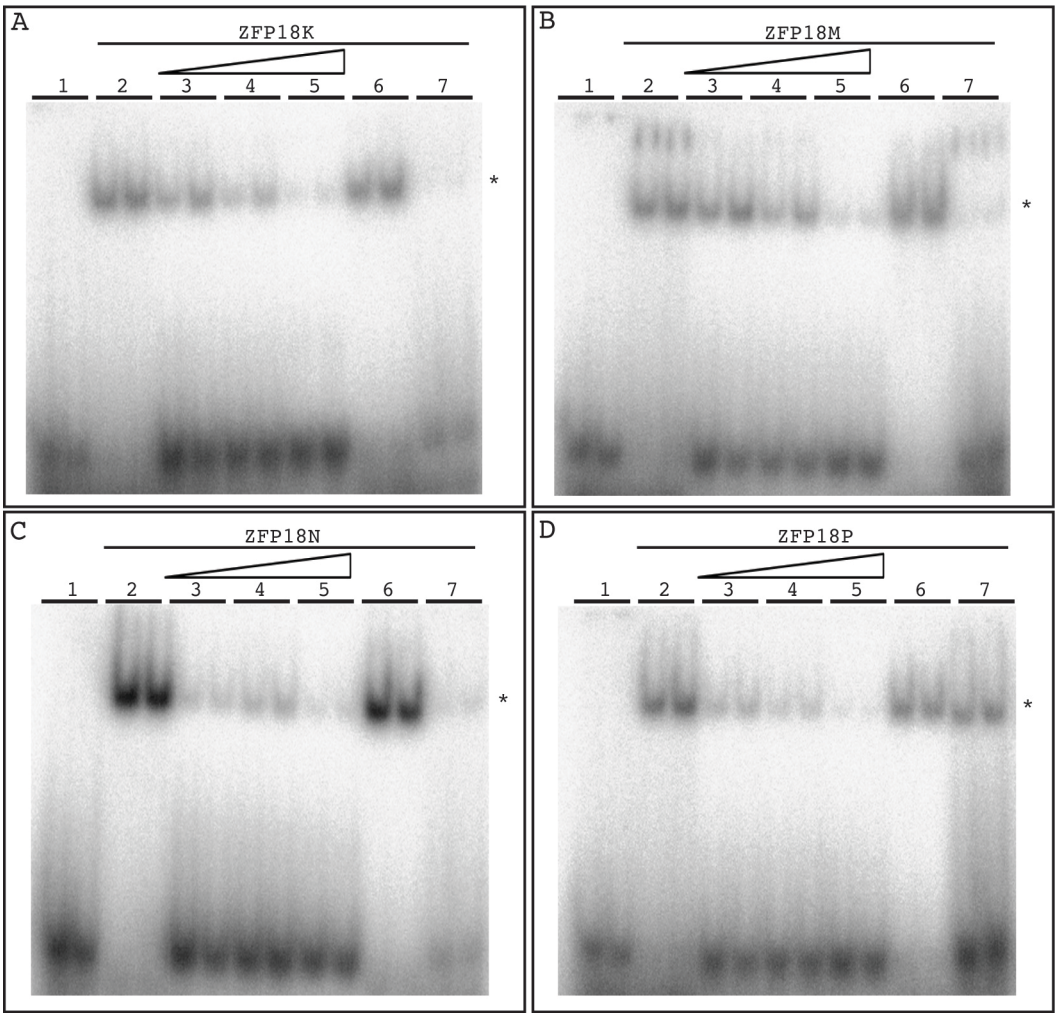

Figure 3.8 - EMSAs to determine the specificity of HBV-specific ZFPs.
Double stranded DNA oligonucleotides with the specific target sequence for each ZFP were radiolabeled with ^{32}P and incubated alone (lane 1) or in the presences of 150-nM ZFP-MBP fusion protein (lanes 2 – 7). In addition, unlabeled specific oligonucleotide competitor DNA was added at 5-μM, 10-μM or 50-μM concentrations (lanes 3 – 5, respectively), or unlabeled non-specific competitor DNA was added at 50-μM concentration (lane 6). Lastly, radiolabeled non-specific probe was incubated with 150-nM ZFP-MBP protein (lane 7). Each sample is in duplicate. The asterisk (*) marks the mobility shift formed when the dsDNA oligonucleotide is bound to the ZFP-MBP fusion protein.

ZFP18M and ZFP18N (Figure 3.8 B & C) demonstrate similar patterns, wherein they are competed by unlabeled specific oligonucleotides (lanes 3 – 5), but not by non-specific competitors (lane 6). Furthermore, they do not bind a non-specific probe (lane 7). ZFP18P, however, did not exhibit the same specificity profile.

Instead, it bound the non-specific probe (Figure 3.8 D, lane 7) to an equal extent as its specific probe. This non-specific binding prompted ZFP18P to be eliminated from further analysis.

3.3.6 SPR on HBV-specific ZFPs

SPR was also performed on the HBV-specific ZFPs. SPR measures the real-time interactions between a ligand (biotinylated dsDNA oligonucleotides) coupled to a detection surface (streptavidin-coated sensor chip) and an analyte (purified ZFP-MBP fusion proteins) that flows over the detection surface. The ZFPs were flowed over the detection surface and a reference flow cell (lacking oligonucleotides) and produced a 1:1 binding scenario with the immobilized oligonucleotides.

SPR was performed using an automated BIAcore 3000 machine on ZFP18K, ZFP18M, ZFP18N, ZFP9X1, ZFP9X2, ZFP9Y1, ZFP9Y2 and ZFP9Z1. ZFP18P was excluded because of its non-specific binding in Figure 3.8 D. ZFP9Z2 could not be cloned, therefore SPR could not be performed on it.

For each ZFP, a range of concentrations was passed over the sensor chip surface, from low to high, with a regeneration step in between each concentration to renew the surface of the sensor chip. Binding was measured as ZFPs passed over the surface, by measuring the change in refraction of light on the sensor surface, caused by analyte binding to ligand. This change is plotted as response difference in resonance units (RU), with more binding producing higher response differences than less binding. The response differences (RU) on the y-axis is plotted against the time (seconds) on the x-axis for each ZFP18K (A), ZFP18M (B), and ZFP18N (C) (Figure 3.9). Each line on these graphs represents a different concentration of ZFP passed over the sensor chip surface. SPR was carried out for the 9-mers as well, but these experiments produced data indicating no binding was occurring. As an example, the representative results obtained with ZFP18M show no binding (Figure 3.9 B). Similar results were obtained with all other ZFP 9-mers.

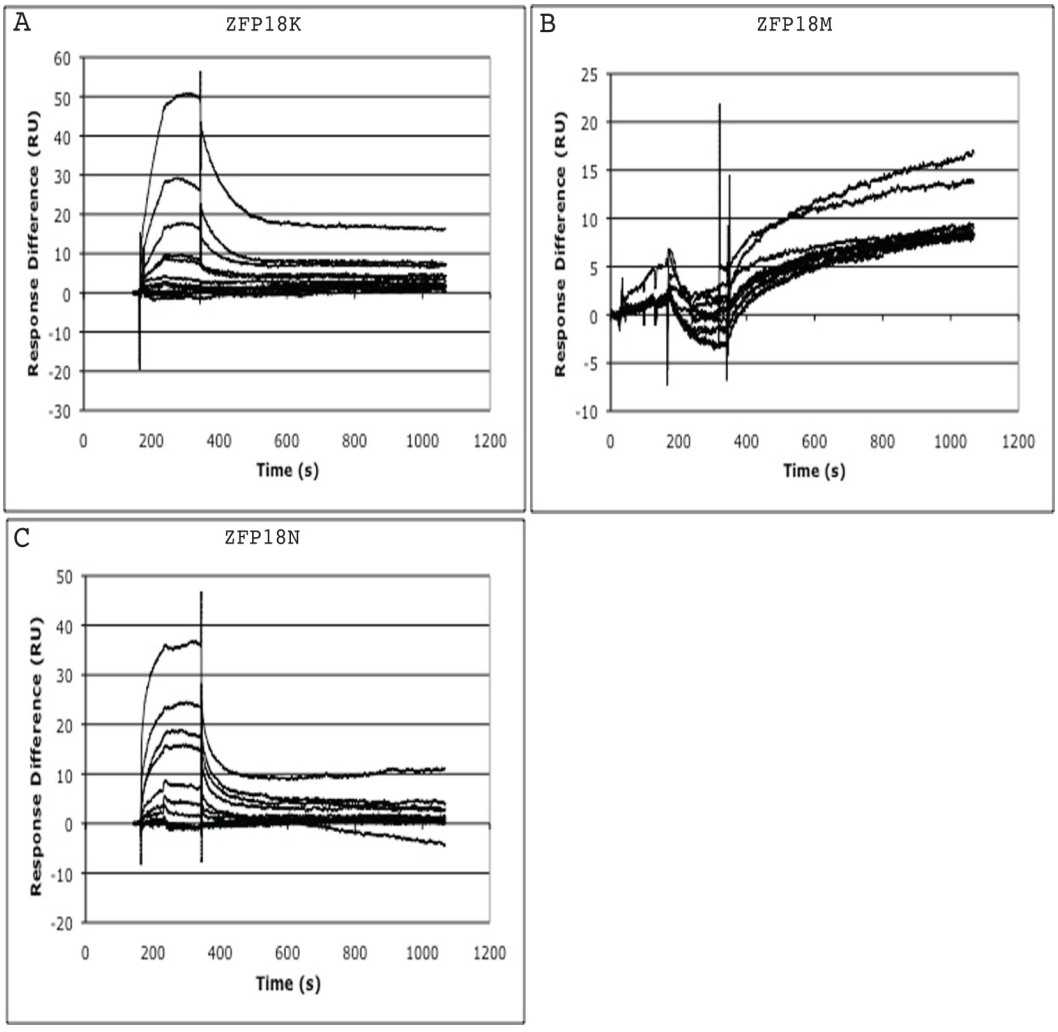

Figure 3.9 - Surface Plasmon resonance on HBV-specific ZFPs.
SPR was performed on HBV-specific ZFP-MBP fusion proteins using the BIAcore 3000 and biotinylated dsDNA oligonucleotides coupled to streptavidin on a Sensor Chip SA. ZFPs were flowed over the sensor chip surface and the amount of ZFP binding to the target DNA was measured by the change in the refractive index on the sensor chip surface. This change is calculated as the response difference in resonance units (RU), and is plotted on the y-axis, against time on the x-axis (seconds). ZFPs were flowed over the sensor chip surface for 3 minutes, followed by 15 minutes of dissociation time. ZFPs were injected at a range of concentrations in duplicate, running from low to high concentrations. Between each round of injections, the surface was regenerated with 0.5% SDS to remove any bound ZFP from the previous round. Each line represents the average of duplicate analysis of one concentration of ZFP. Three blanks were also performed in duplicate. For each sample, measurements from a reference flow cell lacking the oligonucleotides were subtracted.

The dissociation constant was produced by SPR using fitting the data to a 1:1 binding with drifting baseline model. The baseline drift was likely due to incomplete renewal of the sensor chip surface after the regeneration step, due to incomplete removal of ligand bound ZFP during regeneration. The dissociation constants (Table 3.8) are in general agreement with those calculated by EMSA. For example, the dissociation constant for ZFP18N was calculated as 84.6-nM by EMSA and 69.4-nM by SPR, which is only a 1.2-fold difference. The SPR data for ZFP18K, however, calculated a dissociation constant (5.1-nM) almost 8.5-fold lower than that calculated for EMSA (43.6-nM). The data generated by SPR suggests a stronger binding affinity for its target than that suggested by the EMSA. The data for ZFP9Z1 was of poor quality and varied greatly from the model, suggesting the weak binding of ZFP9Z1 for its target resulted in poor data in the SPR procedure. In agreement with the results collected by EMSA, the other ZFP 9-mers (ZFP9X1, ZFP9X2, ZFP9Y1, ZFP9Y2) did not demonstrate any binding.

HBV-specific ZFPs					
Name	Association rate ($M^{-1}s^{-1}$)	Dissociation rate (s^{-1})	Association constant (M^{-1})	Dissociation constant (nM)	Chi^2 value
ZFP18K	3.58×10^{3}	1.84×10^{-5}	1.94×10^{8}	5.1	2.38
ZFP18M	n.b.[a]	n.b.	n.b.	n.b.	n.b.
ZFP18N	8.66×10^{4}	6.01×10^{-3}	1.44×10^{7}	69.4	0.30
ZFP18P	n.d.[b]	n.d.	n.d.	n.d.	n.d.
ZFP9X1	n.b.	n.b.	n.b.	n.b.	n.b.
ZFP9X2	n.b.	n.b.	n.b.	n.b.	n.b.
ZFP9Y1	n.b.	n.b.	n.b.	n.b.	n.b.
ZFP9Y2	n.b.	n.b.	n.b.	n.b.	n.b.
ZFP9Z1	n.b.	n.b.	n.b.	n.b.	n.b.
ZFP9Z2	n.d.	n.d.	n.d.	n.d.	n.d.

Table 3.8 - Kinetic data from SPR on DHBV-specific ZFPs.
[a] No binding. [b] Not done.

The association rate describes the number of ZFP-DNA complexes formed per second in a 1M solution of ZFP and DNA. The association rate was 3.58 x 10^3 $M^{-1}s^{-1}$ for ZFP18K and 8.66 x 10^4 $M^{-1}s^{-1}$ for ZFP18N (Table 3.8). ZFP18N had a faster association rate than ZFP18K. The dissociation rate was 1.84 x 10^{-5} s^{-1} for ZFP18K and 6.01 x 10^{-3} s^{-1} for ZFP18N (Table 3.8). This rate describes the stability of the complex formed by ZFPs and DNA. ZFP18K had a much slower dissociation rate with 0.00184% of the complexes dissociating per second, compared to ZFP18N, which had 0.601% dissociating per second. The association constant describes the binding strength of the ZFP to the DNA. ZFP18K had a stronger binding strength to its target DNA than ZFP18N had (Table 3.8). Lastly, the Chi^2 value is a measurement of the goodness of fit to the model. Smaller values for Chi^2 indicate a better fit to the model: both ZFP18K and ZFP18N had good fit to the model.

3.3.7 Lipofectamine™ 2000 transfection of HepAD38 cells

HepAD38 cells were created by Ladner *et al* (1997) (7) stably transfecting HepG2 human hepatoma cells with a cDNA copy of the HBV strain *ayw* pgRNA under the control of a tetracycline-responsive promoter. HepAD38 cells are useful for testing therapeutics targeting the cccDNA reservoir of HBV because HBeAg is only produced and secreted into the culture supernatant in the presence of cccDNA. Experiments testing protein therapeutics such as the HBV-specific ZFPs require transfection of HepAD38 cells with the ZFP-encoding plasmids. However, HepAD38 cells, like their parental HepG2 line, are difficult to transfect at high efficiencies. Thus, a number of transfection methods were tested on the HepAD38 cells to obtain high enough ZFP-expression to see a therapeutic effect.

Standard LF2000 transfection was tested in the HepAD38 cells by plating the cells in 6-well plates. After overnight incubation, the cells were transfected with the plasmid pd1-EGFPn1 using a variety of DNA to LF2000 ratios, including 2:1, 1:1, 1:2, 1:4 and 1:5. A total amount of 4-µg of DNA was maintained in each treatment. Cells were assessed for GFP expression at 24 and 48 hours post-

transfection by visualization and counting under a fluorescence microscope. The cell viability was also approximated by estimating the number of floating cells present in each well. Table 3.9 summarizes the results from one such experiment. The best transfection efficiency obtained was 25% using a ratio of 1:5. Unfortunately, the viability of the cells with this treatment was quite low by 48 hours. Also, by 48 hours post-transfection, the number of GFP positive cells decreased in all treatment groups, including the 1:5 ratio group to only 10% GFP positive cells.

DNA:LF2000™ ratio	Percent GFP positive cells		Approximate Cell Viability
(µg:µL)	24 hours	48 hours	48 hours
2:1	1%	0%	High
1:1	5%	5.4%	Medium-high
1:2	24%	4.8%	Medium
1:4	24%	3.3%	Medium-low
1:5	25%	10%	Low

Table 3.9 – Results of transfection optimization of HepAD38 cells by varying the ratio of DNA to LF2000.

In an attempt to increase the cell viability, the optimal cell densities were tested while keeping the DNA to LF2000™ ratio constant at 1:5. Cells were plated at densities of 2.0×10^5, 4.0×10^5, 8.0×10^5 and 1.6×10^6 cells/well, then transfected with the plasmid pd1-EGFPn1. GFP positive cells was assessed and counted after 24 hours using a fluorescence microscope. The cell viability was also approximated by estimating the number of floating cells present in each well. Table 3.10 summarizes the results from one such experiment. The best transfection efficiency was obtained when a cell density of 4.5×10^5 cells/well was used, which also had a better cell viability profile than previously determined in Table 3.9.

Cell density at plating	Percent GFP positive cells (24 hours)	Approximate Cell Viability
2.0 x 10^5 cells/well	11%	High
4.0 x 10^5 cells/well	17.5%	Medium-high
8.0 x 10^5 cells/well	10.3%	Medium
1.6 x 10^6 cells/well	0.6%	Low

Table 3.10 – Results of transfection optimization of HepAD38 cells using LF2000 by varying cell density at the time of plating.

A transfection efficiency of 25% proved insufficient to test any therapeutic effect of the transfected ZFPs in HepAD38 cells. This is likely due to the large amount of viral products produced in the HepAD38 cell line, which produces 11-fold more relaxed circular virion DNA than another HBV-harbouring cell line, HepG2.2.15 (7). If less than one quarter of HBV-producing cells are expressing ZFPs, and in this fraction of cells, HBV gene products are reduced by 70% (as was demonstrated with the DHBV-specific ZFPs), the effect of the ZFPs would still be greatly masked by HBV production in the non-transfected cells.

Transfection plasmid	Total cells collected after sorting	Percent of parent population[a]
pcDNA3.1(+)	2.9 x 10^4 cells	2.6%
pcDNA3.1(+)-ZFP18K	3.9 x 10^4 cells	3.8%
pcDNA3.1(+)-ZFP18M	3.5 x 10^4 cells	2.8%
pcDNA3.1(+)-ZFP18N	4.3 x 10^4 cells	3.5%

Table 3.11 - Results of GFP-based cell sorting of LF2000-transfected HepAD38 cells.
[a] percent of GFP positive cells collected after sorting compared to the starting population.

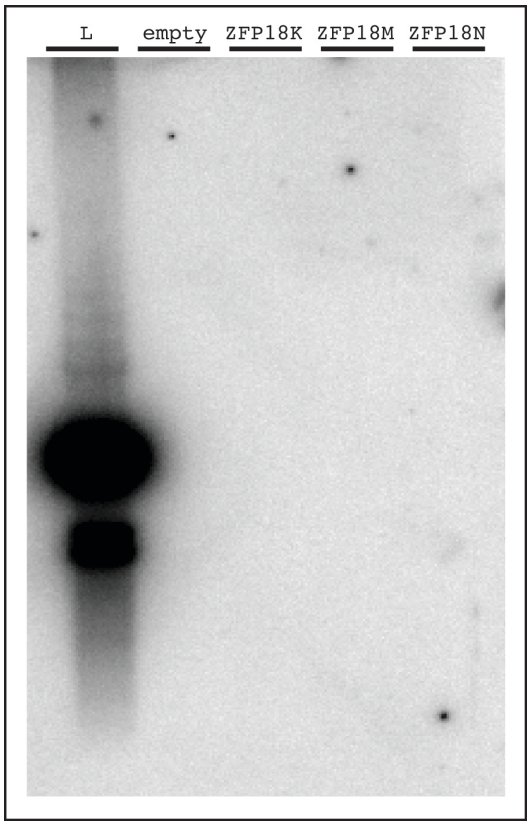

Figure 3.10 – Southern blot of ICV isolated from GFP-based cell sorting of LF2000-transfected HepAD38 cells.
HepAD38 cells were transfected with pcDNA3.1(+)-EGFP and pcDNA3.1(+) (empty) or pcDNA3.1(+)-ZFP18K, ZFP18M or ZFP18N. After 24 hours, the cells were sorted based on EGFP and then ICV was isolated from the enriched fractions. ICV was assessed by Southern blot using an HBV-specific probe, and scanned by a phosphorimager. The ladder (L) was a 1.0-kb DNA ladder that partially cross-reacts with the HBV-specific probe. This experiment was performed twice with similar results.

To attempt to enhance the proportion of ZFP-expressing cells, HepAD38 cells were plated at 4.0 x 10^5 cells/well and co-transfected with pcDNA3.1(+)-EGFP and pcDNA3.1(+) or pcDNA3.1(+)-ZFP18K, ZFP18M or ZFP18N. After 24 hours, the cells were removed from the plates and sorted by flow cytometry for GFP expression. Based upon transfection of the cells with a 4-fold excess of pcDNA3.1(+) or pcDNA3.1(+)-ZFP compared to pcDNA3.1(+)-EGFP, cells that express GFP are likely to also have been transfected with the ZFP-expressing plasmid as well. In an attempt to enrich for ZFP-expressing HepAD38, the GFP positive cells were sorted and collected. Unfortunately, only very small numbers

of GFP positive cells were recovered for each transfection, despite the fact that all the wells from an entire 6-well plate were pooled for an experiment. As can be seen in Table 3.11, only 2.9 x 10^4 - 4.3 x 10^4 cells were collected from each treatment group, which was insufficient for further analysis, as determined by Southern blot for ICV production (Figure 3.10).

In summary, transfection with the LF2000 reagent was insufficient to properly investigate the potential therapeutic effects of the HBV-specific ZFPs in HepAD38 cells.

3.3.8 TransIT®-LT1 and Fugene® 6 transfections of HepAD38 cells

Two other lipid-based transfection reagents were tested in attempts to increase the transfection efficiency of HepAD38 cells. HepAD38 cells were plated in 6-well plates and transfected with the pd1-EGFPn1 plasmid using the TransIT®-LT1 reagent. After both 24 and 48 hours, there were no GFP positive HepAD38 cells, as determined by examination using a fluorescence microscope.

Similarly, HepAD38 cells were transfected with the pd1-EGFPn1 plasmid using the Fugene® 6 transfection reagent. After 24 hour and 48 hours, no HepAD38 cells showed GFP fluorescence, despite the different ratios of DNA to Fugene® 6 tested,. LMH cells similarly transfected, as a positive control, exhibited GFP positive cells after 24 and 48 hours. Thus, both TransIT®-LT1 and Fugene® 6 were discarded as a possible alternatives for transfection of HepAD38 cells.

3.3.9 Electroporation and nucleofection of HepAD38 cells

HepAD38 cells were electroporated with the pd1-EGFPn1 plasmid using standard methods on a Bio-Rad Gene Pulser electroporator. After 24 hours, 1 – 5% of cells expressed EGFP, as determined by visualization and counting under a fluorescence microscope. However, there were no GFP positive cells detected after 48 hours.

The Cell Line Optimization Nucleofactor® Kit was used to optimize nucleofection of plasmid DNA into HepAD38 cells. The Nucleofactor® Device is a specialized electroporation apparatus that provides unique electrical parameters and solutions for electroporation of mammalian cells. Two different electroporation solutions (L and V) were tested with seven different preset programs. HepAD38 cells were nucleofected with the pmaxGFP plasmid provided with the Optimization Kit (see map in Appendix A). The results of nucleofection with Solution L are found in Table 3.12 and with Solution V in Table 3.13. The controls included addition of the pmaxGFP plasmid without any program applied to the cells, and application of the program T-020 with no plasmid DNA added. After 24 and 48 hours post-nucleofection, cells were assessed for expression of GFP by counting under a fluorescence microscope. The cell viability was also approximated at 24 and 48 hours. In general, Solution V resulted in greater percentages of GFP positive cells and higher cell viability compared to Solution L. For Solution L, 10 – 30% of the cells were GFP positive, depending on the program used (Table 3.12). The best program with Solution L was X-001, although the cell viability was moderate after 24 hours and dropped off by 48 hours. The cell viability was quite poor with Solution L and programs T-020, T-030, X-005 and L-029. The program D-023 produced a decent transfection rate of 20% and had good cell viability.

For Solution V (Table 3.13), 2 – 40% of the cells were GFP positive. The best programs with Solution V were T-030 and X-001, although T-030 had poor cell viability. In contrast, the X-001 program had high numbers of GFP positive cells and moderate cell viability. Overall, there was much better cell viability with Solution V, since only program T-020 and T-030 produced low cell viability.

Program	Percent GFP positive cells		Approximate Cell Viability	
	24 hours	48 hours	24 hours	48 hours
No program & DNA	0%	0%	High	High
T-020 & No DNA	0%	0%	High	High
D-023	20%	20%	High	Medium
A-020	10%	10%	High	High
T-020	10%	20%	Low	Low
T-030	15%	20%	Low	Low
X-001	30%	20%	Medium-low	Low
X-005	15%	15%	Low	Low
L-029	10%	5%	Low	Low

Table 3.12 – Results of nucleofection optimization of HepAD38 cells using Solution L.

Program	Percent GFP positive cells		Approximate Cell Viability	
	24 hours	48 hours	24 hours	48 hours
No program & DNA	0%	0%	High	High
T-020 & No DNA	0%	0%	High	High
D-023	15%	15%	High	High
A-020	2%	2%	Medium-high	Medium-high
T-020	30%	30%	Low	Low
T-030	40%	40%	Low	Low
X-001	40%	40%	Medium	Medium-low
X-005	30%	40%	Medium	Medium-low
L-029	10%	10%	High	Medium-low

Table 3.13 – Results of nucleofection optimization of HepAD38 cells using Solution V.

Experiments were performed using Solution V and program X-001, using the plasmid pd1-EGFPn1 as a marker for transfection efficiency. Only 1 – 5% of HepAD38 cells were GFP positive (Figure 3.11 B), compared to high levels of GFP expression in the control LMH cells (Figure 3.11 A). Since pd1-EGFPn1 has been used as the marker for transfection efficiency in all other experiments, it is a more useful indication of transfection efficiency in comparison to other techniques. This suggests that the pmaxGFP provided with the nucleofection kit may give an over-estimation of the transfection efficiency.

3.3.10 ZFP-polyplex transfections of HepAD38 cells

Transfection of HepAD38 cells with ZFP-polyplexes was first optimized using SEAP-polyplexes. These polyplexes contain the plasmid pEF1a-SEAP-wPRE-attB, which expresses secreted alkaline phosphatase (SEAP) in transfected cells. The standard transfection protocol with polyplexes requires incubation with the polyplexes in serum-free media for 2 hours. To attempt to increase the transfection efficiency, SEAP-polyplexes were also incubated for 6-hours and 24-hours. As well, 0.5% DMSO was added to wells and incubated with SEAP-polyplexes for 2- and 6-hours, to enhance cell permeability. The medium was changed after the designated incubation time and the supernatant was assessed for SEAP 48 hours later. The treatment time of 6 hours (without DMSO added) resulted in the greatest production of SEAP from transfected cells (Figure 3.12). The addition of DMSO had no positive effect, and even appeared to dampen the transfection success of the 2- and 6-hour treatment regiments. There was no added benefit of incubating the cells with SEAP-polyplexes for 24 hours, as the amount of SEAP was decreased in the 24-hour incubation treatment.

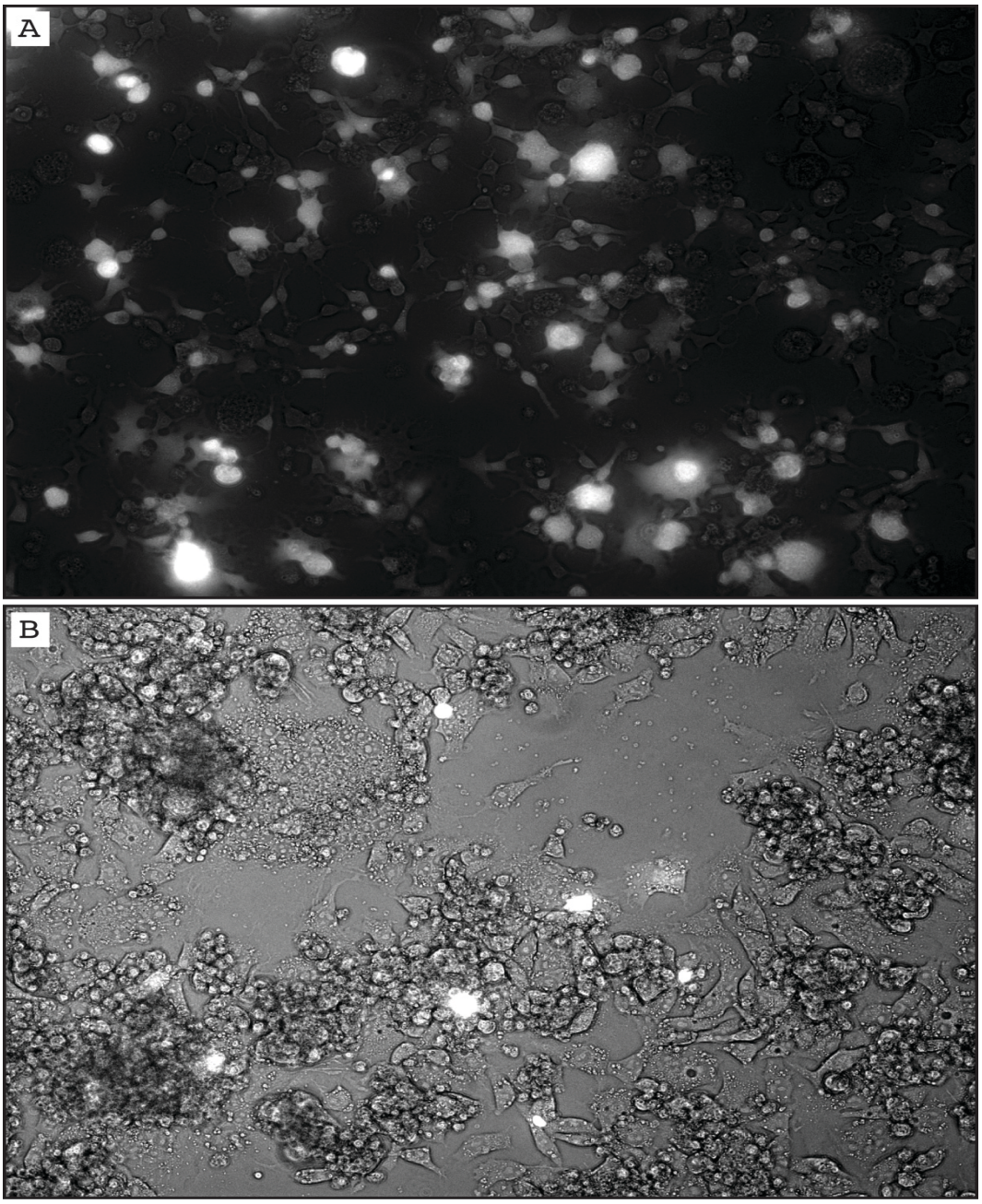

Figure 3.11 – Nucleofection-based transfection of cells using the pd1-EGFPn1 plasmid.
LMH (A) or HepAD38 (B) cells were transfected by nucleofection using the pd1-EGFPn1 plasmid. After 24 hours, the cells were examined and photographed under a fluorescence microscope and lasers for GFP. The GFP positive cells are bright white spots.

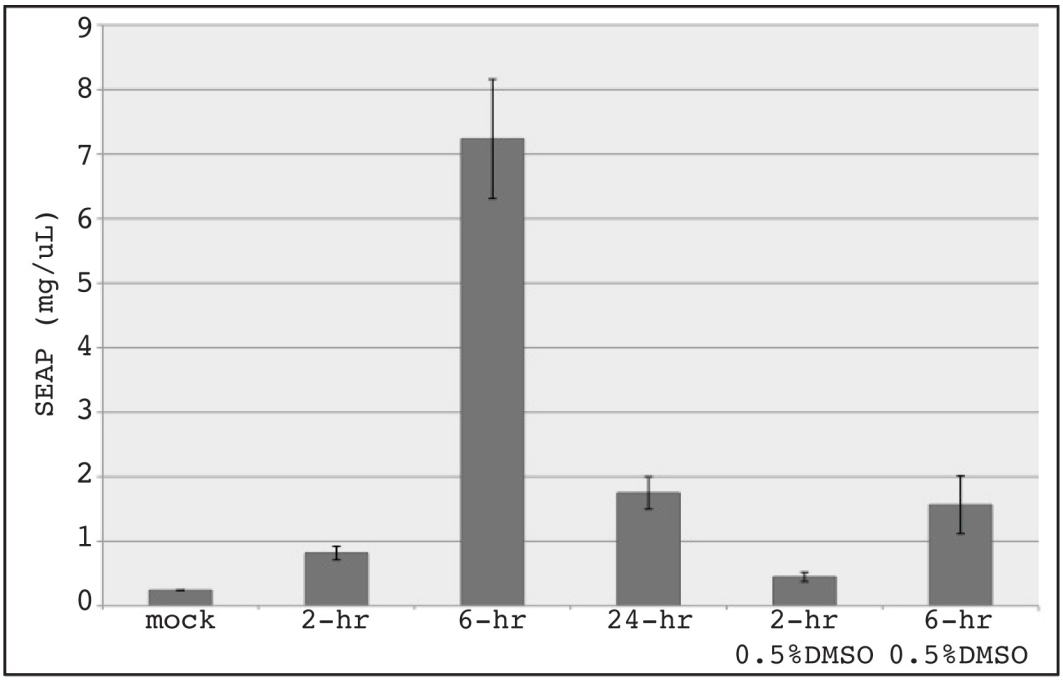

Figure 3.12 – Optimization of the polyplex-based transfection protocol for HepAD38 cells using SEAP-polyplexes.
HepAD38 cells were transfected with 2-μg/well SEAP-polyplexes by varying the time of transfection (2-hr, 6-hr, 24-hr) or adding 0.5% DMSO during the transfection. After 48 hours, the amount of SEAP in the supernatant of cultures was measured and plotted on the y-axis in mg/μL. The average of two duplicate wells is shown and the error bars represent the standard deviation. This experiment was repeated twice.

The cell density of HepAD38 cells at the time of plating was also optimized using ZFP-polyplexes. HepAD38 cells were transfected for 6 hours with ZFP18K-polyplexes in 6-well plates. After 24 hours, the cells were stained with X-Gal to assess the β–galactosidase produced from the mlacZ plasmid, which is present in the polyplexes at one fifth the amount of the pcDNA3.1(+)-ZFP plasmids (Figure 3.13). The positive control (Figure 3.13 A) is LMH cells transfected with the mlacZ plasmid using LF2000.

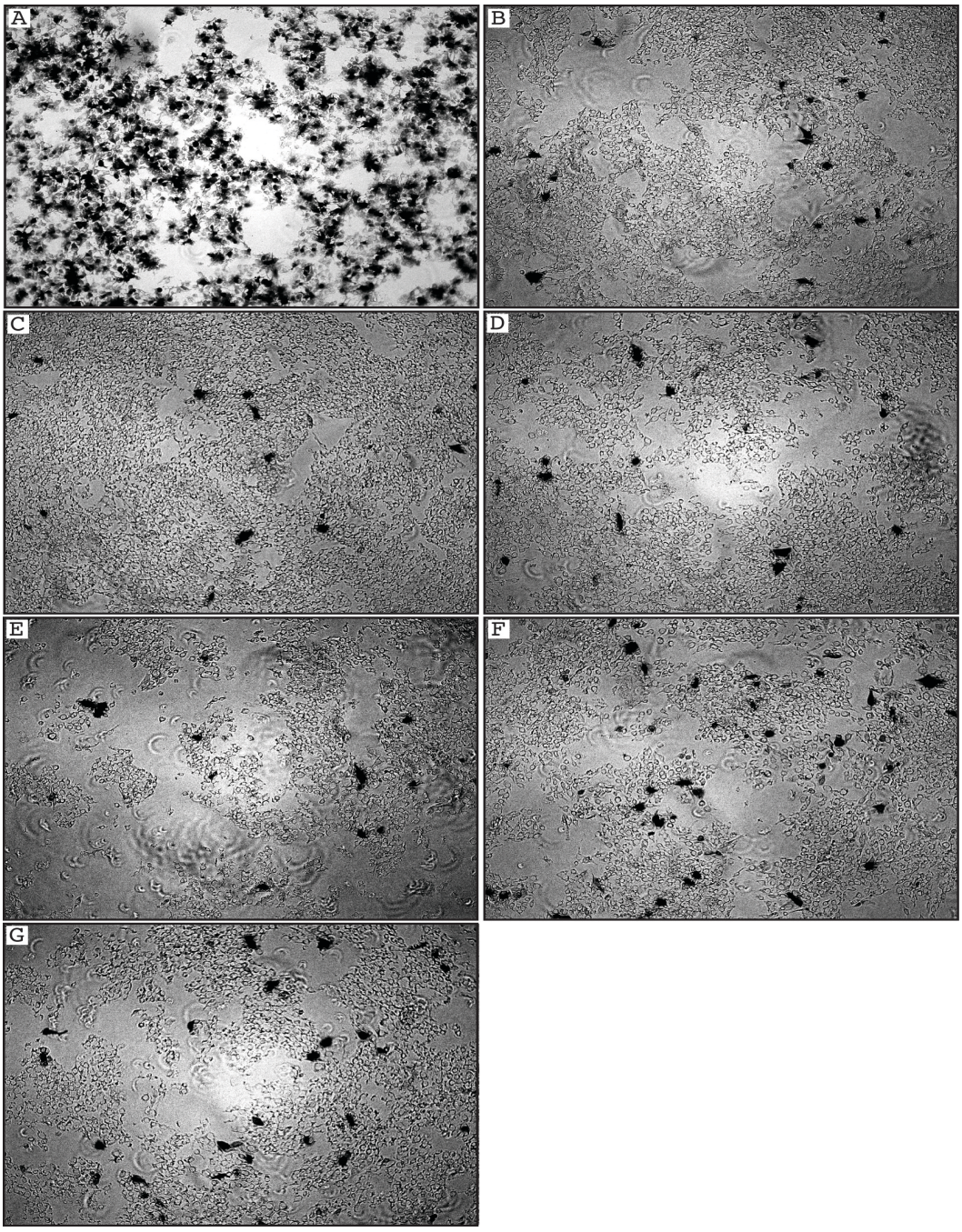

Figure 3.13 - Optimization of transfection protocol for HepAD38 cells by varying the cell density at the time of plating.
HepAD38 cells were plated at varying cell densities, then transfected for 6-hours with 2-μg/well of ZFP18K-polyplexes. After 24 hours, the cells were stained for β–gal expression (black cells) and photos taken under a light microscope. The positive control for staining (A) is LMH cells transfected with the plasmid mlacZ using LF2000™. The HepAD38 cells were plated at the following densities: (B) 1.5 x 10^5 cells/well, (C) 2.0 x 10^5 cells/well, (D) 2.5 x 10^5 cells/well, (E) 3.0 x 10^5 cells/well, (F) 3.5 x 10^5 cells/well, (G) 4.0 x 10^5 cells/well.

Cell density at plating	Percent β-Gal positive cells after 48 hours
1.5 x 10^5 cells/well	2.0%
2.0 x 10^5 cells/well	2.9%
2.5 x 10^5 cells/well	0.8%
3.0 x 10^5 cells/well	1.1%
3.5 x 10^5 cells/well	0.8%
4.0 x 10^5 cells/well	1.3%

Table 3.14 – Results of transfection optimization of HepAD38 cells using ZFP18K-polyplexes by varying cell density at the time of plating

The number of β–Gal positive cells was counted and ranged from 0.8 – 2.9%, with the higher numbers found in wells with lower cell densities (Table 3.13). Because the mlacZ plasmid is present at one-fifth the amount of the pcDNA3.1(+)-ZFP plasmids, the estimated transfection efficiency of pcDNA3.1(+)-ZFP18K is 4 – 14.5%. However, the actual transfection rate can be lower than this if more than one plasmid molecule enters one cell. Similar to previous transfection attempts, this transfection efficiency is too low for effective experiments on the therapeutic value of ZFPs. Western blots were performed on lysates from HepAD38 cells transfected with ZFP18K-, ZFP18N- or ZFP18cA-polyplexes or mock transfected (Figure 3.14). Cells were harvested and assessed for ZFP expression, HBV core expression and actin as a loading control, after 24 (Figure 3.14 A) and 48 hours (Figure 3.14 B). Very faint bands for ZFP are detected in one lane for ZFP18K-polyplexes (Figure 3.14 A) and one lane for ZFP18N-polyplexes (Figure 3.14 B). There is no effect on the HBV core levels in these cells.

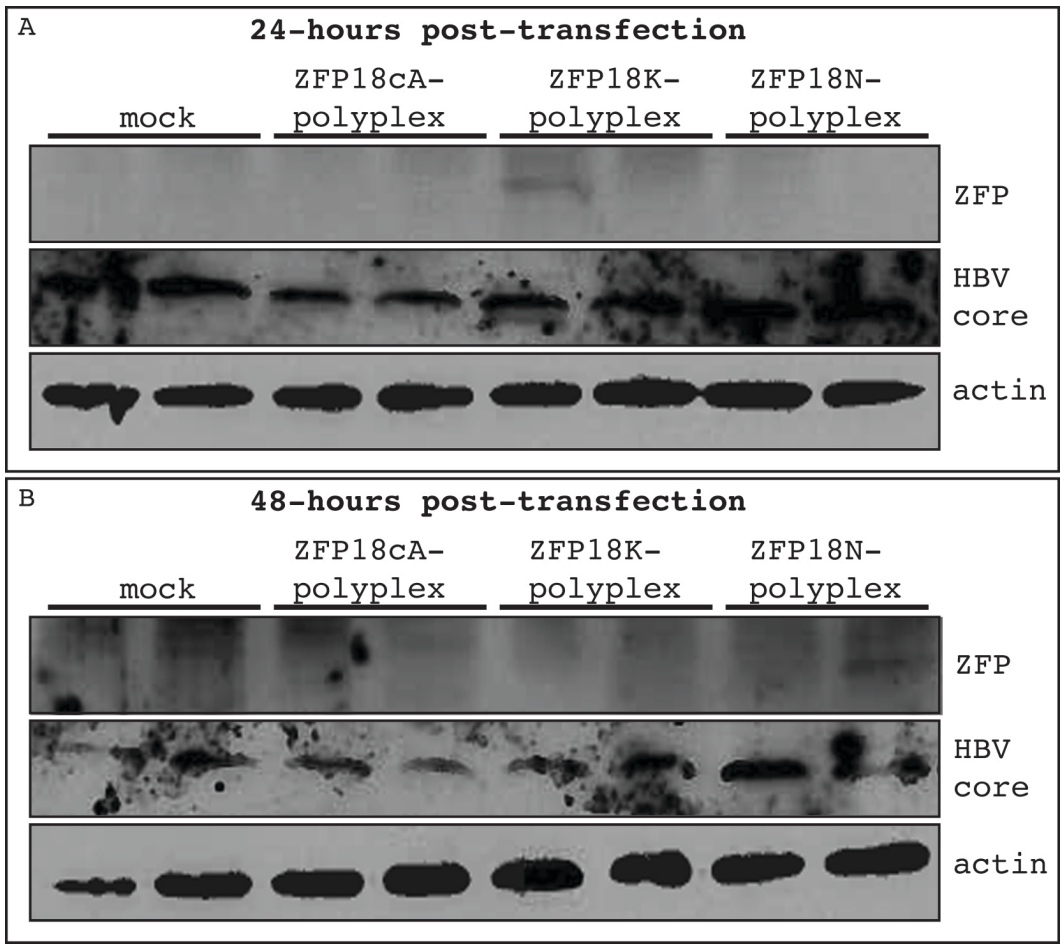

Figure 3.14 - Western blot assessment of protein expression in HepAD38 cells transfected with ZFP-polyplexes.
HepAD38 cells were transfected with 2-μg/well of ZFP18K-, ZFP18N- or ZFP18cA-polyplexes, or were mock transfected. After 24 (A) or 48 hours (B), cells were harvested and assessed by Western blot using anti-ZFP antiserum, anti-HBV core and anti-actin antibodies. Each treatment was performed in duplicate. The asterisk (*) marks the presumptive ZFP band.

3.3.11 Profect-P2 and Targefect-Hepatocyte transfections of HepAD38 cells

Profect-P2 is a non-lipid reagent for the intracellular delivery of intact proteins. It forms non-covalent complexes with proteins and transports them across both the cell and nuclear membranes. Profect-P2 was used to attempt to deliver intact ZFP18K-MBP into HepAD38 cells. The conditions were optimized by varying the amount of ZFP18K-MBP fusion protein from 1 – 10-μg and the volume of Profect-P2 from 1 – 10-μL. Cells were harvested with RIPA and assessed by Western blot for the presence of intracellular ZFP18K-MBP fusion protein after

48 hours (Figure 3.15). The presence of ZFP18K in transfected HepAD38 cells was not detected, regardless of the amount of ZFP18K or volume of Profect-P2 used. Actin was used as a loading control.

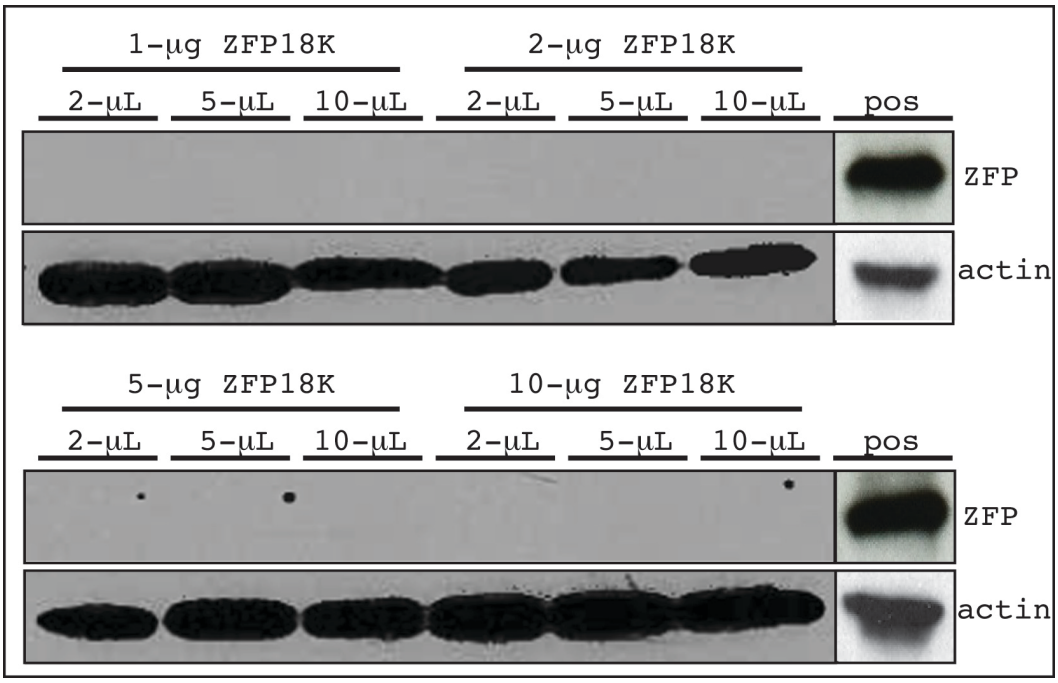

Figure 3.15 - Western blot analysis of HepAD38 cells transfected with ZFP18K-MBP fusion protein using Profect-P2.
HepAD38 cells were transfected with varying amounts (1 – 10-µg) of ZFP18K-MBP in coordination with varying volumes of the Profect-P2 reagent (2, 5, 10-µL). After 48 hours, cells were harvested and assessed by Western blot using anti-ZFP antiserum and anti-actin antibodies. A positive control is added from a parallel blot, where LMH cells were transfected with the pcDNA3.1(+)-ZFP18K plasmid and assessed by Western blot after 24 hours.

Targefect-Hepatocyte is a lipid-based transfection reagent that transfects "difficult-to-transfect" cell lines, including primary hepatocytes. Targefect-Hepatocyte was tested for its ability to transfect HepAD38 cells using the pd1-EGFPn1 plasmid. Different DNA to Targefect-Hepatocyte ratios were tested. HepAD38 cells transfected very poorly with Targefect-Hepatocyte. There were no more than 1% of cells GFP positive after 24 or 48 hours (Table 3.15).

DNA:Targefect ratio (µg:µL)	Total amount of DNA (per well) [a]	Percent GFP positive cells	
		24 hours	48 hours
4:5	2 µg	1%	<1%
2:5	2 µg	1%	<1%
4:15	2 µg	1%	1%
2:5	1 µg	1%	<1%
1:2	3 µg	1%	1%

Table 3.15 - Results of Targefect-Hepatocyte transfection optimization of HepAD38 cells.
[a] for cells in a 6-well plate.

3.3.12 Assessment of the metabolic activity of Huh7 cells expressing HBV-specific ZFPs

The effect of the HBV-specific ZFPs on the metabolic activity of cells was assessed using the MTT assay in Huh7 cells. Huh7 cells were transfected with pcDNA3.1(+), pcDNA3.1(+)-ZFP18K, ZFP18N, ZFP18cA, or not-transfected. There was no difference in the metabolic activity between non-transfected cells, cells transfected with the empty vector, or cells transfected with a ZFP plasmid (Figure 3.16). This confirms that, similar to the DHBV-specific ZFPs, there appears to be little effect on the metabolic activity due to expression of the HBV-specific ZFPs.

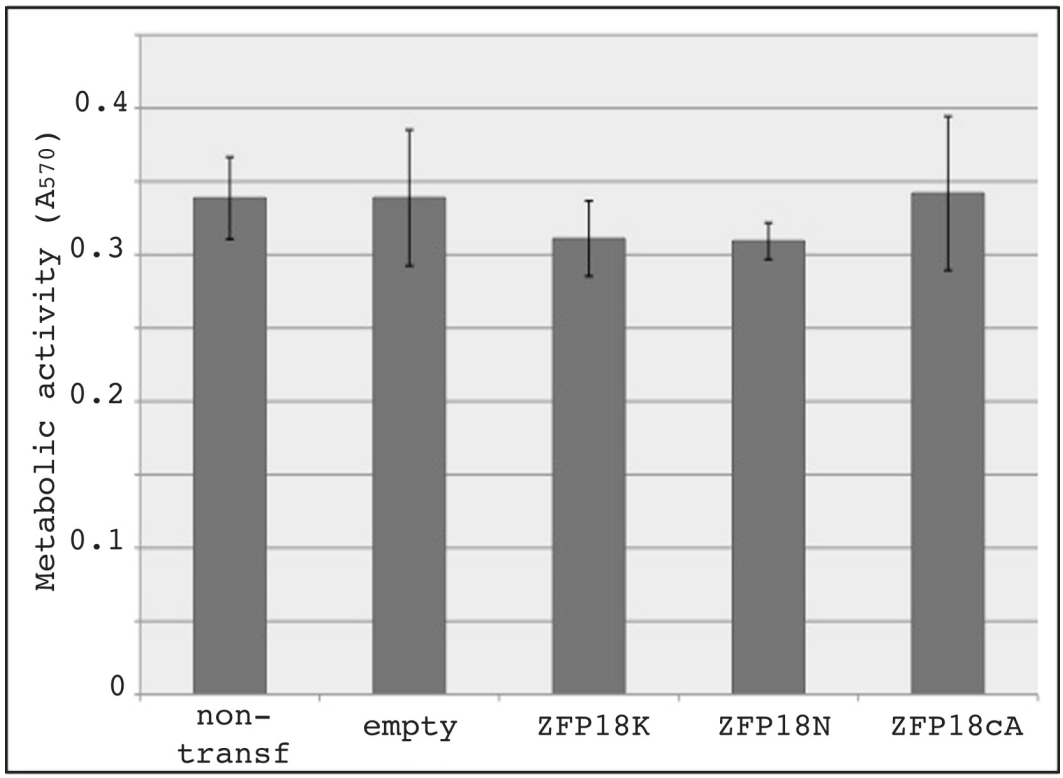

Figure 3.16 - MTT assay to test metabolic activity of Huh7 cells expressing HBV-specific ZFPs.
The cell viability of Huh7 cells not transfected (non-transf), or transfected with pcDNA3.1(+) (empty) or pcDNA3.1(+)-ZFP18K, ZFP18N or ZFP18cA, was tested using the MTT assay. Absorbance (570-nm) is measured in each sample and is plotted on the y-axis. The results are presented as the mean of 16 wells with error bars to indicate the standard deviation. This experiment was performed three times. There was no statistically significant difference between any group. Data is courtesy of Kristen Miller.

3.3.13 Visualization of HBV-specific ZFPs expressed in LMH cells using confocal microscopy

Plasmids expressing ZFPs fused to EGFP were created in the pcDNA3.1(+) background by PCR amplifying EGFP from the pAdTrack-CMV1 plasmid. The PCR amplified product was ligated to pCR4-TOPO, and then transferred into pcDNA3.1(+)-ZFP18K, ZFP18N, ZFP9X1, ZFP9X2, ZFP9Y1, ZFPY2 and ZFP9Z2 by restriction digest and directional ligation. EGFP was not fused with ZFP18M or ZFP9Z1 because these ZFPs could not be cloned into the pcDNA3.1(+) backbone. No positive clones were successfully isolated for pcDNA3.1(+)-ZFP18N, ZFP9X2, ZFP9Y1, ZFP9Y2 and ZFP9Z2, therefore

confocal microscopy was not completed for these ZFPs. LMH cells were used for these experiments because they can be transfected easily.

LMH cells were plated in plastic dishes with glass coverslips in the center. After 24 hours, they were transfected with either pcDNA3.1(+)-ZFP18K-EGFP or pcDNA3.1(+)-ZFP9X1-EGFP. A further 24 hours after transfection, the nuclei were stained with Hoechst 33342. Using a multi-photon microscope, images of LMH cells expressing ZFP-EGFP (green) were collected, with the nuclei stained in blue. The positive control (Figure 3.17 A) and negative controls (Figure 3.17 B) can be compared to the EGFP expression of ZFP18K-EGFP (Figure 3.17 C) and ZFP9X1-EGFP (Figure 3.17 D). Both ZFP18K-EGFP and ZFP9X1-EGFP express EGFP at levels above the background level in the negative control, but at lower levels than the positive control.

3.3.14 Cloning of chimeric ZFP-FokI endonucleases

The *FokI* endonuclease was fused in frame to ZFP18M, ZFP18N and all the ZFP 9-mers, in order to create ZFNs. The hypothesis was that site-specific cleavage of the cccDNA in the nucleus of cells would potentiate instability and the subsequent destruction of the viral reservoir. *FokI* was PCR amplified from the plasmid pML109RM19-1, which contains a 6.0-kb genomic fragment from the bacterium *Flavobacterium okeanokoites*. The primers added *SpeI* sites at both ends of the *FokI* PCR product, which was then cloned into the plasmid pCR4. Positive clones were sequenced with the T7 primer. One point mutation, A586G, was detected at the 5' end of the PCR product, however this is a conservative mutation and the leucine residue was unchanged.

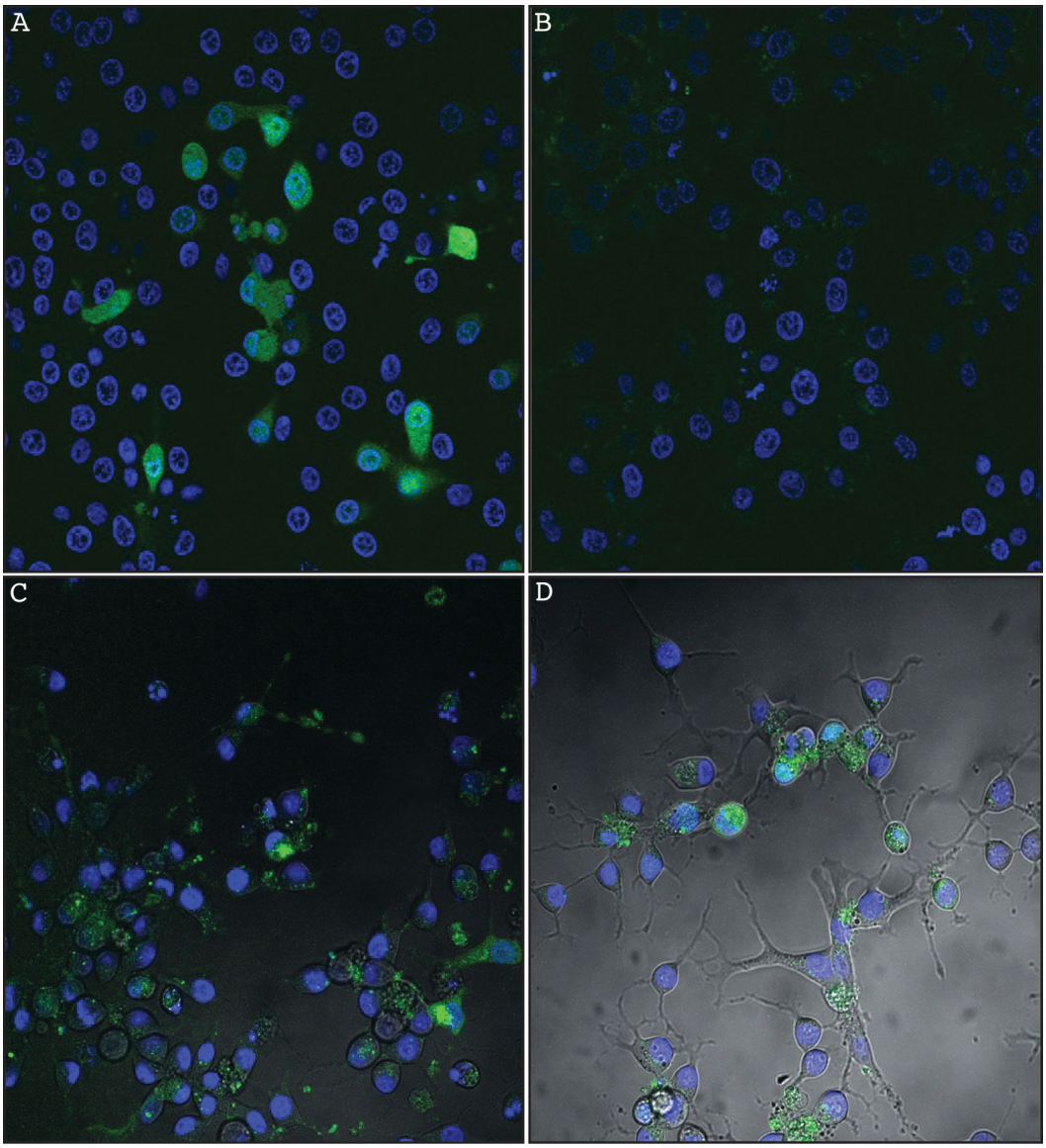

Figure 3.17 - Live cell imaging of HBV-specific ZFP-EGFP expression in transfected LMH cells.
LMH cells were plated in dishes with glass coverslips, then transfected with (A) pcDNA3.1(+)-EGFP (positive), (B) pcDNA3.1(+) (negative), (C) pcDNA3.1(+)-ZFP18K-EGFP or (D) pcDNA3.1(+)-ZFP9X1-EGFP. After 24 hours, the nuclei were stained with Hoechst 33342 and visualized using a multi-photon microscope. EGFP is shown in green and nuclei are shown in blue.

FokI was then cloned into pMAL-ZFP9A1, ZFP9A2, ZFP9B1, ZFP9B2, ZFP9X1, ZFP9X2, ZFP9Y1, ZFP9Y2, ZFP9Z1, ZFP18M and ZFP18N. Clones were screened for the presence of *FokI* by restriction digest. Potentially positive clones were sequenced using an *FokI*-specific primer (Fok.263.fw). A vast

majority of clones had *FokI* inserted in the reverse orientation. Only 20% of clones were in the forward direction. This suggested there was selection against *FokI* fused to ZFPs in the forward direction. Likely, some leaky expression of the ZFP-FokI fusion protein was occurring in the bacteria, proving toxic and selecting against those clones with *FokI* in the forward direction. Of those few clones in the forward direction, there were major problems with their sequences. Three clones had deletions of 6-bps in the middle of the sequence. One clone encoded for a modified ZFP that did not align with the original ZFP inserted into the plasmid. BLAST searches of the ZFP sequence matched it with ZFPs from other organisms. This indicated that the basic sequence was recognizable as a ZFP, but the changes were so great it no longer aligned with the original ZFP sequence. These results further highlight the problems associated with cloning the *FokI* endonuclease in frame with the designed ZFPs.

Recently, a number of *FokI* variants with modified dimerization interfaces were received from Dr. David Segal (University of California, Davis) (11). These modifications prevent homo-dimerization during off-target binding, which lowers the potential toxicity problems that occur during zinc finger nuclease design. The process of cloning these variants in frame with the designed ZFPs targeting HBV or DHBV is currently being performed by Kristen Miller as part of her graduate work.

3.3.15 Cloning of chimeric ZFP-Ho endonucleases

In contrast to the *FokI* endonuclease, which requires dimerization for DNA cleavage, the Ho endonuclease from *Saccharomyces cerevisiae* mediates dsDNA breaks as a monomer. It includes a carboxy-terminal zinc finger domain for target sequence recognition, which functions independently of the amino-terminal endonuclease domain (9). Nahon and Raveh (1998) swapped in a foreign zinc finger domain within Ho to target novel DNA sequences (12). Therefore, I attempted to replace the endogenous zinc finger domain of Ho with the designed ZFP 18-mers. This would create a chimeric endonuclease targeted to DHBV- or

HBV-specific sequences (Figure 3.18). The hypothesis was that site-specific cleavage of the cccDNA in the nucleus of cells potentiates instability and subsequent destruction of the viral reservoir.

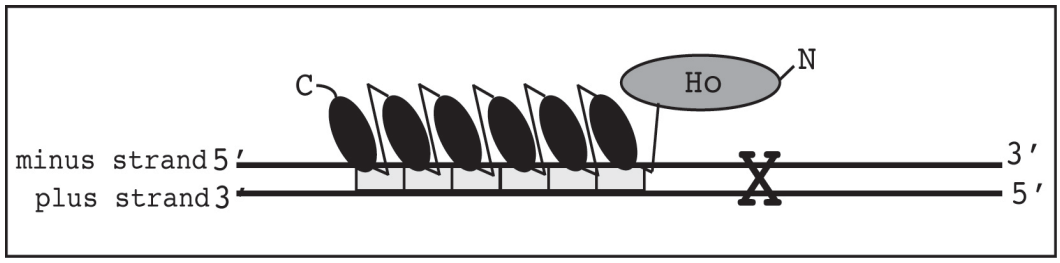

Figure 3.18 - Schematic representation of chimeric endonucleases formed by ZFP 18-mers fused to the Ho endonuclease domain.
Each zinc finger motif of the 18-mer is shown as an oval, with six modules linked in tandem. The grey boxes represent the binding site for the 18-mer. The Ho domain is located at the amino-terminus of the 18-mer. The "X" represents the approximate DNA cleavage site.

The Ho endonuclease was PCR amplified from a plasmid received from Dr. David Stuart (University of Alberta) called YCpGAL::HO, which contained a 2.5-kb fragment encoding the Ho ORF and 171-bp of 3' untranslated region. The PCR product was cloned into pCR4, then transferred into pMAL-ZFP18A, ZFP18B, ZFP18cA, ZFP18K or ZFP18N plasmid backbones. Positive clones were isolated by restriction digest screening and sequencing. However, several mutations were consistently found in all clones. The major mutation was a large deletion of approximately 300-bps, which occurred in a large subset of clones. A number of other point mutations or small deletions were found in different clones isolated over several different attempts at cloning Ho into the pMAL-ZFP18 plasmids. None of these small mutations were consistently found within the clones. It seemed there was selective pressure against the production of unaltered Ho clones.

3.4 Discussion

The concept of using ZFPs as therapeutics targeting HBV cccDNA was demonstrated using the *in vitro* DHBV model virus system. The work was

continued into the HBV system, although a number of barriers were reached using HBV in tissue culture. These barriers are a common problem, and the reason new models of HBV in cell culture are useful.

Ten HBV-specific ZFPs were designed: four 18-mers and six 9-mers. Similar to that seen with the DHBV-specific ZFPs, the 18-mers bound to their target sequences with greater affinity than the 9-mers. One 18-mer (ZFP18P) demonstrated off-target binding and was excluded from further analysis, but the remaining ZFPs were used for further analyses.

There were greater problems cloning the HBV-specific ZFPs than the DHBV-specific ZFPs. The reasons are not apparent, but given the characteristics of the readout during cloning (for example, only attaining clones in the reverse direction), the toxicity of these HBV-specific ZFPs appeared higher than the DHBV-specific ZFPs. For example, ZFP9Z2 could not be cloned in the forward direction of the pMALc vector, and ZFP18M could not be cloned into the pcDNA3.1(+) vector. In addition, the success of cloning the HBV-specific ZFPs in frame with EGFP was much lower than for the DHBV-specific ZFPs. Overall, this led to discontinuities in the analyses of some of the ZFPs described in this chapter.

All of the ZFP 18-mers exhibited dissociation constants in the nanomolar range, which is sufficient for therapeutic development purposes. However, the ZFP 9-mers had very poor binding profiles and only ZFP9Z1 had detectable binding by EMSA. This binding was weak and in the micro-molar range.

The tolerance of ZFP18K to bind target sites with one or two nucleotide changes ("near-target" sites) from the wild-type target site was tested. ZFP18K had high tolerance for binding near-target sites – this could be a major problem during therapeutic expression of ZFPs in patients. Chromatin structure will protect most near-target sites in the host genome from being bound by ZFPs, however it is a

major issue to resolve in order to develop this technology into a viable therapeutic reagent. The off-target binding would have to be eliminated to reduce the danger to patients. This would probably require a method that optimizes the α–helices of the ZFP in relation to the target DNA sequence, such as phage-display or bacterial two-hybrid systems (13, 14). These methods would optimize the ZFP to better discriminate between target and non-target sequences. For example, Choo *et al* (1994) used phage-display to develop a ZFP that discriminated between two sequences with only one nucleotide difference over a 12-bp target sequence (14). Although the Zinc Finger Tools is a convenient and fast method to use for development of sequence-specific ZFPs, it does not optimize ZFPs to be as discriminate as those developed by Choo *et al* (1994). This is because there are some interactions between the α-helix of one zinc finger module and the adjacent triplet DNA recognition sequence (15). For example, in the model ZFP Zif268, a well-studied mouse protein, the α-helix from Finger 2 (Figure 1.10) makes two direct contacts with its DNA target site (site 2), but also makes a hydrogen bond with the opposite strand within the target site of Finger 1 (site 1). This interplay between DNA target subsites is important for exclusivity of site recognition, and is not taken into account when designing ZFPs with the Zinc Finger Tools program. Using a library of α-helix sequences compared to DNA triplet sequences (see Appendix B, Tables 7.1 & 7.2 for complete list) the Zinc Finger Tools program independently assesses each DNA target site and matches it to the amino acid sequence required within the α-helix to bind that site. Then, all of the individually assessed zinc finger modules are strung together linearly. It does not take into account the cross-interaction between the zinc finger motifs and adjacent DNA target sites, nor any possible interfinger interactions. Thus, the recognition of the ZFP for its target site is not as specific as that which would be created using a screening method, such as phage display or a two-hybrid system. This is seen with the results from ZFP18K and its ability to bind near-target sites with approximately equal affinity compared to wild-type site binding.

Testing the ZFPs in tissue culture cells turned out to be a very difficult task. The HBV-harbouring cell lines utilized were difficult to transfect. Despite testing a wide-range of transfection methods and reagents, I was unable to transfect HepAD38 cells to an extent that would allow testing of ZFPs as therapeutics. However, it appears that the baculoviruses described in Chapter 4 are a viable option for transduction of HepG2.2.15 cells, based upon the recent work by Kristen Miller. This avenue will allow further tissue culture assessment of the HBV-specific ZFPs. Further, the baculoviruses can be utilized in the *scid*-Alb/uPA chimeric mouse model infected with HBV.

Fusion of the designed ZFPs to endonuclease domains was a major goal of this project, but a number of difficulties during the cloning process prevented the successful completion of this goal. The apparent toxicity of the endonuclease domain in *E.coli* prevented the successful ligation of wild-type *FokI* or Ho to either HBV-specific or DHBV-specific ZFPs. Despite a number of methods and cloning strategies attempted, no clones were ever isolated that were of wild-type sequence. Recently, a new paper was published that utilized ZFNs based on *FokI* to cleave the cccDNA of HBV (16). This paper used two ZFP 9-mers fused to the *FokI* domain to mediate specific cleavage of the HBV genome *in vitro* and in tissue culture. They were able to demonstrate a 29% decrease in the pgRNA levels, normalized to GAPDH, in the presence of the expressed ZFNs (16). This proof of concept paper demonstrated that designed ZFNs can be used to cleave the episomal form of the viral genome, resulting in impairments in viral fitness. However, a higher efficiency is still an important goal for successful treatment.

In summary, the kinetic experiments demonstrated robust binding capabilities for some of the designed ZFPs, but further examination of their antiviral activity in tissue culture was impaired by the lack of an efficient tissue culture model system for HBV, aside from using the DHBV model virus system. A large number of transfection methods were attempted, but none resulted in transfection levels sufficient to detect antiviral effects by the HBV-specific ZFPs.

3.5 References

1. Bock CT, Schranz P, Schroder CH, & Zentgraf H (1994) Hepatitis B virus genome is organized into nucleosomes in the nucleus of the infected cell. *Virus Genes* 8(3):215-229.
2. Bock CT, Schwinn S, Locarnini S, Fyfe J, Manns MP, Trautwein C, & Zentgraf H (2001) Structural organization of the hepatitis B virus minichromosome. *J Mol Biol* 307(1):183-196.
3. Newbold JE, Xin H, Tencza M, Sherman G, Dean J, Bowden S, & Locarnini S (1995) The covalently closed duplex form of the hepadnavirus genome exists in situ as a heterogeneous population of viral minichromosomes. *J Virol* 69(6):3350-3357.
4. Mandell JG & Barbas CF, 3rd (2006) Zinc Finger Tools: custom DNA-binding domains for transcription factors and nucleases. *Nucleic Acids Res* 34(Web Server issue):W516-523.
5. Elrod-Erickson M, Rould MA, Nekludova L, & Pabo CO (1996) Zif268 protein-DNA complex refined at 1.6 A: a model system for understanding zinc finger-DNA interactions. *Structure* 4(10):1171-1180.
6. Beerli RR, Segal DJ, Dreier B, & Barbas CF, 3rd (1998) Toward controlling gene expression at will: specific regulation of the erbB-2/HER-2 promoter by using polydactyl zinc finger proteins constructed from modular building blocks. *Proc Natl Acad Sci U S A* 95(25):14628-14633.
7. Ladner SK, Otto MJ, Barker CS, Zaifert K, Wang GH, Guo JT, Seeger C, & King RW (1997) Inducible expression of human hepatitis B virus (HBV) in stably transfected hepatoblastoma cells: a novel system for screening potential inhibitors of HBV replication. *Antimicrob Agents Chemother* 41(8):1715-1720.
8. Zhou T, Guo H, Guo JT, Cuconati A, Mehta A, & Block TM (2006) Hepatitis B virus e antigen production is dependent upon covalently closed circular (ccc) DNA in HepAD38 cell cultures and may serve as a cccDNA surrogate in antiviral screening assays. *Antiviral Res* 72(2):116-124.
9. Bakhrat A, Jurica MS, Stoddard BL, & Raveh D (2004) Homology modeling and mutational analysis of Ho endonuclease of yeast. *Genetics* 166(2):721-728.
10. Bibikova M, Carroll D, Segal DJ, Trautman JK, Smith J, Kim YG, & Chandrasegaran S (2001) Stimulation of homologous recombination through targeted cleavage by chimeric nucleases. *Mol Cell Biol* 21(1):289-297.
11. Szczepek M, Brondani V, Buchel J, Serrano L, Segal DJ, & Cathomen T (2007) Structure-based redesign of the dimerization interface reduces the toxicity of zinc-finger nucleases. *Nat Biotechnol* 25(7):786-793.
12. Nahon E & Raveh D (1998) Targeting a truncated Ho-endonuclease of yeast to novel DNA sites with foreign zinc fingers. *Nucleic Acids Res* 26(5):1233-1239.
13. Joung JK, Ramm EI, & Pabo CO (2000) A bacterial two-hybrid selection system for studying protein-DNA and protein-protein interactions. *Proc Natl Acad Sci U S A* 97(13):7382-7387.

14. Choo Y, Sanchez-Garcia I, & Klug A (1994) In vivo repression by a site-specific DNA-binding protein designed against an oncogenic sequence. *Nature* 372(6507):642-645.
15. Segal DJ, Beerli RR, Blancafort P, Dreier B, Effertz K, Huber A, Koksch B, Lund CV, Magnenat L, Valente D, & Barbas CF, 3rd (2003) Evaluation of a modular strategy for the construction of novel polydactyl zinc finger DNA-binding proteins. *Biochemistry* 42(7):2137-2148.
16. Cradick TJ, Keck K, Bradshaw S, Jamieson AC, & McCaffrey AP (2010) Zinc-finger Nucleases as a Novel Therapeutic Strategy for Targeting Hepatitis B Virus DNAs. *Mol Ther* 18(5):947-954.

4 Chapter 4: *Ex vivo* and *in vivo* efficacy of DHBV-specific ZFPs

4.1 Introduction

After demonstration of the antiviral effects of the DHBV-specific ZFP in the tissue culture cell line, further experiments were performed on the Pekin duck model of DHBV infection. The original goal was to clone the DHBV-specific ZFPs into adenovirus vectors for delivery to the liver *in vivo* or *ex vivo* using primary duck hepatocytes (PDH) in culture. However, producing infectious adenoviruses that carried the ZFP genes was unsuccessful. Subsequently, baculoviruses were constructed that expressed the DHBV-specific ZFPs and were used to transduce PDH in tissue culture. Using this approach, DHBV either excluded superinfection of the ZFP-expressing baculoviruses or prevented expression of the ZFPs in the transduced PDHs, limiting the ability to test the ZFPs as a therapeutic option *ex vivo*. Lastly, chitosan-based polyplexes were used to deliver plasmid DNA encoding the DHBV-specific ZFPs to the liver of DHBV-infected ducklings. This method also proved incapable of demonstrating any specific antiviral effect of the ZFPs *in vivo*. A non-specific innate immune response after treatment resulted in a global decrease in viral titres, preventing evaluation of any specific antiviral effect. However, no evidence was found that the ZFPs were expressed subsequent to delivery with the chitosan-based polyplexes, suggesting this delivery method is not optimal for use in the duck model.

4.2 Materials and Methods

4.2.1 Cell lines and culture conditions

Sf9 (*Spodoptera frugiperda*) cells were maintained in SF-900 II SFM media (Invitrogen 10902-088) supplemented with 25-µg/mL gentamycin and incubated at room temperature (25°C) without CO_2. 293A cells were maintained in DMEM (Invitrogen 31600-034) supplemented with 10% (v/v) FCS and 50-IU/mL penicillin and 10-µg/mL streptomycin, and incubated at 37°C with CO_2. LMH cells were maintained as described in Section 2.2.11.

4.2.2 Cloning of duck GAPDH into pCR4

Duck GAPDH was PCR amplified using cDNA made from total RNA from duck liver. The primers Du-GAP.Fw (5'-GGCACTGTCA AGGCTGAGAA TG-3') and Du-GAP.Rv (5'-TGCAAGAGGC ATTGCTGAC-3') were used. The PCR reaction contained 1-µL of template cDNA, 1-µL of 10-mM dNTPs, 12.5 units recombinant *Taq* DNA Polymerase, 1.5-mM MgCl2, 5-µL of 10X PCR Buffer, 0.5-µM of each primer and dH_2O up to 50-µL. The reaction was annealed at 54°C, with an elongation time of 45 seconds and 35 cycles. The PCR product was ligated to pCR4 using the TOPO TA cloning kit by combining 4-µL of PCR product with 1-µL of vector and 1-µL of salt solution. The reaction proceeded for 1 hour at room temperature then 1-µL of the reaction was transformed into TOP10 as described in Section 2.2.3. Positive (white) colonies were used to inoculate 2-mL of LB/Amp mini-preps. Positive clones were identified by *EcoRI* digest of mini-prep DNA isolated by the QIAprep Spin Miniprep Kit (Qiagen 27106) and sequencing with the T7 primer.

4.2.3 Cloning and production of ZFP-expressing adenoviruses

4.2.3.1 Cloning of ZFPs into the AdEasy shuttle vector, pAdTrack-CMV1

Initial cloning attempts using double restriction digests and directional insertion of ZFPs into the AdEasy shuttle vector pAdTrack-CMV1 (see map in Appendix A) were unsuccessful. Therefore, the *EcoRV* restriction site was added flanking each ZFP using the primers in Table 4.1, to replicate the successful cloning process used by Kathie Walters (1).

The PCR reaction was carried out as follows: 1-µL of template plasmid (pCR4-ZFP18A, ZFP18B, ZFP18cA, ZFP18K, ZFP18N), 1-µL of 10-mM dNTPs, 12.5 units recombinant *Taq* DNA Polymerase, 1.5-mM $MgCl_2$, 5-µL of 10X PCR Buffer, 0.5-µM of each primer and dH_2O up to 50-µL. The reaction was annealed at 54°C, with an elongation time of 1 minute and 30 cycles. PCR products were separated on a 0.8% (w/v) agarose gel and cut out using a scalpel. DNA was recovered using the QIAquick Gel Extraction Kit as described in Section 2.2.3.

PCR products were ligated to pCR4 using the TOPO TA cloning kit, transformation of TOP10 *E.coli* and miniprep production of positive clones was performed as described in Section 4.2.2. Clones were screened for positivity by *EcoRI* restriction digest, liberating the PCR insert. Positive clones were sequenced with the T7 primer to confirm the integrity of the ZFP sequence after PCR. Clones with no sequence changes were digested with 10 units of *EcoRV* (Invitrogen 15425-010) in NEB Buffer 3 with 1X BSA for 1.5 hours at 37°C. The backbone, pAdTrack-CMV1 (kanamycin resistant (Kan^R)), was similarly digested. All digests were separated on 0.8% (w/v) agarose gels and the resulting backbone and inserts (546 - 588-bp: 18-mers and 288 - 306-bp: 9-mers) were excised using a scalpel. DNA was recovered using the QIAquick Gel Extraction Kit as described. The pAdTrack-CMV backbone was further treated with SAP (Roche 1758 250) to dephosphorylate the blunt ends. The entire, *EcoRV*-digested backbone was treated with 2-µL (2 units) of SAP and 4-µL of 10X SAP Buffer in 40-µL total volume, brought up with dH_2O. After incubation at 37°C for 10 minutes, the enzyme was heat inactivated at 70°C for 10 minutes. Subsequently, the DNA was purified from protein and buffer using the PCR Purification protocol from the QIAquick Gel Extraction Kit, as described in Section 3.2.16. The sample was eluted in 30-µL dH_2O. The ZFPs were ligated to pAdTrack-CMV1 in a 10-µL reaction containing 6-µL of insert DNA, 2-µL of 5X T4 DNA Ligase Buffer, 1-µL of the pAdTrack-CMV1 backbone (diluted 1:10) and 1-µL (1 unit) of T4 DNA Ligase (Invitrogen 15224-017). Control reactions substituted 6-µL of water for insert. The ligations were incubated overnight at room temperature. The following day, 1-µL of the ligation reaction was transformed into chemically competent TOP10 *E.coli*, and plated on LB/Kan (Kan at 25-µg/mL). Isolated colonies were used to inoculate 2-mL LB/Kan mini-preps, which were incubated overnight at 37°C with agitation. DNA was isolated using the QIAprep Spin Miniprep Kit, and positive clones were determined by restriction digest with *EcoRV*. Positive clones were sequenced with the pAdTrack-MCS.fw primer (5'-GAACTCCATA TATGGGCTAT G-3').

Name	Primer sequence [a]
ZFPa.RV.fw	**GATATC**ATGC ACCATCACCA TCACCAT*CCC*
	*AAGAAAAAGC GTAAGGTC*CT CGAACCCGGC
	GAAAAGCCTT AT [b]
ZFPa.RV.rv	**GATATC**ACTT GTCTTCTTAC CTGTGTGG [c]
ZFPb.RV.fw	**GATATC**ATGC ACCATCACCA TCACCAT*CCC*
	*AAGAAAAAGC GTAAGGTC*CT CGAACCAGGT
	GAAAAACCCT
ZFPb.RV.rv	**GATATC**TGAA GTCTTCTTTC CTGTGTGA
ZFPcA.fw	**GATATC**ATGC ACCATCACCA TCACCAT*CCC*
	*AAGAAAAAGC GTAAGGTC*CT GGAACCCGGC GAGAAAC
ZFPcA.rv	**GAATTC**GGAG GTCTTTTTTC CGGTGTG
ZFPk.RV.fw	**GATATC**ATGC ACCATCACCA TCACCAT*CCC*
	*AAGAAAAAGC GTAAGGTC*GG TGATATCCTG GAGCCCGGC
ZFPk.RV.rv	**GATATC**ACCG ATATCAGACG TCTTCTTAC
ZFPn.RV.fw	**GATATC**ATGC ACCATCACCA TCACCAT*CCC*
	*AAGAAAAAGC GTAAGGTC*GG TGATATCCTC
	GAACCCGGTGA
ZFPn.RV.rv	**GATATC**ACTA GTACCGATAT CGGACGTCTT CTTT

Table 4.1 - Sequences of primers used for pAdTrack-CMV1 cloning and screening of bacmid recombinants.
[a] Sequences are shown 5' to 3'.
[b] *EcoRV* restriction site (**bold**), 6x histidine tag (underlined), SV40 nuclear localization signal (*italics*), unique ZFP sequence (plain text).
[c] *EcoRV* restriction site (**bold**), unique ZFP sequence (plain text).

4.2.3.2 Recombination of the shuttle vector with the AdEasy vector, pAdEasy-1

pAdTrack-ZFP18A, ZFP18B, ZFP18cA, ZFP18K and ZFP18N were linearized by digestion with 10 units of *PmeI* (NEB R0560L) in NEB Buffer 4 with 1X BSA for 1.5 hours at 37°C. The digests were phenol:chlorofom extracted by adding 100-µL each of phenol and chloroform, mixing vigorously for 15 seconds, and centrifuging for 5 minutes at 14,000-rpm. The top aqueous layer was transferred

to a new microfuge tube and the DNA was precipitated with 0.1X volume 3.0-M sodium acetate and 2X volume 95% (v/v) ethanol. The sample was centrifuged for 10 minutes at 14,000-rpm and the pellet washed once with 70% (v/v) ethanol, followed by centrifugation again for 10 minutes at 14,000-rpm. The pellet was air-dried and resuspended in 5-μL of dH_2O. 50-μL of electrocompetent BJ5183-AD-1 (Stratagene 200157), which stably contain the pAdEasy-1 plasmid (Amp^R), were electroporated with 1-μL of the *PmeI*-digested pAdTrack-ZFP DNA in 0.2-cm electroporation cuvettes (Bio-Rad 165-2082) using a Bio-Rad Gene Pulser electroporator at settings of 2.5-kV, 200-Ω and 25-μF. After pulsing, 1-mL of LB was added to the cells and incubated at 37°C for 1 hour with agitation. The transformations were plated on LB/Kan plates and incubated overnight at 37°C. Very small, isolated colonies were used to inoculate 2-mL LB/Kan for mini-preps, which were grown overnight at 37°C with agitation. Plasmid DNA was isolated using the QIAprep Spin Miniprep Kit and digested with 10 units of *PacI* (NEB R0547S) in NEB Buffer 1 with 1X BSA for 1.5 hours at 37°C. Candidate clones yielded a large fragment (near 30-kb) and a smaller fragment (3.0-kb or 4.5-kb). Candidate clones were sequenced using the respective ZFP*x*.RV.rv primer (Table 4.1). These candidate clones were labeled pAdeno-ZFP*x*.

4.2.3.3 Production of recombinant adenoviruses in 293A cells

293A cells were plated in T25 flasks (Sarstedt 83.1810.302) at 1.5 x 10^6 cells/flask and incubated overnight at 37°C in a CO_2 incubator. The next day, 4-μg of mini-prep pAdeno-ZFP18A, ZFP18B, ZFP18cA, ZFP18K or ZFP18N was digested with 10 units of *PacI* in NEB Buffer 1 with 1X BSA for 1.5 hours at 37°C. The enzyme was heat inactivated at 70°C for 20 minutes, then used to transfect 293A cells in T25 flasks, as follows. The digested plasmid DNA was added to 250-μL of Opti-MEM® I reduced-serum medium. In a separate tube, 20-μL of LF2000 was added to 250-μL of Opti-MEM® I reduced-serum medium. Both tubes were incubated at room temperature for 5 minutes then the LF2000 containing solution was added in a drop-wise manner to the DNA solution. After gentle mixing, the solution was incubated for 20 minutes at room temperature.

During this incubation time, each T25 flask was washed once with Opti-MEM® I reduced-serum medium, then the media was replaced with 2.5-mL of Opti-MEM® I reduced-serum medium. The LF2000 solution was added to the flask, and the cells were incubated overnight at 37°C in a CO_2 incubator. The following day, the media was replaced with complete media. The transfection was monitored for 10 days by observing GFP expression using the Zeiss Axiovert 200M fluorescent microscope and lasers for 488-nm excitation of GFP.

Adenoviruses were isolated by scraping cells off the culture flask using a cell scraper and transferring the cells to a new tube. The cells were centrifuged for 5 minutes at 1000-rpm then resuspended in 2-mL 1X PBS. The cells were subjected to four freeze-thaw cycles using liquid nitrogen to freeze and a 37°C water bath to thaw. The samples were subsequently centrifuged briefly and stored at -20°C. 1-mL of the virus supernatant was used to infect 293A cells in T25 flasks, plated the previous day at 1.5 x 10^6 cells/flask. Viral infection was monitored by observing GFP expression using the Zeiss Axiovert 200M fluorescent microscope and lasers for 488-nm excitation of GFP.

4.2.3.4 Assessment of ZFP-expressing adenovirus production in 293A cells

The presence of adenoviruses in culture supernatant of pAdeno-ZFP*x* transfected 293A cells was analyzed by collecting 1-mL of day 4 – 6 culture supernatant. Virus was pelleted by adding 300-µL of ICV Solution 2 (26% (w/v) polyethylene glycol (PEG) 8000, 1.4-M NaCl and 10-mM EDTA), incubating on ice for 1 hour and centrifuging for 10 minutes at 14,000-rpm at 4°C. The supernatant was removed and the pellet was resuspended in 20-µL of SDS-PAGE loading buffer. The entire sample was separated by 10% SDS-PAGE and transferred to nitrocellulose membrane as described in Section 2.2.21. The Western blots were probed with the goat anti-adenovirus hexon antibody (Abcam ab1056) at a dilution of 1:2000. The secondary antibody was donkey anti-goat HRP (Santa Cruz sc-2020) and was used at a dilution of 1:5000. The negative control was untransfected 293A supernatant and the positive control was purified AdCvM-

lacZ (kindly provided by Karl Fischer). The membranes were treated with Supersignal® West Dura Extended Duration Substrate (Pierce 34076) and exposed to film (Kodak XAR-5) to visualize the protein bands. The film was developed using the Kodak M35A X-OMAT Processor.

The presence of the ZFP gene within adenoviruses was determined by PCR. 5-µL of viral supernatant was incubated with 10-µL of proteinase K at 55°C for 1 hour, then the enzyme was heat inactivated at 70°C for 20 minutes. 1-µL of the sample was used for PCR with 1-µL of 10-mM dNTPs, 12.5 units recombinant *Taq* DNA Polymerase, 1.5-mM $MgCl_2$, 5-µL of 10X PCR Buffer, 0.5-µM of each primer and dH_2O up to 50-µL. The reaction was annealed at 52°C, with an elongation time of 30 seconds and 35 cycles. The PCR products were separated on a 0.8% (w/v) agarose gel with 1.5-ng/µL of EtBr and visualized with UV light and the G:box Gel Documentation System.

4.2.4 Cloning and production of ZFP-expressing baculoviruses

4.2.4.1 Cloning of ZFPs into the donor plasmid pFastBac-CMV1

pFastBac-CMV1 (pFB-CMV1, recombination donor plasmid (Amp^R), see map in Appendix A) was produced in house by Karl Fischer and contains the CMV IE promoter upstream of a multiple cloning site (MCS) and an SV40 splice/polyA signal downstream of the MCS. pFB-CMV1 and pcDNA3.1(+)-ZFP18A, ZFP18B, ZFP18cA, ZFP18K and ZFP18N were doubly digested with 10 units of *EcoRI* and 10 units of *BamHI* in NEB Buffer 2 with 1X BSA for 1.5 hours at 37°C. The restriction digests were run in their entirety on a 0.8% (w/v) agarose gel containing 1.5-ng/uL of EtBr and visualized using UV light and the G:box Gel Documentation System. The resulting backbone and inserts (546-588-bp) were excised from the agarose gel using a scalpel blade and the DNA was isolated using the QIAquick Gel Extraction Kit as described. The purified inserts were ligated to the pFastBac-CMV1 backbone in a 10-µL reaction containing 6-µL of insert DNA, 2-µL of 5X T4 DNA Ligase Buffer, 1-µL of the pFastBac-CMV1 backbone (diluted 1:10) and 1-µL (1 unit) of T4 DNA Ligase. Control reactions

substituted 6-µL of water for insert. The ligations were incubated overnight at 16°C in the thermocycler. The following day, 1-µL of the ligation reaction was transformed into 100-µL of chemically competent TOP10 *E.coli* as described in Section 2.2.3. Plates were incubated at 37°C overnight and isolated colonies were used to inoculate 2-mL of liquid LB/Amp cultures in 14-mL (17-mm x 100-mm) polypropylene culture tubes (Simport T406-2A), which were incubated at 37°C overnight with agitation.

Miniprep DNA was isolated using the QIAprep Spin Miniprep Kit, as described in Section 2.2.3. Positive clones were confirmed by restriction digest of 5-µL of miniprep DNA with *EcoRI* and *BamHI*, followed by visualization by EtBr-agarose gel electrophoresis and UV light.

4.2.4.2 Recombination of the donor plasmid with baculovirus bacmid DNA

Positive clones of pFB-ZFP18A, ZFP18B, ZFPc18A, ZFP18K and ZFP18N were transformed into chemically competent DH10Bac™ *E.coli* (Invitrogen 10361-012), which allow recombination between pFB clones and the baculovirus bacmid DNA (bMON14272 from *Autographa californica*). 100-µL of DH10Bac™ cells were thawed on ice and then 50 – 100-ng of pFastBac-ZFP plasmid in 5-µL was gently mixed with the cells (do not vortex). The mixture was incubated on ice for 30 minutes, then heat shocked at 42°C for 45 seconds. 900-µL of SOC was added and the cells were allowed to recover at 37°C with medium agitation for 4 hours. The transformation mixture was plated, as described above, on LB plates containing 7-µg/mL gentamycin, 10-µg/mL tetracycline, 50-µg/mL Kan, 40-µg/mL IPTG and 100-µg/mL X-Gal (LB/GTKIX). The plates were incubated 48 hours at 37°C and assessed for blue and white colonies. Isolated, white colonies were streak plated onto LB/GTKIX plates and incubated 24 hours at 37°C. Colony screen PCR was used to screen bacmid-ZFP clones from the plates as follows: a pipette tip was touched to a colony and then touched into a PCR reaction mixture contained 1-µL of 10-mM dNTPs, 12.5 units recombinant *Taq*

DNA Polymerase, 1.5-mM $MgCl_2$, 5-µL of 10X PCR Buffer, dH_2O up to 50-µL and a final concentration of 0.5-µM of each primer pair (Table 2.6). The annealing temperature was 54°C, with 40 cycles and 45 seconds for elongation. Isolated colonies from positive clones were used to inoculate 2-mL liquid LB with 7-µg/mL gentamycin, 10-µg/mL tetracycline and 50-µg/mL Kan, and incubated overnight at 37°C with agitation.

Bacmid-ZFP DNA was isolated by transferring 1.5-mL of the overnight culture into a 1.7-mL microfuge tube and centrifuging for 1 minute at 14,000-rpm in a micro-centrifuge (Beckman Coulter Microfuge® 18 Centrifuge). The supernatant was removed and the pellet was gently resuspended, by pipetting up and down, with 0.3-mL of Solution I (15-mM Tris-HCl pH 8.0, 10-mM EDTA, 100-µg/mL RNase A). Next, 0.3-mL of Solution II (0.2-N NaOH, 1% (w/v) SDS) was added, mixed gently and incubated at room temperature for 5 minutes. 0.3-mL of 3-M potassium acetate (pH 5.5) was slowly added and then incubated on ice for 5 – 10 minutes, before centrifugation for 10 minutes at 14,000-rpm. The supernatant was gently transferred to a new tube containing 0.8-mL isopropanol, then mixed gently and incubated overnight at -20°C. The sample was then centrifuged for 15 minutes at 14,000-rpm at room temperature, to precipitate the DNA. The supernatant was removed and the pellet rinsed by adding 0.5-mL of 70% (v/v) ethanol to the tube. After inverting several times, the sample was again centrifuged for 5 minutes at 14,000-rpm at room temperature. This wash was repeated a second time, then the supernatant removed as completely as possible, before air-drying the pellet for 5 – 10 minutes. The bacmid-ZFP DNA was gently resuspended by allowing it to sit in 40-µL of TE with gentle tapping. The samples were then stored at 4°C. The bacmid-ZFP DNA preps were analyzed on a 0.5% (w/v) agarose gel made with TAE buffer and containing 0.5-µg/mL EtBr. 5-µL of the bacmid-ZFP DNA prep was loaded onto the gel and electrophoresed at 23-V for 10 hours. The gel was then visualized using UV light and the G:box Gel Documentation System, with most preps showing the high molecular weight bacmid-ZFP DNA band and some additionally demonstrating the presence of

contaminating pFastBac-ZFP plasmid, however this contaminant had no effect on subsequent transfection into Sf9 cells.

4.2.4.3 Production of baculoviruses in Sf9 insect cells

Baculoviruses were produced in Sf9 insect cells using SF-900 II SFM media by plating 9.0 x 10^5 cells/well in 6-well plates with 2-mL media per well. Only cells from a 3 – 4 day old culture were used. The cells were allowed to attach for 1 hour, then the following solutions were prepared: (a) 5-μL of bacmid-ZFP DNA in 100-μL of media without antibiotics; (b) 6-μL of Cellfectin II Reagent (Invitrogen 10362-100) in 100-μL of media without antibiotics. The two solutions were combined gently and incubated for 15-45 minutes at room temperature. The plated Sf9 cells were washed once with 2-mL of media without antibiotics. Then, 0.8-mL of media was added to the transfection solution and the resulting 1-mL of media/transfection solution was overlaid on the SF9 cells for 5 hours in an incubator at room temperature without CO_2. Following this incubation, the transfection mixture was removed and replaced with 2-mL of complete media. After one week, the supernatant was collected to assess the presence of baculoviruses encoding ZFPs. 0.5-mL of supernatant was collected and clarified by centrifugation for 5-minutes at 1000xg (Beckman Coulter Allegra® X-15R centrifuge), then 6-mM $MgCl_2$, 100-μg/mL DNase I (Sigma DN-25) and 10-μg/mL RNase A (Sigma R-5503) were added and the reaction incubated for 30 minutes at 37°C. The sample was centrifuged for 10 minutes at 14,000-rpm and the supernatant was transferred to a new tube. 0.5-mL of PEG Solution (26% (w/v) PEG 8000, 1.4-M NaCl, 25-mM EDTA) was added and mixed gently by inversion (not vortexed, which would cause shearing). The sample was placed on ice for 30 minutes, then centrifuge for 10 minutes at 14,000-rpm at 4°C. The supernatant was carefully removed, then 100-μL TSE (50-mM Tris-HCl pH 8.0, 150-mM NaCl, 10-mM EDTA), 1-μL 10% (w/v) SDS and 5-μL proteinase K (20-mg/mL) were added to the pellet. The sample was incubated at 42°C for 5 hours. The sample was phenol:chloroform extracted by adding 50-μL of phenol and mixing by flicking the tube, then adding 100-μL of chloroform and mixing again.

The sample was then centrifuged for 5 minutes at 14,000-rpm and the aqueous phase transferred to a new tube using a pipette tip cut to have a larger opening size. 0.1X volume of 3-M sodium acetate and 2X volumes of 95% (v/v) ethanol were added and then the sample was chilled at -20°C for 30 minutes. The DNA was collected by centrifugation for 10 minutes at 12,000-rpm at 4°C, then tested for the presence of ZFPs by PCR as above, except 1-uL of isolated DNA was used at the template. All transfections successfully produced ZFP-encoding baculoviruses. Baculovirus production was up-scaled using T175 flasks inoculated with stock baculoviruses. Baculoviruses were harvested by collecting culture supernatant in a sterile tube and clarifying by centrifugation at 500xg for 5 minutes. The supernatant was transferred to a new tube and an aliquot stored long-term at -80°C with the addition of 2% (v/v) FCS. The remainder of the supernatant was concentrated by centrifugation at 22,000-rpm for 90 minutes, then resuspending in 1-mL of 1X PBS supplemented with 2% (v/v) FCS. Titres were determined using the BaculoELISA Titer Kit (Clontech 631412) and baculovirus stocks were stored at 4°C in the dark.

4.2.5 *Ex vivo* assessment of ZFP-expressing baculoviruses using primary duck hepatocytes

4.2.5.1 Perfusion of ducklings and isolation of primary duck hepatocytes

Two-week old Peking ducklings (*Anas platyrhynchos*) were used for the perfusion protocol. Stock solutions of EGTA base, collagenase base, L-15 medium and MEM were prepared ahead of time. EGTA base is prepared by adding 3.9-g NaCl, 0.5-g KCl, 4.5-g glucose and 5.95-g Hepes to 1-L ddH_2O, adjusting the pH to 7.5 and filter sterilizing. Collagenase base is prepared by adding 3.9-g NaCl, 0.5-g KCl, 4.5-g glucose, 5.95-g Hepes and 0.7-g $CaCl_2$ in 1-L ddH_2O, adjusting the pH to 7.5 and filter sterilizing. MEM is prepared by dissolving 10.48-g of MEM suspension powder (Invitrogen 11900-024) in 800-mL of ddH_2O. The pH is adjusted to 7.5 with 1-M Hepes solution. The volume is brought up to 1-L and filter sterilized. L-15 media is prepared by adding 14.69-g of L-15 powder (Invitrogen 41300-039) to 800-mL ddH_2O. 15-mL of 1-M Hepes is added and the

pH is adjusted to 7.5. 120-μL of 10-mg/mL insulin, 170-μL of 10-mg/mL glucose and 1.1-mL of 10-mM hydrocortisone hemisuccinate are added, then the volume is brought up to 1-L and filter sterilized. Other solutions that are required and filter sterilized are 100X pen/strep (5000-IU/mL penicillin, 1-mg/mL streptomycin), 2-mg/mL insulin, 50-mM EGTA and 100X L-Glutamine (200-mM). Immediately before commencing the perfusion protocol, several solutions were prepared. Perfusion solution was prepared by adding 5-mL of 100X pen/strep, 5-mL of 50-mM EGTA and 5-mL of 100X L-glutamine to 500-mL of MEM pH 7.5. Digest solution was prepared by adding 100-μL of 2-mg/mL insulin, 2-mL of 100X pen/strep to 190-mL of collagenase base. Collagenase was prepared by dissolving 200-mg of collagenase (from *Clostridium histolyticum Type IV:* Sigma C5138) in 10-mL of collagenase base and filter sterilizing using a 0.45-μm syringe filter. Collagenase inhibit solution I was prepared by adding 5-mL of 50-mM EGTA, 100-μL of 2-mg/mL insulin and 0.5-mL of 100X pen/strep to EGTA base, up to 50-mL total volume. Collagenase inhibit solution II was prepared by adding 2.5-mL of 50-mM EGTA, 250-μL FCS and 0.5-mL of 100X pen/strep to EGTA base, up to 50-mL total volume. L-15 complete media was prepared by adding 5-mL of 100X pen/strep and 25-mL FCS to 500-mL of L-15 media. Perfusion solution, digest solution and L-15 complete media are warmed at 37°C until use. Both collagenase inhibit solutions are kept at room temperature until use. The collagenase is kept on ice until use. The pump (Pharmacia Pump P-50) should also be prepared ahead of time by running 70% (v/v) ethanol through it several times.

Ducklings were killed by leg-vein injection of 500-μL euthanyl (Bimeda-MTC DIN 00141704, pentobarbital sodium USP 240-mg/mL). The abdomen of the duckling was washed with warm water and soap, followed by 70% (v/v) ethanol. The duckling was placed on a 2-inch thick cushion of paper towels within a 9” x 13” Pyrex glass dish. The outer layer of skin was cut away starting at the thigh, where loose skin can be pulled away from the inner abdominal membrane. The outer skin was cut vertically along both thighs and horizontally at the bottom of

the abdomen, forming a square "U" shape. The skin was then cut away from the inner abdominal membrane upwards towards the chest. Once completed, new pairs of sterile scissors and tweezers were used, and the inner abdominal membrane was opened up such that the liver was exposed but not falling out of the abdominal cavity, and the heart was visible (this requires some cutting of the rib cage). The IV catheter (20 gauge x 1.88 inches: BD Biosciences 381337) was inserted about ¾ cm into the right ventricle of the heart and the inner needle was removed. The pump head was placed into the perfusion solution and allowed to flow for a minute at 40-mL/min until any ethanol was cleared out of the system. The pump was stopped, then the pump head was attached to the catheter. The pump was turned on at 40-mL/min, then the major lobe of the liver was carefully lifted and the portal vein was cut. The portal vein became visible as pressure built in the blood system from the incoming perfusion solution. At least 250-mL of perfusion solution was allowed to flow through, while the liver was gently massaged as the blood cleared out. Next, the complete digest solution was prepared by adding the ice-cold collagenase to the pre-warmed digest solution and immediately run through the pump at 20-mL/min. The liver was not touched more than necessary; the digestion was assessed by pressing the liver with the edge of the tweezers and watching for the "bounce back". If the liver stayed squished down after pressing, digestion was done. This usually required 8-9 minutes of perfusion at 20-mL/min. Collagenase inhibit solution I was run through the pump at 20-mL/min, then solution II was run through at the same speed. The catheter was removed from the heart and discarded in the sharps waste container then ethanol was run through the pump to clean. The liver was removed from the abdominal cavity using an autoclaved, large household spoon and scissors. The liver was placed into a 10-cm petri dish containing 20-mL of L-15 complete media. The liver was diced with scissors and tweezers, which allowed the digested cells to separate into the media. The largest liver pieces were transferred to a second petri dish and diced with scissors and tweezers again. Next, the petri dishes were poured into an autoclaved funnel containing several layers of cheesecloth and strained into a 50-mL tube. The volume was brought up to 50-mL

with L-15 complete media, and the cells were allowed to settle for 30 minutes at 37°C. 80% of the media was decanted off and the volume was again brought up to 50-mL again with L-15 complete media. The cells settled again for 20 minutes at 37°C. These steps were repeated once more (3 washes). The cells were counted using trypan blue and plated at 1.0 x 10^6 cells/well in a 12-well plate (Sarstedt 83.1836.300). The cells were incubated at 37°C without CO_2 buffering. After 24 hours, the cells were rinsed 3X with warm 1X PBS and new L-15 complete media was added. The media was changed every two days for up to 2 weeks.

4.2.5.2 Infection of cells with ZFP-expressing baculoviruses

PDH were infected with Baculovirus-ZFP18A or Baculovirus-ZFP18cA 48 hours after plating. Media was removed from the PDH and replaced with 0.5-mL of complete media containing Baculovirus-ZFP18A or Baculovirus-ZFP18cA at multiplicity of infections (MOI) from 1 to 100. The infection was allowed to proceed overnight with the PDH incubated at 37°C without CO_2 buffering. The following morning, the virus was removed, the cells were washed twice with 1X PBS and fresh media was added. The media was changed every two days thereafter, as usual for PDH cultures. Cells were harvested 24, 48 or 72 hours post-infection.

LMH cells were infected with Baculovirus-ZFP18A or Baculovirus-ZFP18cA, as control cells. LMH cells were plated at 9.0 x 10^4 cells/well in 12-well plates. 24 hours later, the media was replaced with 0.5-mL of media containing Baculovirus-ZFP18A or Baculovirus-ZFP18cA at MOIs from 1 to 100. The infection was allowed to proceed overnight with the LMH incubated at 37°C with 5% CO_2. The following morning, the virus was removed, the cells were washed twice with 1X PBS and fresh media was added. Cells were harvested at 24 and 48 hours post-infection.

4.2.5.3 RNA isolation, cDNA synthesis and PCR on cells infected with ZFP-expressing baculoviruses

RNA was isolated from cells using TRIzol® Reagent as described in Section 2.2.13. cDNA was produced from 1-µg of total RNA using Random Primers (Invitrogen 48190-011) and SuperScript® II RT (Invitrogen 18064-022) according to manufacturer's specifications. Specifically, 2-µL of Random Primers (50-ng/µL), 1-µL of RNase-free dNTPS (10-mM stock) and 5-µg of total RNA were combined in a 1.7-mL microcentrifuge tube with RNase-free water up to a total volume of 12-µL. The sample was heated to 65°C for 5 minutes and quickly chilled on ice. The sample was centrifuged briefly to return the contents to the bottom, then 4-µL of 5X First Strand Buffer and 2-µL of 0.1-M dithiothreitol (DTT) were added. The contents were mixed gently then incubated at 42°C for 2 minutes. 1-µL (200 units) of SuperScript® II RT was added and the reaction allowed to proceed at 42°C for 50 minutes. The reaction was heat inactivated at 70°C for 15 minutes. Standard PCR was performed as described in Section 4.4.2, except that the primers were ZFP18A.RV.fw and ZFP18A.RV.rv, and ZFP18cA.RV.fw and ZFP18cA.RV.rv (Table 4.1), and the elongation time was 30 seconds, the annealing temperature was 54°C and the reaction was cycled 25 times. The primers and PCR protocol for duck GAPDH (Du-GAP.fw, Du-GAP.rv) are described in Section 4.2.2, except that 32 cycles were used.

4.2.5.4 Assessment of cells infected with ZFP-expressing baculoviruses

SDS-PAGE and Western blots were performed on Sf9, LMH and PDH cells as described in Sections 2.2.21-2.2.23.

4.2.6 *In vivo* assessment of ZFPs as therapeutics by portal vein injection of ZFP-polyplexes

4.2.6.1 Surgical procedure for portal vein injection

Pekin ducks ranging in age from 3 – 5 weeks old were used for the surgical procedure, after being pre-screened for DHBV levels in the serum as described in

Section 4.2.6.2. The ages and treatments of the ducklings can be found in Table 4.2.

ID number[a]	Surgery date	Treatment[b]	Age at surgery
4	08-Nov-20	ZFP18A polyplex, 150-μL	3 weeks
41	08-Nov-20	ZFP18cA polyplex, 150-μL	3 weeks
63	08-Nov-20	ZFP18A polyplex, 150-μL	3 weeks
69-1	08-Nov-20	ZFP18cA polyplex, 150-μL	3 weeks
22	09-Feb-11	ZFP18cA polyplex, 150-μL	4.5-5 weeks
26	09-Feb-11	ZFP18cA polyplex, 150-μL	4.5-5 weeks
86-1	09-Feb-11	ZFP18A polyplex, 150-μL	4.5-5 weeks
91	09-Feb-11	ZFP18A polyplex, 150-μL	4.5-5 weeks
69-3	09-Mar-18	ZFP18cA polyplex, 600-μL	4.5-5 weeks
82	09-Mar-18	ZFP18A polyplex, 600-μL	4.5-5 weeks
97	09-Mar-18	ZFP18cA polyplex, 600-μL	4.5-5 weeks
421	09-Mar-18	ZFP18A polyplex, 600-μL	4.5-5 weeks
412	09-Apr-22	1X PBS, 600 μL	5 weeks
25	09-Apr-22	pcDNA3.1(+)-ZFP18A & mlacZ in 1X PBS, 600-μL	5 weeks
72	09-Apr-22	pcDNA3.1(+)-ZFP18cA & mlacZ in 1X PBS, 600-μL	5 weeks
67	No surgery	No surgery, no injection	5 weeks
80	09-Jul-14	1X PBS, 600-μL	4 weeks
86-2	09-Jul-14	Chitosan in 97% sucrose, 600-μL	4 weeks
100	No surgery	No surgery, no injection	4 weeks

Table 4.2 - Summary of ducklings and their treatments for portal vein injection with polyplexes.
[a] Identification number of each animal from leg-tag.
[a] Type of treatment and volume injected during surgery.

Twenty-four hours prior to surgery, blood was collected from the leg vein of experimental animals and serum was isolated by centrifugation at 5000-rpm for 5 minutes at room temperature. Immediately prior to surgery, blood was again collected then ducks were injected with 20-mg/kg of ketamine. Once planar anesthetic was achieved, ducks were maintained under sedation with isofluorane using the Narkomed Anesthesia System (North American Drager). Dr. Lin Fu Zhu performed the microsurgeries in a surgical suite operated by Health Sciences Lab Animal Services. The abdomen of the ducks were washed with 70% ethanol and a small area was removed of feathers. A vertical incision in the abdomen was used to expose the liver. The portal vein was exposed under the retracted liver and either 150-μL (22 copies ZFP plasmid/cell) (ducks 4, 41, 63, 69-1, 22, 26, 86-1, 91) or 600-μL (88 copies ZFP plasmid/cell) (ducks 69-3, 82, 97, 421) of chitosan-based polyplexes was slowly injected using a 1-mL syringe through a 30-gauge needle. Upon removal of the needle, pressure was applied to ensure cessation of bleeding and then the animals were sutured closed using synthetic absorbable sutures (Surgik 1023-42). The ducks were taken off isofluorane and antibiotic cream was applied to the suture site. Ducks received intramuscular administration of 0.1-mg/kg hydromorphone every 24 hours until euthanasia. Ducks were allowed to recover under a warming lamp and then returned to their pens. Blood was collected at either 12 or 24 hour intervals from the leg vein. Control animals underwent similar surgery and were injected with 600-μL of 1X PBS (duck 80, 412), 600-μL of chitosan in 97% (w/v) sucrose solution (duck 86-2), or 600-μL of naked DNA at equivalent concentrations as in the polyplexes (pcDNA3.1(+)-ZFP18A/mlacZ: duck 25 and pcDNA3.1(+)-ZFP18cA/mlacZ: duck 72. 90-μg of pcDNA3.1(+)-ZFP*x* and 18-μg of mlacZ were used in each mixture). Animals that did not undergo surgery were also euthanized for comparison (ducks 67 and 100). A summary of the ducks and their treatment can be found in Table 4.2. Ducks were sacrified by euthanyl injection in the leg vein. Necropsy included collection of the liver, pancreas, spleen, duodenum and kidney for histology. Liver pieces were snap frozen in 1.8-mL Nunc cryovials (368632) using liquid nitrogen.

4.2.6.2 Assessment of DHBV DNA in duck serum by dot-blot hybridization

One-week old ducklings were pre-screened for surgery by collecting blood from the leg vein. Serum was separated by centrifugation at 5000-rpm for 5 minutes at room temperature and collected into a new tube. 100-μL of 1X PBS was added to the serum sample, which was then assessed using dot-blot hybridization, as described below. Ducklings with DHBV DNA at detectable levels in the serum were selected for surgery. Blood from surgically treated ducklings was also collected and assessed in the following way. A dot blot 96 apparatus was prepared by applying a water-soaked piece of Whatmann filter paper to the bottom grid, followed by a water-soaked nylon membrane (Hybond-XL). The top adaptor of the apparatus was fastened and a vacuum line attached. The serum samples were applied to each well and the liquid pulled through by vacuum, after which the membrane was removed and placed face-up for 30 minutes on filter paper soaked with denaturation solution (0.5-M NaOH, 1.5-M NaCl). The membrane was next placed face-up for 30 minutes on filter paper soaked with neutralization solution (0.5-M Tris-HCl pH 8.0, 1.5-M NaCl). UV cross-linking for 3 minutes affixed the nucleic acids to the membrane before pre-hybridization in a hybridization oven (Robbins Scientific® Model 1000) for 2 hours at 65°C with pre-hybridization solution (5X SSC, 2% (w/v) SDS, 1X Denhardt's Solution, 0.5-mg/mL herring sperm DNA) in a glass hybridization tube. [α-^{32}P]dCTP-labeled DHBV probe (prepared as described in Section 2.2.16) was added to the membrane in the glass tube and allowed to hybridize overnight at 65°C. The next day, the membrane was washed twice with 1X SSC/0.1% (w/v) SDS for 15 minutes and once with 0.1X SSC/0.1% (w/v) SDS for 15 minutes, before being exposed to an image plate overnight and scanned by a Fujifilm FLA5100 phosphorimager (Fuji Photo Film Co. Ltd). Quantification of DHBV serum levels was done using Science Lab 2003 Image Gauge software v4.22 (Fuji Photo Film Co. Ltd).

4.2.6.3 Isolation of viral DNA from serum using the High Pure Viral Nucleic Acid Kit

Some ducks had DHBV titres too low to detect by dot-blot. Viral DNA from serum was isolated using the High Pure Viral Nucleic Acid (HPVNA) kit (Roche 11 858 874 001) according to manufacturer's specifications. Specifically, working solution was prepared using 200-µL/sample of Binding Buffer and 4-µL/sample of PolyA (provided in kit). Next, 50-µL of serum was combined with 150-µL of 1X PBS, 200-µL of working solution and 50-µL of proteinase K (provided in kit). Samples were incubated for 10 minutes at 72°C, after which 100-µL of Binding Buffer was added to the tube and centrifuged briefly to pellet contents. The entire sample contents were transferred to a provided filter tube and centrifuged at 8000xg for 1 minute at room temperature. The filter tube was rinsed once with 500-µL of Inhibitor Removal Buffer and twice with 450-µL of Wash Buffer, centrifuging at 8000xg for 1 minute after each addition and discarding the flow-through. After the last wash, filter tubes were spun an additional 10 seconds at maximum speed to ensure complete removal of wash buffer. Samples were eluted with 50-µL of Elution Buffer and centrifugation at 8000xg for 1 minute.

4.2.6.4 Assessment of DHBV DNA in duck serum by semi-quantitative PCR

PCR was performed on HPVNA isolated from Section 4.2.6.3 using the DHBV-specific JS-16 primer (5'-TCCGTCAGAT ACAGCAAG-3') and the 1039/57 primer (5'-CTCAAGAGAT TCCTCAGCC-3'). The PCR reaction contained 2-µL of HPVNA template, 1-µL of 10-mM dNTPs, 12.5 units recombinant *Taq* DNA Polymerase, 1.5-mM $MgCl_2$, 5-µL of 10X PCR Buffer, 0.5-µM of each primer and dH_2O up to 50-µL. The reaction was annealed at 52°C, with an elongation time of 30 seconds and 26 cycles. PCR products were separated on a 0.8% (w/v) agarose gel and visualized using UV light and the G:box Gel Documentation System. The program GeneTools v.3.06, (Synoptics Ltd, Cambridge UK) was used to quantify the bands.

4.2.6.5 SDS-PAGE and Western blot of liver lysates

Whole cell lysates were produced from liver using RIPA buffer (10-mM Tris-HCl pH 8.0, 140-mM NaCl, 0.1% (w/v) SDS, 1% (v/v) Triton X-100, 1% (w/v) deoxycholic acid, 0.025% (w/v) sodium azide). Specifically, 300-μL of RIPA was added to a piece of liver less than 250-mg in weight and the liver was homogenized using a 16-gauge needle. The sample was centrifuged at 14,000-rpm for 10 minutes. A 21-gauge needle was used to collect the lysate below the fat layer. SDS-PAGE, Western transfer and Western blot were performed as described in Section 2.2.21-2.2.23. Primary and secondary antibodies as described in Section 2.2.23.

4.2.6.6 Preparation of tissue for histological assessment

Samples were placed in plastic cassettes and placed in formalin for 24 hours at room temperature with slight agitation. Formalin was drained and then 70% (v/v) ethanol was added for 1 hour, followed by two washes with absolute ethanol for 1.5 hours each. Finally, butanol was added for 24 hours, then replaced twice with fresh butanol for another 24 hours each (72 hours total). Samples were paraffin embedded by vacuum infiltration and sectioned at 4 microns by a Shandon Histocentre 2 microtome for histological analysis.

Liver pieces used for the X-Gal staining protocol (Section 4.2.6.7) were fixed in 2% paraformaldehyde for 1 hour at room temperature. They were rinsed twice with 1X PBS pH 7.2 and soaked overnight at 4°C in 1X PBS pH 7.2 containing 30% sucrose and 2-mM $MgCl_2$. The samples were then embedded in O.C.T. compound (Tissue-Tek 4583) and frozen on dry ice. Samples were sectioned at 5-mm thick by a Leica CM1900 UV cryotome.

4.2.6.7 Histological assessment of tissue sections

The standard protocol for hematoxylin and eosin (H&E) staining of tissue sections was completed by Suellen Lamb. Slides were visualized using a Zeiss Axio Imager M1 microscrope.

Frozen tissue sections were stained with X-Gal stain (1X PBS pH 7.2 containing 2-mM $MgCl_2$, 2-mM potassium ferricyanide, 4-mM potassium ferrocyanide and 1-mg/mL X-Gal (dissolved in DMF)) and counterstained with nuclear fast red. Nuclear fast red was produced by dissolving 2.5-g of aluminum sulfate in 50-mL dH_2O, then adding 50-mg of nuclear fast red and heating the solution. Once the powders were dissolved, the solution was cooled and filtered using Whatman 3MM filter paper. Slides were rehydrated in 1X PBS pH 7.2 with 2-mM $MgCl_2$ for 5 minutes. 500-µL of X-Gal stain was added to each section and then incubated in a humidity chamber for 16 – 18 hours at 37°C. The next day, slides were rinsed with 1X PBS pH 7.2 and counterstained with 500-µL of nuclear fast red for 5 minutes. The slides were rinsed one more time with 1X PBS pH 7.2 and dehydrated for mounting, by passing slides through subsequent washes of ethanol to xylene. Slides were visualized using a Zeiss Axio Imager M1 microscrope.

4.2.6.8 Ortho-nitrophenyl-beta-galactoside (ONPG) assay to measure β–Gal activity in liver tissue

Liver pieces were homogenized in 1X PBS using a 16-gauge needle. Lysates were centrifuged briefly at 10,000-rpm and the lysates were transferred to a new tube. Several solutions were made ahead of time. 0.1-M sodium phosphate (pH 7.5) was prepared by mixing 41-mL of 0.2-M $Na_2HPO_4{\cdot}2H_20$ with 9-mL of 0.2-M $NaH_2PO_4{\cdot}2H_2O$ in 50-mL of dH_2O. 100X Mg solution consisted of 0.1-M $MgCl_2$ and 4.5-M β-mercaptoethanol in dH_2O. 1X ONPG consisted of 4-mg/mL ONPG in 0.1-M sodium phosphate (pH 7.5). 10-µL of liver lysate was mixed with 1-µL of 100X Mg solution, 22-µL 1X ONPG and 65-µL of 0.1-M sodium phosphate (pH 7.5). The reaction was incubated at 37°C for 2 hours before stopping it with the addition of 167-µL of 1-M Na_2CO_3. The optical density was measured at 420-nm using a SpectraMAX Plus 384 plate reader (Molecular Devices) (2). Measurements were converted to activity of β-Gal according to the following formula:

$$\text{Units/mg} = (\text{OD} \times 0.1^*)/(4.6 \times t_{min})(\text{weight of liver piece})$$

where * is the final reaction volume.

4.2.6.9 Isolation of total RNA from liver samples

Total RNA was isolated from liver samples using Trizol reagent (Invitrogen 15596-018). 1-mL of Trizol was added to a piece of liver less than 250-mg in weight and the liver was homogenized using a 16-gauge needle. Samples were incubated on a rotating platform for 30 minutes at room temperature then centrifuged at 3000-rpm for 5 minutes to remove large chunks. The supernatant was transferred into a new tube then 0.3-mL of chloroform was added. Samples were shaken vigorously for 15 seconds then incubated on a rotating platform for 10 minutes at room temperature. Next, samples were centrifuged at 12,000xg for 15 minutes at 4°C and the top aqueous layer collected into a new tube. The extraction was repeated by adding 0.5-mL chloroform to the aqueous layer, vortexing for 20 seconds, incubating at room temperature on a rotating platform for 2 minutes and centrifuging at 12,000xg for 15 minutes at room temperature. The aqueous phase was again collected and RNA precipitated by adding 2-μg of yeast tRNA as carrier and one half volume each of isopropanol and high salt solution (0.8-M sodium citrate, 1.2-M NaCl). After mixing by inversion, samples were incubated at -20°C overnight, then centrifuged at 12,000xg for 30 minutes at 4°C. After discarding the supernatant, the RNA pellet was washed twice with 1-mL of 75% (v/v) ethanol (RNase free) and centrifuged at 13,000-rpm for 5 minutes at room temperature. Traces of ethanol were removed, the RNA pellet was briefly air-dried and resuspended in 20-μL dH_2O. RNA was measured by diluting 1:100 in RNase-free water and measuring on the spectrophotometer (Pharmacia Biotech UltraSpec® 3000) at A_{260}/A_{280}.

4.2.6.10 cDNA synthesis from total RNA from liver

cDNA was produced from 5-μg of total RNA as described in Section 4.2.5.3.

4.2.6.11 Quantitative PCR on duck liver samples

Quantitative PCR was performed on cDNA made from total RNA from the liver using the Bio-Rad CFX-96 using the iQ SYBR Green Supermix kit (#170-8880) and the primers as shown in Table 4.3. Specifically, 12.5-μL of 2X iQ Supermix

was mixed with 2-µL of each primer (5-µM stock), 2.5-µL of template and water up to 25-µL.

Name	Primer sequence [a]
IFNaF	GACAGCGCCT TCGCCTGGGA CAG[b]
IFNaR	GTGGCGTGCG GTGTGGAGCC AGT[b]
Duck.GAPDH.F	GGCACTGTCA AGGCTGAGAA TG
Duck.GAPDH.R	TGCAAGAGGC ATTGCTGAC
IL1bF	CCCGTGTACC GCTACACCCG CTCC[b]
IL1bR	GATGTCCCTC ATGACGGCGG CCTC[b]
GBP-F	AGTCCTTCCT CATGAACCGG CTG[c]
GBP-R	GTACACCAGG GTGCTGGAGA GCA[c]
OAS5'-2.1	CTGCAGCCCA GCACGGAATT CAGCA[c]
OAS3'-2	CAGGATGTCG ACGTCGATGG ACTC[c]

Table 4.3 - Primer sequences for quantitative and standard PCR reactions.
[a] Sequences are shown 5' to 3'.
[b] Sequence from Kathy Magor, Department of Biological Sciences, University of Alberta.
[c] Sequence from Karl Fischer, Tyrrell lab.

4.2.7 Standard PCR on duck liver samples

Standard PCR was performed on cDNA from total RNA isolated from duck liver. Primer sequences can be found in Table 4.3. The PCR reaction contained 2-µL of cDNA template, 1-µL of 10-mM dNTPs, 12.5 units recombinant *Taq* DNA Polymerase, 1.5-mM $MgCl_2$, 5-µL of 10X PCR Buffer, 0.5-µM of each primer and dH_2O up to 50-µL. The reaction was annealed at 52°C, with an elongation time of 30 seconds and 28 cycles (GBP, OAS) or 32 cycles (GAPDH). PCR products were separated on a 0.8% (w/v) agarose gel and visualized using UV light and the G:box Gel Documentation System. Blank samples had water only without template, and positive samples had 2-µL of pCR4-Du.OAS, -Du.GBP or -Du.GAPDH plasmids.

4.3 Results

4.3.1 Production of adenoviruses encoding ZFPs

The AdEasy System was used to develop adenovirus vectors encoding DHBV- and HBV-specific ZFPs. ZFP18A, ZFP18B, ZFP18cA, ZFP18K and ZFP18N were cloned into the shuttle vector pAdTrack-CMV1. The successful clones were then linearized and transformed into BJ5183-AD-1 *E.coli*, which contain the AdEasy vector, pAdEasy-1, and allow for recombination between the shuttle vector and the AdEasy vector. The resulting recombinants (pAdeno-ZFP18A, -ZFP18B, -ZFP18cA, -ZFP18K, -ZFP18N) contain the genetic material to produce adenoviruses in the packaging cell line 293A. Clones for each construct were sequenced for the presence of each ZFP. Positive matches were used for further experimentation. Five clones for each construct were used to transfect 293A cells, and the transfection was monitored under the fluorescent microscope by observing GFP expression, which is encoded by the pAdeno-ZFP plasmids. A typical timeline for production of adenovirus particles is observation of GFP positive cells around day 2, followed by the appearance of adenovirus-producing foci by 5 – 7 days (3). The foci are formed by the production of infectious adenovirus particles, which infect adjacent 293A cells. By day 3, about half of the clones had produced appreciable numbers of GFP positive cells. pAdeno-ZFP18A had one clone (A101) with 10% GFP positive cells after 3 days, while the other four clones had 1% or less. pAdeno-ZFP18B had three clones (B101, B102, B103) with 10% GFP positive cells and pAdeno-ZFP18N had one clone (N104) with 10% GFP positive cells. All the remaining clones, including those for pAdeno-ZFP18K and pAdeno-ZFP18cA, had only 1 – 2% GFP positive cells.

In addition to the low amounts of GFP positive cells, which may only indicate poor transfection efficiencies, no clones ever developed adenovirus-producing foci after even 10 days of culture. When the supernatant of all the clones were harvested for adenovirus, and used to re-infect new flasks of 293As, none produced any subsequent GFP expression. The supernatants of these clones were collected and assessed using Western blot to detect adenovirus hexon (Figure

4.1). Adenovirus hexon protein was not detected in any of the supernatants of transfected 293A cells. Figure 4.1 is a representative Western blot for all the pAdeno-ZFP clones tested, and shows a strong signal from the positive control, which was purified AdCvM-lacZ adenovirus.

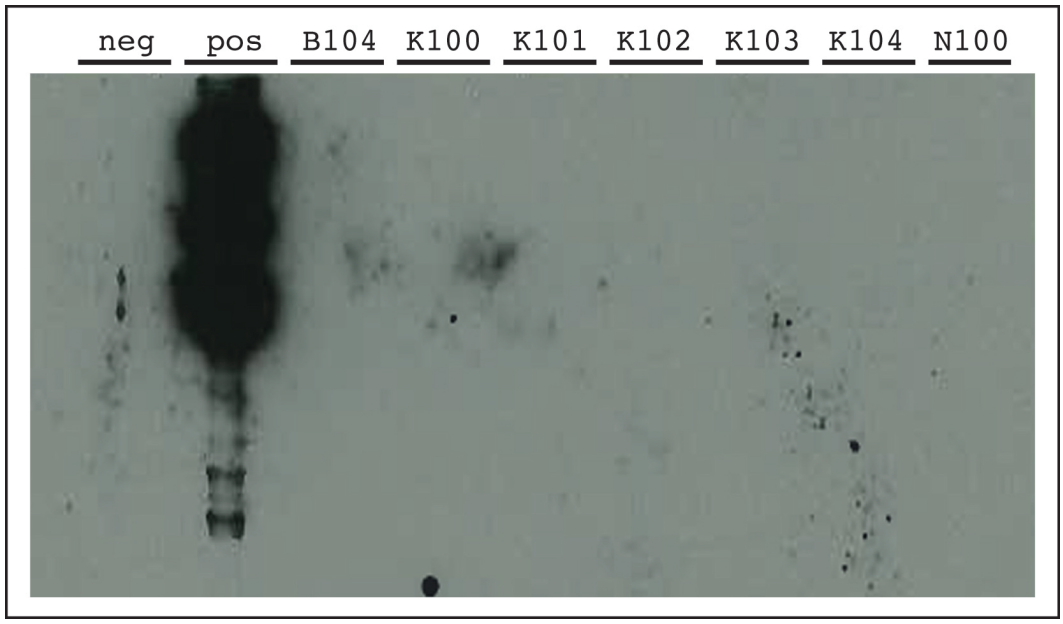

Figure 4.1 - Western blot for adenovirus hexon protein in supernatants from pAdeno-ZFP-transfected 293A cells.
293A cells were transfected with pAdeno-ZFP clones and after day 4 – 6, supernatants were collected and analyzed by Western blot using an anti-adenovirus hexon antibody. The negative control (neg) was non-transfected 293A supernatant and the positive control (pos) was purified AdCvM-lacZ adenovirus. This blot is representative for all pAdeno-ZFP clones tested, but shows one clone of pAdeno-ZFP18B (B104), five clones of pAdeno-ZFP18K (K100 – K104) and one clone of pAdeno-ZFP18N (N100).

Subsequently, 293A cells were transfected with pAdeno-ZFP18A and -ZFP18cA plasmids that were concentrated into a smaller volume. These cells were 1 – 5% GFP positive after 2 days. When supernatants from these cells were used to infect new 293A cells, a few clones (cA100, cA101, cA103, A103) produced GFP positive cells, indicating the presence of infectious adenovirus. The supernatant from these cultures was collected and viral nucleic acid was isolated. PCR specific for each respective ZFP was carried out to determine if the adenoviruses

still encoded ZFPs. As seen in Figure 4.2, clones cA100, cA101, cA103 and A103 did not encode their respective ZFP, since no band like that seen in the positive control lanes was detected. The blank sample using ZFP18cA-specific primers brought up a smaller band, but since none of our samples were positive, there is no concern that a false positive may have resulted in the sample lanes.

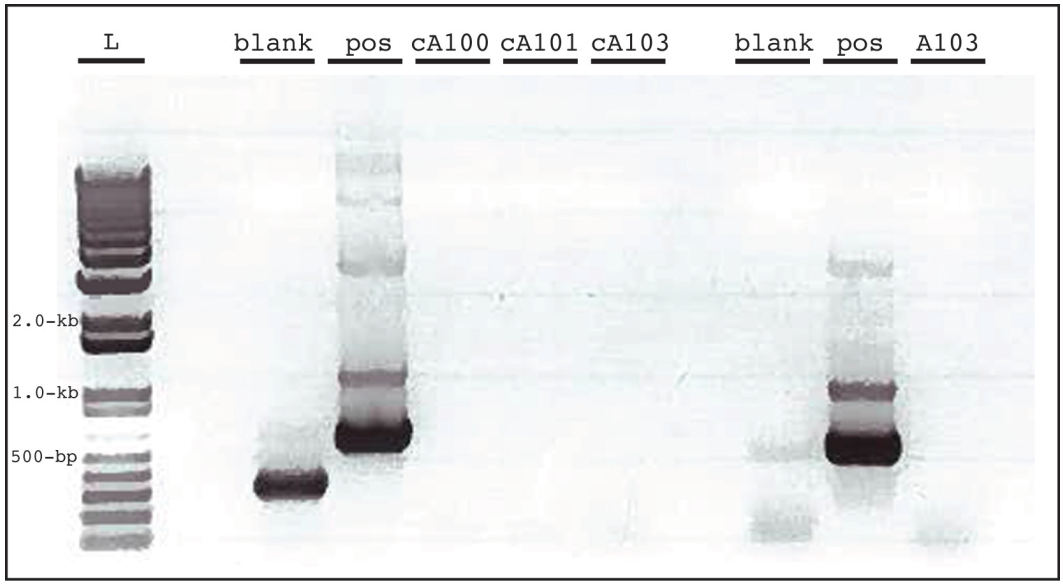

Figure 4.2 - PCR for ZFPs on adenovirus nucleic acid isolated from the supernatant of adenovirus-infected 293A cells.
Nucleic acid was isolated from the supernatants of adenovirus-infected 293A cells and analyzed by PCR. The clones cA100, cA101 and cA103 were analyzed using ZFP18cA-specific primers. The positive control was pcDNA3.1(+)-ZFP18cA and the negative control was water alone. The clone A103 was analyzed using ZFP18A-specific primers. The positive control was pcDNA3.1(+)-ZFP18A and the negative control was water alone. The ladder (L) is shown on the left with some size markers.

In summary, the construction of adenoviruses-encoding ZFPs failed. First of all, 293A cells failed to produce infectious adenovirus particles for the majority of clones. Secondly, the few clones that did produce infectious adenovirus particles no longer contained the gene for the ZFPs. This suggests that the presence of the ZFPs in the adenovirus clones prohibited the production of infectious adenoviruses. Those "escape mutants" that eliminated the presence of the ZFP gene were able to produce infectious adenovirus particles.

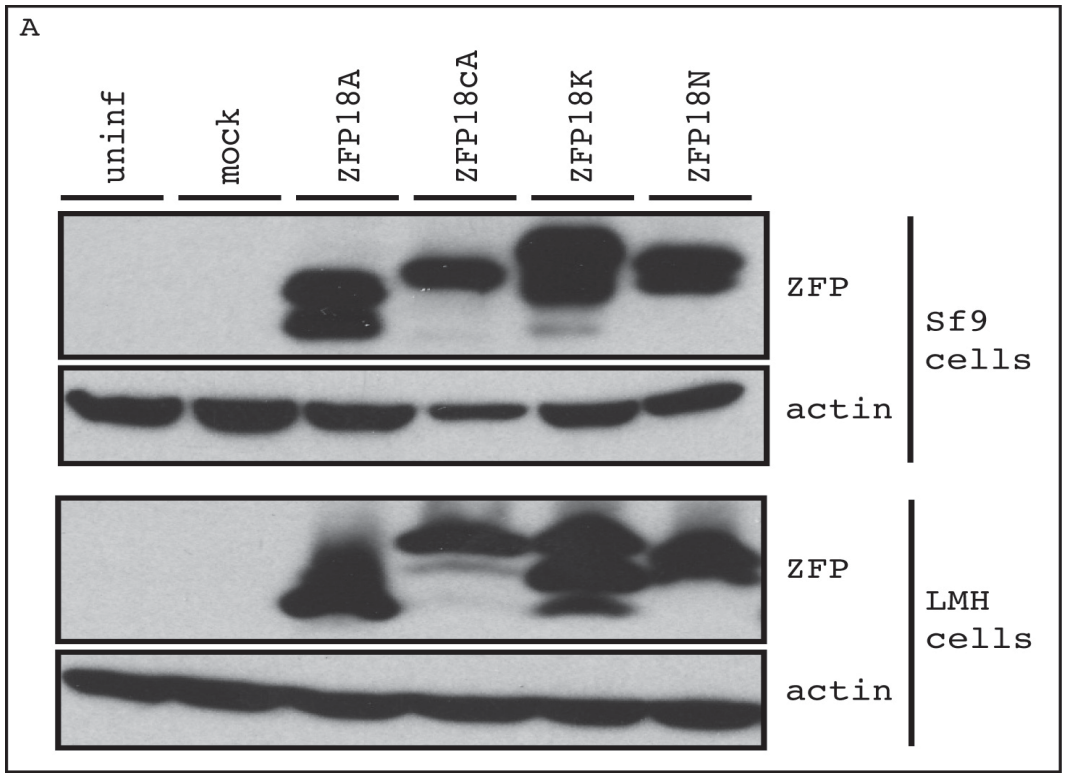

Figure 4.3 - Western blots of baculovirus-producing Sf9 and baculovirus-infected LMH lysates.
Sf9 cells were transfected with Bacmid-ZFP18A, -ZFP18cA, -ZFP18K, or -ZFP18N, mock transfected (mock) or not-transfected ("uninf"). After 10 days of baculovirus production, cell lysates were collected and assessed by Western blot using anti-ZFP antiserum and anti-actin antibodies. LMH cells were infected with the harvested baculovirus-ZFP18A, -ZFP18cA, -ZFP18K, or –ZFP18N, mock infected with lysates from the mock-transfected Sf9s (mock) or uninfected (uninf). After 48-hours, cell lysates were collected and assessed by Western blot using anti-ZFP antiserum and anti-actin antibodies.

4.3.2 Production of baculoviruses encoding ZFPs

Next, baculoviruses expressing ZFPs were constructed as an alternative method to deliver ZFPs into PDH and duck liver *in vivo*. Baculoviruses are known to be capable of infecting the liver (4), and have been shown to transduce both duck and chicken cells (5). ZFP18A, ZFP18cA, ZFP18K and ZFP18N were cloned into the baculovirus recombinant donor plasmid pFB-CMV1 and then recombined with the baculovirus bacmid resident in DH10Bac *E.coli*. Positive clones were used to produce ZFP-encoding baculoviruses in Sf9 insect cells. Expression of ZFPs from the ZFP-encoding baculoviruses was tested by Western blots on

baculovirus-producing Sf9 cell lysates after 10-days of baculovirus production (Figure 4.3). LMH cells were also infected with baculoviruses and harvested after 48-hours for Western blot analysis on cell lysates (Figure 4.3). Compared to uninfected and mock-transfected (Sf9) or mock-infected (LMH) lysates, ZFP protein expression was strongly detected in both Sf9 and LMH cells for Baculovirus-ZFP18A, ZFP18cA, ZFP18K and ZFP18N. These Western blots demonstrate ZFP-expression by the constructed ZFP-encoding baculoviruses.

4.3.3 Infection of PDH with ZFP-encoding baculoviruses

The ability for the baculoviruses to infect the liver of ducks was first assessed *ex vivo* in PDH, which were isolated by perfusion and collagenase digestion of congenitally-infected Pekin ducklings. After plating, the PDH were infected with Baculovirus-ZFP18A or –ZFP18cA at varying MOIs. In parallel, LMH cells were also infected with the same MOIs, for comparison between the PDH and a cell line known to be efficiently transduced by the ZFP-encoding baculoviruses. After 24, 48 and 72 hours, whole cell lysates were collected and assessed by Western blot for ZFP expression, and actin expression as a loading control (Figure 4.4). As seen in the LMH cells (Figure 4.4 A), increasing MOIs resulted in increasing amounts of ZFP expression. ZFP expression could be strongly detected at 24 and 48 hours, and was still faintly visible at 72 hours. In contrast, ZFP expression in PDH was not detected at any time point, including 24, 48 or 72 hours (Figure 4.4 B).

The levels of ZFP transcripts were also investigated by harvesting total RNA from PDH infected with baculovirus-ZFP18A or ZFP18cA at an MOI of 10 after 48 hours. ZFP transcripts were not detected in PDHs (Figure 4.5), suggesting that either the baculoviruses do not infect PDHs or that the ZFPs cannot be expressed in the PDHs.

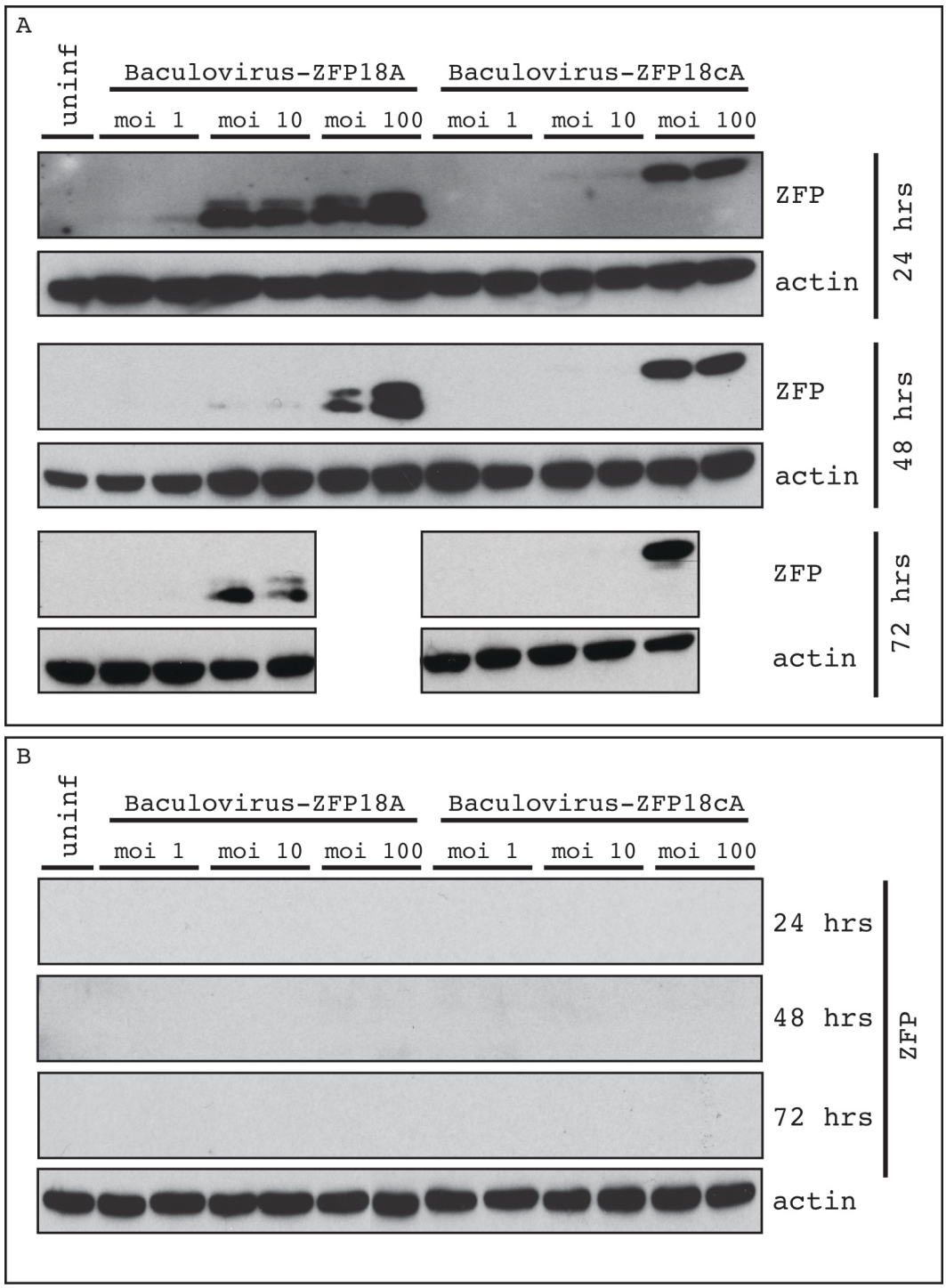

Figure 4.4 – Western blot analysis of LMH and PDH cells infected with ZFP-encoding baculoviruses.

LMH cells (A) and PDHs (B) were infected with baculovirus-ZFP18A or –ZFP18cA at MOIs of 1, 10 or 100, or left uninfected ("uninf"). After 24, 48 and 72 hours, cell lysates were collected and assessed by Western blot using anti-ZFP antiserum and anti-actin antibodies. This experiment was performed twice.

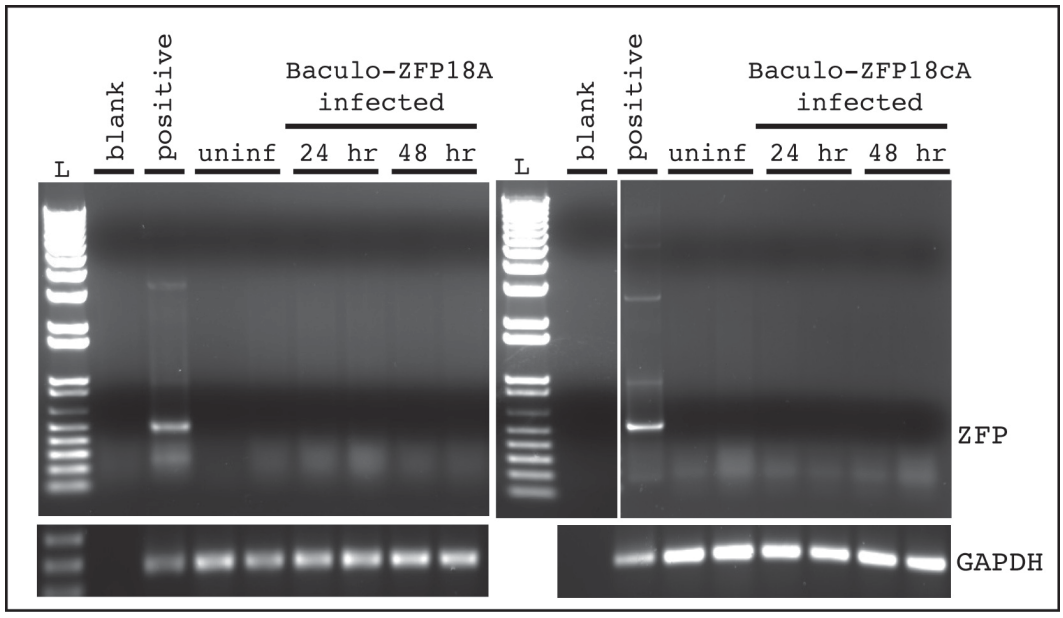

Figure 4.5 – PCR analysis for ZFP transcripts in baculovirus-infected congenital PDH.
Congenitally-infected PDH cells were infected with baculovirus-ZFP18A or –ZFP18cA at an MOI of 10, or left uninfected ("uninf"). After 24 and 48 hours, total RNA was collected, made into cDNA and assessed by PCR for the presence of ZFP transcripts, or GAPDH as a control. Negative control samples ("blank") had no template added, and positive control samples ("positive") had either pCR4-ZFP18A, -ZFP18cA or –Duck.GAPDH as template.

To investigate the reason for the paucity of ZFP expression in congenitally-infected PDH, two non-congenital Pekin ducklings were perfused and infected with baculovirus-ZFP18A or –ZFP18cA at an MOI of 1, 10 and 50. After 48 hours, total RNA was isolated and made into cDNA. PCR for ZFP transcripts was performed, with GAPDH as a control. As seen in Figure 4.6, transcripts for both ZFP18A and ZFP18cA were detected at increasing levels relative to the MOI. This suggests that baculoviruses are able to infect and express ZFP transcripts in PDH in the absence of a pre-existing DHBV infection. This is supported by Western blots for ZFP expression in baculovirus-infected non-congenital PDH (Figure 4.7). Both ZFP18A and ZFP18cA can be detected in the PDH infected with an MOI of 50, although ZFP expression was not detected in PDH infected with lower MOIs (1 or 10).

In summary, it appears that the presence of DHBV in PDH excludes the subsequent infection of or gene expression by baculoviruses encoding therapeutic ZFPs.

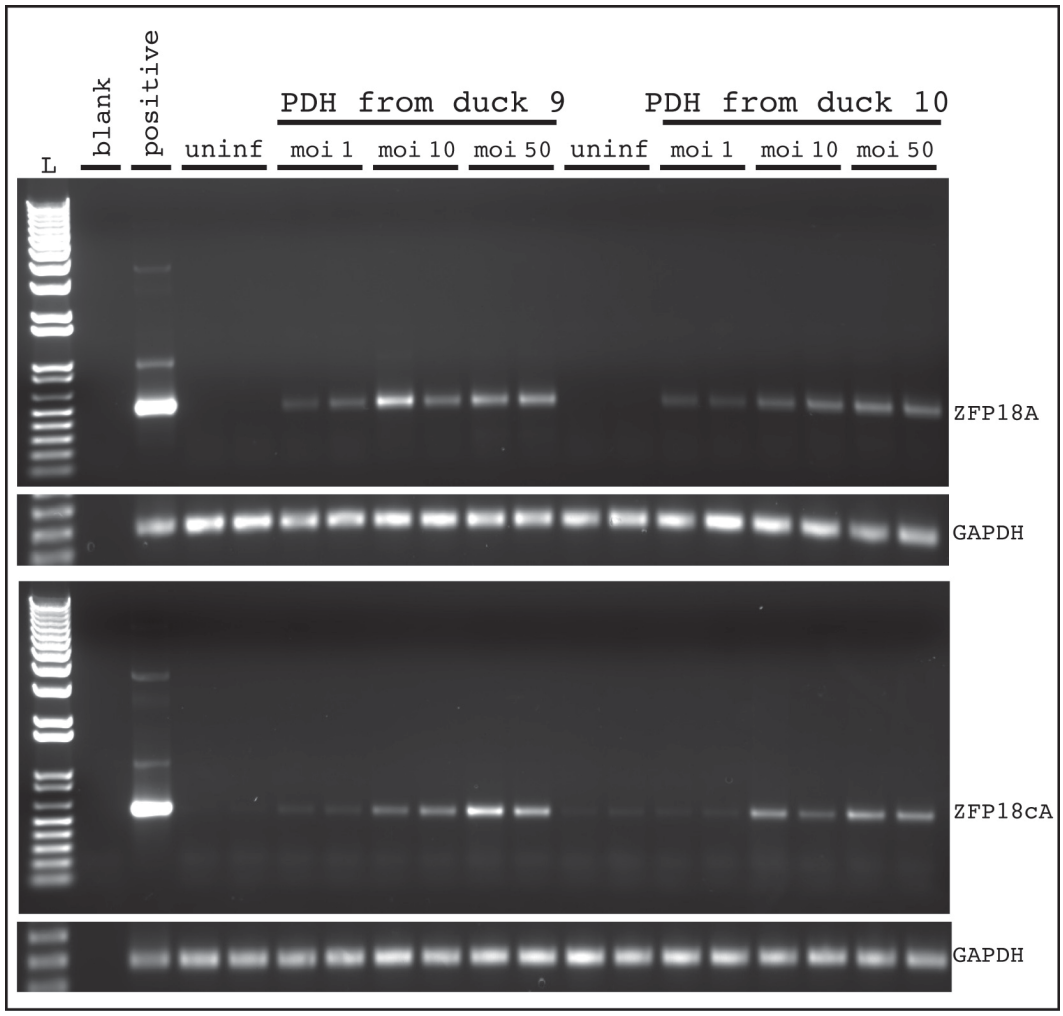

Figure 4.6 - PCR analysis for ZFP transcripts in baculovirus-infected non-congenital PDH.
Non-congenital PDH were infected with baculovirus-ZFP18A or –ZFP18cA at an MOI of 1, 10, or 50, or left uninfected ("uninf"). After 48 hours, total RNA was collected, made into cDNA and assessed by PCR for the presence of ZFP transcripts, or GAPDH as a control. Negative control samples ("blank") had no template added, and positive control samples ("positive") had either pCR4-ZFP18A, -ZFP18cA or –Duck.GAPDH as template.

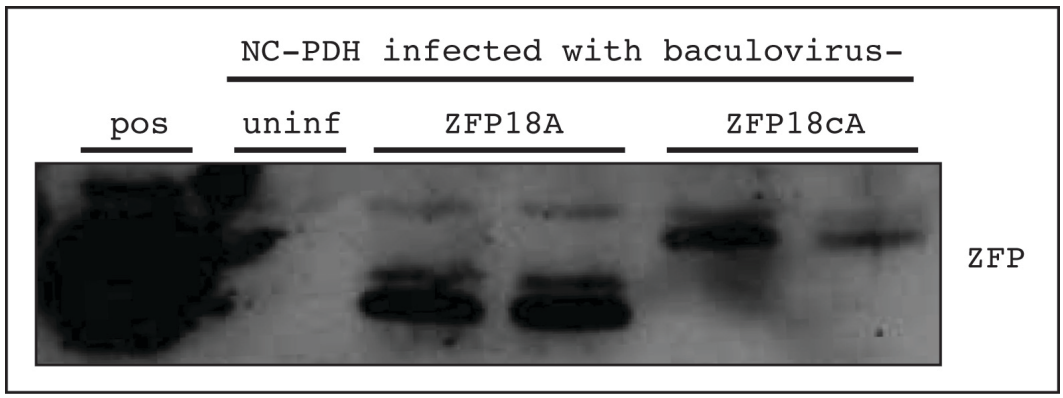

Figure 4.7 – Western blot for ZFP expression in baculovirus-infected non-congenital PDH.
Non-congenital PDH cells were infected with baculovirus-ZFP18A or –ZFP18cA at an MOI of 50, or left uninfected ("uninf"). After 48 hours, whole cell lysates were collected and assessed by Western blot using anti-ZFP antiserum. A positive control (pos) was included, which was cell lysate from LMH cells transfected with the pcDNA3.1(+)-ZFP18A plasmid.

4.3.4 *In vivo* assessment of ZFP-polyplexes as therapeutics targeting DHBV

4.3.4.1 Experimental design

ZFP-polyplexes were used to deliver plasmids encoding ZFPs into DHBV-infected Pekin ducklings. ZFP18A-polyplexes and ZFP18cA-polyplexes were tested in a series of experiments. Since polyplexes transfect cells regardless of tissue or host type, the polyplexes were injected directly into the portal vein of ducklings. This ensured the polyplexes were delivered directly into the liver, not systemically. Systemic delivery would dilute the potential effectiveness of the therapeutic. Congenitally-infected Pekin ducklings aged 3 – 5 weeks were used for the experimental protocol. The main read-out of therapeutic effectiveness was DHBV levels in the serum of treated ducklings, however organs were also harvested at the time of necropsy and used for further assessment, as outlined below. In general, the greatest threat to the ducklings' survival was the anesthetics used during the surgical procedure itself. Once the surgery was completed and the duckling had regained consciousness, there were no incidents of post-operative death. Additionally, no ducks exhibited symptoms of septicemia or infection at the surgical site. All animals resumed normal duck behavior patterns once consciousness was regained and the anesthetics wore off completely.

The first eight animals were treated with 150-μL of ZFP-polyplex, which equates to 22 copies/hepatocyte, if it is assumed that 1.0-g of liver has 10^9 cells and an average duck liver weighs 200-g. Half of the animals were treated with ZFP18A-polyplexes and half with ZFP18cA polyplexes. The next four animals were treated with four times the volume; 600-μL, or 88 copies/hepatocyte. Additionally, control animals were treated with 600-μL of 1X PBS, or 600-μL of chitosan alone in 97% sucrose (chitosan is the structural component of the polyplexes). Other control animals were treated with 600-μL of pcDNA3.1(+)-ZFP18A or ZFP18cA plasmid DNA in 1X PBS at the same copy number and ratio to mlacZ as the ZFP-polyplexes. Lastly, animals that did not undergo the surgical procedure were used as controls.

Samples were collected at approximately the same time each day, to minimize any effects due to the natural oscillation of DHBV levels in the blood of infected ducklings throughout the 24-hour cycle, which are tied to the diurnal rhythm of the ducklings (6).

4.3.4.2 Analysis of DHBV levels in the serum of ducklings

The first surgical round ("experiment 1") included two animals (duck 4, duck 63) treated with 150-μL of ZFP18A-polyplex and two animals (duck 41, duck 69-1) treated with 150-μL of ZFP18cA-polyplex. These animals were monitored on days -1, 2, 4, 6 and 7 by collecting blood and isolating the serum. The serum was analyzed by dot blot for DHBV (Figure 4.8 A). The levels of DHBV in the serum of ducks 63 and 69-1 were too low to detect by dot blot, therefore semi-quantitative PCR was carried out on the serum (Figure 4.8 B). Both animals treated with ZFP18A-polyplexes show a similar trend of decline in DHBV levels between day -1 and day 2, with a rebound starting at day 4. In fact, in duck 4 (ZFP18A-treated, Figure 4.8 A ◆), DHBV levels in the serum were decreased by 83.0% by day 2, and 48.4% by day 4, compared to the pre-surgical levels. Duck 63 (ZPF18A-treated, Figure 4.8 A ▲) had DHBV levels decrease by 35.7% on day 2 and 38% by day 4 compared to pre-surgical levels.

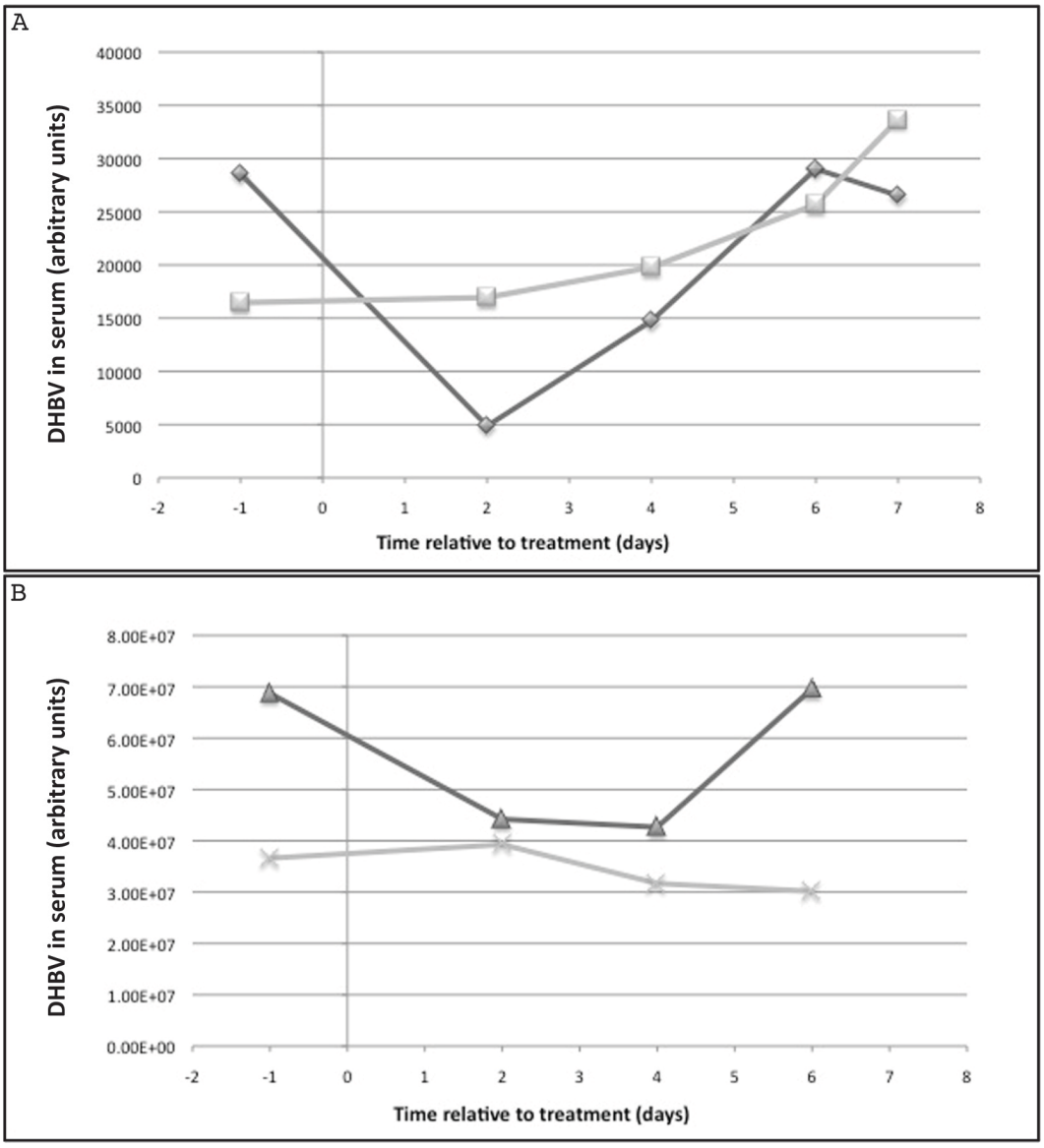

Figure 4.8 - Quantification of the DHBV serum levels of ducks treated with ZFP-polyplexes in experiment 1.
Four ducklings were injected into the portal vein with 150-µL of ZFP18A-polyplexes (duck 4 ◆ & duck 63 ▲) or ZFP18cA-polyplexes (duck 41 ■ & duck 69-1 ×). From days -1 to 7 relative to surgical treatment, blood was collected and DHBV levels were assessed by dot blot (A) or semi-quantitative PCR (B).

By day 6, both animals had returned to pre-surgical levels. In contrast, the ZFP18cA-polyplex treated animals exhibited no decrease in the amount of DHBV in the serum by day 2. There started to be some variability in the amount of DHBV in the blood by day 4 and 6; duck 41 (Figure 4.8 B ■) had DHBV levels

increase by 20.3% and duck 69-1 (Figure 4.8 B ×) decreased by 13.5%. This variance is likely due to natural changes in DHBV levels in the ducks throughout their infection (6). There was no statistical difference between the ZFP18A- versus ZFP18cA-treated ducks, however the data suggested that with greater numbers of animals a trend might be identified.

Next, four animals were similarly treated in "experiment 2", except they were monitored at 12 hour intervals over 24 or 48 hours. Two animals (duck 86-1, duck 91) were treated with 150-μL of ZFP18A-polyplex and two animals (duck 22, duck 26) were treated with 150-μL of ZFP18cA-polyplex. Ducks were monitored 24-hours prior to surgical treatment, and then at 12-hour intervals thereafter. Blood was collected and DHBV levels were assessed by dot blot, which was quantified using arbitrary units and plotted against time (Figure 4.9 A). Two ducks (duck 86-1, duck 22) were euthanized at 24-hours post-surgery and two (duck 91, duck 26) were euthanized at 48-hours post-surgery. With the examination of time points closer to the surgery, it became evident that the decreases in DHBV levels observed in the serum of ducklings treated with ZFP18A-polyplexes was also occurring in the ducklings treated with the control ZFP18cA-polyplexes, albeit to a lesser degree (Figure 4.9 A). The amount of DHBV in the serum of ZFP18A-treated ducks started to decrease between 12- and 24-hours post-surgery. Duck 86-1 (Figure 4.9 A ◆) and duck 91 (Figure 4.9 A ▲) had DHBV levels drop by 47.8% and 74.4%, respectively, at the 24-hour time point, compared to the pre-surgical levels. Duck 86-1 was euthanized at the 24-hour time point, but duck 91 was monitored for a further 24-hours. By 36-hours post-surgery, duck 91 retained DHBV decreases of 68.3%, but by 48-hours, viral rebound was occurring, because DHBV levels were only decreased by 47.7% at that point. In comparison, the ZFP18cA-treated ducklings also demonstrated decreases in DHBV levels by the 12- and 24-hour time points. Duck 22 (Figure 4.9 A ■) and duck 26 (Figure 4.9 A ×) had decreases of 37.1% and 68.1%, respectively, at 12-hours, and 62.0% and 71.5%, respectively, at 24-hours, compared to pre-surgical levels. These decreases are equivalent to that seen in the

ZFP18A-treated ducks – there was no statistical difference between the means of the two groups at any time point. Duck 22 was euthanized at the 24-hour time point, but duck 26 was monitored for a further 24-hours. By 36-hours post-surgery, duck 26 demonstrated DHBV levels 55.9% lower than pre-surgical levels. Viral rebound was occurring by 48-hours post-surgery in duck 26, because DHBV levels were back up to 87.7% of pre-surgical levels. Since both ZFP18A-treated and control ZFP18cA-treated animals were exhibiting decreases in DHBV levels, this suggested that the treatment with ZFP-polyplexes was not acting specifically. This non-specific effect was highlight in the next experiment ("experiment 3") where the dose was quadrupled to 600-μL of ZFP-polyplex (88 copies/hepatocyte).

Two animals (duck 82, duck 421) were treated with 600-μL of ZFP18A-polyplex and two animals (duck 69-3, duck 97) were treated with 600-μL of ZFP18cA-polyplex in "experiment 3". These animals were monitored at 24-hour intervals by collecting serum and assessing the levels of DHBV by dot blot quantification. As seen in Figure 4.9 B, injection of a larger volume of ZFP-polyplex, whether ZFP18A or ZFP18cA, resulted in dramatic decreases in DHBV in the serum at 24- and 48-hours post-surgical treatment. By 24-hours post-treatment, the decreases in DHBV levels were as follows: 76.6% for duck 421 (Figure 4.9 A ◆), undetectable (100%) for duck 82 (Figure 4.9 A ▲), 75.6% for duck 69-3 (Figure 4.9 A ■) and 72.7% for duck 97 (Figure 4.9 A ×). Duck 421 and 69-3 were euthanized at the 24-hour time point, but duck 82 and duck 97 were monitored for a further 24-hours. At 48-hours post-surgery, duck 82 and duck 97 had DHBV levels at 93.6% and 68.4%, respectively, compared to pre-surgical levels. There was no statistical difference between the treatments at any time point.

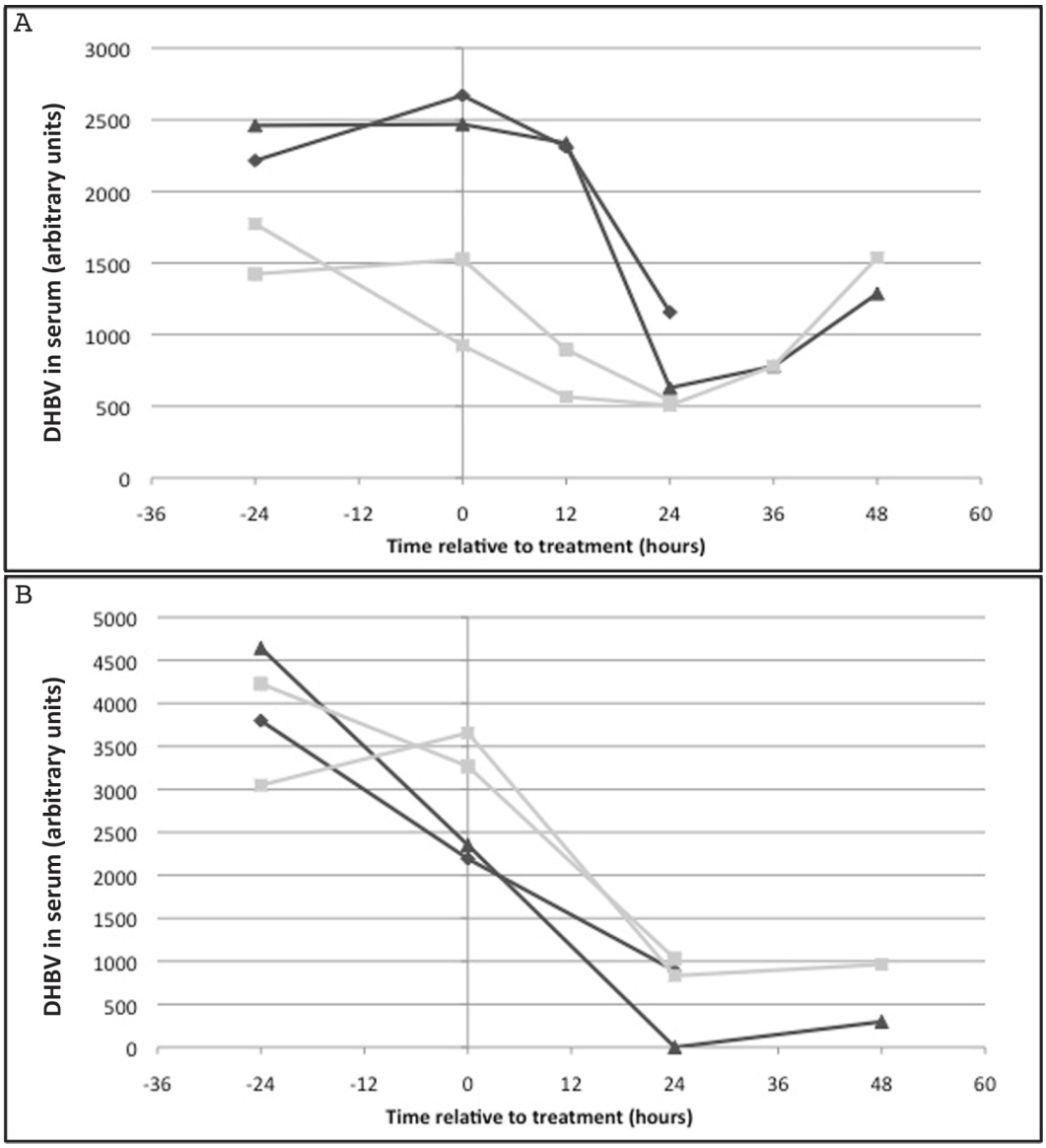

Figure 4.9 - Quantification of the DHBV serum levels of ducks treated with ZFP-polyplexes in experiment 2 & 3.

(A) Four ducklings were injected into the portal vein with 150-µL of ZFP18A-polyplexes (duck 86-1 ◆, duck 91 ▲) or ZFP18cA-polyplexes (duck 22 ■, duck 26 ×). 24-hours prior to surgery and at 12-hour intervals after surgical treatment, blood was collected and DHBV levels were assessed by dot blot. (B) Four ducklings were injected into the portal vein with 600-µL of ZFP18A-polyplexes (duck 421 ◆, duck 82 ▲) or ZFP18cA-polyplexes (duck 69-3 ■, duck 97 ×). 24-hours prior to surgery and at 12-hour intervals after surgical treatment, blood was collected and DHBV levels were assessed by dot blot. There was no statistical difference between the treatments at any time point.

Seven animals were used for control experiments. Two animals, duck 67 and duck 100, were untreated with no surgery and were euthanized along with the following controls. The DHBV levels in these two ducks were not monitored. Two animals (duck 412 and duck 80) were injected with 600-μL of 1X PBS. One animal (duck 86-2) was injected with 600-μL of chitosan in 97% sucrose. This is the structural component of the polyplexes, without the plasmid DNA associated. Two animals were injected with 600-μL of plasmid DNA alone in 1X PBS, without the chitosan of the polyplexes: duck 25 was injected with 90-μg of pcDNA3.1(+)-ZFP18A and 18-μg of mlacZ and duck 72 was injected with 90-μg of pcDNA3.1(+)-ZFP18cA and 18-μg of mlacZ. These amounts replicate the concentration of plasmid injected into the ducks when in the polyplex form, based upon the 600-μL dose. The control animals were monitored 24-hours prior to and 24-hours after surgery by dot blot (Figure 4.10 A) or semi-quantitative PCR (Figure 4.10 B). In general, there was little change in DHBV levels of control animals. One of the two PBS-treated animals had no change in DHBV levels at 24-hours post-surgery (duck 80, Figure 4.10 B ●) and the other animal had a decrease of 61% at 24-hours post surgery (duck 412, Figure 4.10 A ◆), compared to pre-surgical levels. The chitosan-treated duck had no change in DHBV levels due to surgery (duck 86-2, Figure 4.10 B ×). The two ducks treated with plasmid DNA alone had small decreases. Duck 25 was treated with pcDNA3.1(+)-ZFP18A/mlacZ and had an 8.0% decrease in DHBV levels by 24-hours (Figure 4.10 A ■). Duck 72 was treated with pcDNA3.1(+)-ZFP18cA/mlacZ and had a 27.1% decrease compared to pre-surgical levels (Figure 4.10 A ▲).

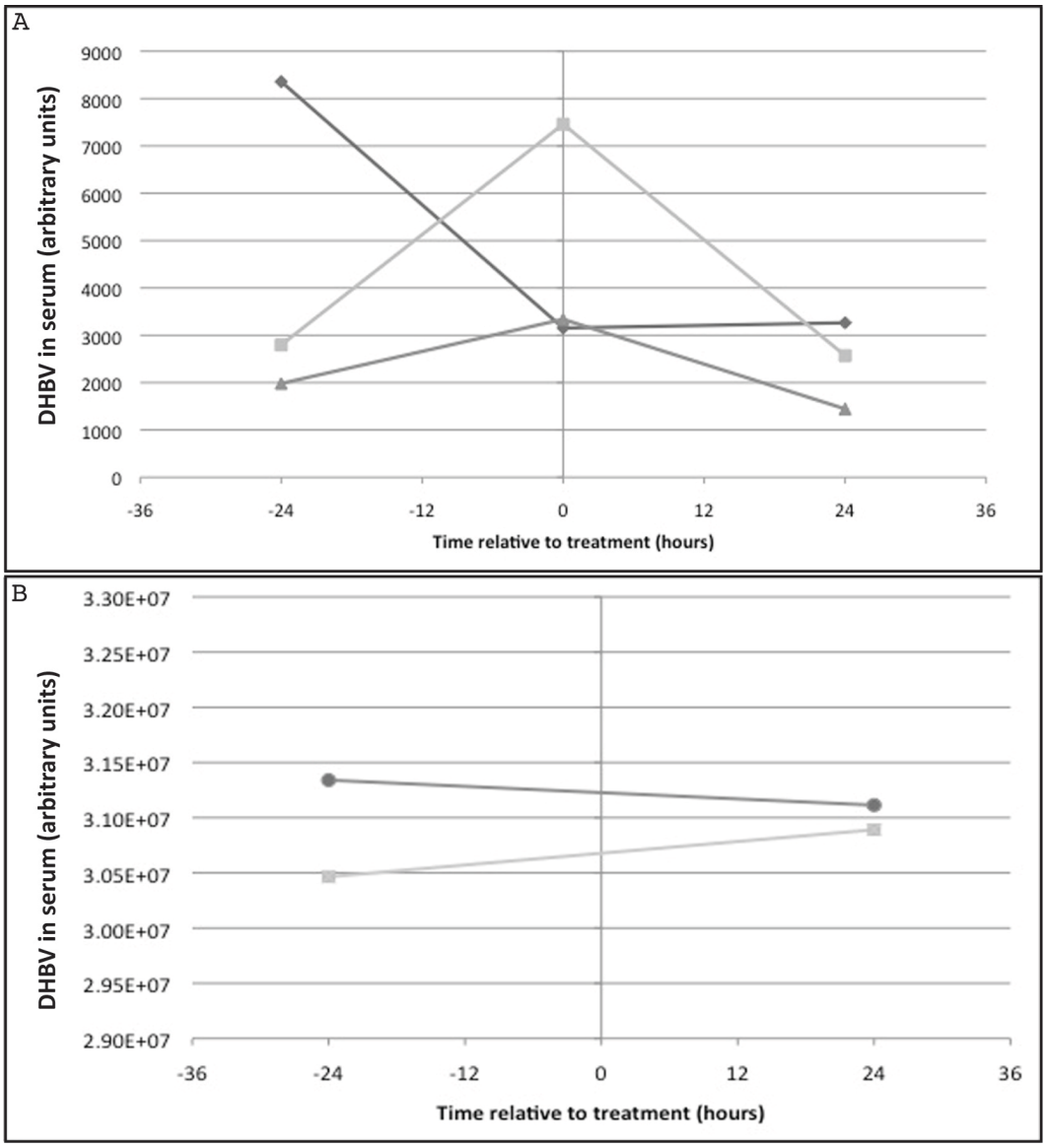

Figure 4.10 - Quantification of the DHBV serum levels of control ducks.
Control ducks were injected into the portal vein with 600-µL of PBS (duck 412 ◆, duck 80 ●), 600-µL of chitosan alone in 97% sucrose (duck 86-2 ×), 600-µL of pcDNA3.1(+)-ZFP18A/mlacZ DNA in 1X PBS (duck 25 ■) or 600-µL of pcDNA3.1(+)-ZFP18cA/mlacZ DNA in 1X PBS (duck 72 ▲). At 24 hours prior and 24 hours after, blood was collected and DHBV levels were assessed by dot blot (A) or semi-quantitative PCR (B). There was no statistical difference between the treatments at any time point.

In general, it appears that injection of the ZFP-polyplexes causes the decrease in DHBV levels in the serum of ducks. The individual components (chitosan or plasmid DNA) had little effect on the levels of DHBV. PBS treatment had a small

effect, suggesting that the surgery and/or the injection might be responsible for some of the decrease of DHBV.

4.3.5 Western blot assessment of DHBV and ZFP protein expression in duck liver

Pieces of liver from polyplex-treated ducks were collected at the time of euthanisia to assess the protein expression levels after treatment. Western blots were performed to detect ZFPs, DHBV core and preS proteins, and actin as a loading control. The animals in experiment 1 were euthanized 7 days post-treatment, after viral rebound had occurred, Western blots were not performed on these animals because it was not anticipated that any effect on DHBV protein levels would be observed. Western blots for animals from experiment 2 (Figure 4.11 A) and experiment 3 (Figure 4.11 B) do not show any detectable ZFP protein expressed in the liver of treated animals. Experiment 2 animals also show a variable amount of DHBV core and preS proteins (Figure 4.11 A), although there does not appear to be any consistency between the expression of the two DHBV proteins in each liver piece. For example, duck 86 has low core protein levels, yet high preS levels. Duck 26 has the opposite pattern. The loading control, actin, shows relatively equal loading of protein. There appears to be no difference in DHBV protein levels depending on the time of euthanasia. Duck 86 and duck 22 were euthanized at 24-hours post-treatment, whereas duck 91 and duck 26 were euthanized at 48-hours post-treatment. All animals had approximately the same amount of decrease in DHBV at euthanasia except duck 26, which had higher levels of DHBV at euthanasia. This might correlate with the higher level of DHBV core in duck 26, but is contrary to the amount of preS in the liver piece. Western blots of the animals from experiment 3 (Figure 4.11 B) do not show the same trend seen in experiment 2. Across all the animals treated, there is an equivalent level of DHBV core and preS produced.

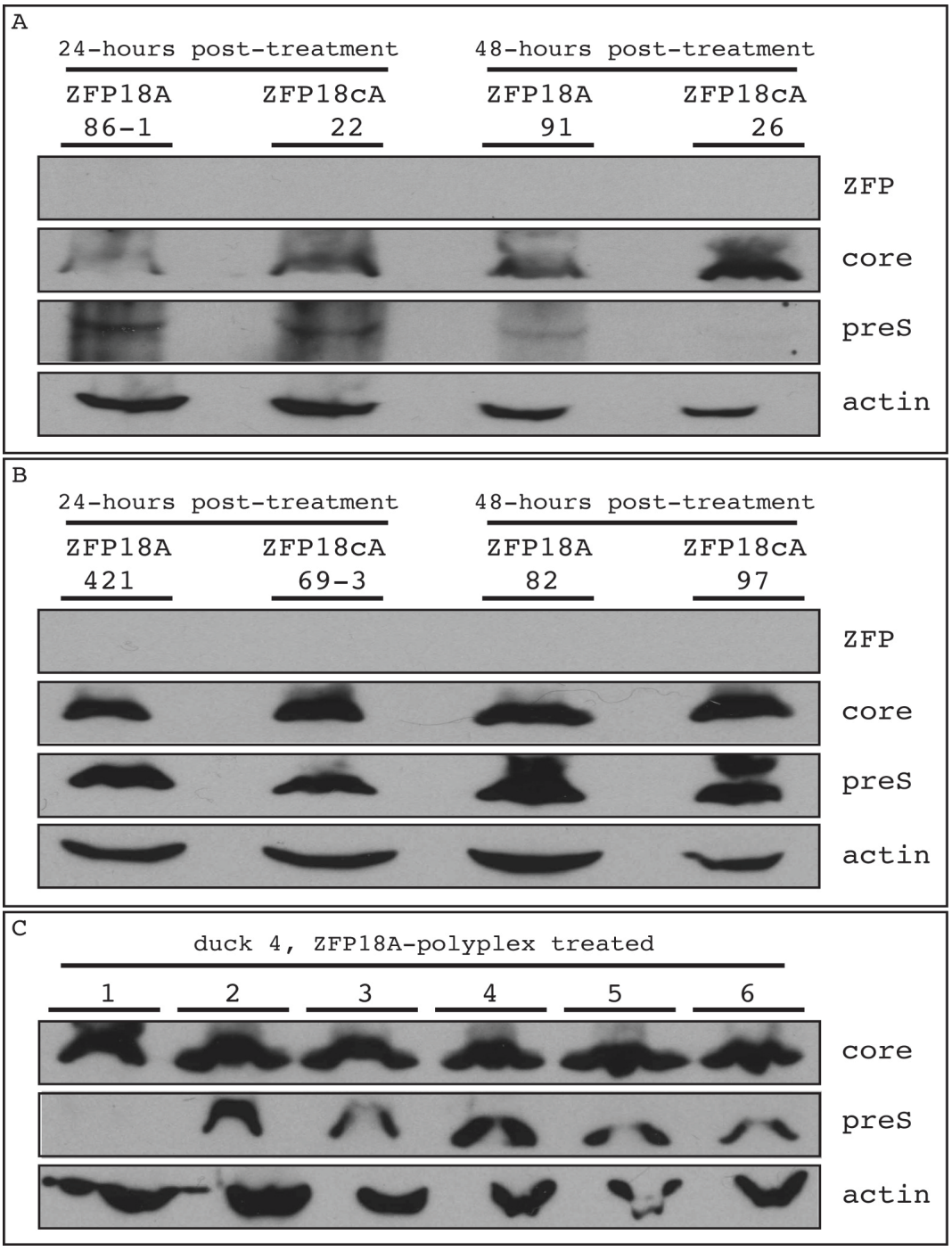

Figure 4.11 - Western blots on liver lysates from ZFP-polyplex treated ducks. Western blots were performed on liver lysates from ducks from experiment 2 (A), experiment 3 (B) or from duck 4 (C). Anti-ZFP antiserum, anti-DHBV core (J112), anti-DHBV preS (1H1) and anti-actin antibodies were used. Ducks were euthanized at the indicated time points post-treatment (A, B) and duck 4 was euthanized at 7 days post-treatment (C). The type of treatment (ZFP18A-polyplex versus ZFP18cA-polyplex) is labeled above each lane (A, B).

Because the liver is a large and diverse organ, several pieces of liver from one animal (duck 4) were assessed by Western blot, to evaluate possible differences in protein expression (Figure 4.11 C). Actin was used as a loading control. DHBV core and preS were assessed in six different pieces. The levels of preS appeared to vary to a greater extent than the amount of core in liver pieces (Figure 4.11 C). For example, piece 1 from duck 4 had barely detectable preS protein compared to piece 2, but their core protein levels were relatively equivalent. This suggests that there is a heterogeneous distribution of DHBV proteins in the liver, and while comparing one piece of liver from one animal to one piece of liver from another animal is convenient, it likely does not give an accurate picture of the entire organ. However, liver pieces were selected from regions surrounding large vascular vessels, which should provide the most relevant picture of the therapeutic effects on DHBV in liver tissue: after injection of the ZFP-polyplexes into the portal vein, it is reasonable to assume the cells closest to the blood vessels carrying the ZFP-polyplexes would get the greatest proportion of therapeutics.

Analysis of protein expression by Western blot failed to demonstrate a trend that showed any therapeutic difference between ZFP18A-polyplex-treated versus ZFP18cA-polyplex-treated animals. However, there was a non-specific decrease in DHBV in the serum, regardless of which polyplex was used to treat the animals.

4.3.6 β–galactosidase assessment of lacZ expression in the liver of ZFP-polyplex treated ducks

Western blots of duck liver did not show any ZFP expression in the liver of ZFP-polyplex-treated ducks. Two methods based upon the marker plasmid, mlacZ, were employed to test for uptake of polyplexes and gene expression from the associated plasmid. mlacZ was included in the polyplex preps at one fifth the amount of the pcDNA3.1(+)-ZFP18A or –ZFP18cA plasmids. Expression of β-Gal from mlacZ was assessed by staining frozen liver sections with the X-gal reagent, or by an ONPG colorimetric assay of liver lysates.

Frozen sections of liver were stained with X-Gal to detect β–Gal activity, and counterstained with nuclear fast red. Representative images for duck 22 (Figure 4.12 A) and duck 26 (Figure 4.12 B) showed no sign of β–Gal activity, which would be visible as dark blue spots (counterstain is pink). No obvious strong expression of β–Gal from mlacZ was detected by staining of tissue sections. An ONPG colorimetric assay was performed to re-test this result. Liver pieces were homogenized and tested for the presence of β–Gal by the ability of the lysates to hydrolyze ONPG into galactose and the yellow ortho-nitrophenol compound, which is measured on a spectrophotometer at 420-nm. There was no increase in β–Gal activity in the livers of ducks treated with ZFP-polyplexes (Figure 4.12 C, ZFP18A-polyplex: dark grey bars. ZFP18cA-polyplex: light grey bars) compared to control ducks (white bars). With the Western blot data showing no ZFP expression, and the X-Gal staining and ONPG assays showing no β–Gal activity, it is suggestive that either the polyplexes failed to deliver the associated plasmids into the hepatocytes, or the plasmids failed to express their respective proteins. Since all three plasmids contained within the ZFP-polyplex complex express their genes-of-interest through the strong CMV promoter, it seems more likely that the polyplexes failed to deliver the plasmids into the hepatocytes.

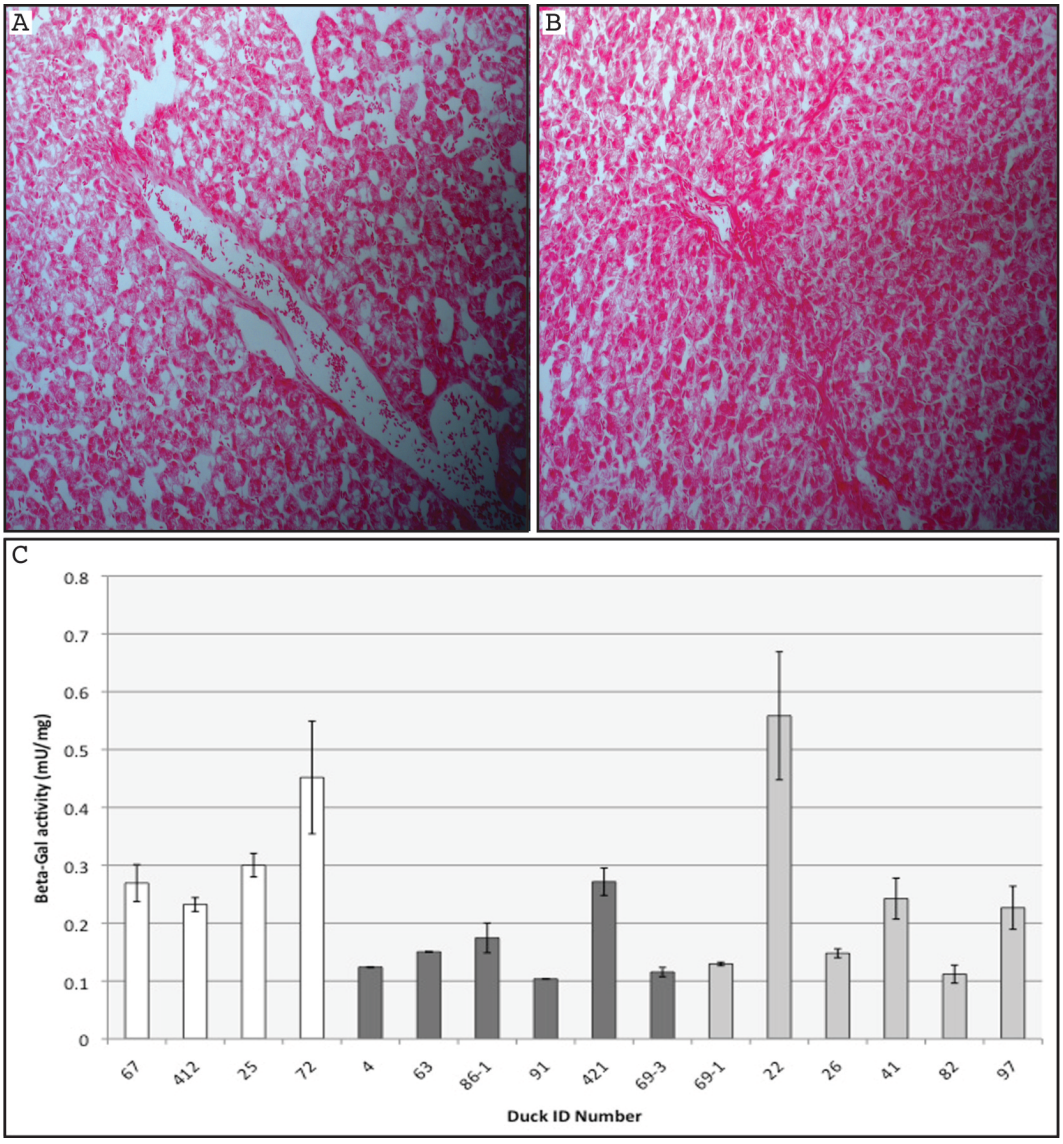

Figure 4.12 - Assessment of β-Gal activity in the liver of ZFP-polyplex treated ducks.

Pieces of duck liver from duck 22 (A) or duck 26 (B) were frozen, sectioned, stained with X-Gal for β-Gal activity (dark blue) and counterstained with nuclear fast red (pink). (C) Pieces of duck liver from experiments 1 – 3 and control ducks were used for an ONPG colorimetric assay measuring β-Gal activity. The bars indicate the means of duplicate wells and the error bars represent the standard deviation. Control ducks are shown in white bars, ZFP18A-polyplex-treated ducks are shown in dark grey bars and ZFP18cA-polyplex-treated ducks are shown in light grey bars. The ONPG assay was repeated twice.

4.3.7 Assessment of the type I interferon response in the liver of ducks treated with ZFP-polyplexes

Total RNA was isolated from liver pieces from polyplex-treated ducks and converted into cDNA for quantitative and standard PCR analyses. The duck genome has not been sequenced; therefore the innate immune genes that can be examined are quite limited. Primer sets for duck interferon-α (IFN-α), duck interleukin 1-β (IL1β), avian 2'-5'-oligoadenylate synthetase 1 (OAS1), avian guanylate-binding protein (GBP) and duck GAPDH were developed in house. Other primer sets designed for IFN-β, CD4, CD8, myxoma resistant GTPase (Mx), interferon stimulated gene 20 (ISG-20), ISG-15, IL-6 and dsRNA-dependent protein kinase (PKR) were not successful at identifying a duck homologue.

Quantitative PCR was performed on the isolated cDNA for duck IFN-α, duck IL1β and duck GAPDH. Measurements were normalized to GAPDH and compared to the non-surgical control duck, duck 67 (Figure 4.13). Strikingly, all animals that underwent a surgical procedure, whether injected with saline, plasmid DNA or ZFP-polyplex, had a 4 to 8 log increase in IFN-α production in the liver (Figure 4.13 A). There didn't appear to be any difference between animals treated with ZFP18A-polyplex (dark grey bars) versus ZFP18cA-polyplex (light grey bars). Interestingly, by day 7 post-surgery, as for ducks 4, 41, 63 and 69-1, IFN-α levels remained high, even though viral levels were rebounding by that point in these animals. The same pattern was not observed for IL1β - in general, animals that underwent a surgical event had lower levels of IL1β transcript than the non-surgical animal.

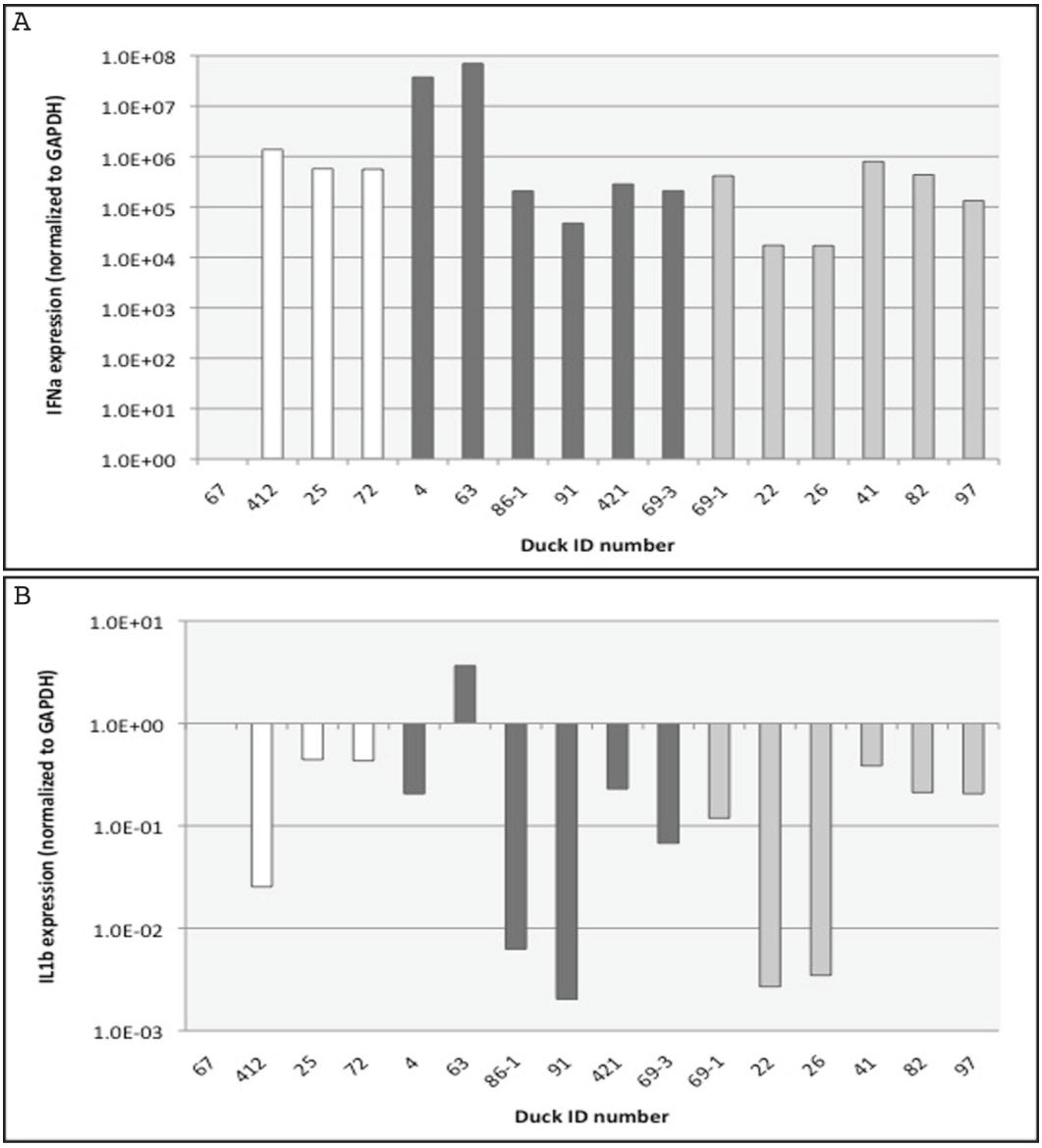

Figure 4.13 - Quantitative PCR for IFN-α and IL1β expression in the liver of ducks treated with ZFP-polyplexes.
Quantitative PCR for duck IFN-α, IL1β and GAPDH was performed on cDNA from duck liver pieces. IFN-α and IL1β measurements were normalized to GAPDH and compared to the non-surgical control duck, duck 67. Control ducks are shown in white bars, ZFP18A-polyplex-treated ducks are shown in dark grey bars and ZFP18cA-polyplex-treated ducks are shown in light grey bars.

Standard PCR was performed with the remaining primers, to gain an indication of their general levels in different animals. As seen in Figure 4.14, OAS was not detected in any of the liver samples. GBP was variably detected, again with no trend. GAPDH was used as a loading control. This data suggests that while there

was a large increase of IFN-α transcript in the liver of surgically-treated ducks, there was no similar trend in the other type I interferon genes detected by PCR.

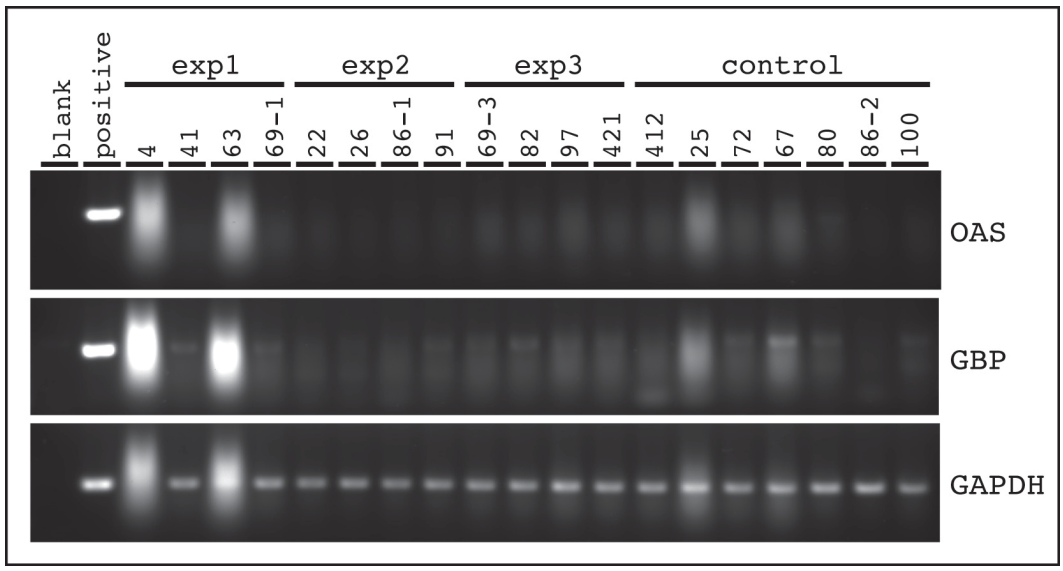

Figure 4.14 – PCR analysis on duck liver for the expression of duck OAS, GBP and GAPDH.
Total RNA was isolated from duck liver and made into cDNA. Standard PCR was performed using primers for OAS, GBP or GAPDH as a loading control. PCR products were separated on agarose gel and visualized using EtBr and UV light.

4.4 Discussion

The AdEasy adenovirus system proved to be a difficult method to work with, limiting my ability to use adenoviruses to deliver the ZFPs. The initial cloning of the ZFPs into pAdTrack-CMV1 was quite difficult, since directional cloning failed a number of times. Moreover, the recombination event with pAdEasy-1 was challenging as well. Although this system claims it is an easy technique for developing recombinant adenovirus vectors, the system could be further optimized to make it more practical for use. First of all, the visual map of the MCS in pAdTrack-CMV1 lists the restriction sites in a different order than in the actual plasmid, as examined in a sequencing program. I could not be confident that the two restrictions sites I was using were actually in the correct orientation for successful ligation of the insert. Secondly, the recombination event of pAdTrack-CMV1 and pAdEasy-1 in the bacteria is an inefficient process. I overcame this by purchasing the BJ5183-AD-1 *E.coli* directly from the company,

which increased the recombination frequency since the pAdEasy-1 plasmid was already found within these bacteria. Lastly, the inability for me to obtain infectious adenoviruses that carried the ZFP genes was puzzling – it would be surprising if this phenomenon were caused by a toxicity problem, especially considering the absence of toxicity during transfection of ZFPs into LMH cells and Huh7 cells in Chapters 2 & 3. Additionally, Rebar *et al* (2002) have used adenoviruses, and indeed the AdEasy-1 system, to deliver ZFPs to cell lines and even a mouse model (7). Therefore it was surprising that the DHBV- and HBV-specific ZFPs were so difficult to work with in the AdEasy-1 system in my hands.

Utilization of baculoviruses to deliver the ZFPs appeared to be a promising approach based on the ease of cloning and viral production. However, an unexpected barrier was encountered when it was observed that DHBV either excludes secondary infection of baculoviruses or prevents gene expression of the ZFPs from the baculoviruses. DHBV has been shown to exclude superinfection of itself, but not for other viruses including adenoviruses, herpes simplex virus-1 and vesicular stomatitis virus (1). It is unclear why DHBV might block the infection of the baculoviruses. The receptor for entry for baculoviruses is unidentified, but perhaps DHBV infection downregulates the expression of the unidentified cell surface receptor for baculovirus infection. DHBV is hypothesized to exclude superinfecting DHBV particles by shuttling incoming nucleocapsids into the secretory pathway, due to an excess amount of surface proteins found in the cell once infection is established (8). It seems unlikely that a similar mechanism is at work regarding baculovirus infection, since the nucleocapsids of baculovirus would not associate with the DHBV surface proteins. Baculoviruses could be used to deliver the ZFPs into PDHs prior to infection with DHBV to test their prophylactic capabilities, however the goal of this project was to target the pre-existing pool of cccDNA in the nucleus of cells. Therefore, pre-treatment of the cells with ZFPs negates the purpose of developing a therapeutic to target cccDNA.

The chitosan-based polyplexes used to deliver the plasmids to the duck liver were developed using a proprietary recipe and protocol by Engene Inc. Chitosan is a polysaccharide composed of linear β-(1-4)-linked monosaccharides (9). It is made by the deacetylation of chitin, a chemically inert polysaccharide found abundantly in marine crustaceans (9). Compared to a number of other natural polymers, chitosan is positively charged, making it useful in pharmaceutical applications (9). Chitosan polymers can be incredibly large in size, and the cross-linking of different size chitosan polymers directly impacts the size of the nanospheres produced (10). Chitosan is also favorable for therapeutic use because it does not cause allergic reactions or rejection, and it slowly degrades into harmless products which are absorbed by the body (9).

Chitosan is useful for gene therapy approaches because it masks the negative charge on the plasmid DNA and delivers it to the negatively charged cell membrane. Chitosan nanospheres also protect the DNA from degradation by extracellular nucleases (10). The DNA is tightly packed within the chitosan nanospheres, and it is thought that the positively charged nanospheres aggregate together and facilitate cell contact, enhancing delivery of the cargo (10).

Chitosan-based polyplexes have been used in other models for gene delivery. Leong *et al* (1998) compared transfection protocols using lipofectamine, calcium phosphate and chitosan nanospheres (11). They found that the nanospheres could transfect different cell lines to varying degrees, although in general it appeared to have lower transfection efficiencies than the other two transfection reagents (11). For example, transfection of 293 cells with nanospheres resulted in 6% positive cells, as compared to 20% with lipofectamine and 15% with calcium phosphate. Similarly in B7-1 cells, 10% were transfected with nanospheres, 37% with lipofectamine and 50% with calcium phosphate (11). Erbacher *et al* (1998) compared chitosan nanosphere transfection to polyethylenimine-mediated transfection in HeLa cells (12). HeLa cells were efficiently transfected with the nanospheres, and exhibited prolonged expression of the reporter gene compared

to the polyethylenimine transfection method (12). These studies show that even in tissue culture, chitosan-based nanospheres are not necessarily better at transfection than traditional reagents. However, they do offer a non-viral method for gene delivery *in vivo*. Despite their potential for gene delivery, delivery of ZFPs to the duck liver was not observed in our studies. There are a number of reasons why the ZFP-polyplexes were unsuccessful in the duck model, as discussed below.

It is unclear what size of nanospheres is optimal for efficient transfection of cells. Nakanishi and Noguchi (2001) have shown that the optimal particle size of chitosan microspheres for gene delivery is 400-nm to 1400-nm (13). MacLaughlin *et al* (1998) found microspheres ranging in size from 80-nm to 500-nm during a transfection protocol (14), while Erbacher *et al* (1998) had particles with sizes between 1000-nm and 5000-nm (12). The ZFP-polyplexes used in the duck model ranged in size from 113-nm to 127-nm, which is much smaller than any micromolar sized particles, but within the range of the study by MacLaughlin *et al* (1998) (14). Therefore, it is difficult to tell if the size of the ZFP-polyplexes is a factor in the transfection efficiency of the cells, since the ideal characteristics for transfection with chitosan nanospheres is not clear and appears to vary depending on the system.

The pH of the medium can play a role in the transfection efficiency of chitosan microspheres. Sato *et al* (2001) found that transfections were better at a slightly acidic pH of 6.9, compared to pH 7.6 (15). The pH of human blood is between 7.35 and 7.45, although the blood pH of ducks is not known. It is likely similar to that of humans, suggesting that the pH of blood is not optimal for transfection with the ZFP-polyplexes. Additionally, the positive charge of the chitosan may result in interactions with different blood components, leading to opsonisation by the reticulo-endothelial system (16). Blood monocytes were transfected only 9% by nanospheres in tissue culture, therefore ZFP-polyplexes injected into the bloodstream would not be expected to greatly affected by any potential off-target

transfection effects within the blood (10). In summary, a number of factors may have affected the ability of the ZFP-polyplexes to enter the liver tissue and express the delivered plasmids.

The innate immune response to portal vein injection of ZFP-polyplexes appears to support the histological and biochemical evidence that plasmid DNAs were not delivered into the cytoplasm of hepatocytes. TLR9 on hepatocytes can recognize extracellular plasmid dsDNA as a pathogen associated molecular pattern (PAMP), based upon the CpG content arising from production in *E.coli* (17). This recognition event can transmit a signal cascade to induce the production of type I interferons, including IFN-α (17). The low levels of IL1β further support the suggestion that the delivered plasmid DNA stayed external to the cytoplasm. The presence of DNA in the cytoplasm of cells results in increased transcription of IL1β, which was not observed (17). IL1β is an inflammatory response mediator and plays a role in cell proliferation, differentiation and apoptosis (18). The presence of cytoplasmic DNA, detected by as yet unidentified DNA receptors, can result in the transcriptional up-regulation of the pro-cytokines pro-IL1β and pro-IL-18 (17, 18). These pro-cytokines are subsequently activated by the recognition of cytoplasmic DNA by the AIM2-inflammasome (18). IFN-α levels were high and IL1β levels were low in the liver. These results strongly support the hypothesis that the polyplexes failed to deliver the plasmid DNA into the cytoplasm of the hepatocytes.

Despite the high levels of IFN-α detected in the liver of surgically-treated ducks, there was no apparent up-regulation of OAS in these animals. OAS up-regulation would be expected because IFN-α binds to the IFN receptor complex IFNAR1 and IFNAR2 to stimulate the Jak/STAT pathway (19). Activation of the Jak/STAT pathway leads to the transcription of a number of IFN-stimulated genes (ISG) including OAS, PKR, Mx and RNA-specific adenosine deaminase (ADAR) (19). Unfortunately, primers could not be developed to detect most of these transcriptional products, therefore a fuller picture of the innate immune

environment is not yet available. It is not clear why high levels of OAS were not detected, but the primers developed may not be optimal to detect the endogenous OAS transcripts from the duck liver.

GBP is a GTPase that is induced by IFN-γ signaling through the IFNγR (20). Although the mechanism of antiviral activity for the family of GBP proteins is not entirely elucidated, it appears that it might limit viral spread by limiting cell proliferation (20). The low levels of GBP found in the duck liver suggest that IFN-γ was not produced in response to the surgical event.

In summary, a number of difficulties were faced in utilizing the duck model to test the *in vivo* and *ex vivo* efficacy of the ZFPs as therapeutics. Construction of viral vectors for delivery resulted in the inability to produce ZFP-producing clones, as the case with the adenoviruses, or the inability to infect DHBV-infected PDHs, as for the baculoviruses. Lastly, it appears that chitosan-based nanospheres to elicit gene delivery into the duck liver is not an ideal delivery method, since the method of portal vein injection of ZFP-polyplexes did not result in viral clearance specifically due to the expression of the therapeutic ZFPs.

4.5 References

1. Walters KA, Joyce MA, Addison WR, Fischer KP, & Tyrrell DL (2004) Superinfection exclusion in duck hepatitis B virus infection is mediated by the large surface antigen. *J Virol* 78(15):7925-7937.
2. Sambrook J FE, Maniatis T. (1989) Strategies for Studying Gene Regulation. *Molecular Cloning: A Laboratory Manual*, ed Nolan C (Cold Spring Harbor Laboratory Press, USA), 2 Ed Vol 2, pp 16.56-16.67.
3. He TC, Zhou S, da Costa LT, Yu J, Kinzler KW, & Vogelstein B (1998) A simplified system for generating recombinant adenoviruses. *Proc Natl Acad Sci U S A* 95(5):2509-2514.
4. Nishibe Y, Kaneko H, Suzuki H, Abe T, Matsuura Y, & Takaku H (2008) Baculovirus-mediated interferon alleviates dimethylnitrosamine-induced liver cirrhosis symptoms in a murine model. *Gene Ther* 15(13):990-997.
5. Song J, Liang C, & Chen X (2006) Transduction of avian cells with recombinant baculovirus. *J Virol Methods* 135(2):157-162.
6. Addison WR, Walters KA, Wong WW, Wilson JS, Madej D, Jewell LD, & Tyrrell DL (2002) Half-life of the duck hepatitis B virus covalently

closed circular DNA pool in vivo following inhibition of viral replication. *J Virol* 76(12):6356-6363.
7. Rebar EJ, Huang Y, Hickey R, Nath AK, Meoli D, Nath S, Chen B, Xu L, Liang Y, Jamieson AC, Zhang L, Spratt SK, Case CC, Wolffe A, & Giordano FJ (2002) Induction of angiogenesis in a mouse model using engineered transcription factors. *Nat Med* 8(12):1427-1432.
8. Walters KA (2003) Superinfection Exclusion in Duck Hepatitis B Virus Infection. Doctor of Philosophy (University of Alberta, Edmonton).
9. Agnihotri SA, Mallikarjuna NN, & Aminabhavi TM (2004) Recent advances on chitosan-based micro- and nanoparticles in drug delivery. *J Control Release* 100(1):5-28.
10. Guang Liu W & De Yao K (2002) Chitosan and its derivatives--a promising non-viral vector for gene transfection. *J Control Release* 83(1):1-11.
11. Leong KW, Mao HQ, Truong-Le VL, Roy K, Walsh SM, & August JT (1998) DNA-polycation nanospheres as non-viral gene delivery vehicles. *J Control Release* 53(1-3):183-193.
12. Erbacher P, Zou S, Bettinger T, Steffan AM, & Remy JS (1998) Chitosan-based vector/DNA complexes for gene delivery: biophysical characteristics and transfection ability. *Pharm Res* 15(9):1332-1339.
13. Nakanishi M & Noguchi A (2001) Confocal and probe microscopy to study gene transfection mediated by cationic liposomes with a cationic cholesterol derivative. *Adv Drug Deliv Rev* 52(3):197-207.
14. MacLaughlin FC, Mumper RJ, Wang J, Tagliaferri JM, Gill I, Hinchcliffe M, & Rolland AP (1998) Chitosan and depolymerized chitosan oligomers as condensing carriers for in vivo plasmid delivery. *J Control Release* 56(1-3):259-272.
15. Sato T, Ishii T, & Okahata Y (2001) In vitro gene delivery mediated by chitosan. effect of pH, serum, and molecular mass of chitosan on the transfection efficiency. *Biomaterials* 22(15):2075-2080.
16. Basarkar A & Singh J (2007) Nanoparticulate systems for polynucleotide delivery. *Int J Nanomedicine* 2(3):353-360.
17. Hornung V & Latz E (2010) Intracellular DNA recognition. *Nat Rev Immunol* 10(2):123-130.
18. Bryant C & Fitzgerald KA (2009) Molecular mechanisms involved in inflammasome activation. *Trends Cell Biol* 19(9):455-464.
19. Yoneyama M & Fujita T (2010) Recognition of viral nucleic acids in innate immunity. *Rev Med Virol* 20(1):4-22.
20. MacMicking JD (2004) IFN-inducible GTPases and immunity to intracellular pathogens. *Trends Immunol* 25(11):601-609.

5 Chapter 5: General Discussion, Conclusions and Future Directions

This thesis proposes a novel method to directly target the cccDNA of HBV, by utilizing the specificity and affinity of ZFPs for target DNA. cccDNA is currently not directly targeted by therapeutics. Its long half-life allows it to endure throughout antiviral therapy, such that the viral reservoir is maintained in infected hepatocytes when therapy is stopped. The infection is reactivated from the cccDNA, since all viral transcription occurs from this viral episome.

A subset of the designed ZFPs demonstrated the ability to bind their target sequences with high affinity. In the DHBV model system, the DHBV-specific ZFPs were able to discriminate between the target DNA sequence and host sequences, as demonstrated by their ability to specifically decrease the amounts of viral transcript and protein production. Unfortunately, similar experiments could not be performed with the HBV-specific ZFPs, since it was very difficult to transfect cell lines carrying an integrated copy of the HBV genome. This aspect of the project will be continued using ZFP-encoding baculoviruses to transduce HepG2.2.15 cells. Additionally, the baculoviruses can be used to transduce the *scid*-Alb/uPA chimeric mouse model, when these mice are infected with HBV.

The therapeutic ability of the ZFPs was tested in Pekin ducks, which were congenitally infected with DHBV. Chitosan-based nanospheres loaded with plasmid DNA encoding the DHBV-specific ZFPs were delivered directly to the infected duck liver by portal vein injection of the nanospheres. This process was utilized because the construction of adenoviruses as viral vectors was unsuccessful, and ZFP-encoding baculoviruses could not infect DHBV-infected PDH *ex vivo*. Although initial data from the treated ducks appeared promising, subsequent data demonstrated a non-specific viral decrease in treated animals, regardless of whether a DHBV-specific ZFP or a control ZFP was injected.

The use of ZFPs as a therapeutic in the future relies on the ability to deliver the ZFPs to the target liver. As a large protein, ZFPs are much more difficult to deliver than small molecule drugs, thus gene delivery is the most likely method to be used in the near future. Viral vectors offer the easiest and most efficient method of gene delivery. Viral vectors that have been used for gene expression include lentiviruses (LV), simplex virus (HSV), adeno-associated virus (AAV) and vaccinia virus (VV) (1). VV and LV are capable of infecting a wide range of cells, and AAV is capable of infecting muscle and liver, as well as other cell types (1).

AAV is a small non-enveloped virus with a linear dsDNA genome (2). In the presence of a helper virus, such as adenovirus or herpesvirus, AAV undergoes a productive infection cycle. In the absence of the helper, however, AAV will set up latency by integrating itself into a specific site within the host genome (2). This is the only virus know to do this, and its capability could allow for long-term transgene expression for insertional mutagenesis to correct diseases (2). However, current vectors do not encode for integrase activity, therefore it is not currently part of the AAV gene therapy protocol. AAV has become a vector of choice for liver-directed gene therapy because intrahepatic delivery in mice, dogs and non-human primates lead to long-term hepatic expression of the therapeutic gene (3). Further, AAV does not initiate a potent inflammatory response, likely because of low innate immunity to AAV and the inefficiency of AAV to infect dendritic cells or macrophages (3). However, AAV has some disadvantages, including a small capacity for transgene size, the requirement of helper virus in viral production, low rates of gene transfer and high rates of pre-existing immunity to the capsid protein (1, 3). Despite these limitations, AAV has been used in 38 protocols of human clinical trials (2), due to the discovery of new serotypes, the favorability of the long-term responses of gene delivery in animal models, and the targeting of gene therapy for specific organs to effect greater therapeutic benefit (2). Despite these clinical trials, no clinical cures have yet been reported (2).

LV is another viral vector widely used for gene delivery. Lentiviruses are members of the *Retroviridae* family, with the prototypic member being HIV-1 (4). LVs have a high efficiency of *in vivo* transduction, infect a large variety of cell types, and offer stable transgene expression via integration of the viral genome into the host genome (1). Individuals are unlikely to have pre-existing immunity to LVs, barring HIV positive subjects (3). However, the robust adaptive immune response to the LV-delivered transgene is a major problem for using LVs in the liver (3). This immune response arises because of an early innate response to the viral RNA, followed by an adaptive response against the transgene (3). This has been overcome by expressing a hematopoietic lineage micro-RNA that leads to the degradation of the transgene in antigen presenting cells (3).

VV is a member of the orthopoxvirus subfamily and has a large dsDNA genome. It has a number of advantages for its use during gene delivery, including its wide host range and ability to infect many types of cells (1, 5). It can also accommodate a very large transgene: up to 25-kb or more of foreign DNA has been inserted into the viral genome (1, 5). Further, it produces high levels of expressed protein and can be produced at high titres for use (5). However, like all virus vectors, VV has some disadvantages. It activates a very strong immune response to viral proteins, it has potential cytopathic effects and there are a large number of virally encoded proteins with unknown functions (5). Most individuals born after the 1970's have not been vaccinated for smallpox by VV, however, any older patients would be immune to VV (5). VV has most recently been used as an oncolytic virus for cancer virotherapy, and has been in several clinical trials for treating tumours (5).

Non-viral vectors can still offer promise for gene delivery of ZFPs. They fall into two main categories: (1) cationic lipids and (2) cationic polymers, of which chitosan is a member (6). Non-viral gene delivery methods should, at best, not elicit immune response, not cause insertional mutagenesis and should not be infectious (6). Further, they should efficiently deliver the gene of interest to the

target organ, and should be biodegradable after delivery. Non-viral vectors associate with the DNA to form complexes of micro- or nano-sphere shape (6). They mask the negative charge of the DNA and deliver it to the cytoplasm of the cells. Cationic lipids are amphiphilic molecules that have a cationic head to condense DNA and a lipid moiety to enhance penetration into cells (6). They are very efficient at delivering plasmid DNA and can protect DNA from extracellular nucleases during *in vivo* delivery (6). A number of clinical trials are ongoing with different cationic lipids, suggesting that their abilities at gene delivery are a viable option for delivering ZFPs to the liver (6).

Gene therapy using cationic polymers is a new concept, and all of the technical difficulties have not been resolved. In general, cationic polymers self assemble with negatively charged plasmid DNA to form complexes (6). The original cationic polymer was diethylaminoethyl-dextran (DEAE-dextran), which is useful for transient expression of transgenes, but not for long-term goals (6). Other cationic polymers include polyethyleneimine, poly-L-lysine, polyallylamine, chitosan, and dendrimers. All of these have lower gene delivery potential than any viral vector, and chitosan appears to have the lowest transfection efficiency of them all, suggesting that another polymer might be a better choice for delivery of the DHBV-specific ZFPs to duck liver (6). However, poly-L-lysine and polyallaylamine are highly toxic, also limiting their usefulness (6). Future work to better define the characteristics and mechanisms of efficient gene delivery by cationic polymers is needed to optimize their use, however they hold the potential to be powerful gene delivery tools someday.

In summary, this thesis presents the proof-of-concept that ZFPs can act as antiviral therapeutics by targeting the genome of HBV or DHBV. Although the delivery methods for *in vitro* assessment of the HBV-specific ZFPs and the *in vivo* assessment of the DHBV-specific ZFPs were not successful, there are a number of delivery methods that offer promise for continued therapeutic confidence in ZFPs for the treatment of chronic HBV. In fact, the scientific and

clinical data suggest that a number of gene therapy methods that are currently in clinical trial will open the path for gene delivery of ZFPs in the HBV field in the near future.

5.1 References

1. Lu Y & Madu CO (2010) Viral-based gene delivery and regulated gene expression for targeted cancer therapy. *Expert Opin Drug Deliv* 7(1):19-35.
2. Daya S & Berns KI (2008) Gene therapy using adeno-associated virus vectors. *Clin Microbiol Rev* 21(4):583-593.
3. LoDuca PA, Hoffman BE, & Herzog RW (2009) Hepatic gene transfer as a means of tolerance induction to transgene products. *Curr Gene Ther* 9(2):104-114.
4. Goff SP (2007) Retroviridae: The Retroviruses and their replication. *Fields Virology*, eds Knipe DM & Howley PM (Lippincott Williams & Wilkins, Philadelphia), Vol 2, pp 1999 - 2070.
5. Guo ZS & Bartlett DL (2004) Vaccinia as a vector for gene delivery. *Expert Opin Biol Ther* 4(6):901-917.
6. Pathak A, Patnaik S, & Gupta KC (2009) Recent trends in non-viral vector-mediated gene delivery. *Biotechnol J* 4(11):1559-1572.

6 Appendix A – Plasmid Maps

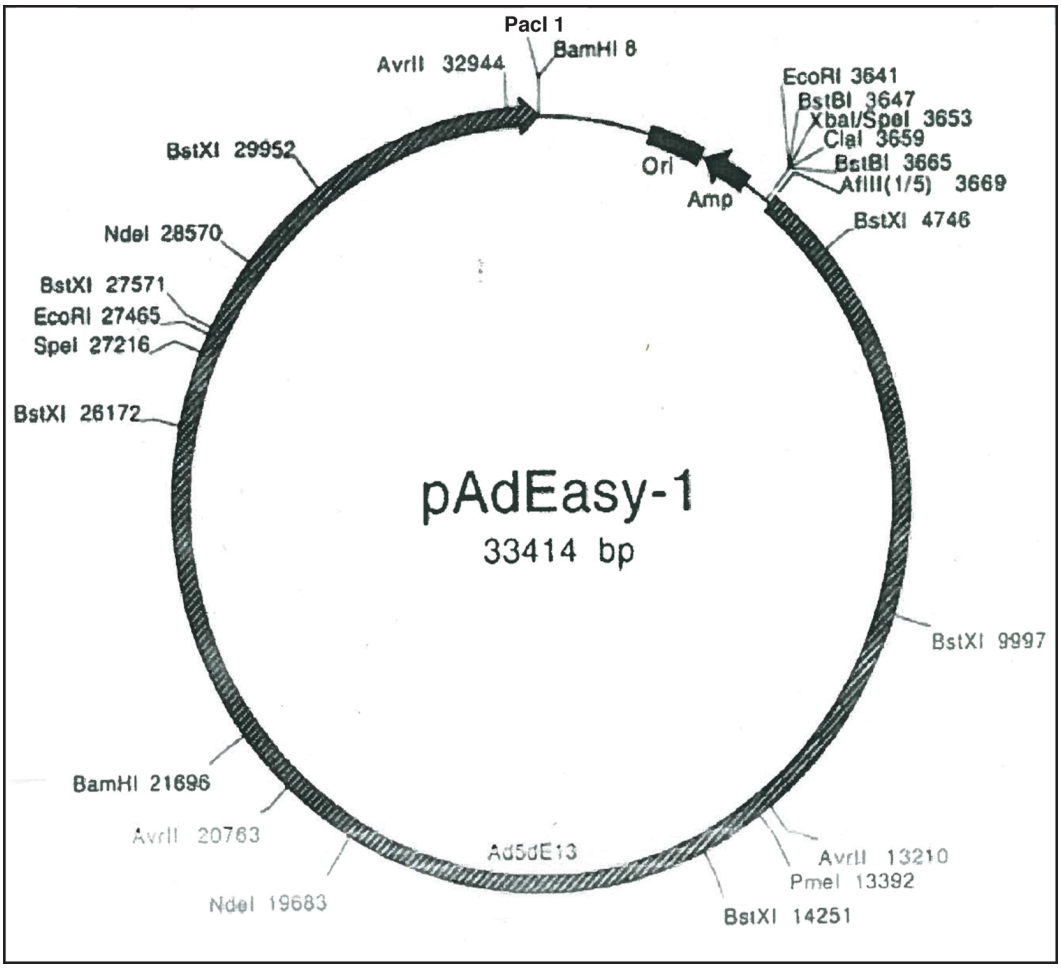

Figure 6.1 - Plasmid map of pAdEasy-1.

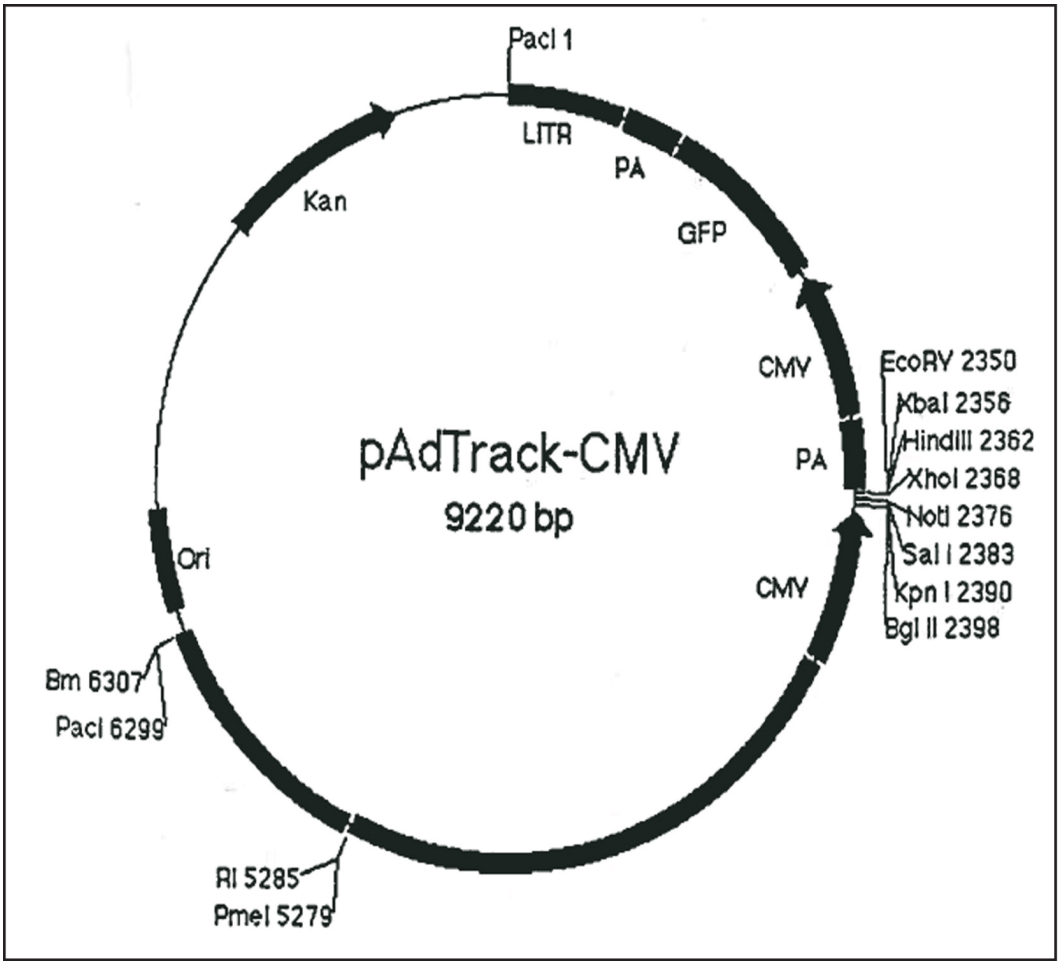

Figure 6.2 - Plasmid map of pAdTrack-CMV.

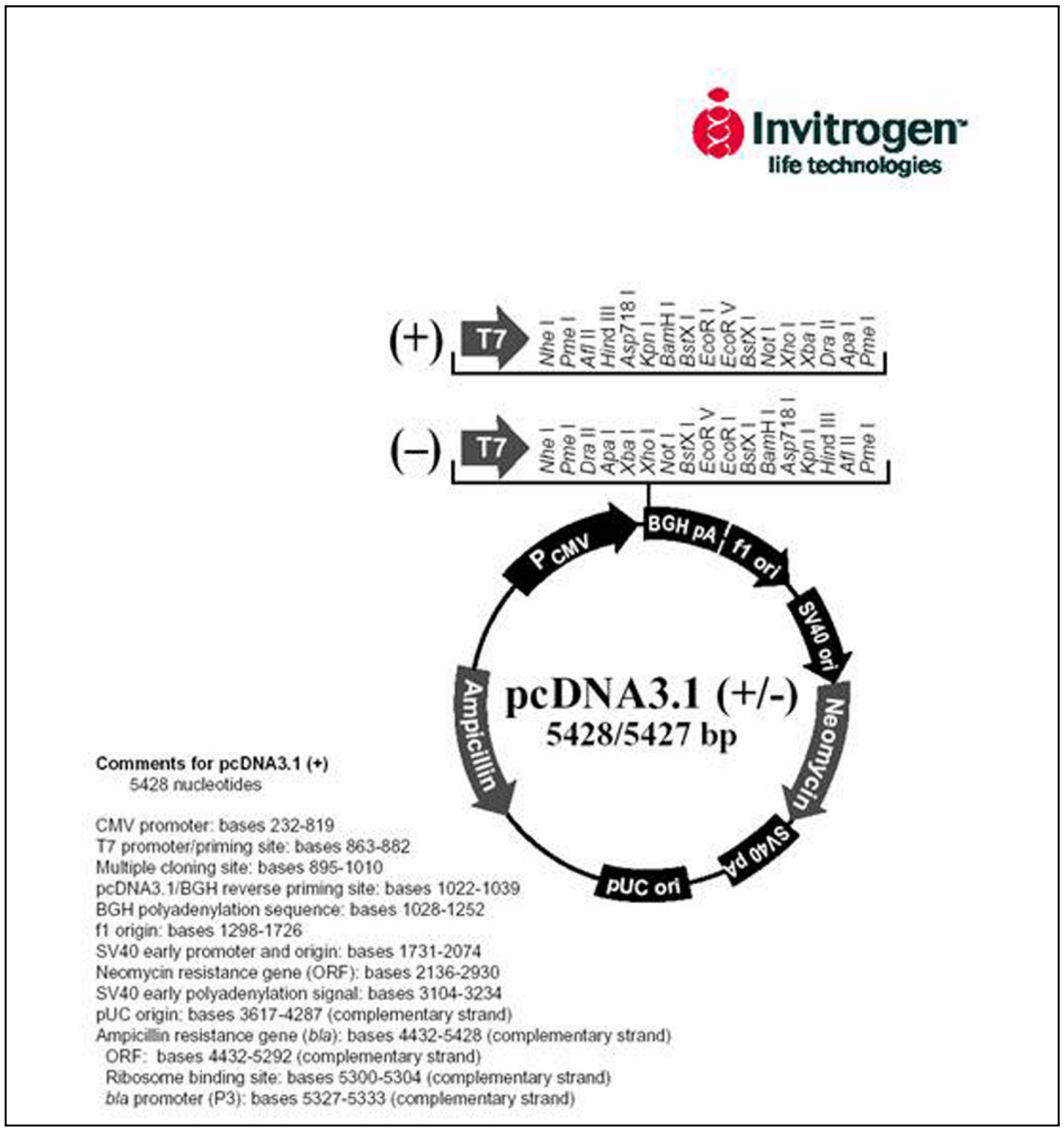

Figure 6.3 - Plasmid map and information for pcDNA3.1(+).
Image from the manual for pcDNA3.1(+) (Invitrogen V795-20).

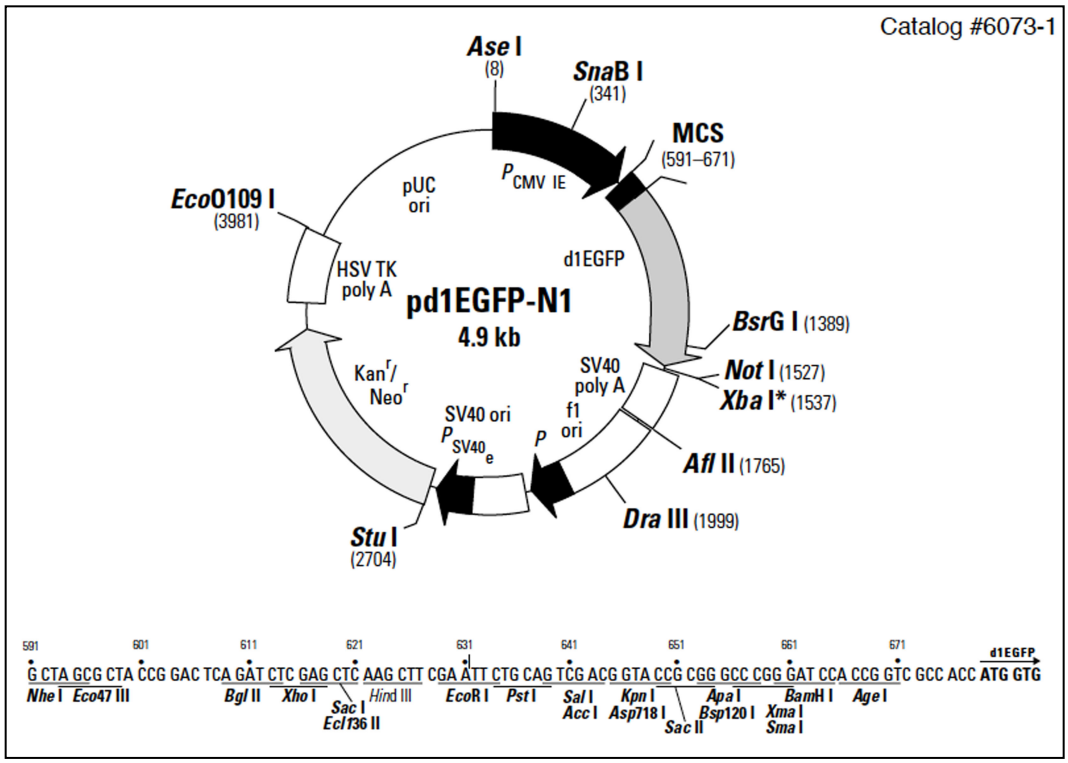

Figure 6.4 - Plasmid map and MCS map of pd1EGFP-N1.
Image from the manual for pd1EGFP-N1 (Clontech #6073-1).

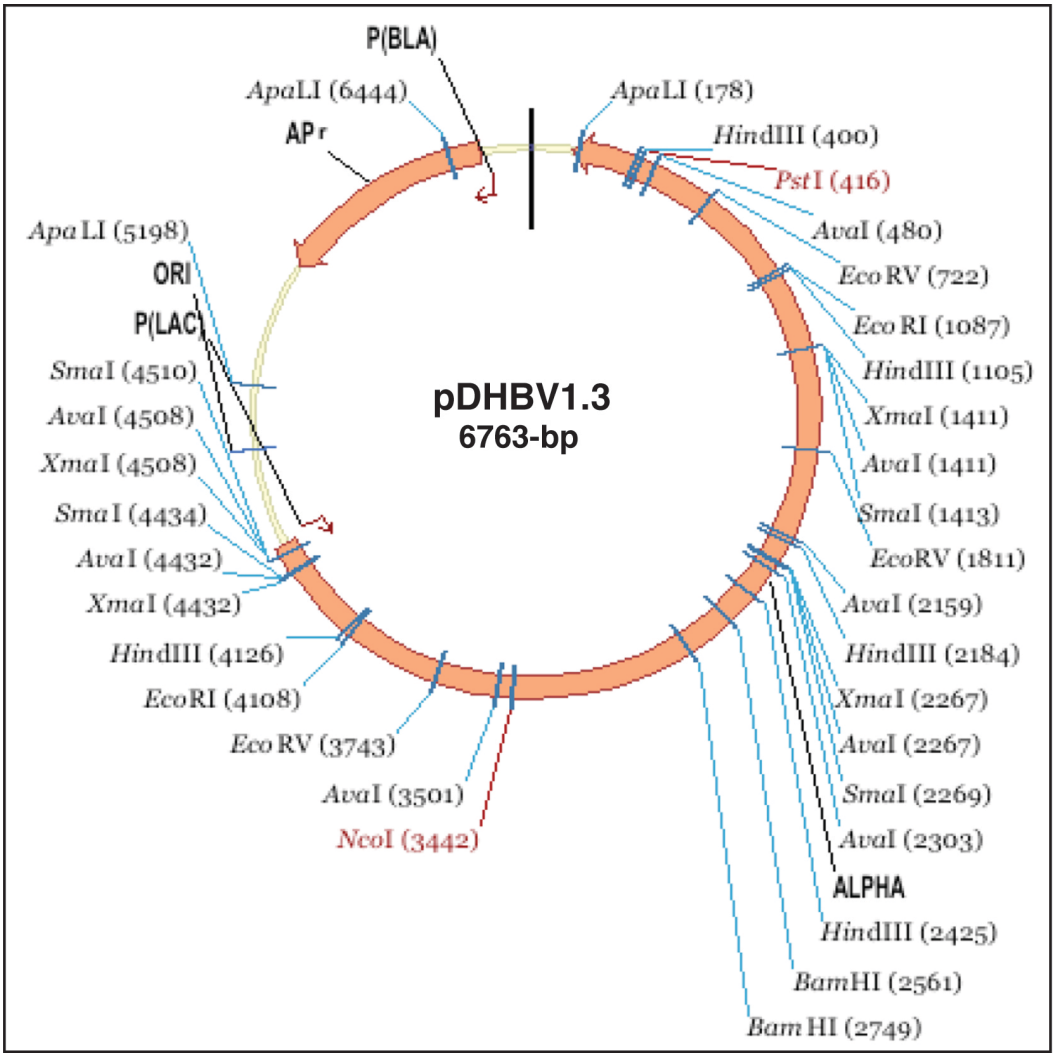

Figure 6.5 - Plasmid map of pDHBV1.3.

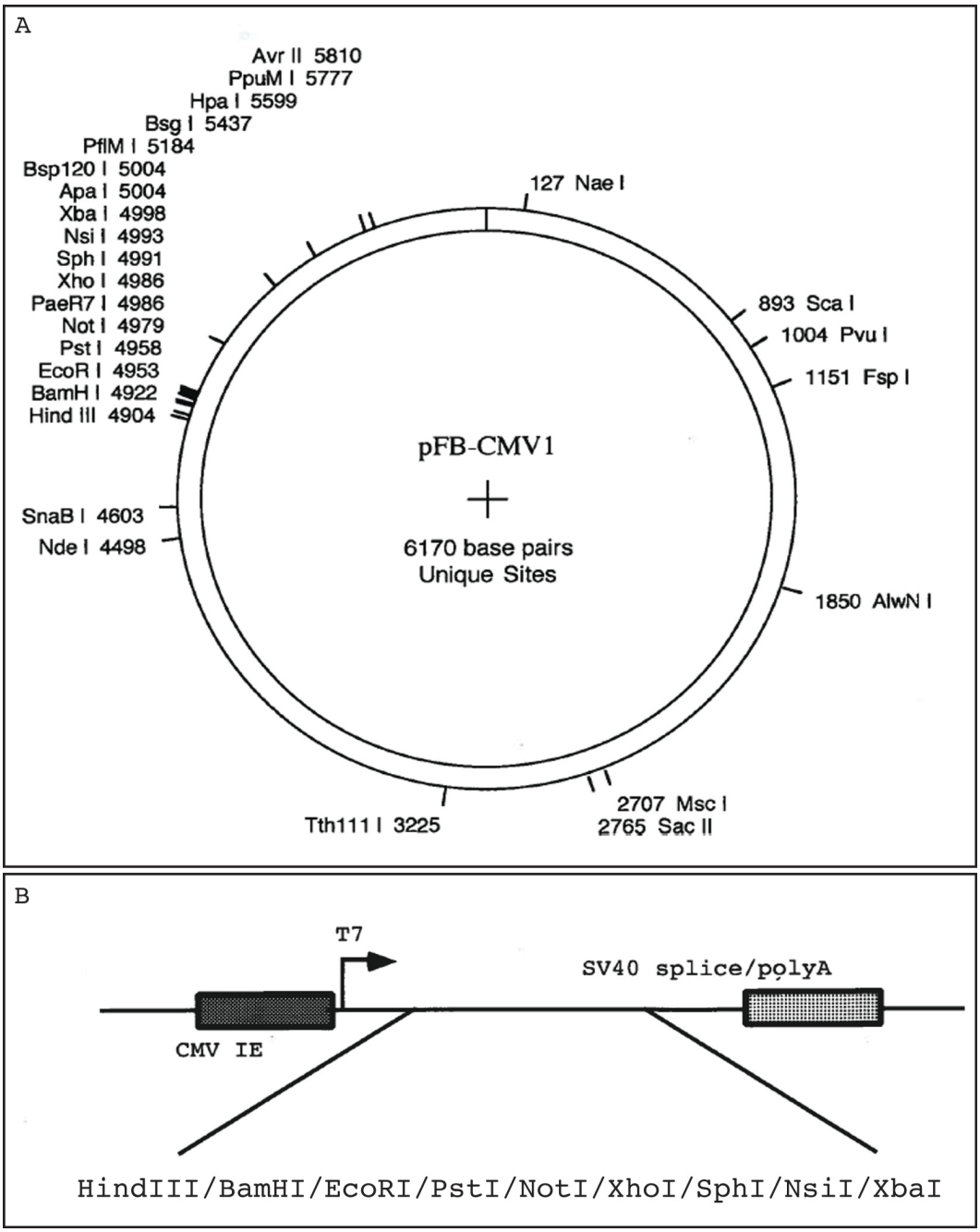

Figure 6.6 - Plasmid map and MCS map of pFB-CMV1.
(A) Plasmid map of pFB-CMV1. (B) Promoter and MCS map of pFB-CMV1.

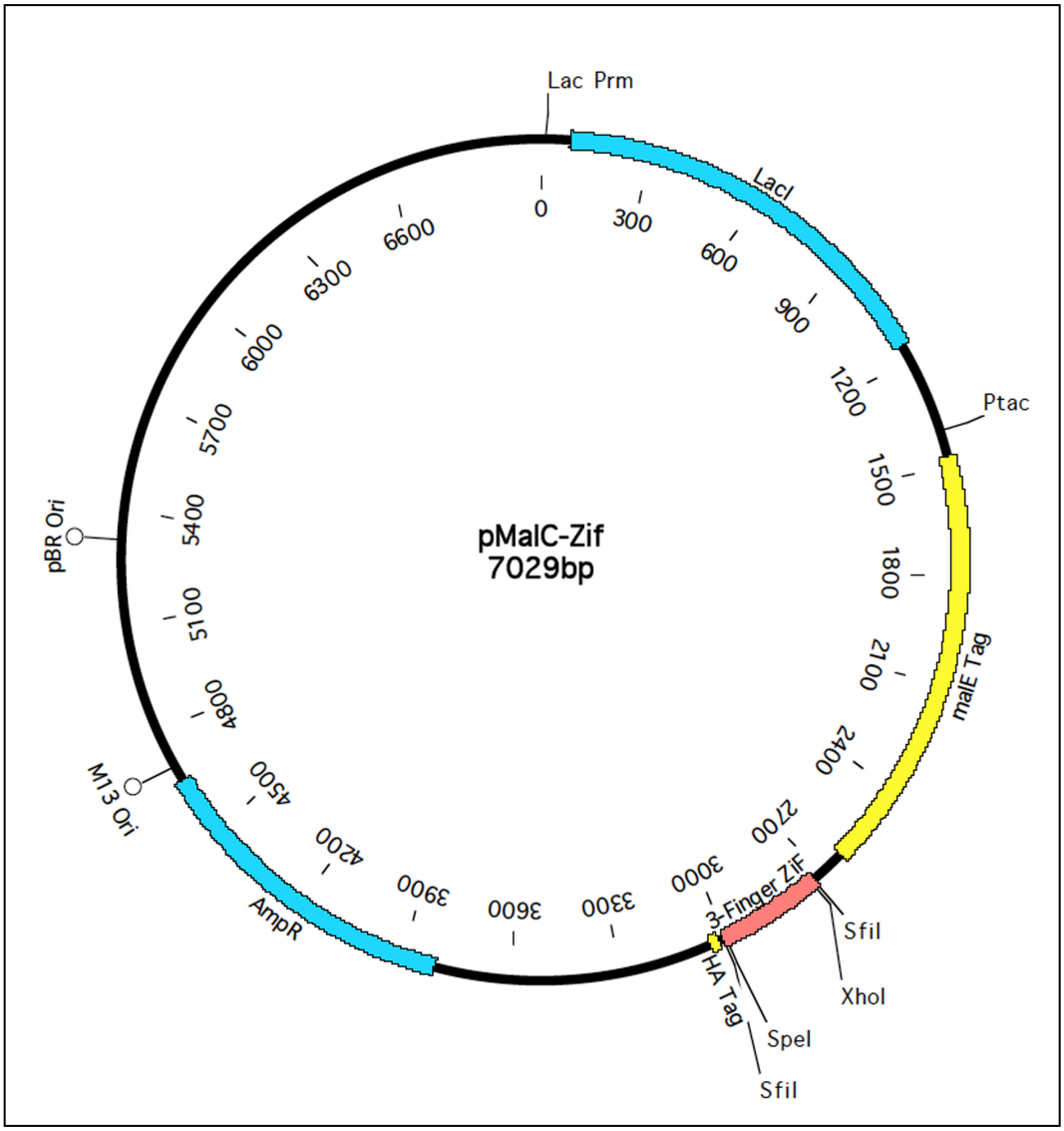

Figure 6.7 – Plasmid map of pMALc with a generalized ZFP inserted in the MCS.

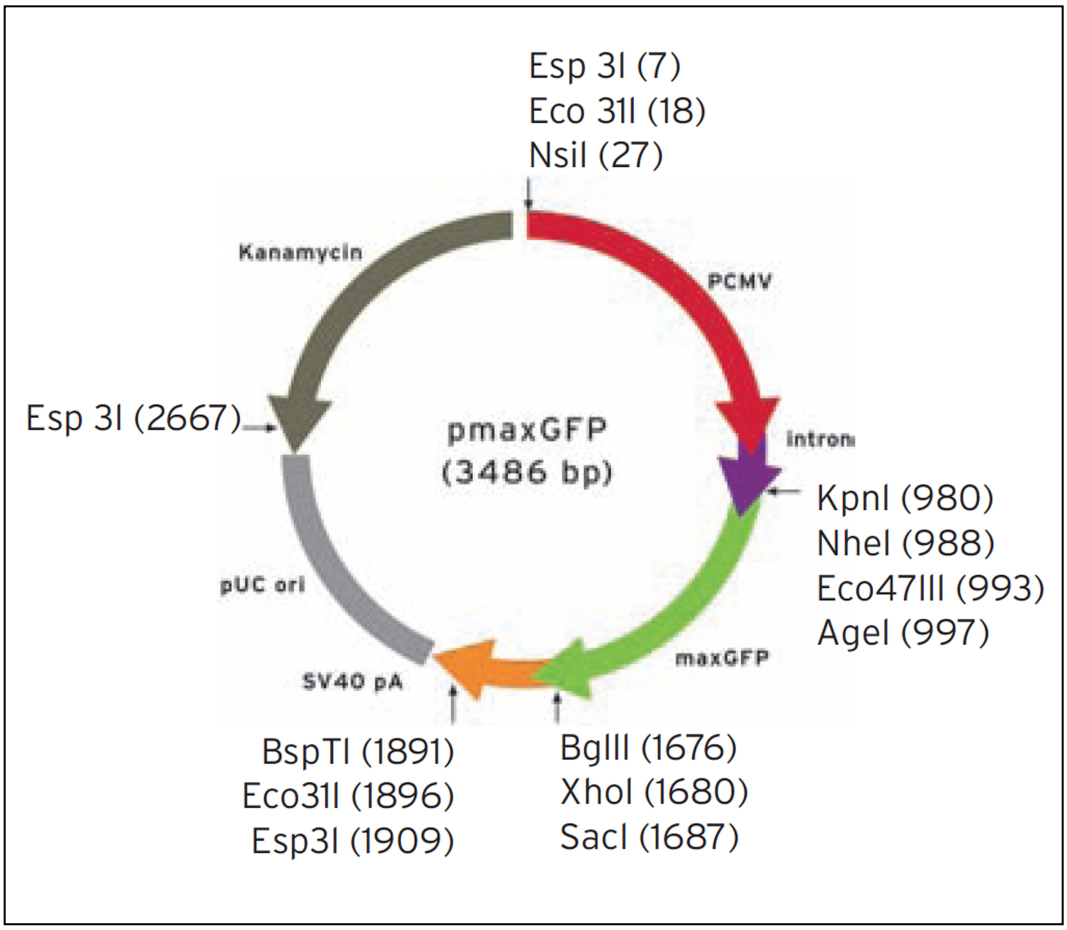

Figure 6.8 - Plasmid map of pmaxGFP, provided in the Nucleofection Optimization Kit.

Image from the manual for the Cell Line Optimization Nucleofector® Kit (Lonza Bio AAD-1001).

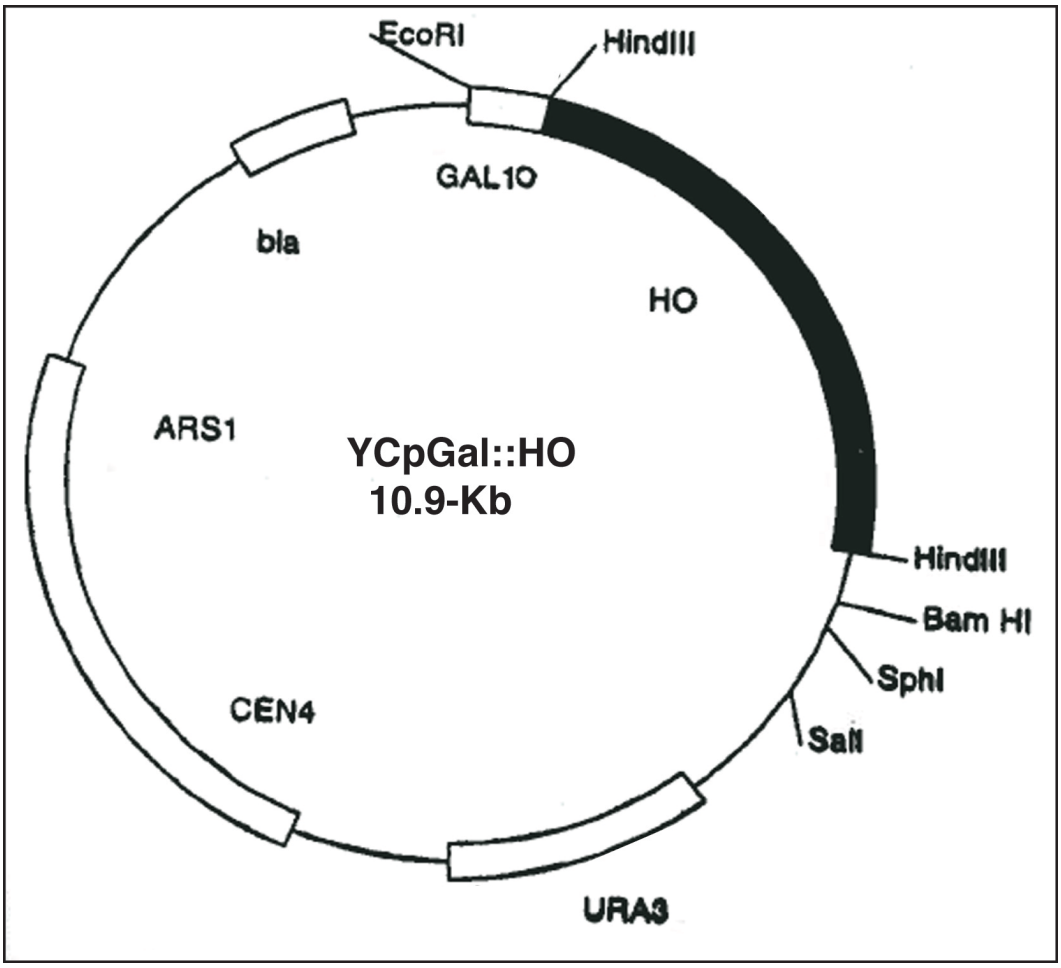

Figure 6.9 - Plasmid map of YCpGal::HO.

7 Appendix B – ZFP Sequence Information

7.1 Amino acid sequences of ZFPs and the corresponding DNA binding site

DNA site	Amino acid sequence	DNA site	Amino acid sequence
AAA	QRANLRA	TAA	Not avail
AAT	TTGNLTV	TAT	Not avail
AAC	DSGNLRV	TAC	Not avail
AAG	RKDNLKN	TAG	REDNLHT
ATA	QKSSLIA	TTA	Not avail
ATT	HKNALQN	TTT	Not avail
ATC	Not avail	TTC	Not avail
ATG	RRDELNV	TTG	Not avail
ACA	SPADLTR	TCA	Not avail
ACT	THLDLIR	TCT	Not avail
ACC	DKKDLTR	TCC	Not avail
ACG	RTDTLRD	TCG	Not avail
AGA	QLAHLRA	TGA	QAGHLAS
AGT	HRTTLTN	TGT	Not avail
AGC	ERSHLRE	TGC	Not avail
AGG	RSDHLTN	TGG	RSDHLTT

Table 7.1 - DNA target site and corresponding amino acid sequence of the α-helix in the zinc finger motif: A-- and T-- codons.

Sequences from "Zinc Finger Tools" program (Mandell JG, and Barbas CF, 3rd (2006) Zinc Finger Tools: custom DNA-binding domains for transcription factors and nucleases. *Nucleic Acids Res* 34(Web Server Issue):W516-523.)

DNA site	Amino acid sequence	DNA site	Amino acid sequence
CAA	QSGNLTE	GAA	QSSNLVR
CAT	TSGNLTE	GAT	TSGNLVR
CAC	SKKALTE	GAC	DPGNLVR
CAG	RADNLTE	GAG	RSDNLVR
CTA	QNSTLTE	GTA	QSSSLVR
CTT	TTGALTE	GTT	TSGSLVR
CTC	Not avail	GTC	DPGALVR
CTG	RNDALTE	GTG	RSDELVR
CCA	TSHSLTE	GCA	QSGDLRR
CCT	TKNSLTE	GCT	TSGELVR
CCC	SKKHLAE	GCC	DCRDLAR
CCG	RNDTLTE	GCG	RSDDLVR
CGA	QSGHLTE	GGA	QRAHLER
CGT	SRRTCRA	GGT	TSGHLVR
CGC	HTGHLLE	GGC	DPGHLVR
CGG	RSDKLTE	GGG	RSDKLVR

Table 7.2 - DNA target site and corresponding amino acid sequence of the α-helix in the zinc finger motif: C-- and G-- codons.

Sequences from "Zinc Finger Tools" program (Mandell JG, and Barbas CF, 3rd (2006) Zinc Finger Tools: custom DNA-binding domains for transcription factors and nucleases. *Nucleic Acids Res* 34(Web Server Issue):W516-523.)

7.2 Nucleotide and amino acid sequences for DHBV-specific ZFPs

Nucleotide sequence (5' – 3'):
CTGGAGCTCGAACCCGGCGAAAAGCCTTATAAGTGCCCAGAATGCGG CAAATCATTCAGCCAACGGGCCAACCTGAGGGCTCATCAGCGCACAC ACACAGGTGAGAAGCCATACAAATGTCCAGAATGTGGTAAGTCTTTCT CTCACAAGAACGCCCTGCAAAACCACCAGCGGACCCACACAGGCGAG AAGCCCTACAAGTGCCCCGAGTGTGGCAAGTCTTTCAGCAGAAGGGA CGAGCTGAATGTTCATCAAAGGACTCATACTGGAGAGAAGCCATACA AATGTCCTGAATGCGGCAAGAGCTTCAGCCAGAAATCCAGTCTGATCG CACACCAGCGAACGCACACTGGGGAGAAACCTTACAAATGCCCAGAA TGTGGTAAATCTTTCAGCCGTAAAGATAACCTTAAGAACCACCAACGC ACCCACACAGGGGAAAAACCTTATAAGTGTCCCGAATGCGGCAAATC CTTCAGTGACTGCAGGGACCTCGCCCGCCATCAGCGGACACACACAG GTAAGAAGACAAGTACTAGT
Amino Acid Sequence (N – C):
LELEPGEKPYKCPECGKSFSQRANLRAHQRTHTGEKPYKCPECGKSFSHK NALQNHQRTHTGEKPYKCPECGKSFSRRDELNVHQRTHTGEKPYKCPEC GKSFSQKSSLIAHQRTHTGEKPYKCPECGKSFSRKDNLKNHQRTHTGEKP YKCPECGKSFSDCRDLARHQRTHTGKKTSTS
DNA binding site:
In DHBV Canada isolate (AF047045) 2276-2293 on the minus strand. 5'-GCCAAGATAATGATTAA-3'

Table 7.3 - Nucleotide, amino acid and DNA binding site sequence information for ZFP18A.

Nucleotide sequence (5’ – 3’):
CTCGAGCCAGGTGAAAAACCCTACAAGTGCCCTGAGTGTGGCAAAAG CTTTTCTCAAGCAGGACATCTCGCTAGTCATCAAAGGACTCACACCGG TGAAAAGCCCTATAAGTGCCCCGAATGCGGAAAATCTTTTAGCCATAG GACCACACTGACAAACCACCAGCGAACACATACAGGGGAGAAGCCTT ATAAGTGTCCCGAATGCGGGAAGTCTTTTTCTCAGCGGGCAAACCTAA GAGCTCATCAGAGAACACACACAGGCGAAAAACCTTACAAGTGTCCA GAGTGCGGAAAAAGCTTTTCAGATTCTGGAAATCTTCGAGTGCACCAA AGAACTCACACGGGAGAGAAGCCTTATAAGTGCCCCGAATGCGGCAA ATCCTTCTCTCAGAGTGGCGACCTACGGAGACACCAGCGCACTCATAC TGGCGAGAAGCCCTATAAGTGCCCTGAGTGTGGTAAATCCTTTTCTAG AAGAGACGAGCTGAATGTGCACCAACGGACTCACACAGGAAAGAAGA CTTCAACTAGT
Amino Acid Sequence (N – C):
LELEPGEKPYKCPECGKSFSQAGHLASHQRTHTGEKPYKCPECGKSFSHR TTLTNHQRTHTGEKPYKCPECGKSFSQRANLRAHQRTHTGEKPYKCPEC GKSFSDSGNLRVHQRTHTGEKPYKCPECGKSFSQSGDLRRHQRTHTGEKP YKCPECGKSFSRRDELNVHQRTHTGKKTSTS
DNA binding site:
In DHBV Canada isolate (AF047045) 690-707 on the plus strand. 5’-ATGGCAAACAAAAGTTGA-3’

Table 7.4 - Nucleotide, amino acid and DNA binding site sequence information for ZFP18B.

Nucleotide sequence (5’ – 3’):
ACTAGTGCCTTGGAGTTGGAACCCGGCGAAAAACCCTACAAGTGCCC AGAATGCGGCAAGTCTTTTAGCACCAGCGGGAGTCTCGTTAGACACCA GCGGACGCACACAGGCGAGAAGCCATACAAATGTCCAGAGTGTGGTA AGTCATTTTCAAGATCCGACGACCTGGTGAGGCACCAGAGAACCCATA CTGGAGAGAAGCCCTACAAATGTCCAGAATGTGGGAAAAGTTTCTCTG AGCGTTCTCACTTGAGGGAACATCAGAGAACTCATACAGGAGAGAAG CCCTATAAATGCCCCGAGTGCGGAAAAAGCTTTTCAGATCCAGGTAAT CTTGTGAGGCATCAGAGAACACATACAGGAGAAAAGCCATACAAGTG CCCTGAGTGTGGAAAGAGCTTCAGCCAACTGGCCCATCTTCGTGCACA TCAGAGAACGCATACTGGGGAAAAACCATATAAGTGCCCTGAATGTG GGAAATCTTTCTCACAAAAATCCAGCCTTATAGCTCACCAGCGTACAC ATACAGGAAAAAAGACATCTACTAGT
Amino Acid Sequence (N – C):
LEPGEKPYKCPECGKSFSTSGSLVRHQRTHTGEKPYKCPECGKSFSRSDDL VRHQRTHTGEKPYKCPECGKSFSERSHLREHQRTHTGEKPYKCPECGKSF SDPGNLVRHQRTHTGEKPYKCPECGKSFSQLAHLRAHQRTHTGEKPYKC PECGKSFSQKSSLIAHQRTHTGKKTS
DNA binding site:
In DHBV Canada isolate (AF047045) 713-730 on the plus strand. 5’-ATAAGAGACAGCGCGGTT-3’

Table 7.5 - Nucleotide, amino acid and DNA binding site sequence information for ZFP18C.

Nucleotide sequence (5’ – 3’):
CTGGAGCTGGAGCCCGGTGAGAAGCCCTACAAGTGCCCTGAGTGCGG TAAAAGCTTTTCTCAGAAGTCATCCCTAATTGCACATCAGAGAACACA CACAGGAGAAAAACCCTATAAATGTCCAGAGTGCGGAAAGAGCTTCA GTACGTCTGGAAATCTGGTTAGGCACCAACGTACACACACAGGGGAG AAACCATACAAGTGTCCTGAATGCGGTAAAAGTTTCTCTCAGCTGGCT CATTTGAGAGCTCATCAGCGCACACACACAGGTAAAAAGACGAGCAC TAGT
Amino Acid Sequence (N – C):
LELEPGEKPYKCPECGKSFSQKSSLIAHQRTHTGEKPYKCPECGKSFSTSG NLVRHQRTHTGEKPYKCPECGKSFSQLAHLRAHQRTHTGKKTSTS
DNA binding site:
In DHBV Canada isolate (AF047045) 2237-2245 on the minus strand. 5’-AGAGATATA-3’

Table 7.6 - Nucleotide, amino acid and DNA binding site sequence information for ZFP9A1.

Nucleotide sequence (5’ – 3’):
CTGGAGTTGGAGCCCGGGGAGAAGCCCTACAAATGCCCTGAATGTGG AAAATCCTTTAGTCAGCGGGCAAACCTGCGTGCCCATCAGCGAACCCA TACCGGCGAGAAACCTTACAAATGCCCTGAGTGTGGAAAGTCTTTCTC TGAGAGGAGCCACCTCAGGGAGCACCAGAGGACACATACTGGAGAGA AACCCTACAAATGCCCAGAATGTGGTAAGAGCTTCAGCCAGAGAGCA AATCTCCGTGCACACCAACGGACACACACAGGCAAAAAGACCAGCAC TAGT
Amino Acid Sequence (N – C):
LELEPGEKPYKCPECGKSFSQRANLRAHQRTHTGEKPYKCPECGKSFSER SHLREHQRTHTGEKPYKCPECGKSFSQRANLRAHQRTHTGKKTSTS
DNA binding site:
In DHBV Canada isolate (AF047045) 794-782 on the plus strand. 5’-AAAAGCAAA-3’

Table 7.7 - Nucleotide, amino acid and DNA binding site sequence information for ZFP9A2.

Nucleotide sequence (5’ – 3’):
CTGGAGCTCGAACCAGGAGAGAAGCCCTATAAGTGCCCAGAGTGCGG AAAGTCCTTTTCACATAAAAACGCTCTCCAGAATCATCAACGCACACA CACAGGAGAAAAGCCATACAAATGCCCAGAATGCGGGAAGTCCTTCT CAAGACGTGACGAGCTGAACGTTCACCAACGCACTCACACCGGTGAA AAGCCATACAAGTGTCCAGAGTGCGGTAAGAGCTTCAGCCAAAAAAG TAGTCTCATAGCACACCAGAGAACTCATACAGGTAAAAAGACTTCTAC TAGT
Amino Acid Sequence (N – C):
LELEPGEKPYKCPECGKSFSHKNALQNHQRTHTGEKPYKCPECGKSFSRR DELNVHQRTHTGEKPYKCPECGKSFSQKSSLIAHQRTHTGKKTSTS-
DNA binding site:
In DHBV Canada isolate (AF047045) 2282-2290 on the minus strand. 5’-ATAATGATT-3’

Table 7.8 - Nucleotide, amino acid and DNA binding site sequence information for ZFP9B1.

Nucleotide sequence (5’ – 3’):
CTGGAGCTGGAGCCAGGTGAAAAGCCATACAAATGTCCTGAGTGCGG TAAGTCTTTTTCCAGTCCCGCCGACCTTACTCGTCACCAGCGCACACAC ACAGGAGAGAAACCCTATAAATGCCCAGAATGCGGAAAGAGTTTTAG CCGCAAGGATAATCTTAAGAATCATCAGAGAACACATACCGGCGAAA AACCATACAAATGCCCTGAGTGTGGGAAGTCTTTCTCTGACTCCGGAA ATCTCAGGGTCCACCAACGGACACATACTGGAAAGAAGACCTCAACT AGT
Amino Acid Sequence (N – C):
LELEPGEKPYKCPECGKSFSSPADLTRHQRTHTGEKPYKCPECGKSFSRKD NLKNHQRTHTGEKPYKCPECGKSFSDSGNLRVHQRTHTGKKTSTS
DNA binding site:
In DHBV Canada isolate (AF047045) 749-757 on the plus strand. 5’-AACAAGACA-3’

Table 7.9 - Nucleotide, amino acid and DNA binding site sequence information for ZFP9B2.

7.3 Nucleotide and amino acid sequences for HBV-specific ZFPs

Nucleotide sequence (5' – 3'):

CTCGAGGGTGATATCCTGGAGCCCGGCGAGAAACCGTATAAATGCCC
CGAGTGCGGCAAGTCCTTTAGCCAGAGGGCGCACCTGGAACGGCACC
AAAGAACACATACTGGGGAAAAGCCATACAAGTGCCCTGAGTGCGGC
AAGTCATTCTCTTCACCCGCCGACCTGACAAGGCACCAGAGAACTCAC
ACTGGCGAAAAGCCATACAAGTGCCCTGAATGCGGGAAATCCTTTTCC
CGGGCTGACAATCTGACCGAGCATCAGCGCACCCACACAGGCGAGAA
GCCTTACAAGTGCCCGGAGTGTGGCAAGAGCTTTTCACACACGGGGCA
CCTGTTGGAACATCAAAGGACTCACACTGGCGAAAAGCCCTATAAATG
TCCGGAGTGTGGGAAGAGTTTTAGCACCACCGGGAATCTGACCGTACA
CCAACGGACACACACAGGCGAGAAACCCTACAAGTGCCCCGAATGTG
GCAAATCTTTCAGCGATAAGAAAGATTTGACAAGGCATCAGAGAACA
CACACTGGTAAGAAGACGTCTGATATCGGTACTAGT

Amino Acid Sequence (N – C):

LEPGEKPYKCPECGKSFSQRAHLERHQRTHTGEKPYKCPECGKSFSSPAD
LTRHQRTHTGEKPYKCPECGKSFSRADNLTEHQRTHTGEKPYKCPECGKS
FSHTGHLLEHQRTHTGEKPYKCPECGKSFSTTGNLTVHQRTHTGEKPYKC
PECGKSFSDKKDLTRHQRTHTGKKTS

DNA binding site:

In HBV subtype *ayw* (U95551) at 3105-3121 on the minus strand: 5'-ACCAATCGCCAGACAGGA-3'

FINGER	**TRIPLET**	**HELIX**
1	GGA	QRAHLER
2	ACA	SPADLTR
3	CAG	RADNLTE
4	CGC	HTGHLLE
5	AAT	TTGNLTV
6	ACC	DKKDLTR

Table 7.10 - Nucleotide, amino acid and DNA binding site sequence information for ZFP18K.

Nucleotide sequence (5’ – 3’):

CTCGAGGGTGATATCCTGGAGCCAGGAGAAAAACCTTACAAATGCCC
GGAATGTGGAAAGTCCTTCTCACAGAGCGGCAATCTGACGGAGCACC
AGCGCACGCACACTGGGGAAAAGCCCTACAAGTGTCCAGAATGCGGG
AAGTCCTTTTCCCAGAACAGCACGCTGACCGAACACCAGCGCACCCAT
ACTGGTGAGAAGCCCTATAAGTGCCCAGAGTGCGGCAAGTCTTTTAGT
CAGAAATCTAGTCTGATTGCTCATCAGCGGACTCATACCGGGGAAAAG
CCCTACAAGTGTCCGGAGTGTGGCAAGAGCTTCTCCGATCCAGGCCAT
CTCGTCCGGCACCAGCGAACCCATACAGGGGAGAAACCATATAAATG
CCCTGAGTGTGGAAAGTCTTTCAGTCGAGCCGACAATCTGACCGAACA
CCAACGCACCCACACCGGTGAGAAACCATACAAATGCCCAGAATGCG
GCAAGTCTTTTTCCACAAGTGGAGAACTCGTTCGGCACCAGAGGACGC
ACACTGGTAAAAAGACATCAGATATCGGTACTAGT

Amino Acid Sequence (N – C):

LEPGEKPYKCPECGKSFSQSGNLTEHQRTHTGEKPYKCPECGKSFSQNSTL
TEHQRTHTGEKPYKCPECGKSFSQKSSLIAHQRTHTGEKPYKCPECGKSFS
DPGHLVRHQRTHTGEKPYKCPECGKSFSRADNLTEHQRTHTGEKPYKCP
ECGKSFSTSGELVRHQRTHTGKKTS

DNA binding site:

In HBV subtype *ayw* (U95551) at 3056-3074 on the minus strand: 5’-GCTCAGGGCATACTACAA-3’

FINGER	**TRIPLET**	**HELIX**
1	CAA	QSGNLTE
2	CTA	QNSTLTE
3	ATA	QKSSLIA
4	GGC	DPGHLVR
5	CAG	RADNLTE
6	GCT	TSGELVR

Table 7.11 - Nucleotide, amino acid and DNA binding site sequence information for ZFP18M.

Nucleotide sequence (5’ – 3’):

CTCGAGGGTGATATCCTCGAACCCGGTGAGAAACCTTATAAGTGTCCC
GAATGTGGGAAGAGTTTCTCCCGCAGCGACGATCTTGTGCGCCACCAA
AGGACACACACAGGGGAGAAACCTTATAAGTGCCCCGAGTGTGGGAA
GAGCTTCAGTCGGTCTGATAACCTGGTGAGGCACCAGAGGACACACA
CCGGCGAAAAACCTTATAAATGTCCCGAGTGCGGCAAAAGTTTTTCAC
GAGCCGATAACCTCACTGAGCATCAACGAACCCATACAGGGGAAAAA
CCATACAAGTGCCCTGAGTGCGGTAAGAGTTTTTCAAGAAGCGACCAC
CTGACTAATCACCAGCGCACCCACACTGGCGAGAAGCCCTACAAGTG
CCCAGAATGCGGTAAATCTTTTTCTCGGTCTGATCACCTTACTACACAC
CAGAGAACGCATACTGGAGAGAAGCCGTACAAATGTCCCGAGTGCGG
AAAGAGCTTTAGCCGCAGTGATCATCTGACCACTCACCAGCGAACCCA
TACCGGAAAGAAGACGTCCGATATCGGTACTAGT

Amino Acid Sequence (N – C):

LEPGEKPYKCPECGKSFSRSDDLVRHQRTHTGEKPYKCPECGKSFSRSDN
LVRHQRTHTGEKPYKCPECGKSFSRADNLTEHQRTHTGEKPYKCPECGK
SFSRSDHLTNHQRTHTGEKPYKCPECGKSFSRSDHLTTHQRTHTGEKPYK
CPECGKSFSRSDHLTTHQRTHTGKKTS

DNA binding site:

In HBV subtype *ayw* (U95551) at 3091-3108 on the plus strand: 5’-TGGTGGAGGCAGGAGGCG-3’

FINGER	**TRIPLET**	**HELIX**
1	GCG	RSDDLVR
2	GAG	RSDNLVR
3	CAG	RADNLTE
4	AGG	RSDHLTN
5	TGG	RSDHLTT
6	TGG	RSDHLTT

Table 7.12 - Nucleotide, amino acid and DNA binding site sequence information for ZFP18N.

Nucleotide sequence (5’ – 3’):

CTCGAGGGTGATATCTTGGAACCAGGCGAAAAGCCATATAAATGTCCT
GAGTGCGGGAAGTCTTTCAGTACCAAGAACTCTCTTACCGAGCACCAG
CGCACACACACAGGAGAGAAACCCTACAAGTGCCCCGAATGCGGAAA
GAGTTTCAGCAGGAATGATGCTCTTACCGAGCACCAGAGGACTCACAC
GGGCGAAAAACCATACAAGTGTCCCGAGTGTGGGAAGAGTTTCAGCA
GGTCCGACCATCTTACTAATCATCAGCGCACACACACTGGAGAGAAGC
CCTATAAATGTCCAGAGTGCGGCAAAAGTTTCAGTACTTCCGGACATC
TCGTGCGGCACCAAAGGACACATACTGGCGAAAAGCCTTACAAGTGT
CCCGAGTGTGGCAAGTCCTTTAGTCGCTCTGACAAGCTCACTGAGCAT
CAGAGAACACACACTGGAGAGAAACCATACAAGTGCCCCGAGTGTGG
GAAATCCTTCAGCAGGGCAGACAATCTGACCGAACACCAACGGACCC
ATACAGGAAAAAAAACCAGCGATATCGGTACTAGT

Amino Acid Sequence (N – C):

LEPGEKPYKCPECGKSFSTKNSLTEHQRTHTGEKPYKCPECGKSFSRNDA
LTEHQRTHTGEKPYKCPECGKSFSRSDHLTNHQRTHTGEKPYKCPECGKS
FSTSGHLVRHQRTHTGEKPYKCPECGKSFSRSDKLTEHQRTHTGEKPYKC
PECGKSFSRADNLTEHQRTHTGKKTS

DNA binding site:

In HBV subtype *ayw* (U95551) at 3123-3140 on the plus strand: 5’-CAGCGGGGTAGGCTGCCT-3’

FINGER	**TRIPLET**	**HELIX**
1	CCT	TKNSLTE
2	CTG	RNDALTE
3	AGG	RSDHLTN
4	GGT	TSGHLVR
5	CGG	RSDKLTE
6	CAG	RADNLTE

Table 7.13 - Nucleotide, amino acid and DNA binding site sequence information for ZFP18P.

Nucleotide sequence (5’ – 3’):

CTCGAGGGTGATATCTTGGAACCCGGTGAAAAACCATACAAATGTCCG
GAATGCGGAAAATCCTTCAGTAGGAACGACACCCTGACTGAACATCA
GAGAACACACACCGGCGAAAAGCCATACAAGTGTCCCGAGTGTGGAA
AATCCTTTTCCACAAAAAATTCCCTGACTGAGCACCAGCGGACGCATA
CAGGGGAGAAACCATACAAATGCCCAGAGTGTGGGAAGTCATTTTCC
AGGTCTGACCATCTGACCAACCATCAAAGGACCCACACCGGCAAAAA
GACAAGCGATATCGGTACTAGT

Amino Acid Sequence (N – C):

LEPGEKPYKCPECGKSFSRNDTLTEHQRTHTGEKPYKCPECGKSFSTKNSL
TEHQRTHTGEKPYKCPECGKSFSRSDHLTNHQRTHTGKKTS

DNA binding site:

In HBV subtype *ayw* (U95551) at 3029-3037 on the plus strand: 5’-AGGCCTCCG-3’

FINGER	**TRIPLET**	**HELIX**
1	CCG	RNDTLTE
2	CCT	TKNSLTE
3	AGG	RSDHLTN

Table 7.14 - Nucleotide, amino acid and DNA binding site sequence information for ZFP9X1.

Nucleotide sequence (5’ – 3’):

CTCGAGGGTGATATCCTGGAGCCTGGCGAAAAGCCTTACAAATGCCCT
GAATGTGGAAAGAGTTTTTCCAGAGCAGACAATTTGACAGAGCATCA
GCGGACCCATACAGGAGAAAAGCCTTATAAATGCCCCGAGTGTGGTA
AGAGTTTTTCTACTAAGAATAGTCTGACTGAACATCAACGAACTCACA
CTGGAGAGAAGCCTTATAAATGTCCCGAGTGTGGGAAATCTTTTTCCG
AAAGATCCCACCTTAGAGAACACCAGCGGACACATACAGGGAAGAAA
ACCTCTGATATCGGTACTAGT

Amino Acid Sequence (N – C):

LEPGEKPYKCPECGKSFSRADNLTEHQRTHTGEKPYKCPECGKSFSTKNS
LTEHQRTHTGEKPYKCPECGKSFSERSHLREHQRTHTGKKTS

DNA binding site:

In HBV subtype *ayw* (U95551) at 3048-3056 on the minus strand: 5’-AGCCCTCAG-3’

FINGER	**TRIPLET**	**HELIX**
1	CAG	RADNLTE
2	CCT	TKNSLTE
3	AGC	ERSHLRE

Table 7.15 - Nucleotide, amino acid and DNA binding site sequence information for ZFP9X2.

Nucleotide sequence (5’ – 3’):

CTCGAGGGTGATATCCTTGAGCCCGGAGAGAAGCCATACAAATGCCCT
GAGTGTGGAAAGAGCTTCTCCTCTAAGAAGCACCTGGCCGAGCATCAA
CGAACCCACACGGGGGAGAAACCTTATAAATGCCCGGAGTGTGGCAA
ATCATTTTCCAGAAGAGATGAACTTAATGTTCACCAGAGGACCCACAC
AGGTGAGAAGCCTTACAAGTGTCCCGAATGTGGAAAATCCTTTAGCCA
CCGCACTACGCTCACTAATCACCAGCGAACCCACACTGGCAAAAAGA
CATCTGATATCGGTACTAGT

Amino Acid Sequence (N – C):

LEPGEKPYKCPECGKSFSSKKHLAEHQRTHTGEKPYKCPECGKSFSRRDE
LNVHQRTHTGEKPYKCPECGKSFSHRTTLTNHQRTHTGKKTS

DNA binding site:

In HBV subtype *ayw* (U95551) at 3062-3070 on the plus strand: 5’-AGTATGCCC -3’

FINGER	**TRIPLET**	**HELIX**
1	CCC	SKKHLAE
2	ATG	RRDELNV
3	AGT	HRTTLTN

Table 7.16 - Nucleotide, amino acid and DNA binding site sequence information for ZFP9Y1.

Nucleotide sequence (5’ – 3’):

CTCGAGGGTGATATCCTGGAGCCCGGAGAGAAGCCATACAAATGTCC
AGAGTGTGGCAAATCCTTCAGCACAACAGGCAATCTGACTGTGCATCA
GCGCACGCATACTGGAGAGAAACCATACAAATGTCCAGAGTGCGGCA
AGAGCTTCTCACAGAGCGGTGACCTGCGCAGACACCAGAGGACACAC
ACCGGTGAAAAACCCTATAAATGTCCCGAATGCGGAAAATCCTTCTCA
ACTAGCCATAGTCTGACTGAGCACCAGCGCACGCATACCGGCAAGAA
GACCTCTGATATCGGTACTAGT

Amino Acid Sequence (N – C):

LEPGEKPYKCPECGKSFSTTGNLTVHQRTHTGEKPYKCPECGKSFSQSGD
LRRHQRTHTGEKPYKCPECGKSFSTSHSLTEHQRTHTGKKTS

DNA binding site:

In HBV subtype *ayw* (U95551) at 3081-3089 on the minus strand: 5’-CCAGCAAAT -3’

FINGER	**TRIPLET**	**HELIX**
1	AAT	TTGNLTV
2	GCA	QSGDLRR
3	CCA	TSHSLTE

Table 7.17 - Nucleotide, amino acid and DNA binding site sequence information for ZFP9Y2.

Nucleotide sequence (5’ – 3’):

CTCGAGGGTGATATCCTGGAGCCAGGCGAAAAGCCATACAAGTGCCC
AGAGTGCGGCAAGAGCTTCTCACGCTCAGACCACCTCACTACACACCA
GCGGACCCACACCGGCGAGAAGCCGTACAAATGTCCCGAATGTGGCA
AGAGTTTCTCAACTTCAGGAAATCTTGTACGGCATCAGAGAACTCACA
CAGGAGAGAAACCATATAAGTGTCCTGAATGTGGTAAAAGTTTCTCCG
ACCCCGGACATCTCGTGCGCCACCAGAGGACCCATACAGGCAAGAAG
ACATCAGATATCGGTACTAGT

Amino Acid Sequence (N – C):

LEPGEKPYKCPECGKSFSRSDHLTTHQRTHTGEKPYKCPECGKSFSTSGNL
VRHQRTHTGEKPYKCPECGKSFSDPGHLVRHQRTHTGKKTS

DNA binding site:

In HBV subtype *ayw* (U95551) at 3106-3114 on the plus strand: 5’-GGCGATTGG -3’

FINGER	**TRIPLET**	**HELIX**
1	TGG	RSDHLTT
2	GAT	TSGNLVR
3	GGC	DPGHLVR

Table 7.18 - Nucleotide, amino acid and DNA binding site sequence information for ZFP9Z1.

Nucleotide sequence (5’ – 3’):

CTCGAGGGTGATATCCTCGAACCAGGCGAAAAACCGTACAAATGTCCT
GAGTGTGGCAAGTCATTCAGCGATAAGAAGGACCTTACTAGACATCA
ACGGACACATACCGGGGAAAAACCCTACAAGTGTCCAGAATGCGGCA
AGAGTTTTTCCACTAAAAATAGTCTGACAGAACATCAAAGAACCCACA
CCGGGGAGAAACCTTATAAATGCCCTGAATGTGGGAAATCCTTCTCCC
GGGCTGATAACTTGACAGAGCATCAGAGGACTCACACCGGTAAAAAG
ACGTCCGATATCGGTACTAGT

Amino Acid Sequence (N – C):

LEPGEKPYKCPECGKSFSDKKDLTRHQRTHTGEKPYKCPECGKSFSTKNS
LTEHQRTHTGEKPYKCPECGKSFSRADNLTEHQRTHTGKKTS

DNA binding site:

In HBV subtype *ayw* (U95551) at 3126-3134 on the minus strand: 5’-CAGCCTACC -3’

FINGER	**TRIPLET**	**HELIX**
1	ACC	DKKDLTR
2	CCT	TKNSLTE
3	CAG	RADNLTE

Table 7.19 - Nucleotide, amino acid and DNA binding site sequence information for ZFP9Z2.